A Mathematical Model for the Simulation of Paper Drying Energy Consumption

by

Shaun Anthony Reardon, B.E. (Hons)

Submitted in fulfilment of the requirements

for the degree of

Doctor of Philosophy

Department of Civil and Mechanical Engineering

University of Tasmania

November 1994

This thesis contains no material which has been accepted for the award of any other degree or diploma in any tertiary institution and to the best of my knowledge and belief nor does it contain any material previously published or written by another person, except where due reference is made in the text of the thesis.

Shaun A Reardon

This thesis may be made available for loan and limited copying in accordance with the Copyright Act of 1968.

Shaun A Reardon

Abstract

A detailed analysis of the dryer section of a paper machine was undertaken in this study. The mathematical model developed relates initial sheet conditions, paper sheet properties, drying conditions and dryer section configuration to the variation of the moisture content and temperature in the paper sheet as well as energy consumption per unit production.

The theoretical model was based on mass and energy balance equations about a slice of paper composing pulp fibres, free and bound water, water vapour and air. Time-varying boundary conditions, corresponding to the movement of the paper sheet over the 40-50 drying cylinders, were assigned and the equations were converted to finite difference form and solved by computer using standard linear algebra methods.

The heat and mass transfer coefficients which control evaporation rates in the dryer section were investigated experimentally. Drying trials and boundary layer analysis were performed to establish the effects of dryer fabric permeability and tension, air flow, cylinder surface temperature, pulp furnish and sheet basis weight on paper drying rates.

A number of paper sheet properties were investigated as part of the study. The pore size distribution, permeability and sorptive behaviour of machine made newsprint were investigated experimentally and theoretically. Other paper properties correlated from literature for the purposes of this study included thermal conductivity, specific heat capacity, density, fibre saturation point, diffusibility and shrinkage.

A number of simulations were performed on the two Australian Newsprint Mills paper machines that formed the focus of this study. A comparison with actual machine moisture content values showed the model's prediction of moisture change during drying and specific steam consumption under different operating conditions to be within 2% and 10% respectively.

A series of simulations were performed to demonstrate the effect of the paper condition on drying, specifically, initial moisture content, sheet thickness, sheet basis weight and initial temperature. These graphs provided a useful insight into the effect on achievable machine speed and specific steam consumption as a function of such variables. An alternative perspective on the analysis was to specify the machine speed as constant,

as often occurs in a production environment, and determine the necessary change in each of pocket temperature, pocket humidity and cylinder temperature to maintain this speed. In each case, increases in the drying duty were handled most energy efficiently by increasing the temperature of the pocket ventilation air.

Two dryer section configuration changes were also considered. ANM's PM3 was examined from the perspective of an optimal design. The results showed the current lengths of individual cylinder wraps and open draws to be within 10cm of the optimal case from the viewpoint of drying capacity.

The second prospective change examined was that of PM2's conversion to an initial dryer sub-section with seven foot diameter cylinders, in a bid to improve heat transfer and hence drying rate and also improve runnability in this critical wet section. The simulation predicted that this would lead to a production increase of almost 20 m/min, just over 2%. This suggested the project would not be feasible on the basis of increased drying rate alone but would need to be co-justified by other factors.

Acknowledgement

I would like to acknowledge a number of people who have provided various forms of assistance which has contributed to the overall success of this project.

Firstly I would like to thank Australian Newsprint Mills (ANM) as a group for the provision of financial support for the term of this project. This together with key support services such as their corporate library, paper testing laboratory and access to technical and engineering staff for advice and guidance, provided a solid footing for the project.

Within ANM I am particularly grateful to John Brodribb for his efforts in making the entire project possible. John has provided much useful input into the project and my career development and this is greatly appreciated.

Other ANM personnel to have significant impact on the project include paper machine superintendents Kim Brown and Guy Mycroft who assisted with obtaining paper sheet samples from the machine every fifth Wednesday at 7am, Tony Parsons and Paul Banham from the Research Division who provided assistance in operating the sheet former and other testing equipment, and George Fam and the boiler attendants who helped with the collection of steam consumption data.

At the University my key support was obtained from supervisor Dr Peter Doe and associate supervisor Professor Mike Davis. Peter and Mike were available whenever needed and our weekly meetings were always very thought-provoking. The efforts of the department's workshop staff in preparing the experimental rigs for testing and making modifications upon request was a great help. Terry McNicol, who put together all the electronics and instrumentation associated with datalogging the drying test rig and also performed the photography used in this thesis, deserves many thanks for his efforts.

On a personal note I would like to thank my wife, Katrina, for her encouragement and support over the duration of this project during what has also been a very challenging time in her career. I am also grateful to my parents for their limitless support which put me in a position to take on such a study.

Table of Contents

SECTION A - INTRODUCTION

SECTION B - MODEL

SECTION C - HEAT AND MASS TRANSFER COEFFICIENTS

SECTION E - MODEL PREDICTIONS

SECTION G - APPENDICES

1. Background

Paper provides the medium for recording, storing and disseminating a large proportion of the world's information. Since the patent of the first continuous papermaking machine by Nicholas-Louis Robert in France in 1798 there have been innumerous attempts at improving the speed and quality of paper production.

The concept of energy efficiency in papermaking has come to the fore in the past 10-20 years as energy costs have risen significantly and the level of competition has increased substantially as the growing number of paper manufacturers have sought to set new benchmarks in all areas of paper production.

There are three major cost components involved in the production of paper - raw materials, labour and energy. The unit cost of raw materials is largely governed by the paper mill's location which will dictate the availability of and competition for natural resources such as wood, coal and fresh water. The costs associated with supply of these commodities will be affected by environmental and legislative considerations as well as the available transport infrastructure. Thus, given an existing mill there is little control over these factors. This leaves energy usage and labour costs as the key avenues for reducing a mill's unit cost of production.

Energy consumption, which is to be the underlying focus of this study, is therefore one of two generic areas which can be investigated with a view to improving the specific cost of production. Within the bounds of energy consumption at an integrated pulp and paper mill there are the categories of electrical and thermal energy which are usually comparable in terms of annual gigajoules (GJ). As electricity is inherently a very efficient transfer medium and the majority of it is used in driving rotating machinery it was considered that provided the motors were relatively efficient and operating at an appropriate speed for the application there is little motivation for a detailed process analysis in a bid to reduce this component of energy costs.

Approximately 80% of a paper mill's steam requirements are made by the paper machines' dryer sections. Along with the electricity demand of the pulping refiners, dryer section steam generally represents the site's largest energy consumer. With this in mind it is quite reasonable to concentrate attempts to improve energy efficiency in this area. Fractional

improvements even of the order of 5-10% will translate to significant monetary savings due to the large volume of energy involved. Smook (1988) confirms that the dryer section is by far the most expensive part of the paper machine from both a capital and operating cost viewpoint and concludes that any attempts to increase evaporation rate and reduce steam consumption are well justified.

For the above reasons the operation of the dryer section of the paper machine was selected as the focus of this study. At this point it is useful to outline the major components of the paper machine to indicate where the dryer section fits into the overall process.

Papermaking is essentially a process of dewatering. A relatively dilute pulp solution is fed into the stock inlet of the paper machine. To ensure a uniform distribution to the headbox the stock is fed from a constant head tank referred to as the *stuffbox* through the basis weight control valve and into the suction line of the *fan pump* which transfers the flow, which is a mix of the main stock with recycled white water, to the headbox at a consistency of around 0.8-1.0% solids. The objective of the inlet piping is to distribute the papermaking fibres evenly across the width of the paper machine.

The function of the *headbox* is to take the stock delivered by the fan pump and convert the pipeline flow into a uniform rectangular flow equal in width to the paper machine and at uniform velocity in the machine direction. It is essential that an even flow is discharged from the headbox slice opening onto the forming wire at the correct location and angle. The speed and width of the pulp jet is critical to the quality and structure of the final paper sheet. This is achieved with the headbox slice, a full width nozzle which is completely adjustable to give the appropriate flow.

The jet from the headbox is directed onto what has historically been called the *fourdrinier wire*, so named after brothers who were early pioneers of continuous papermaking. The fourdrinier or forming wire is an endless, finely woven belt which travels between the breast roll near the headbox and the couch roll at the other end. Drainage on the forming wire is accomplished by hydraulic pressure gradients induced as the sheet passes over perforated rotating rolls and stationary contoured supports. Further down the wire various vacuum devices are also employed to remove water. As the paper sheet leaves the couch roll the solids content represents around 20% of the total sheet weight. Modern paper machines have evolved further from the fourdrinier former to the twin wire former

which allows dewatering from both sides often along a vertical path. This aids the symmetry of both fibre structure and surface properties of the paper sheet.

The next stage of the process is *pressing* which aims to remove water and consolidate the web. It is an extension of the water removal process that was started on the wire. The wet pressing of paper is carried out in contact with a felt between two rolls in the press nip. The mechanical compression expels water from the sheet. Most press sections have either two or three nips where the sheet is compressed and water removed. The final wet basis moisture content is usually around 60%, or 40% solids.

Improvements in pressing efficiency have a large impact on the subsequent duty in the dryer section. Improving the moisture content at press section output from by 1% from 60% to 59% is equivalent to dropping the water content from 1.50 kg_{water}/kg_{fibre} to 1.44 kg_{water}/kg_{fibre} representing a 4% reduction in drying duty.

The *dryer section* is the final part of the moisture removal process. Attwood (1964) estimated the relative costs of water removal in the dryer section as fifty times greater than the fourdrinier wire and eight times more expensive than the press section. Whilst specific costs have changed since then the same relativity still applies. This is the motivation for minimising the sheet moisture content after the press section and maximising the performance of the dryer section.

The dryer section is composed of 40-50 steam-heated cast iron cylinders configured in two rows. The paper sheet is heated as it wraps around successive cylinders. Between cylinders the sheet is exposed to the ventilating air which is heated to provide moisture carrying capacity to evacuate the evaporating moisture from the region. The whole section is an enclosed region which operates at conditions which are controlled to maintain a constant sheet moisture content at exit, around 10% water and 90% fibre.

The final section of the paper machine is the *calender stack* which is a vertical arrangement of typically six rotating metal rolls which compress the sheet and in doing so impart an improved surface finish which aids printability. After calendering the paper sheet is wound onto the main reel and is later rewound into smaller widths for the customer.

A schematic view of the papermaking processes is shown in Figure 1.1.

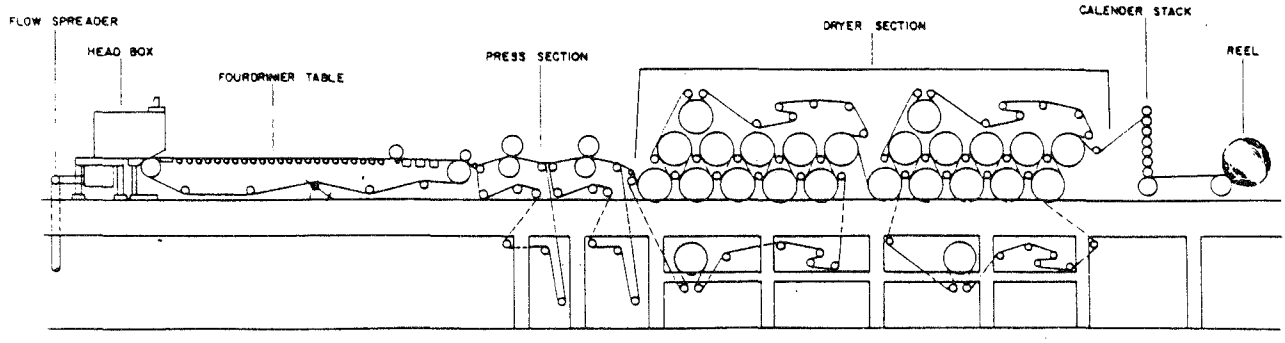

FIGURE 1.1
Fourdrinier paper machine schematic (Smook, 1988)

Australian Newsprint Mills (ANM) who are the co-sponsors of the current study operate two newsprint machines at their Boyer, Tasmania, site. The machines, designated PM2 and PM3 respectively, are approximately 30 years old and together produce in excess of 230 000 tonnes of paper per year. The paper grades vary from telephone directory paper with a basis weight of 36-40 g/m^2 to standard newsprint at 45-48.8 g/m^2 and a brighter, heavier grade especially suitable for four colour offset printing with a basis weight between 52-55 g/m^2. The machines have been subject to relatively recent rebuilds which have made them quite competitive with more modern machines in terms of both quality and production quantity. The photos presented overleaf in Figures 1.2 and 1.3 give a clear indication of the size and complexity of a paper machine.

Figure 1.2 shows a three quarter view from the wet end of PM3. The curved pipe in the foreground transfers stock to the machine. The twin wire former is the tall structure after the head box and is followed by the fourdrinier wire which now acts more as a transfer device rather than a sheet former. The press section is followed by the long dryer section which trails off to the right hand end of the photo.

Figure 1.3 shows PM2 from the dry end. The main winding reel and the calender stack are in the foreground. The extended region on the right is the dryer hood enclosure.

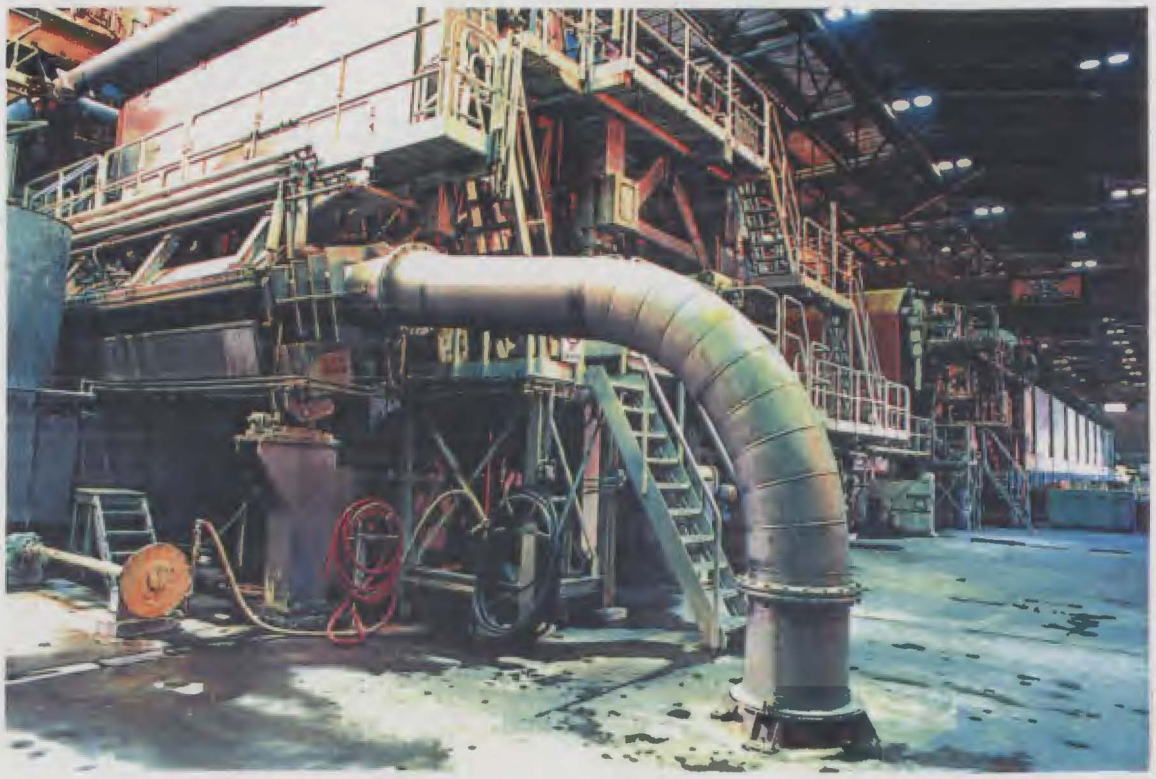

FIGURE 1.2
Photo showing ANM PM3 from the wet end

FIGURE 1.3
Photo showing ANM PM2 from the dry end

The two photos indicate that the dryer section itself is generally inaccessible due to the need to keep it well sealed to reduce the incidence of unconditioned ambient air infiltrating into the dryer hood. Despite this a photo was obtained whilst the side doors were raised for some operating adjustments and this is presented in Figure 1.4.

The photo in Figure 1.4 illustrates a double-felted region about half way through the PM3 dryer section. The paper sheet can be seen passing from the upper to lower cylinders as it weaves its way through its 200m path in the dryers. Each of the 48 steam-heated cylinders are 1.5m diameter and are continually filled with steam at a temperature of between 95-130°C. The dryer section is divided into five sub-sections which are each controlled to distinct drying conditions and have their own support fabrics. The dryer fabric (felt) is a synthetic monofilament material which compresses the paper sheet to the hot cylinders to improve heat transfer and also acts as a physical support for the sheet in some transfer regions.

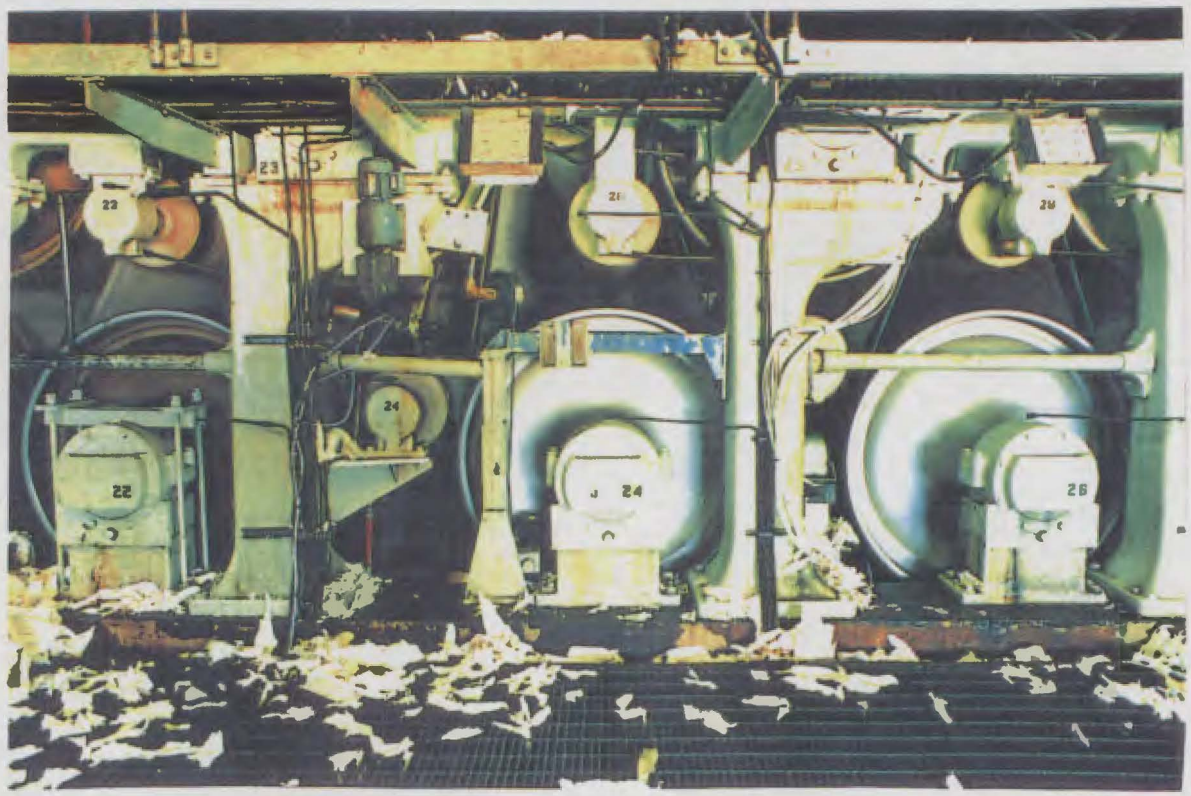

FIGURE 1.4
Photo of ANM's PM3 dryer section

Like most areas of the paper-making process the dryer section is a relatively complex region for which to construct a dynamic thermal model. There are a very large number of parameters which affect the drying process and need to be taken into account when modelling it. There are four main groups of parameters which need to be considered.

The first group of variables contains those machine conditions which are clearly related in a direct way to drying rate and energy consumption. These operating conditions include the machine speed, temperature of the drying cylinders, temperature and humidity of air in the dryer hood, permeability of the supporting drying fabrics and tension of the drying fabric. Most of these variables will change throughout the dryer run. Paper dryers are generally divided into about five sub-sections and in each of these regions the conditions can be expected to be approximately constant. There will also be mild cross-machine variations but these are very difficult to model. Mean values of these control parameters are available from the control modules located in the paper machine room.

The second group of parameters which must be input into the dryer model is the paper sheet conditions. These include the sheet basis weight, thickness, initial moisture content and temperature. The final moisture content required at the dryer section exit would also fall into this category. Basis weight, thickness and final moisture content are available from an on-line scanning device. Initial moisture content is measured in the laboratory by taking a batch sample of wet paper before entry to the dryer section and weighing before and after oven drying. Inlet sheet temperature has only a mild effect on drying and is not easily measured but is obtained as an estimate from several paper machine superintendents.

The heat and mass transfer characteristics of the dryer section form the third major group of model parameters. These coefficients describe the degree of heat transfer between the steam and the cylinder shell, the cylinder surface and the paper sheet, the paper sheet and the ambient air, and the mass transfer from the sheet as a function of machine speed and the presence of dryer fabrics which tend to impede evaporation. These coefficients warrant some detailed investigation to determine how they fluctuate with operating conditions. This will form a significant part of the current study.

The final collection of parameters which intimately affect the drying process is the range of the physical properties of paper. These include density, specific heat capacity, thermal conductivity, diffusibility,

structural permeability, sorptive behaviour, fibre saturation point, shrinkage and the paper sheet geometrical pore size distribution. Many of these properties are documented in some form in the paper industry literature. The complicating factor is the enormous variety of paper furnishes used worldwide. Differences in wood composition between species and vastly different pulping processes lead to paper sheets which are extremely diverse in their range of physical properties.

ANM, Boyer, has historically used four and now uses three different pulps in the production of paper. ANM produces thermo-mechanical pulp (TMP), cold caustic soda pulp (CCS) and purchases kraft pulp, a chemical pulp which is necessary in small quantities for the added strength it gives to the paper sheet. The stone groundwood process is now obsolete at the mill. Of the two pulps made on site, each is made on two distinct lines using different equipment. This effectively leads to a total of four pulp varieties, all with different physical and chemical properties which can be mixed in varying proportions for different paper sheets. Due to the variety of pulps available it was not considered reasonable to simply make use of mean data from the literature for all properties. Consequently some experimental and theoretical work was undertaken to define certain paper properties more closely.

The overall aim, therefore, of this study is to provide a comprehensive description of the behaviour of a sheet of paper as it travels through the dryer section of a paper machine. As discussed in Chapter 2, other researchers have investigated the phenomenon of paper drying in various contexts. What has been missing to date is a study which reviews *all* aspects theoretically and experimentally, and which takes the mathematical model with appropriate input parameters and transforms it into a relevant and practical tool for operators and designers of paper machine dryer sections. The link between drying rate and energy consumption has not been emphasised in the past yet it is one of the key areas which affects the unit cost of production.

Some other, slightly more subtle, features which the current work aims to investigate include the effect of paper sheet structure as it relates to the various drying mechanisms. Whilst paper fibres are hygroscopic, the variability of sorption isotherms between pulps and the subsequent effect of both reduced vapour pressure and the differential heat of sorption on drying behaviour have not always been fully appreciated in previous work in this area. The effect of sheet shrinkage during drying also needs addressing.

There is a need for a dryer section study which, while having a solid theoretical base and making use of parameters which are shown to be relevant to the component pulps used in manufacture of the paper sheet, provides a direct practical link between the fundamental concepts needed to describe the drying process and actual parameters which are important in a production environment, such as achievable machine speed and specific steam consumption. The current study seeks to achieve this niche in an area which has for a long time been acknowledged as important but not fully developed in a way that investigates all aspects.

It should be noted here that the paper industry is essentially self-supporting from the viewpoint of research, literature and equipment. Many terms used are specific to the industry and there are also a number of common abbreviations used, some of which are employed in this volume. For this reason a brief glossary of relevant paper industry terms is presented in Appendix 2 of this thesis.

It should also be emphasised that much of the literature on paper-making and more specifically paper drying is contained within a number of paper industry journals and publications which fall outside the mainstream realm of academic literature. As the narrow focus of these works greatly increases their relevance to the current study they are referred to frequently throughout this study and this will become evident in the literature review.

2. Literature Review

Due to the worldwide prevalence of the paper industry and the intrinsic part that drying plays in the paper manufacturing process it is understandable that there have been many investigations into and descriptions of the paper drying process during the past forty years. These studies take differing perspectives depending upon the nature of the researching institution, the paper grade in question and the underlying objective of the project.

Paper-making companies tend not to have the time to embark on detailed process descriptions themselves and in-house work is therefore usually confined to on-line measurements of select dryer section operating conditions. Such empirical work is certainly reliable and relevant but cannot alone explain the mechanisms of drying. Consequently, there is difficulty in relating dryer operating conditions to their impact on the paper sheet. It is therefore common for paper mills to engage either commercial consultants, frequently in the form of paper machine manufacturers, or local academic institutions to provide a deeper analysis of the paper drying operation.

Paper machine manufacturers require their own dryer models both for initial design purposes as well as fine-tuning and upgrading their clients' existing equipment. These models vary greatly in depth from rigorous finite difference analyses to simple energy accounting approaches. Assessment of some of these drying models is made impossible by the barrier of 'proprietary information' which prohibits general access.

Links with a particular branch of the paper industry also influence the focus of the drying study. Tissue manufacturers dry paper with a single, but very large, steam-heated Yankee dryer. Coated papers generally require a degree of infra-red heating. Recent developments in high intensity drying increase drying rate by the simultaneous application of heat and pressure. However, the situation is still that 80% of paper machines dry paper by means of the multi steam-heated cylinder approach described in the introductory chapter. This form of drying applies to the newsprint machines that are of particular interest in this study.

As the body of paper drying literature grows so does the opportunity to create a comprehensive mathematical model. A reliance on others' data is

necessary due to the plethora of physical data required to implement the drying equations in a reliable and thorough fashion. A collection of correlations for paper drying properties such as permeability, diffusivity, thermal conductivity, shrinkage, pore structure, sorption isotherms, specific heat, density and heat and mass transfer coefficients gives one confidence to utilise them within the framework of a reasonably complex model.

The remarkable development of computers over the past few decades is really the foundation upon which such extensive theorising can be undertaken. It is interesting to note that Depoy's (1972) calculations are based upon use of an analogue computer to solve his paper drying simulation. Attwood (1964) reported that Nissan's solution of the paper drying equations had taken 160 hours. Prahl's doctoral thesis (1968) dealing with the sorptive properties of paper made use of 'the eyeball approach' to obtain a best fit description for the bulk of his data. Such researchers were clearly at a disadvantage by today's standards.

In general terms it can be said that in spite of the quantity of paper drying studies over the years there are few that take a comprehensive view of all of the properties and parameters affecting the process. By assuming such a broad scope this study will reap benefits through the ability to apportion the contribution of each drying mechanism in the overall process. This enables the limiting properties and operating parameters to be identified with more certainty and appropriate adjustments made.

2.1 Paper drying models

From 1950 Nissan was the pioneer of serious attempts to describe the drying of paper in detailed analytical terms. His publications with Kaye (1955), Hansen (1960) and George and Hansen (1962) were the first comprehensive descriptions of conventional steam-heated cylinder paper drying. Their work is credited with defining the four phases of multi-cylinder drying which is necessary when implementing a numerical solution with representative, varying, boundary conditions. The solution calculates temperature change only, based on Fourier's heat transfer equation, with moisture change measured experimentally in trials on a 1mm thick sheet of muslin cloth. Whilst the study on the felt's impact on drying is of great interest, it is no longer relevant due to subsequent changes in felt philosophy and design. Modern paper machines employ

highly synthetic, hydrophobic, permeable *felts* which do not hold moisture but allow vapour and air to pass through with little resistance.

Han (1964) examined the hot surface drying of fibre mats. He was the first worker to analyse the internal moisture transfers occurring as paper dries. Han observed a quasi-steady-rate drying period and noted the very large capillary pressure gradients brought about by the very wide pore size distribution. The analytical model was based upon Fick's law of diffusion for water vapour transport and Darcy's law for the permeation of liquid water. Neither bulk flow of vapour nor the effect of the sorptive behaviour of paper is catered for. Han acknowledged shrinkage of the fibre mat during drying but did not quantify it. Han was no doubt frustrated by the intense computational burden that his drying model created, for in summarising the qualitative work on paper drying by Sherwood, Dreshfield, Cowan and himself, he remarked that a quantitative analysis of the process remained to be accomplished.

Soon after, Han published a further paper in conjunction with Matters (1966) which concentrated on the vapour diffusion component of paper drying. They obtained correlations for the diffusibility of vapour in a fibre matrix and concluded that normal diffusion accounts for 40% of the total drying rate.

Depoy (1972) extended Nissan's work by including a calculation for moisture removal based on surface differentials. The model complexity was limited by the use of analog computer solution. Depoy quoted experimental results for both absorbent felts and open weave synthetic fabrics. Use of the latter was shown to allow double the drying rate under dynamic conditions. Such results provided the confidence for industry to make the transition to a different felt philosophy.

Meisel (1977) followed in the path of Depoy. Using the Fourier heat transfer equation Meisel calculated moisture evaporation based on vapour pressure gradient at the surface. It was necessary to include a *falling rate drying correction factor* in the boundary condition to tune the model towards a realistic prediction. This form of model calibration overrides much of the first principles' analysis and ensures the model will be correct for the single operating point for which the correction factor applies.

Hartley and Richards (1974) advanced the quest to describe the paper drying process with a diffusion based model. Their paper acknowledged Corte's work (1957, 1962) which showed the occurrence of capillary flow

within the drying sheet, yet chose to construct the model on the basis of both liquid and water vapour diffusion. The model restricted itself to hot surface drying and as such did not address the varying boundary conditions prevalent within a paper machine. It was suggested that shrinkage be considered as a factor in future drying models.

Snow (1980) put forward a drying model within which moisture evaporated from the hot surface, diffused towards the sheet surface and condensed. Capillary liquid flow was also a component of Snow's model. Hygroscopic effects and the possibility of bulk vapour flow were not addressed.

During the 1980's several research groups each published a number of articles relating their ongoing experiences in attempting to model the paper machine dryer section adequately. Lee and Hinds (1979, 1980, 1981) compiled comprehensive mass and energy equations to describe the drying process. Like Hartley and Richards they stated that liquid transport in a porous medium occurs primarily as a result of differences in local capillary pressures but then proceed to describe liquid movement with a general diffusivity based term. They obtained reasonable correlations to describe the liquid, vapour and thermal transport coefficients. However, their physical data were determined for 600 g/m^2 linerboard rather than the 50 g/m^2 newsprint of interest in this current study.

In a later paper Hinds and Neogi (1983) updated the model to include vapour transport by bulk convection. They also introduced boundary conditions based on the Chilton-Colburn analogy and acknowledge the use of the PhD work by Prahl (1968) on the sorption properties of paper.

Within a similar time frame to the aforementioned work of Lee, Hinds and Neogi, Karlsson (1980), Soininen (1980) and, Soininen et al (1985) also made several publications within the field. These Finnish researchers also employed a diffusion-based liquid transport description in addition to the use of Prahl's sorption isotherms. In their model, vapour diffusivity was a function of a porosity/tortuosity ratio whilst the *moisture conductivity factor* that described liquid flow was inferred indirectly from experimental tests. Their theoretical system did not allow for the possibility of sheet shrinkage nor bulk vapour flow due to total pressure differential at temperatures greater than 100°C.

Allan, Ghosh and Harris (1988) continued the work of Lee and Hinds (1979, 1980, 1981) with a similar model which differed only in several

minor areas. Allan et al extended their drying model to include the interaction of the steam side of the drying cylinder upon the process. This modification enabled the drying rate to be related to the energy consumption of the section. The model provided a comprehensive list of the correlations used for paper properties and transport coefficients. The use of Lee and Hinds' transport coefficients for vapour, liquid and heat flow is likely to be questionable in the current study due to the variations in furnish and basis weight from the Douglas fir kraft fibres at 600 g/m^2 studied by Lee and Hinds. The other uncertain aspect of the investigation of Allan et al lies in the definition of the contact heat transfer coefficient as that value which allows the model to dry the paper to the desired exit moisture content by the end of the dryer section. This final adjustment negated much of the benefit associated with constructing such a thorough and complex model and made it difficult to assess the model so as to determine whether it faithfully apportions each of the mechanisms of heat and mass transfer within the web.

Iida (1985a) was another to rely heavily upon the work of Lee and Hinds in developing his version of a paper drying model. Iida was particularly interested in creating a one-layer version which could run on a personal computer within a reasonable time. Details of the model were difficult to assess as they were presented exclusively in Japanese (1985b, 1985c) in the Japan Tappi journal. In the English based conference paper the use of a correction factor was noted. The factor modified the cylinder-paper heat transfer coefficient and "...is determined by preliminary simulations to make a web dry just at the final cylinder".

Papers by Kerttula (1984) and Eskelinen (1985) of the Valmet paper machine manufacturing company provide very little in terms of theoretical detail and useable properties and transfer coefficients, presumably because of the sensitivity of such proprietary information. Nonetheless there were some interesting results from their simulations and on-line measurements. They did note, however, that liquid flow is caused by capillary pressure differences resulting from variations in web internal moisture. Both also quoted a moisture level of approximately 20%, below which liquid water cannot flow any more and hygroscopically bound moisture must be removed with the associated increased evaporation energy requirement.

Pounder and Ahrens (1987) presented a model of high intensity paper drying. This phenomenon occurs when the heated surface of the wet web is at or above the thermodynamic saturation temperature corresponding to the ambient pressure. Their work focussed on bulk flow as the dominant

mechanism associated with paper drying and was aimed at drying systems operating at temperatures from 175°C to 400°C in tandem with pressures from 7 kPa to 5 MPa. For these reasons their model assumptions and results were not specifically applicable to the current study.

Harrmann and Schulz (1990) put forward a comprehensive and plausible description of the convective drying of paper. Their work was significant due to the description of the influence of water on the web structure during drying. Their paper explained how water absorption and desorption cause a change of fibre thickness as opposed to length and why it is reasonable to assume that shrinking during drying does not influence the pore structure but only the pore length. These principles provided the platform for calculating the variation of sheet caliper with hygroscopic moisture content during drying. This model appeared very comprehensive as it included sorptive effects, shrinkage, liquid flow by Darcy's Law and a thorough description of the relevant paper properties and transfer coefficients used in the analysis.

Ramaswamy (1990) identified the need for a comprehensive study of the paper drying process. His distributed parameter model was strongly influenced by the work of Dreshfield and Han (1956) and Han (1964). Ramaswamy acknowledged the main transfer processes as vapour diffusion, bulk vapour flow due to total pressure gradients and liquid flow due to local variation in capillary pressures. The model was quite thorough but encouraged further investigation for a number of reasons. Firstly, the work was related specifically to the drying of linerboard, which at 0.45mm thickness has many significantly different characteristics from newsprint at around 0.07mm. These differences are particularly important in the area of internal web flow dynamics as a function of the diffusibility and permeability. This model would be further well served by including an allowance for web shrinkage during drying in addition to a more extensive consideration of the heat and mass transfer coefficients which are the key first order parameters which control drying rates.

Several detailed literature reviews have been published in an attempt to consolidate knowledge on the subject. McConnell (1980) presented a summary of drying research in all areas of the pulp and paper industry. His paper which included 127 references noted that over 80% of dryer sections were the conventional multi-cylinder design.

Nederveen et al (1991) consulted a number of drying experts to provide a summary of the current direction of drying research. This article was of

interest both for its reinforcement of the prevailing drying mechanisms in addition to the useful heat and mass transfer correlations quoted. It also supported the concept of obtaining drying rate information from experimental testing based on drying paper on a curved hot plate in a duct as performed by Ahrens et al (1984). Nederveen's review noted that there have been no experiments on the function of drying fabrics in contact drying. It noted the degree of conflict between authors concerning the percentage of evaporation occurring in the free draw of the paper machine as opposed to that occurring whilst the sheet is in contact with the hot cylinder surface where some authors quote a figure of 10% whilst others claim 40%. The article by Nederveen et al suggests there is considerable scope for further experimental work to describe quantitatively all phenomena related to evaporation within the paper machine.

2.2 Other drying theory

Whilst there is a significant background of information on paper drying within the paper industry itself, it is also advantageous to conduct an examination of the more general literature on drying. This can be achieved by targeting research dealing with porous, hygroscopic materials.

Berger and Pei (1973) studied the drying of hygroscopic capillary porous solids. Their mass and energy balance equations described liquid and vapour movement by Fick's diffusion law and allowed for evaporation internal to the material. The work was very theoretically oriented and did not define the porous material to which the results refer.

Experimental and theoretical work performed by Kisakurek and Gebizlioglu (1978) on the drying of unglazed pottery supported the conclusion of others that the mechanism of solid drying can not be accounted for by a single type of flow phenomena, but is a complex mechanism in which both diffusional and capillary effects coexist. The drying theory presented utilised a description of Darcy's law controlling liquid movement under capillary pressure differences arising from a non-uniform pore size distribution. The theory did not deal with heat fluxes and also appeared to have difficulty in defining a pore size distribution function which was both physically realistic and also amenable to the theory.

Food chemists Szentgyorgyi and Molnar (1978) set up a drying theory to describe evaporation from 8cm thick, wet, granular material into air at 45°C. The solution is effected through definition of an evaporation front

which penetrates into the material with time. This concept is not applicable to the comparatively thin paper sheet.

The drying of wet textile materials, principally wool, was analysed by Nordon and Bainbridge (1971). The model catered for the evaporation of free liquid only and the authors acknowledged that the hygroscopic phase was significant and would affect the later part of the drying curve.

Keey's textbook (1972) is useful for its presentation of characteristic drying curves for differently structured materials. Keey suggested that in a highly hygroscopic substance, such as a potato, the progression from free liquid removal to bound moisture evaporation can be observed as a critical point discontinuity on the drying rate curve. He noted that this feature is typically not the case for paper pulps where the critical point is barely discernible.

Keey also described the two-pore theory for the drying of capillary porous materials. The concept involves the internal transfer of liquid from the wide capillary to the narrow one from where it evaporates from the free surface. The main difficulty in applying this description exists in the relatively arbitrary assigning of the two relevant pore sizes.

2.3 Paper properties and drying parameters

Supplementing the aforementioned attempts to mathematically describe the drying of paper there have also been many investigations aimed at quantifying both the physical properties of paper and the thermal transfer coefficients associated with the paper drying process. It is appropriate here to outline the major sources of such information whilst providing a complete record of supporting data in later chapters.

As a hygroscopic material, the drying of paper is strongly influenced by sorptive effects. Wink et al (1958) obtained the desorption isotherm for an unnamed wood pulp furnish at 93°C. Their data was in excellent agreement with that of Prahl (1968) whose doctoral thesis appears to be the most comprehensive experimental treatment of the topic available. Prahl obtained both adsorption and desorption isotherms over the temperature range of 21°C to 80°C for a number of different pulp furnishes. Regression analysis performed in the current study has allowed this body of data to be encompassed by a single continuous equation relating relative humidity to temperature and moisture content. Prahl also

obtained the related data describing the differential heat of sorption associated with hygroscopic materials.

Information on the related subject of pore size distribution has been obtained by Corte (1957, 1962, 1982), who has contributed much to the literature concerning the porosity of paper. Corte compared pore size distribution curves generated from both mercury porosimetry as well as the gas displacement method and suggests that the latter method provides a more realistic description of the paper sheet's internal pore geometry. This view is supported by Ruthven (1984) who acknowledges that surface constrictions will bias mercury porosimetry results. More recently Yamauchi and Kibblewhite (1988a, 1988b) have published articles on the pore structure of thermo-mechanical pulp (TMP) paper webs. This has relied on mercury porosimetry techniques and generated results which suggest that the pore sizes are distributed primarily through the range 1-20 μm. These findings are consistent with the drying model of Harrmann and Schultz (1990), which assumes the maximum pore radius to be 16μm, based on the work of Rhodius (1980).

Others to have addressed the area of pore size distribution include Bristow (1986), d'A Clark (1981), McKnight et al (1958), Stone and Scallan (1966), and Murakami and Imamura (1984).

Paper sheet permeability is dealt with in detail by Bliesner (1964). Based on a Darcy law description of fluid flow through the fibre network, he used the Kozeny-Carman (1927, 1937) equation which expresses permeability in terms of porosity, specific volume, specific surface area and a dimensionless variable referred to as the Kozeny factor. Bliesner obtained a correlation for the Kozeny factor as a function of porosity. Ingmanson et al (1959) have also contributed in this area, and both groups agreed that the Kozeny factor is constant below a porosity of 0.8.

On a theoretical level the work of Haring and Greenkorn (1970, 1983) can be used quite conveniently to incorporate experimental values for pore size distribution into a mathematical description which can be employed by a drying model. Their statistical description of porous media assumes an incomplete beta function distribution. The importance of such work to a drying model lies in the liquid flow description which makes use of a relation between capillary pressure, pore radius and liquid volume content.

The physical properties of cellulose have been widely documented. Values for density, specific heat and thermal conductivity are provided in articles

by Sutermeister (1941), Han and Ulmanen (1958), Stone and Scallan (1968), Depoy (1972) and Nakagawa and Shafizadeh (1984), and are found to be quite consistent. Harrmann and Schultz's drying model (1990) expresses the fibre saturation point for paper in terms of an empirical temperature dependent relationship developed by Rhodius (1980). This correlation is found to agree satisfactorily with data presented by Skaar (1988).

Several research reports, internal to the pulp and paper company supporting this study, provided further assistance in obtaining precise values for paper properties. The reports by Young (1989) and Banham and Cox (1989) were particularly useful in that they referred to pulps and paper products specifically investigated under the current study.

The dynamics of paper drying are primarily controlled by the heat and mass transfer coefficients. Any first estimation of the rate of open surface mass and energy transfers must begin with the Chilton-Colburn analogy in j-factor form (Chilton and Colburn, 1934). The drawback of using such an analogy lies in the uncertainty of the relative velocity between paper and air. A first approximation will assume the paper machine speed to be the relative velocity, but the accuracy of this assumption is dependent upon the degree of air entrainment with the paper sheet and dryer felt. For this reason it is preferable to rely on experimental results from laboratory and on-line machine tests, such as those presented by Karlsson (1980) and Lee and Hinds (1979, 1980, 1981).

Correlations for the contact heat transfer coefficient between the steam-heated drying cylinder and the paper sheet are entirely empirical due to the uncertain quality of contact arising from the non-homogeneous nature of the paper structure and the variations induced by changing water content. Kerekes (1980) provides a summary of previous investigations into this parameter for various paper grades. Ng et al (1991) examine the contact conductance between paper and metal for bone-dry paper under varying pressure. Asensio et al (1991) performed similar tests for paper of varying moisture content. Depoy (1972), Nissan and Hansen (1960) and Hinds and Neogi (1983) also reported variations of contact heat transfer coefficient with paper sheet moisture. Riddiford (1969) interpreted the contact between paper sheet and drying cylinder as an air gap which varies with felt permeability and tension. This method would appear to have difficulty with accounting for the interaction between the varying paper sheet moisture content and sheet surface roughness.

Whilst there has been a lack of investigation into the influence of felts on paper drying as discussed by Nederveen (1991) in his review of present drying theory, Fagerholm (1990) did attack the question of the aerodynamic properties of dryer fabrics on paper machines. The paper focussed on the topic from the viewpoint of improving sheet runnability by minimising disturbance of the paper sheet associated with air entrainment with the dryer felt. It was concluded that appropriate felt design could minimise the volume of air dragged by the dryer felt and therefore reduce the incidence of sheet breaks and wrinkles. The relevance of this work to drying rates lies in the quantifying of boundary layer development on the felt. There is also some information on the direction of airflows within a single dryer pocket. These data allow the surface heat and mass transfer coefficients to be calculated more accurately throughout the various parts of the dryer section.

3. Model Development

The aim of the drying model is to calculate the temperature and moisture content of an element of paper during its passage from the press section exit through the length of the dryer section. Throughout this drying process the paper sheet is subjected to a series of alternating boundary conditions as the two sides of the sheet sequentially come in contact with the dryer cylinder surface, the hood air and the dryer felt.

An initial simplification of the problem is therefore to restrict the analysis to hot surface drying only. This defines a situation where the paper sheet is heated on one side by a hot, impermeable surface whilst the opposite side of the sheet is exposed to conditioned air which transports the evaporated moisture away. When this interim solution has been obtained the implementation of the full dryer section simulation is simply a matter of varying the surface boundary conditions with time.

The advantage of separating the model development into two stages is twofold. Assessing the model response and numerical stability is much simplified when performing trials on a system which has constant boundary conditions. Secondly, the hot surface drying scenario itself is directly relevant to the experimental testing performed in this study to determine correlations for the transfer coefficients.

3.1 Drying mechanisms

The development of the mathematical model to describe the drying process is centred around the consideration of the paper sheet as a porous, hygroscopic material which releases moisture to the surroundings via the combined mechanisms of liquid capillary flow, diffusional vapour flow and bulk vapour flow as a consequence of the total pressure gradient throughout the sheet.

Liquid flow within the paper sheet occurs due to the capillary pressure differentials created by the non-uniform pore structure of the paper sheet. As capillary pressure is proportional to the inverse of pore radius, for the case of water, large pore radii are at higher pressures than small pore radii. This sets up a pressure gradient which transfers liquid from large pore radii

to the smaller ones. The rate of liquid flow is then controlled by Darcy's law.

Vapour flow by diffusion is driven by the vapour concentration gradient which primarily occurs due to the non-uniform temperature distribution across the sheet. In this case Fick's law of diffusion governs the mass flow rate. The cross-sectional area for diffusion-based vapour transfer increases as drying progresses and the paper sheet's macro-pores empty themselves of liquid.

The third major mechanism for moisture removal from the sheet is that of bulk vapour flow. This differs from the diffusion term in that the flow is pressure driven rather than concentration driven. Darcy's law is used to describe this mechanism which becomes relevant when the partial pressure of the water vapour within the paper exceeds that in the ambient air within the dryer hood. Given that the pressure within the dryer hood is close to atmospheric, this phenomenon therefore occurs if the paper sheet temperature exceeds 100°C. Hence, the relevance of the bulk vapour flow mechanism to paper drying is effectively determined by the steam pressure within the drying cylinders. The steam pressure is closely related to the saturation steam temperature which governs the temperature of the dryer cylinder surface and ultimately that of the paper sheet.

3.2 Paper structure

The pore size distribution of the paper sheet is very important in determining sheet porosity, and hence permeability, and also the capillary pressure differentials which control liquid flow within the sheet. This distribution is defined by relative frequency data for the pore radii over the range from zero up to the maximum pore radius present. The pore size distribution will be a function of fibre length and diameter and the degree of inter-fibre bonding.

Ideally the pore size distribution would be specified directly from observations of relative occurrence of various pore size ranges. Chapter 6, which collates empirical data describing the pore size distribution, explains how the complexity of the actual paper structure makes this approach impractical. It further explains that the pore size distribution can be inferred from the relationship between cumulative fractional volumetric saturation and applied pressure for a given sample.

The statistical pore model of Haring and Greenkorn (1970) uses the beta function, *g(r;a,b)*, to describe the probability distribution function for pore radii. This function was selected since the random variable, dimensionless radius (r), had a range of zero to one and the distribution has a spectrum of skew and symmetric shapes depending on the choice of parameters (a,b) :

$$g(r;a,b) = \frac{(a+b+1)!}{a!\,b!} r^a (1-r)^b \qquad (3.1)$$

Many other two-parameter distributions lack the flexibility to simulate many natural phenomena and particularly suffer from the difficulty of handling an infinite range.

The pore size distribution, *g(r)*, defined in equation 3.1, covers the complete spectrum of intra-fibre pores (micro-pores) which contain *bound* water to inter-fibre pores (macro-pores) which are said to contain *free* water. The bound water forms in the cavities of the cell walls of the pulp fibre. These cavities are smaller in size than the macro-pores which form between fibres. The enthalpy of moisture within these micro-cavities is lower than that of ordinary liquid water (or free water) for two reasons. Firstly the vapour pressure of water in these micro-capillaries is affected by the curvature of the air-water meniscus in a capillary. This lowering of vapour pressure can be described by the Kelvin equation as reported by Skaar (1988),

$$\ln\left(\frac{1}{\phi}\right) = \frac{2\sigma}{R R_w T}, \qquad (3.2)$$

where,
- σ = surface tension [N/m],
- R_w = gas constant for water [0.462 kJ/kg.°K],
- R = pore radius [m],
- T = temperature [°K], and,
- ϕ = relative vapour pressure [-].

Whilst indicating the general effect, the Kelvin equation cannot be used alone to describe the sorptive behaviour of paper. This is because of the presence of water-soluble extractives in the capillary water which further reduces the vapour pressure below that predicted by the capillary-meniscus based Kelvin equation. For this reason the sorptive behaviour is generally determined experimentally and this is detailed in Chapter 9.

At this point it is sufficient to note that there is a continuum of pore sizes. At the large end of the scale there are pores formed between separate fibres where sorptive effects are negligible. Small pores are generally found within cavities of the fibre cell walls and the Kelvin equation predicts the nature of this vapour pressure reduction. The cross-over between the two regimes is designated the fibre saturation point (FSP). This refers to the moment that the macro-pores are empty whilst the fibres themselves remain fully saturated (micro-pores). Whilst defined as a single point the FSP is not a discontinuity in the sorption or drying behaviour. It simply represents the point at which moisture notionally begins evaporating from within the fibres themselves. In the context of the drying model to be developed in this chapter, the FSP is not a necessary parameter from a mathematical viewpoint but rather gives an appreciation of the internal distribution of moisture in the paper sheet. The information governing the FSP is implicitly contained in the pore size distribution.

The system's defining equations, developed in the following sections, express liquid mass flow in terms of capillary pressure differentials. Given that the final mass and energy balance equations are solved in terms of moisture content it is necessary to relate capillary pressure to moisture content.

The pore size probability distribution function, *g(r)*, is the basis for defining the incremental volume, *dV*, associated with adding the volume occupied by pores in the radii range from *R* to *R+dR* to the cumulative volume. Given *N* pores per unit area and a sheet thickness of *L* the incremental volume per unit sheet area is expressed as,

$$dV = N\pi R^2 L\, g(r)\, dr. \tag{3.3}$$

The number of pores per unit area is related to the sheet's porosity, ε, by,

$$N\pi < R^2 >= \varepsilon. \tag{3.4}$$

Combining equations 3.3 and 3.4 and defining the dimensionless radius, r, as, R/R_{max}, the ratio of actual radius to maximum pore radius, gives,

$$dV = \frac{\varepsilon r^2 L\, g(r) dr}{< r^2 >}, \tag{3.5}$$

where the second moment of the distribution function, $<r^2>$, is defined by,

$$< r^2 > = \int_0^1 r^2 \, g(r) \, dr, \tag{3.6}$$

and can be expressed as,

$$< r^2 > = \frac{(a+1)(a+2)}{(a+b+2)(a+b+3)}. \tag{3.7}$$

Given the Kelvin equation,

$$P_c(R) = -\frac{2\sigma \, Cos\gamma}{R}, \tag{3.8}$$

where, σ = surface tension [N/m],
γ = contact angle [°],
R = pore radius [m], and,
P_c = capillary pressure [Pa],

and integrating equation 3.5 over the range from 0 to R, enables the local moisture content to be related to capillary pressure by the equation,

$$S = \frac{V(R)}{V(R_{max})} = \beta\left(\frac{p_c(R_{max})}{p_c(R)}; a+2, b\right), \tag{3.9}$$

where, S = fractional volumetric saturation [-],
R_{max} = maximum pore radius [m],

β is the incomplete beta function which is defined by,

$$\beta(r; a, b) = \int_0^r g(r) \, dr, \tag{3.10}$$

and the expression for capillary pressure can be written as,

$$\frac{p_c(R_{max})}{p_c(R)} = \frac{R}{R_{max}} = r. \tag{3.11}$$

The fractional volumetric saturation, S, can be converted to the moisture content term, M, used in the subsequent defining equations, with the relation,

$$M = S\frac{\rho_L \varepsilon L}{b_{wt}}, \tag{3.12}$$

where, M = sheet moisture content [kg_{water}/kg_{fibre}],
ρ_L = density of liquid water [kg/m^3],
ε = paper sheet porosity [-],
L = sheet thickness [m], and,
b_{wt} = dry basis weight of paper sheet [kg/m^2].

The moisture content, M, refers to the total moisture content within the paper sheet. This therefore includes both free water in the macro-pores and notionally bound water within the micro-pores of the fibre cell walls.

The parameters *a* and *b* used in the probability distribution function, g(r), must be selected to fit the experimental data obtained from mercury porosimetry tests which generate results which can be interpreted on the basis of equation 3.9. An explanation of mercury porosimetry and the estimation of *a* and *b* is provided in Chapter 6.

3.3 Mass transfer

3.3.1 Liquid capillary flow

The theory developed in the previous section allows the liquid flow due to capillary pressure differentials to be calculated. Darcy's law is used to describe the process :

$$\dot{m}_L = -\frac{\rho_L \kappa_L}{\mu_L}\frac{\partial P_c}{\partial y}, \tag{3.13}$$

where, $\dot{m}_L$ = liquid mass flux [$kg/m^2.s$],
ρ_L = density of liquid water [kg/m^3],
κ_L = liquid permeability [m^2],
μ_L = liquid viscosity [kg/m.s],
P_c = capillary pressure [Pa], and,
y = dimension of fluid flow [m].

It should be noted that the liquid pressure is deemed equal to the capillary pressure. This is based on the premise that centripetal and gravitational acceleration terms prove negligible. An order analysis shows that under nominal machine operating conditions the relative pressures are 10 000, 20 and 0.5 Pa for the capillary, centripetal and gravitational pressures respectively.

The variation of liquid density and viscosity with temperature is considered negligible over the range of interest. However, the effective liquid permeability of the paper sheet, which is derived from the paper structure's intrinsic permeability and the relative permeability due to partial saturation, changes significantly with moisture content and this relation has been correlated by Robertson (1963) for a typical paper sheet. Details of this are presented in Chapter 8.

3.3.2 Diffusional vapour flow

Vapour flow by means of diffusion complements the liquid moisture transfers due to capillary mechanisms. The driving gradient is vapour concentration. Making the assumption that water vapour behaves as an ideal gas the concentration, ρ_v, can be expressed as :

$$\rho_v = \frac{P_v}{R_w T}, \tag{3.14}$$

where, P_v = vapour pressure [Pa],
T = temperature within the paper sheet [°K], and,
R_w = gas constant for water vapour [0.462 kJ/kg.°K].

The sheet temperature is the primary parameter which determines the local vapour pressure :

$$P_v = \phi(M,T)P_{sat}(T), \tag{3.15}$$

where M is the local moisture content previously defined in equation 3.12 and ϕ the sorption isotherm function which describes the reduction in vapour pressure below the saturation pressure due to the hygroscopic nature of paper which carries bound water within intra-fibre pores and through surface adsorption. A more detailed explanation of sorption isotherms and experimental correlations for ϕ as a function of moisture content and temperature are presented in Chapter 9.

Fick's law of diffusion, on a per unit area basis, then states :

$$\dot{m}_v = -D_v \frac{\partial \rho_v}{\partial y}, \tag{3.16}$$

where, $\dot{m}_v$ = vapour mass flux [kg/m².s],
ρ_v = vapour concentration [kg/m³],
D_v = diffusion coefficient [m²/s], and,
y = dimension of fluid flow [m].

An estimate for the effective diffusion coefficient is based upon the value for the binary diffusion of water vapour in air, together with an allowance for temperature variation and cross sectional area available for diffusion processes. Thus, the effective coefficient increases during the drying process as the pores evacuate and more area becomes available to the vapour phase. This is discussed further in Chapter 10.

3.3.3 Bulk vapour flow

As mentioned earlier this mechanism becomes relevant at temperatures above the boiling point of water. As the dryer hood is at a pressure very close to atmospheric this equates approximately to a temperature threshold of 100°C below which bulk flow may be ignored. At temperatures above this, the total pressure increases above the dryer hood pressure and provides a vigorous mechanism for the evacuation of vapour. This dual-range concept can be summarised by the equation :

$$P_{tot} = \text{Max}(P_{atm}, \phi P_{sat}(T)), \tag{3.17}$$

where the total web pressure, P_{tot}, is the larger of atmospheric pressure ($P_{atm} \cong$ dryer hood pressure) and the vapour pressure ($\phi.P_{sat}(T)$). With this definition the mass flow of vapour per unit area due to bulk flow may be expressed by Darcy's law as :

$$\dot{m}_v = -\rho_v \frac{\kappa_v}{\mu_v} \frac{\partial P_{tot}}{\partial y}, \tag{3.18}$$

where, $\dot{m}_v$ = vapour mass flux [kg/m².s],
ρ_v = vapour concentration [kg/m³],

κ_v = vapour permeability [m^2],
μ_v = vapour viscosity [kg/m.s],
P_{tot} = total web pressure [Pa], and,
y = dimension of fluid flow [m].

When $P_v < P_{atm}$, $\frac{\partial P_{tot}}{\partial y} = 0$, and $\dot{m}_v = 0$.

At high temperatures when $P_v > P_{atm}$, the equation becomes :

$$\dot{m}_v = -\rho_v \frac{\kappa_v}{\mu_v} \frac{\partial P_v}{\partial y}. \qquad (3.19)$$

Vapour permeability refers to the relative intrinsic permeability of the paper structure. As for the liquid flow case, the intrinsic structural permeability of paper is related to its porosity by the Kozeny-Carman relation (Kozeny, 1927 and Carman, 1937) and is independent of fluid properties. The relative intrinsic permeability is the product of the saturated intrinsic permeability and the relative permeability which is a dimensionless correction for partial vapour saturation within the paper web. These correlations are elaborated upon in Chapter 8.

The vapour viscosity is a weak function of temperature as detailed in Chapter 10. The vapour concentration must be broken down into its ideal gas form (equation 3.14) to express equation 3.18 with vapour pressure and temperature as the independent variables.

3.3.4 Mass balance equation

Having identified the prevailing evaporation mechanisms and mathematically quantified their behaviour, it is now possible to assemble the equation describing mass transfer within the paper sheet. This equation can be generated through a simple mass balance approach,

$$\text{accumulation of mass} = \sum \text{mass}_{in} - \sum \text{mass}_{out}. \qquad (3.20)$$

An element of paper sheet of thickness *dy* is shown in the diagram below. A typical slice contains fibres and pores in the ratio $(1 - \varepsilon) : \varepsilon$. Also the pore volume will be divided between liquid water and water vapour in the ratio S : (1-S).

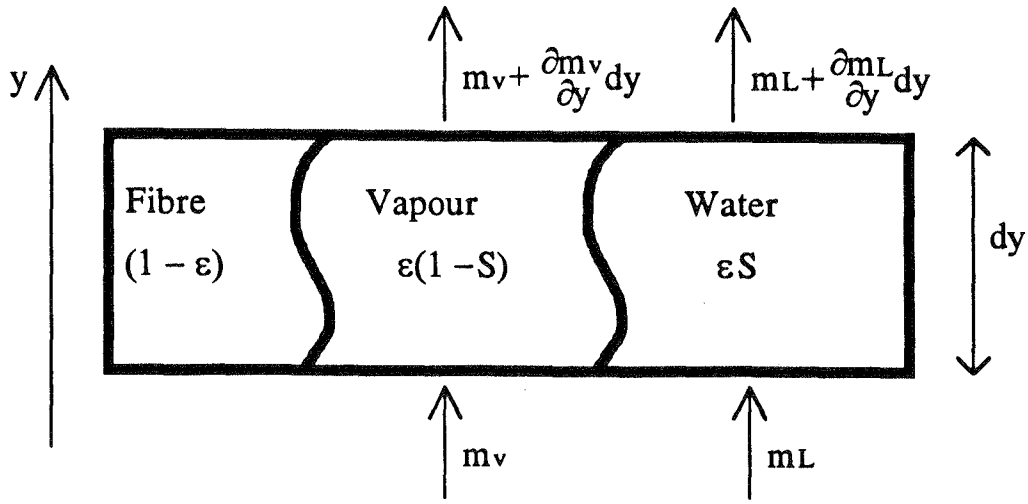

FIGURE 3.1
Shows mass transfers through an element of the paper sheet

Equating the net flow of water into the slice with the rate of change of mass within the slice gives the defining equation :

$$\frac{\partial M}{\partial t}\frac{b_{wt}}{dy} = -\frac{\partial \dot{m}_L}{\partial y} - \frac{\partial \dot{m}_{V_{diff}}}{\partial y}\left(-\frac{\partial \dot{m}_{V_{bulk}}}{\partial y}\right), \qquad (3.21)$$

where b_{wt} = dry basis weight of the paper sheet [kg/m^2].

Substituting the mass flow rate equations for each of the three transfer mechanisms produces the first of two governing differential equations describing the drying of paper,

$$\frac{\partial M}{\partial t} = \frac{\rho_L \kappa_L}{\mu_L}\frac{\partial^2 P_L}{\partial y^2}\frac{dy}{b_{wt}} + D_v\frac{\partial^2 \rho_v}{\partial y^2}\frac{dy}{b_{wt}}\left(+\frac{\rho_v \kappa_v}{\mu_v}\frac{\partial^2 P_v}{\partial y^2}\frac{dy}{b_{wt}}\right). \qquad (3.22)$$

The parentheses indicate that the bulk flow term is included only when the internal web pressure exceeds atmospheric. The dy/b_{wt} term appears in this

equation as a result of the definition of moisture content M as mass of water per unit mass of dry fibre rather than the more conventional concentration in mass per unit volume. The selection of this definition for M is made to integrate with standard nomenclature and units from the paper industry.

Before equation 3.22 can be implemented in finite difference form for computer solution the liquid pressure, P_L, must be expressed in terms of moisture content, M, and the vapour concentration must be replaced by its ideal gas law representation. Because the second derivatives of these terms in their most fundamental form are a little unwieldy the expansion is omitted here but presented in Appendix 5.

3.4 Energy transfer

3.4.1 Convection heat transfer

The transfer of mass by each of the three mechanisms outlined previously is associated with a simultaneous transfer of energy. This component of energy transfer within the paper sheet may be termed convection heat transfer. Quantitatively it may be expressed as the product of the mass flow of each phase and its enthalpy. Enthalpy values for both liquid water and water vapour over a range of temperatures are obtained from the steam tables of Rogers and Mayhew (1989). The best fit correlations used are given in Chapter 10.

3.4.2 Conduction heat transfer

Heat is also transported through the paper web by conduction. Fourier's law must be applied to the mixture of stratified fibres, liquid water and water vapour :

$$Q = -k\frac{\partial T}{\partial y}, \tag{3.23}$$

where, Q = heat flux [W/m^2],
k = thermal conductivity [W/m°K],
T = temperature [°K], and,
y = dimension of fluid flow [m].

The value for thermal conductivity must be determined as a combination of the individual conductivities for each of the three components. It should also be noted that thermal conductivity is generally a very weak function of temperature. More information on thermal conductivity and appropriate correlations are presented in Chapter 10 which deals with physical properties.

3.4.3 Energy balance equation

A similar procedure to that followed earlier for the mass balance can be employed to compose an equation based on energy inputs and outputs. In this case the net energy into a given slice of the paper sheet should be equated to the accumulation of energy within that element, i.e., a temperature change for the materials composing the element. A schematic diagram depicting the relevant transfers is shown in Figure 3.2.

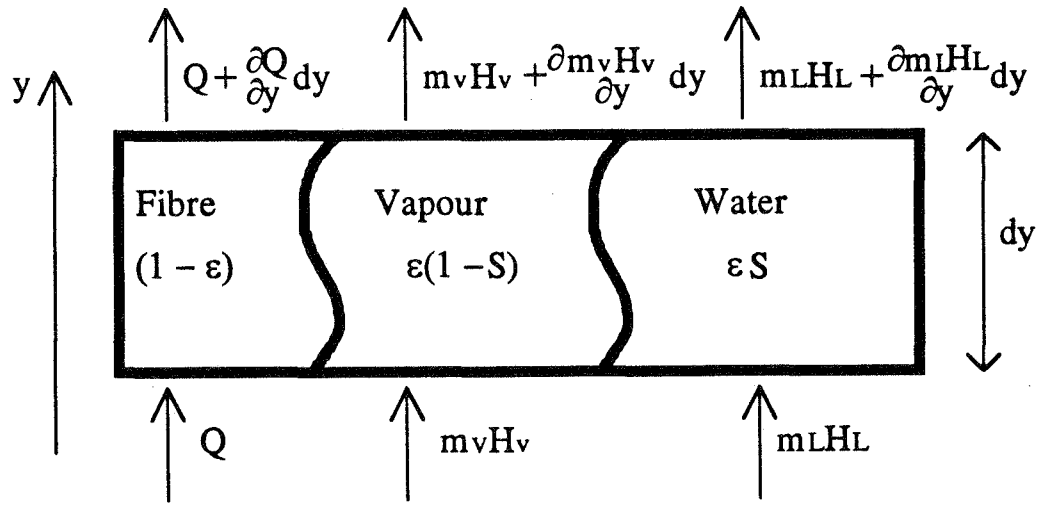

FIGURE 3.2
Shows energy transfers through an element of the paper sheet

The energy equation can therefore be written as,

$$\frac{\partial CT}{\partial t} = -\frac{\partial Q}{\partial y} - \frac{\partial}{\partial y}\left(\dot{m}_L H_L\right) - \frac{\partial}{\partial y}\left(\dot{m}_v\left(H_v + Q_s\right)\right), \qquad (3.24)$$

where, C = combined specific heat capacity of paper slice [kJ/kg°K],
Q_s = heat of sorption [kJ/kg],

H_{fg} = heat of vaporisation for water [kJ/kg],
H_v = enthalpy of vapour [kJ/kg], and,
H_L = enthalpy of liquid [kJ/kg].

The heat of sorption represents the additional energy beyond the latent heat of vaporisation required to evaporate a unit mass of liquid due to the bonds formed by adsorption in hygroscopic materials. This is quantified and related to the sorption isotherms in Chapter 9. The combined specific heat capacity, C, is a function of the moisture content of the sheet and the relative specific heat values for the fibre, water and vapour components. This together with expressions for the enthalpies of liquid water and water vapour are described in detail in Chapter 10.

The energy equation can be partially expanded and written as :

$$\frac{\partial CT}{\partial t} = k\frac{\partial^2 T}{\partial y^2} + \frac{\rho_L \kappa_L}{\mu_L} H_L \frac{\partial^2 P_L}{\partial y^2} + D_v(H_v + Q_s)\frac{\partial^2 \rho_v}{\partial y^2}\left(+ \frac{\rho_v \kappa_v}{\mu_v}(H_v + Q_s)\frac{\partial^2 P_v}{\partial y^2}\right) \tag{3.25}$$

Again the final bulk flow term, in parentheses, is only relevant when the total vapour pressure exceeds atmospheric.

The two major differential equations developed (equations 3.22 and 3.25) must be solved simultaneously to obtain the variation of paper sheet moisture content and temperature with time and sheet thickness under a given set of external drying conditions. The finite difference implementation of the two equations is presented in detail in Appendix 5.

3.5 Internal sheet interactions

The heart of the mathematical model of paper drying is described by the differential equations 3.22 and 3.25. Given a material with constant physical properties and a simple internal geometry the solution of these equations would be relatively straightforward. However, the paper sheet does not fit this description and so the overall internal mechanisms associated with its drying behaviour become quite complex. The solution of equations 3.22 and 3.25 will be strongly driven by correlations developed to describe the sheet's characteristics.

The major cause of computational complexity in the evaluation of the drying model is the seemingly random pore structure of any given paper sheet. The distribution of pore sizes is a vital component of a complete drying model as it directly governs the liquid capillary pressure differentials which promote liquid flow within the sheet. The pore size distribution also affects the sorptive behaviour of the sheet, its structural permeability and the fibre saturation point (FSP). Definition of the pore size distribution is described in detail in Chapter 6, but at this stage it is sufficient to note that the outcome, which is summarised in general terms by equation 3.9 and obtained at considerable computational expense, is a first order parameter in describing liquid transfers within the sheet. The progressive evacuation of liquid from the larger macro-pores through to the micro-pores within individual fibres is a key component of the overall drying representation and this description is strongly reliant on available pore size data for paper samples.

The permeability of the paper sheet is a direct consequence of the pore size distribution. Permeability controls pressure driven flow through porous media (Darcy's Law). In this instance the paper sheet has an intrinsic permeability which is purely a function of the sheet structure and related to the pore size distribution. This intrinsic permeability must be modified by a factor which varies between zero and unity depending upon the extent to which the sheet is saturated with either liquid or vapour. Thus the permeability referred to in the defining equations will not only be a function of pore size distribution but also of instantaneous moisture content.

The hygroscopic nature of paper fibres means that sorptive effects are also significant. At moisture contents below the FSP when the macro-pores are empty and the remaining water resides within the fibres themselves, two effects emerge which tend to inhibit drying rates. The partial pressure of the water vapour within the paper sheet is reduced and the heat of vaporisation of the remaining liquid is increased by an amount known as the differential heat of sorption. These effects are pursued in Chapter 9 and manifest themselves in the model where the vapour pressure, vapour density or heat of vaporisation terms appear. In this sense they create an iterative type of dependence on the two key independent variables, moisture content and temperature.

Many other physical properties form an integral part of the defining differential equations and are also dependent upon both moisture content and temperature. The paper sheet is a mixture of paper fibre, liquid

moisture and vapour and thermal conductivity and specific heat relationships must reflect this composition. Correlations for these are presented in Chapter 10 along with values for fluid specific properties such as viscosity, enthalpy, diffusivity, density and heat of vaporisation.

The whole environment of the drying model presented is one of inter-dependence between variables and an emphasis on the fundamental sheet properties which will control drying at a micro-level. Providing this form of detailed reference to sheet specific properties gives a solid foundation for the model to deal with external factors such as the drying conditions and interfacial transfer coefficients. This is a considerably more thorough means of addressing the drying question compared with the alternative approach of developing a simpler description based on constant properties and subsequently assigning an anonymous *drying rate correction factor* to bring the model's predictions into agreement with actual paper machine observations. The benefits of the fundamental approach become evident when evaluating the drying of different paper grades or pulps, but do admittedly carry a significant algebraic and computational premium.

3.6 Boundary conditions

3.6.1 Boundary conditions for single-sided drying

During the process of single-sided hot surface drying the paper sheet sees an impermeable heated surface on one face and is exposed to a body of conditioned air on the other face. Figure 3.3 shows the physical situation schematically and should be read in conjunction with the following variable definitions :

T_{air} Air temperature within dryer hood [°K],
ϕ Air relative humidity within dryer hood [-],
T_c Temperature of hot drying surface [°K].
h_c Contact heat transfer coefficient [W/m^2°K],
h_s Open surface heat transfer coefficient [W/m^2°K], and,
h_m Surface transfer coefficient [m/s].

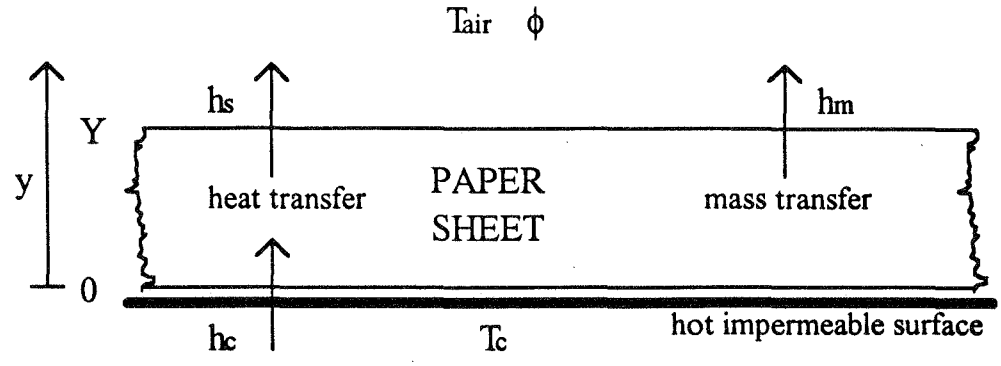

FIGURE 3.3
Illustrates boundary conditions and transfer coefficients

Denoting the side of the paper in contact with the heated surface by the subscript $_0$, the boundary conditions are defined as :

$$-k\left.\frac{\partial T}{\partial y}\right|_0 = h_c(T_c - T_0), \tag{3.26}$$

$$\left.\frac{\partial \rho_v}{\partial y}\right|_0 = 0, \tag{3.27}$$

$$\left.\frac{\partial P_L}{\partial y}\right|_0 = 0, \tag{3.28}$$

and,

$$\left.\frac{\partial P_{tot}}{\partial y}\right|_0 = 0. \tag{3.29}$$

The temperature boundary condition (3.26) relates the heat transfer through the interface to the heat conduction at the paper surface. The other three mass boundary conditions are consistent with a zero mass flux across the impermeable cylinder surface.

The boundary conditions at the open side of the sheet are given below with the subscript $_Y$ denoting this interface :

$$-k\left.\frac{\partial T}{\partial y}\right|_Y = h_s(T_Y - T_{air}), \tag{3.30}$$

$$-D_v\left.\frac{\partial \rho_v}{\partial y}\right|_Y = h_m(\rho_Y - \rho_{air}), \tag{3.31}$$

$$\left.\frac{\partial^2 P_L}{\partial y^2}\right|_Y = 0, \tag{3.32}$$

and,

$$\left.\frac{\partial^2 P_{tot}}{\partial y^2}\right|_Y = 0. \tag{3.33}$$

The heat conduction term at the open surface is equated to the surface convection heat transfer through the surface heat transfer coefficient h_s in equation 3.30. In a similar fashion the vapour diffusion flow at the open air interface is related to the external vapour density gradient by the surface mass transfer coefficient, h_m. In this equation ρ_{air} refers to the concentration of water vapour in the drying air. The final two boundary conditions are derived on the premise that the surface offers no resistance to the pressure driven flows of liquid and vapour.

Initial conditions must also be assigned for the controlling variables moisture content, temperature and pressure,

$$M(t=0) = M_0, \tag{3.34}$$

$$T(t=0) = T_0, \tag{3.35}$$

$$P(t=0) = P_{sat}(T_0). \tag{3.36}$$

The initial moisture content and temperature are determined from paper sheet measurements made after the sheet's exit from the press section. Vapour in the sheet is saturated and the vapour pressure is therefore calculated directly from the temperature according to equation 3.36 where $P_{sat}(T_0)$ refers to the saturation pressure for water vapour at the initial temperature T_0.

3.6.2 Extension to alternating boundary conditions

As mentioned previously the solution of the problem was segregated into two stages to facilitate debugging and allow correlations with experimental results to be made. To implement the full paper machine dryer section simulation requires no change to the internal transport mechanics, merely the external boundary conditions. Rather than calculating the drying rate subject to *constant* external conditions it is now necessary to introduce *time dependent* boundary conditions. The surface relations will therefore vary as a function of the sheet's location within the dryer section. The following sketch, Figure 3.4, depicts the possible boundary condition configurations for a double-felted dryer section.

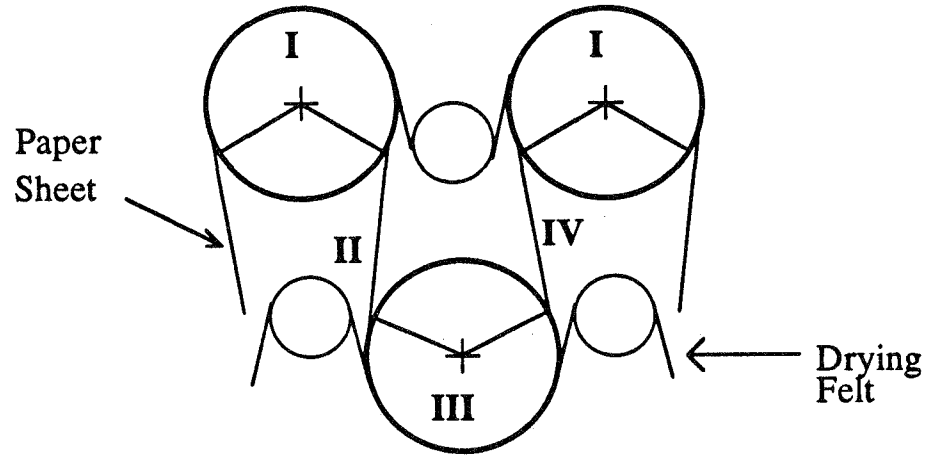

FIGURE 3.4
Four boundary condition regions for each drying cylinder pair in the double felted region of the dryer section

Section **I** is identical to the configuration for hot surface drying as described earlier. The surface mass transfer coefficient applied here must take account of the restricting nature of the adjacent felt. In section **II** both sides of the sheet are open to the local air flows. There is no heating supplied and the sheet cools quickly due to the dual-sided evaporation. There is no felt in contact with the sheet so evaporation occurs unimpeded. Section **III** is the reverse of **I**; the sheet is heated from its 'top' side whilst moisture removal can occur through the dryer felt on the 'bottom' side. Section **IV** is identical to **II**.

The cyclic changes of surface transfer coefficients are essentially the same for both single and double felted parts of the dryer section. The general pattern of boundary conditions is the same but in the case of double felted drying sections the surface heat and mass transfer coefficients must be modified for the absence of the dryer felt during the free draw. Figure 3.5 depicts this cyclic variation.

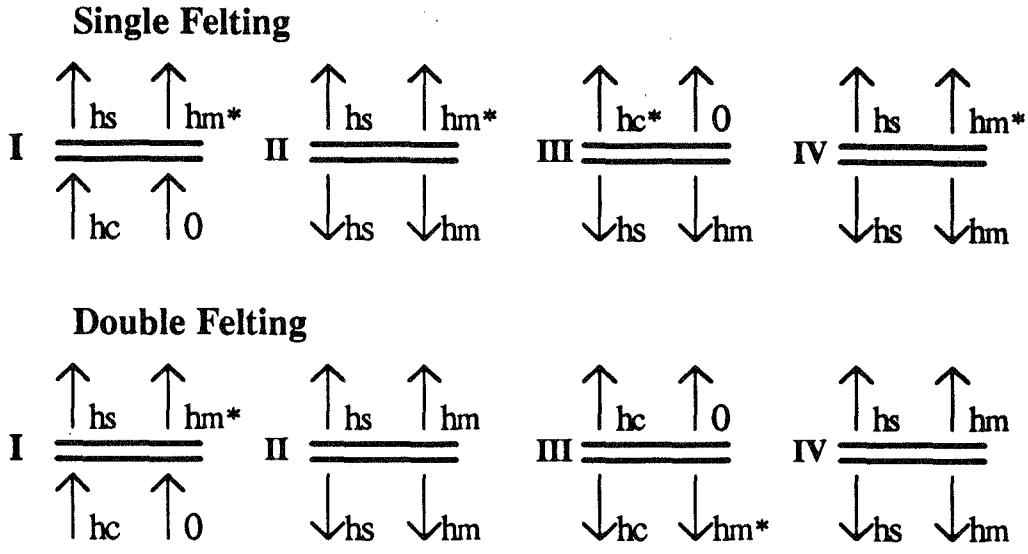

FIGURE 3.5
Variation of surface transfer coefficients through Phases I-IV

In Figure 3.5 h_c represents the cylinder contact heat transfer coefficient, h_s is the open surface heat transfer coefficient, and, h_m is the open surface mass transfer coefficient. The * superscript indicates the presence of the dryer fabric (felt).

It should be noted that the double felted boundary condition definition is slightly simplified from the commonly quoted version proposed by Nissan and Kaye (1955). The disparity lies in their decision to define the short region between the felt leaving the drum and the paper sheet leaving the drum as a distinct section. Given that this region, highlighted in Figure 3.6, represents approximately 5% of the drying run it is not a serious omission. The motivation for combining these drying zones arises from the uncertainty existing around values for the contact heat transfer coefficient and surface mass transfer coefficient at this point. In this region the paper sheet is under tension but is not compressed to the drying cylinder by the felt so it is not clear what quality of contact exists between the sheet and

cylinder. It is probable that the absence of the felt would generate an increase in local drying rate. However, there is also likely to be a zone of highly humid air between the sheet and felt. This localised patch of high water vapour concentration would act to reduce the drying gradient somewhat.

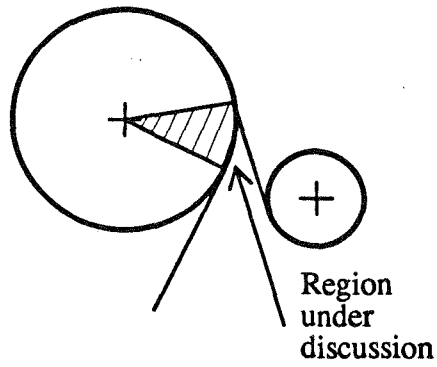

FIGURE 3.6
Region of paper wrap but no felt wrap (≅20°)

The boundary conditions used in this model assumes that the zones do not change until the paper sheet leaves the cylinder surface. As discussed above any discrepancy is likely to be small since the paper sheet is under tension itself which will maintain its intimate contact with the surface of the drying cylinder despite the absence of the dryer felt for this short time.

3.7 Solution by finite differences

Even without the complication of time-varying boundary conditions it would be impossible to solve this problem, in the depth presented, without computational aid. The complexity of the defining equations removes any possibility of finding an analytic solution. Consequently, a numerical method must be implemented to attain a solution for temperature and moisture content at a finite number of positions across the thickness of the paper web and at a number of discrete time increments. It was noted that in the early 1960's Nissan required 160 hours of manual calculations to complete a single dryer length simulation. Nissan's drying model was an order of magnitude simpler than the current one and did not allow for the variation of properties and transfer coefficients as a result of changes in the independent variables.

The widespread availability and increasing processing power of computers has brought the solution to such a problem within reach of the desktop and made it feasible to perform the drying rate integration defined by equations 3.22 and 3.25 for a large number of permutations corresponding to different model input parameters. To achieve these goals it is first necessary to present the problem in a form which can be digested by computer. This is achieved by utilising the method of finite differences.

Finite difference methods are considered approximate since derivatives at a point are represented by difference quotients over a small interval :

$$\partial M/\partial t \cong \delta M/\delta t, \text{ provided } \delta t \text{ is sufficiently small.}$$

Bearing in mind the uncertainty which prevails in some of the model input parameters it is reasonable to assume that any errors associated with a numerical approach are negligible - provided the solution is stable and the time increment is sufficiently small.

A fully implicit method based on central differencing is used to solve the drying problem under study. An implicit method increases the computational requirements over the simpler explicit method by demanding simultaneous solution of the defining equations at all grid points, but is inherently more stable. This allows much larger time increments to be taken and the overall calculation time to be shortened. According to Smith (1978) the implicit finite difference solution of the non-dimensional equation,

$$\frac{\partial M}{\partial t} = \frac{\partial^2 M}{\partial y^2}, \qquad (3.37)$$

is convergent and stable for all finite values of $\delta t/\delta y^2$ whereas the explicit method is only stable for $\delta t/\delta y^2 < 0.5$. However, this freedom does not appear to apply to the significantly more complex set of equations which are to be solved here. Whilst the implicit method is found to be far superior to the explicit method it is certainly not unconditionally stable in the current context.

Central differencing is an alternative to forward or backward differencing as a representation of the first derivative. It offers more symmetry to the solution than the other two approaches, e.g.,

$$\frac{\partial M}{\partial y} \cong \frac{M_{i+1,j+1} - M_{i-1,j+1}}{2\delta y}. \qquad (3.38)$$

The second derivative terms are represented in the form :

$$\frac{\partial^2 M}{\partial y^2} \cong \frac{M_{i+1,j+1} - 2M_{i,j+1} + M_{i-1,j+1}}{\delta y^2}. \qquad (3.39)$$

In the above expressions the $_i$ subscript refers to position in the *y* direction, whilst the $_j$ subscript refers to the variable value at time *t*; by extension, $_{j+1}$ relates to the value at time t+δt. The full expansion of equations 3.22 and 3.25 into finite difference form is presented in Appendix 5.

Determining a suitable combination of δt and δy is a matter of trial and error, given the complexity of the defining equations. For the newsprint sheet of interest it was deemed adequate to set δy equal to 1/5 of the sheet thickness. This is in line with the work by Ramaswamy (1990) which examined linerboard with a caliper of 457μm and divided the sheet into ten elements. For the comparatively thin newsprint sheet under study (70μm) in this investigation there turns out to be very little variation of moisture content and temperature across the paper web. Given a sufficiently small value of δt the results are found to be stable and consistent with sample calculations where the number of elements across the sheet is increased to 20. The motivation for using the minimum number of sheet slices lies in the desire to minimise computer calculation time. For comparison sake Lee and Hinds (1980) made use of six slices across the paper sheet in their analysis of paper drying.

It is of interest to briefly summarise the computational load associated with such an implementation. The defining equations are compiled under Turbo Pascal version 6.0 on a personal computer running at 33Mhz with an 80486 processor operating with numeric co-processor. A reliable solution for the dryer length simulation was attainable for δt = 1ms. The corresponding 12,000 steps of the integration were carried out by the computer in around ten minutes. This was observed to output moisture contents and temperatures which converged to within 1.0% of the asymptotic results. The close approach towards such asymptotic results was inferred by reducing the time increment in steps by a factor of ten each time until at δt = 1μs the calculation was observed to have converged to within 0.01% of the final values resulting from the δt = 10μs calculation.

4. Laboratory Tests I - Boundary Layers

The mathematical model for paper drying developed in this study requires the knowledge of both heat and mass transfer coefficients over a range of operating conditions. To quantify these relationships it was necessary to conduct a series of experimental measurements on a laboratory model. This physical model replicates the key principles of an actual paper machine dryer and thus enables the parameters which control drying rate to be varied over a range which is relevant to paper machine operation. There are numerous combinations of drying variables possible and consequently a large number of drying tests need to be performed.

A test rig was designed and built for the purpose of monitoring key parameters in the drying of paper. The measurement of fundamental quantities such as temperature, air speed and moisture content was the basis for further analysis to determine the transfer coefficients.

Two streams of testing were undertaken. It was first necessary to characterise the set-up of the testing configuration and this was achieved by investigating the boundary layer development over the curved hot plate mounted in a square duct. This provided a description of air flows across the test hot plate and allowed the surface heat transfer coefficient to be estimated. Measurements of the thermal boundary layer enabled the contact heat transfer coefficient between the hot plate and paper sheet to be estimated. The data gathered also hold much significance for evaluation of the comparative effects of drying fabrics of different permeabilities. Comparison was made with the findings of others investigating similar geometries.

The data inferred from the boundary layer measurements are crucial for the determination of mass transfer coefficients in the subsequent chapter. This second strand of laboratory testing monitors paper sheet drying rates for a number of drying conditions. The mass transfer coefficient for each drying trial is extracted by fitting the experimental results to the model's prediction. The previously determined values for surface and contact heat transfer coefficient must be input into the model at this point.

The largely independent results from the two sets of testing can then be compared through the use of analogies relating mass transfer to the surface heat transfer coefficient.

It may be noted that much of the work in this chapter has been presented in a previous publication (Reardon, 1992).

The significance of dryer fabrics

In a typical paper machine a number of different dryer fabrics are used throughout the dryer section run. These fabrics vary in permeability and are selected on the basis of their ability to control the amount of air flow exposed to the paper sheet within each dryer pocket. Fabrics with low permeability (75cfm) are typically selected for use in the wet end of the dryer section where the moisture content of the sheet is relatively high and the sheet strength is therefore low. The low permeability restricts air flow into the dryer pocket and consequently limits sheet disturbance and the possibility of a break. As drying progresses, the fabrics in subsequent sub-sections have higher permeability ratings (215-350cfm) and therefore pump greater quantities of air into the pockets and therefore promote greater drying rates.

This variation in the permeability of drying fabrics through the dryer section run prompts questions concerning their varying aerodynamic behaviour. The amount of air dragged by a fabric whilst travelling through the dryer section at speeds of 15-20 m/s is significant from two points of view. Firstly, the boundary layer profile will influence heat and mass transfer from the paper sheet, through the felt and into the hood air. Secondly, the air layer entrained by the fabric is cyclically pumped into and out of dryer pockets as the fabric negotiates the turning rolls. The air currents generated by this process may cause paper sheet instability. This is undesirable as it may result in paper breaks if the sheet oscillations are significant or encourage sheet wrinkles and folded edges which are forbidden from a quality viewpoint. Figure 4.1 demonstrates air being entrained by both the dryer fabric and the paper sheet itself.

Paper sheet instability resulting from felt-induced turbulence is a complex phenomenon in its own right and is outside the scope of the current study. It is an issue which has been addressed previously by Soininen and Nurminen (1974) and Soininen (1982).

The drying fabrics also act as a physical impediment to moisture evacuation from the paper sheet. The area restriction the felt imposes on the surface of the paper sheet implies that drying rates over the felt-

wrapped cylinders will be substantially less than those in the open draw between cylinders. This effect is investigated in Chapter 5.

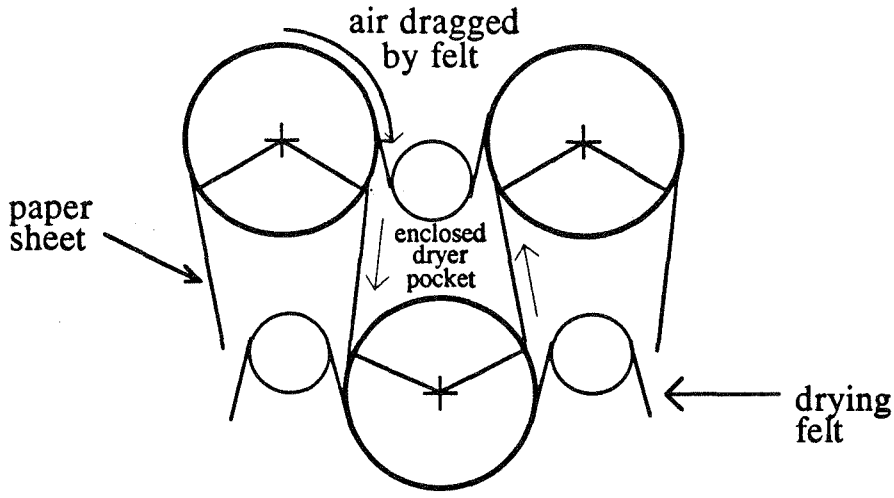

FIGURE 4.1
Schematic diagram illustrating air boundary layer development during the paper drying process

Measurements of the thermal boundary layer over a drying surface will also prove useful in assessing the contact heat transfer coefficient between the hot plate and the thin aluminium backing plate used in the drying rate experiments. This information will be useful in isolating the variation of mass transfer coefficient in the drying trials. It is anticipated that the contact heat transfer coefficient should increase with felt tension. These data will be required in the analysis of the following chapter.

4.1 Experimental set-up

The experimental rig fabricated for the drying trials described in Chapter 5 provided the curved felt surface for which the boundary layer development was monitored. The testing rig comprised a square sectioned duct (225×225mm) with radiant electric heating elements positioned beneath a curved aluminium hot plate. As discussed in Chapter 5 the hot plate contour was selected both for practical purposes, to assist with the mounting of the relatively stiff dryer fabric, and due to the fact that it is largely representative of the machine drying situation. The three elements were enclosed by a semi-circular stainless steel reflector that was thermally insulated by a combination of sindayno board and loose

fibreglass matting. The hot plate was fitted with nine thermocouples in its top surface. The output from these was monitored by a datalogging computer together with the ambient air temperature and relative humidity.

A piece of dryer fabric was attached to the leading edge of the hot plate. The fabric was drawn over the hot plate and taken out through a downstream slot in the base of the duct. This end of the dryer fabric was then connected to a fixed support by means of a ratchet and turnbuckle arrangement that allowed the fabric to be stretched to a pre-determined tension which was measured by a load cell connected in series with the fabric.

A schematic diagram of the test set-up is shown in Figure 4.2.

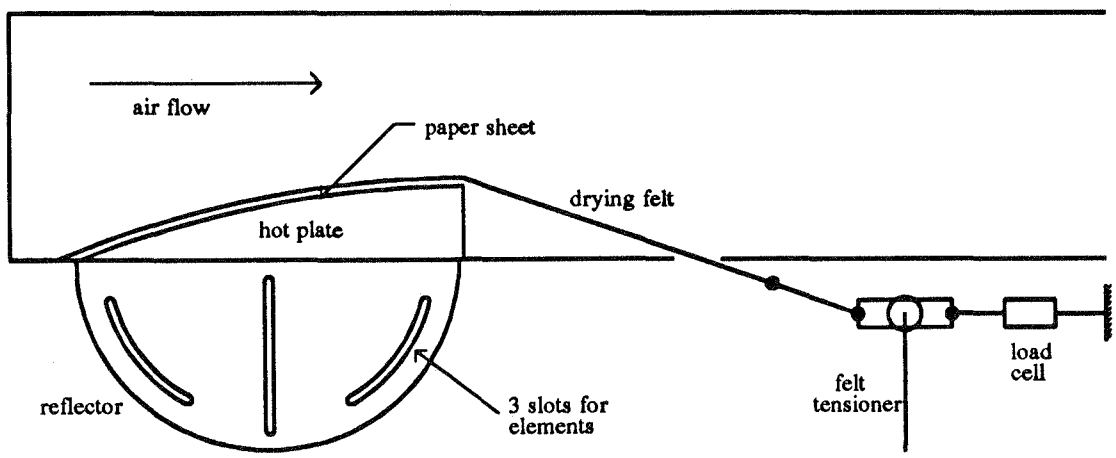

FIGURE 4.2
Schematic diagram of laboratory paper drying rig

For the boundary layer measurements a traversing dial gauge was mounted on rails above the roof of the test duct. A straight-armed hot wire probe and probe support were mounted to the traversing block to allow measurement of both fluid velocity and temperature in the boundary layer forming over the tensioning fabric. This arrangement is depicted in Figure 4.3.

The Mitutoyo dial gauge used for traversing the hot wire probe was calibrated in 0.01mm units and it was possible to take measurements within 0.10mm of the fabric surface. The measured profiles over the dryer

fabrics were found to be sufficiently steady to reliably extrapolate the data to the nominal traversing datum. The data obtained from these turbulent boundary layer measurements were used to assign skin friction coefficients for the drying fabrics along the hot plate.

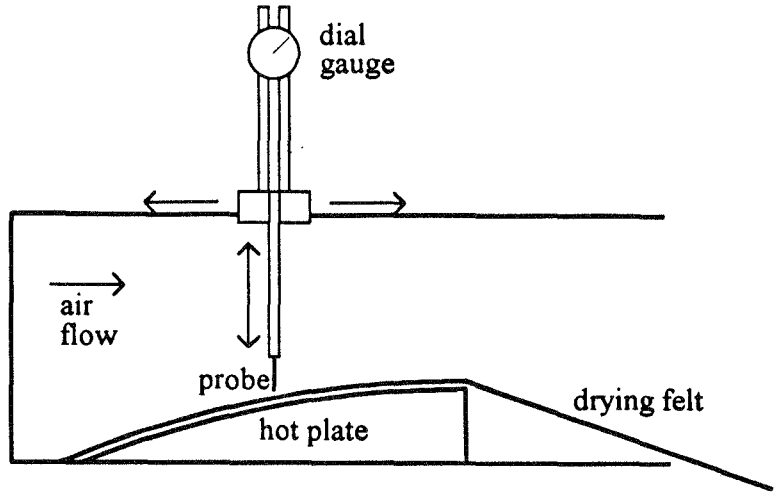

FIGURE 4.3
Set-up for boundary layer measurements

Velocity boundary layer measurements were made on three different drying felts. Two of these trials made use of actual paper machine drying fabrics with rated permeabilities of 75cfm and 350cfm where *cfm* is the paper industry ranking in terms of cubic feet per minute of air transmitted through a square foot of the felt under a differential pressure of 1/2" water gauge. The third trial configuration replaced the felt with a number of nylon lines which were tensioned to hold the hot plate in place without disturbing the air flow over the smooth curved aluminium surface. Photos of the experimental set-up are shown in Figures 4.4 and 4.5.

A boundary layer traverse was made at several axial locations along the centreline of the hot plate. Due to the rough nature of the dryer fabric surface it was difficult to determine a datum for the probe to operate from. The relatively large protrusions of the monofilament polyester weave into the flow demonstrate that the surface datum will necessarily be a somewhat arbitrary definition. This is illustrated by the scanning electron micrographs of Figures 4.6 and 4.7. The zero datum was estimated by extrapolating the linear section of the momentum boundary layer profile to a point where the no-slip condition is satisfied. Since velocities as low as $0.1U_\infty$ were able to be measured near the surface the extrapolation is expected to be satisfactory.

FIGURE 4.4
Photo showing general laboratory set-up and instrumentation for boundary layer measurements

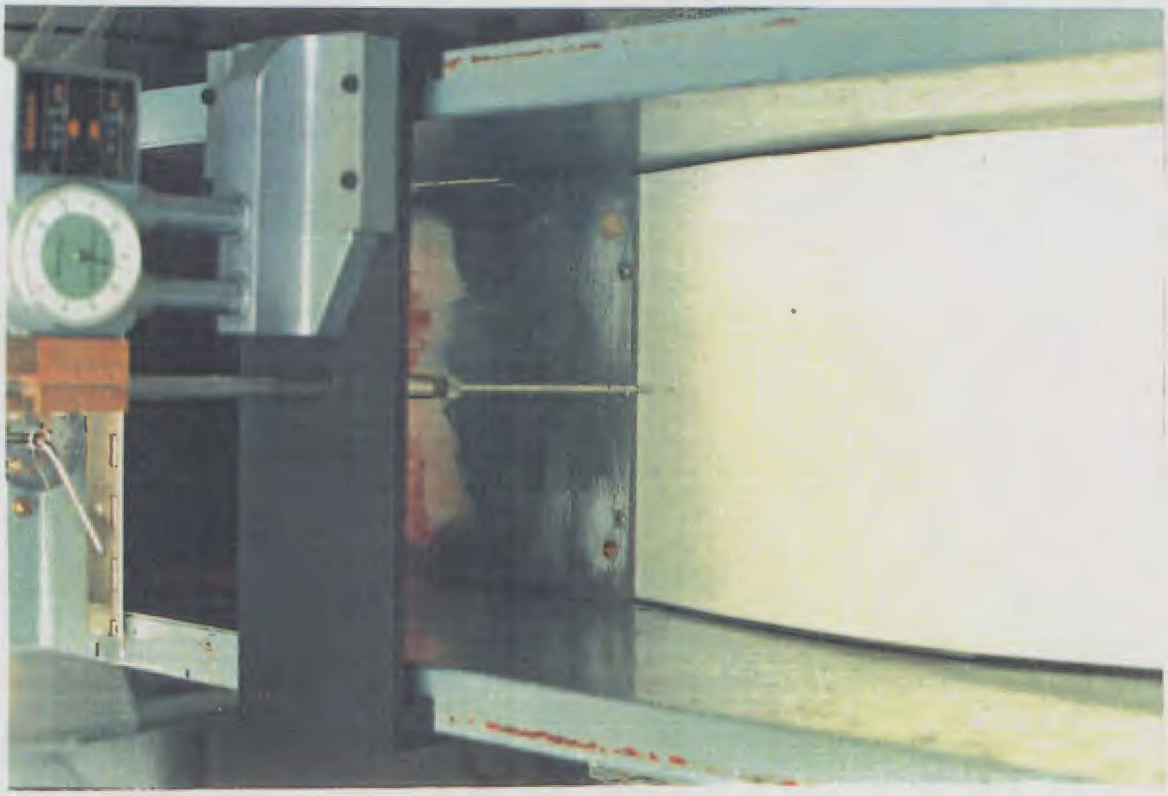

FIGURE 4.5
Photo showing the hot wire probe, controlled from the dial gauge, near the surface of the dryer fabric

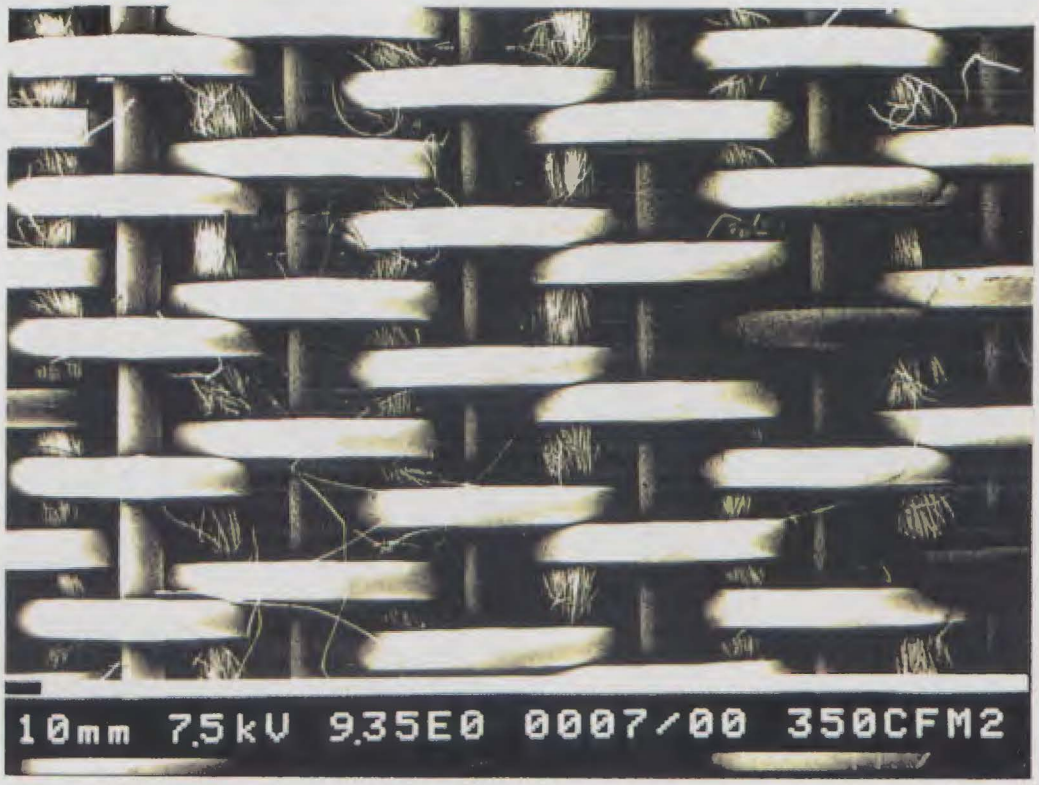

FIGURE 4.6
Scanning electron micrograph of a 350cfm dryer fabric showing surface construction (x14)

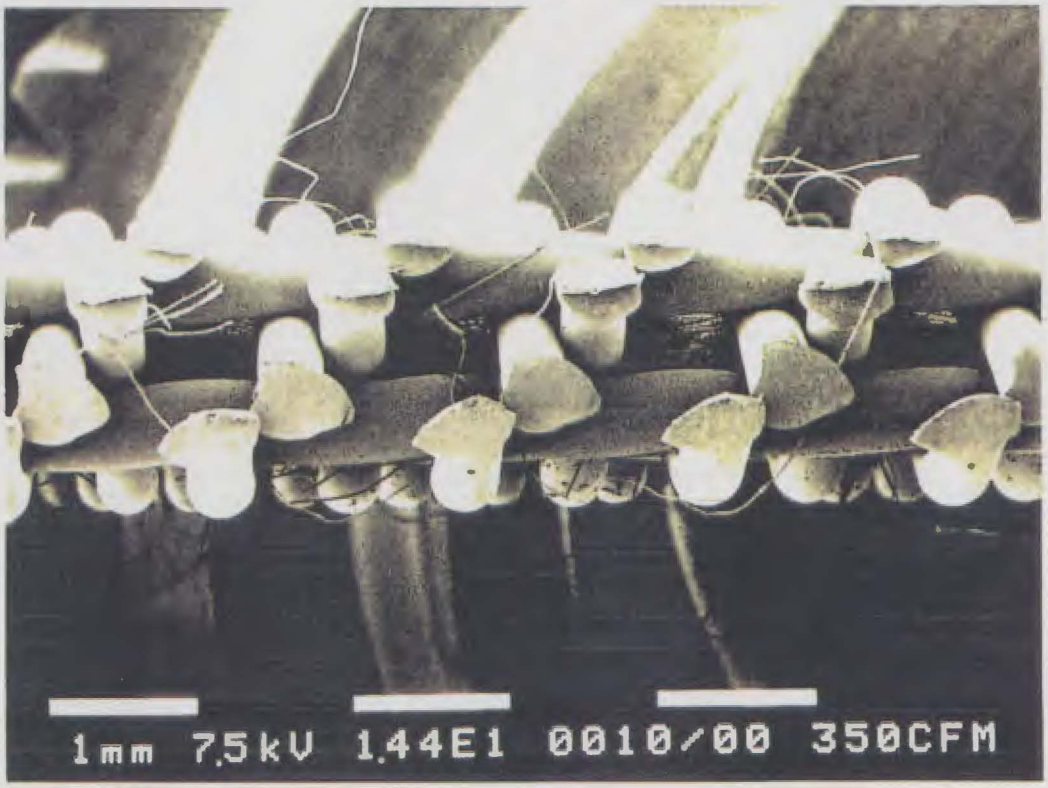

FIGURE 4.7
Scanning electron micrograph of a 350cfm dryer fabric showing edge construction (x14)

The hot wire probe was also utilised to measure the temperature boundary layer above the curved hot plate whilst the thin aluminium backing plate was in contact with it, under tension from the nylon tensioning line which acts as a felt substitute as depicted in Figure 4.8.

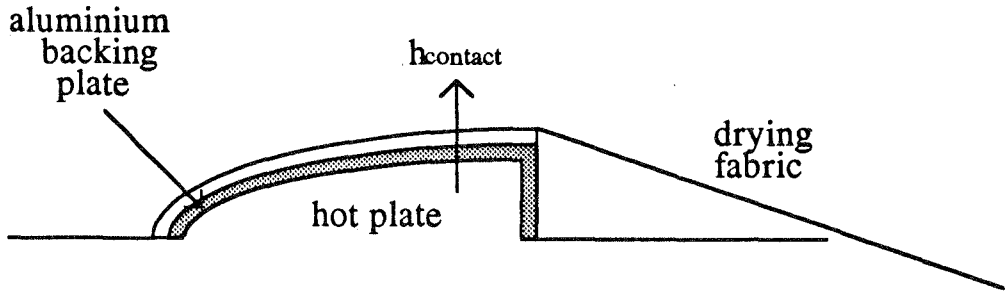

FIGURE 4.8
Heat transfer between hot plate and aluminium backing plate.

A DISA type 55 P01 hot wire probe was used for the boundary layer measurements. It was calibrated over the range 0-20 m/s by a Betz micromanometer which operates with a precision of ± 0.1 mmH_2O. Temperatures were obtained by measuring the probe's resistance at the local conditions and using its temperature coefficient of resistivity to relate this to resistance at standard conditions. For the platinum wire the temperature coefficient of resistivity is 0.0036/°C.

Using the hot wire probe as a resistance thermometer enabled the temperature layer to be defined. Comparing this profile with other correlations then enabled the heat flux to be determined. The hot plate temperature was measured with embedded thermocouples and hence the surface heat transfer coefficient was able to be estimated. This set of data also provided the opportunity to calculate the contact heat transfer coefficient between hot plate and thin backing plate which supports the paper sheet. The contact heat transfer coefficient was expected to exhibit change in response to changing felt tension.

The average velocity and turbulence intensity through the boundary layer were measured via a channel of the analog-to-digital board installed in the datalogging computer. Each data point was determined from 10,000 samples which were generated from the I/O board at a rate of 600Hz. The calibration of the datalogging facility was achieved through establishing a

linear relationship between the probe voltage and the digital word input to the datalogging program,

$$\text{probe voltage} = A \times \text{Word} + B, \qquad (4.1)$$

where A and B are the appropriate regression constants.

The probe voltage was then mapped to a velocity value through use of the probe calibration curve which is expressed by,

$$\text{velocity} = 5.369\times10^{-4}\ \text{probe voltage}^{7.108} - 0.6597. \qquad (4.2)$$

Velocity traverses to define the dryer fabric skin friction coefficient were performed at three longitudinal locations (see Figure 4.9) for fabrics of three different permeabilities. In addition a traverse was made across the hot plate itself for the case where the dryer fabric was replaced by the nylon tensioning line. It was in this configuration that the temperature traverses were made to define the thermal boundary layer next to the smooth aluminium backing plate.

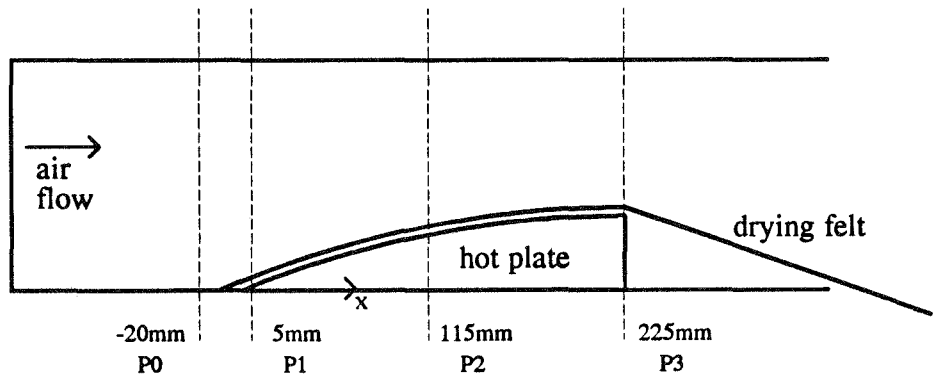

FIGURE 4.9
Diagram showing the four longitudinal locations for boundary layer traverses. The distances are relative to the leading edge of the curved hot plate. The four positions are denoted by P0, P1, P2 and P3 respectively along the horizontal axis.

4.2 Boundary layer results

As the aim of the study was to differentiate between drying felts on the basis of their aerodynamic behaviour it was considered sufficient to measure velocity profiles and calculate skin friction coefficients at three longitudinal locations along the centreline of the duct. Given that the curved hot plate has an axial span of 225mm, the measurement sites were selected as 5mm, 115mm and 225mm relative to the leading edge. Results were obtained at a Reynolds number of 2.5×10^5, which corresponds to a flow of 14 m/s through the 225mm wide duct.

4.2.1 Velocity profile

The velocity profile for boundary layer air flowing over the dryer felts can be expressed in terms of the wall law relationship. This makes use of the dimensionless parameters u^+ and y^+ which are defined, in accordance with the notation of Schetz (1993), as,

$$u^+ = \frac{u}{u^*}, \quad u^* = \sqrt{\tau_w / \rho}, \text{ and, } \quad y^+ = \frac{y\,u^*}{\nu}, \tag{4.3}$$

where,

u	=	fluid velocity [m/s],
u^*	=	friction velocity [m/s],
$U\infty$	=	free stream velocity [m/s],
τ_w	=	wall shear stress [N/m^2],
ρ	=	density of air [kg/m^3],
ν	=	kinematic viscosity [m^2/s],

and the skin friction coefficient, C_f, is defined by,

$$\tau_w = \frac{C_f}{2}\rho U_\infty{}^2. \tag{4.4}$$

The nondimensional length y^+ is effectively a Reynolds number and is used as the independent variable in the law of the wall,

$$u^+ = f\left(y^+\right). \tag{4.5}$$

For smooth, flat surfaces the viscous sublayer, $y^+<7$, is described by,

$$u^+ = y^+, \tag{4.6}$$

whilst the turbulent inner wall region is generally described by Clauser's (1956) correlation,

$$u^+ = 5.6\log\left(y^+\right) + 4.9, \qquad (4.7)$$

Figures 4.10, 4.12 and 4.14 show the wall law relationship, $u^+ \sim y^+$, obtained for each of the three axial positions whilst Figures 4.11, 4.13 and 4.15 demonstrate the normalised axial RMS velocity profile for the various surfaces.

In these graphs the boundary layer thickness, δ, is defined as the point at which the velocity in the boundary layer is 99% of the local free stream velocity.

The wall law plot for the roughened felt surface shows a dual slope characteristic after the initial low turbulence parabolic region which corresponds to the $u^+ = y^+$ region. The inner turbulent layer lies in the approximate range $50<y^+<300$, which varies with the specific test conditions, where the du^+/dy^+ value is independent of surface roughness.

The two key differences between the widely documented smooth, flat plate data and the results of this study are surface roughness and the presence of an axial pressure gradient caused by the curved hot plate profile. Schetz (1993) quotes the work of Ludwieg and Tillmann (1950) which demonstrates that the inner turbulent flow is insensitive to pressure gradients provided separation is not induced. Thus the wall law plot can be expected to hold for all pressure gradients, except in the immediate area of separation.

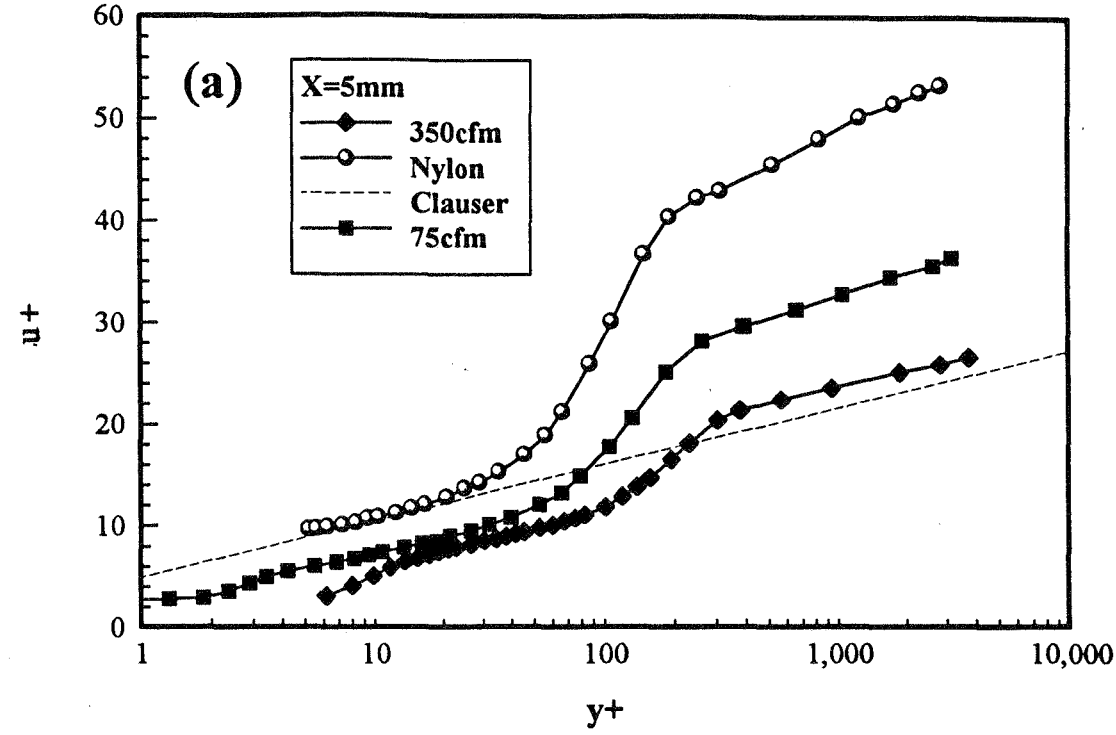

FIGURE 4.10
Wall law plot for the three felt arrangements x=5mm

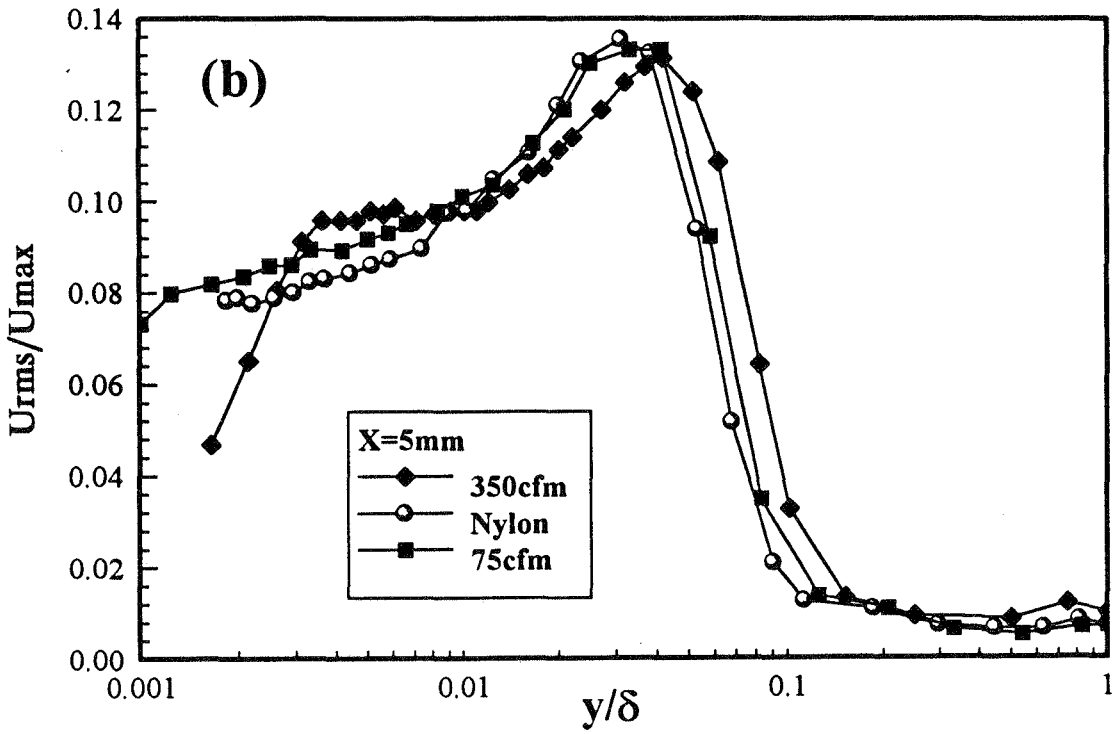

FIGURE 4.11
Turbulence intensity plot at x=5mm

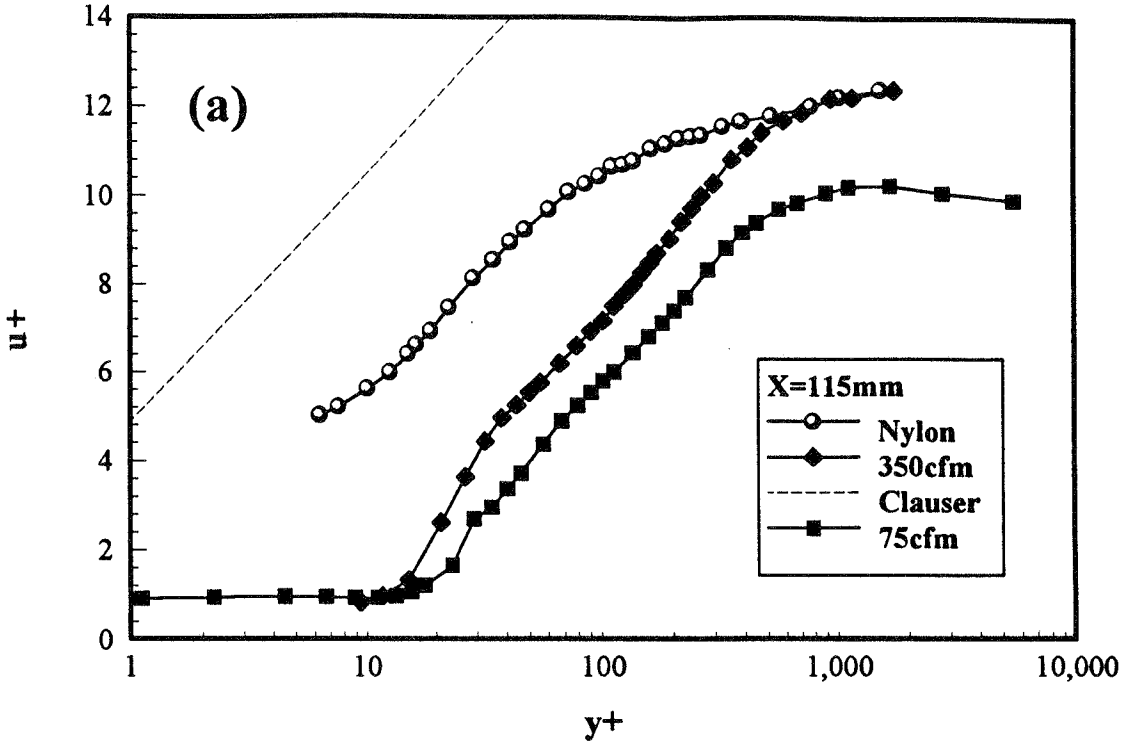

FIGURE 4.12
Wall law plot for the three felt arrangements x=115mm

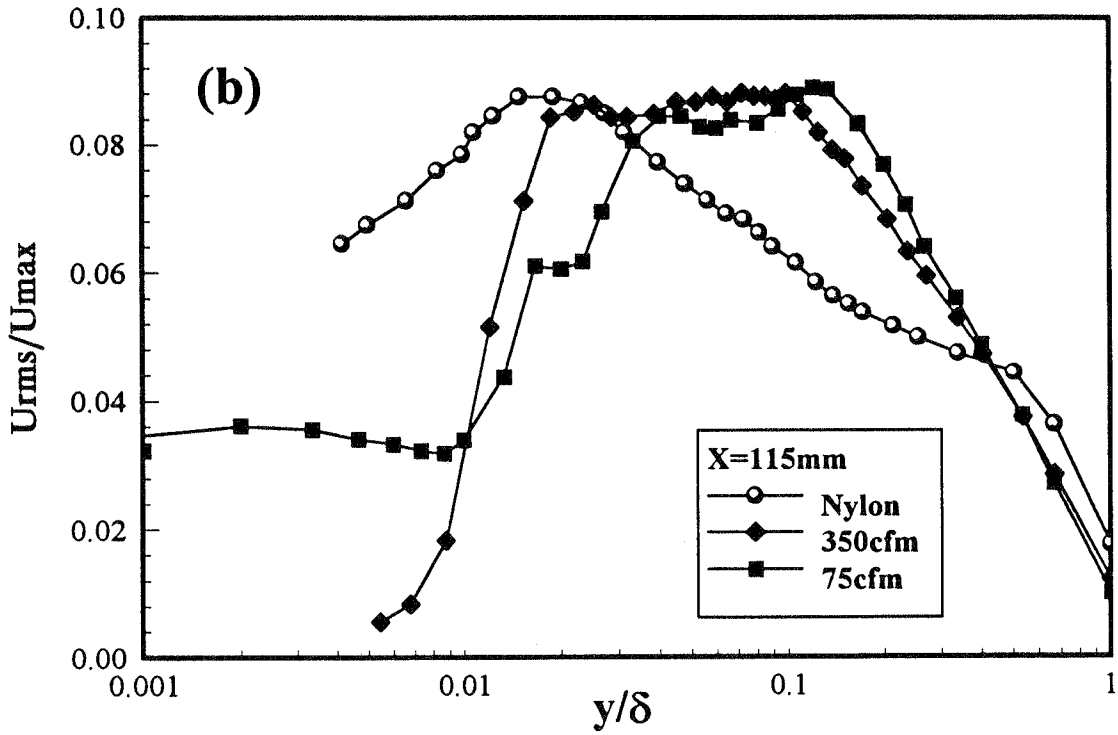

FIGURE 4.13
Turbulence intensity plot at x=115mm

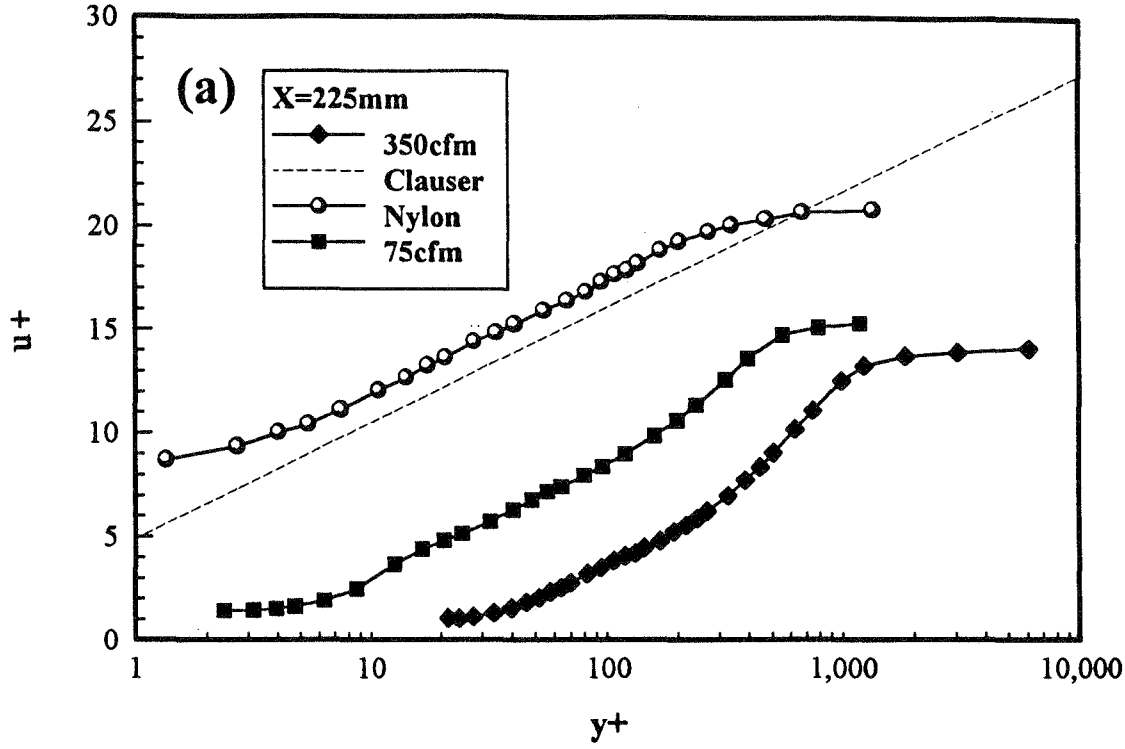

FIGURE 4.14
Wall law plot for the three felt arrangements at x=225mm

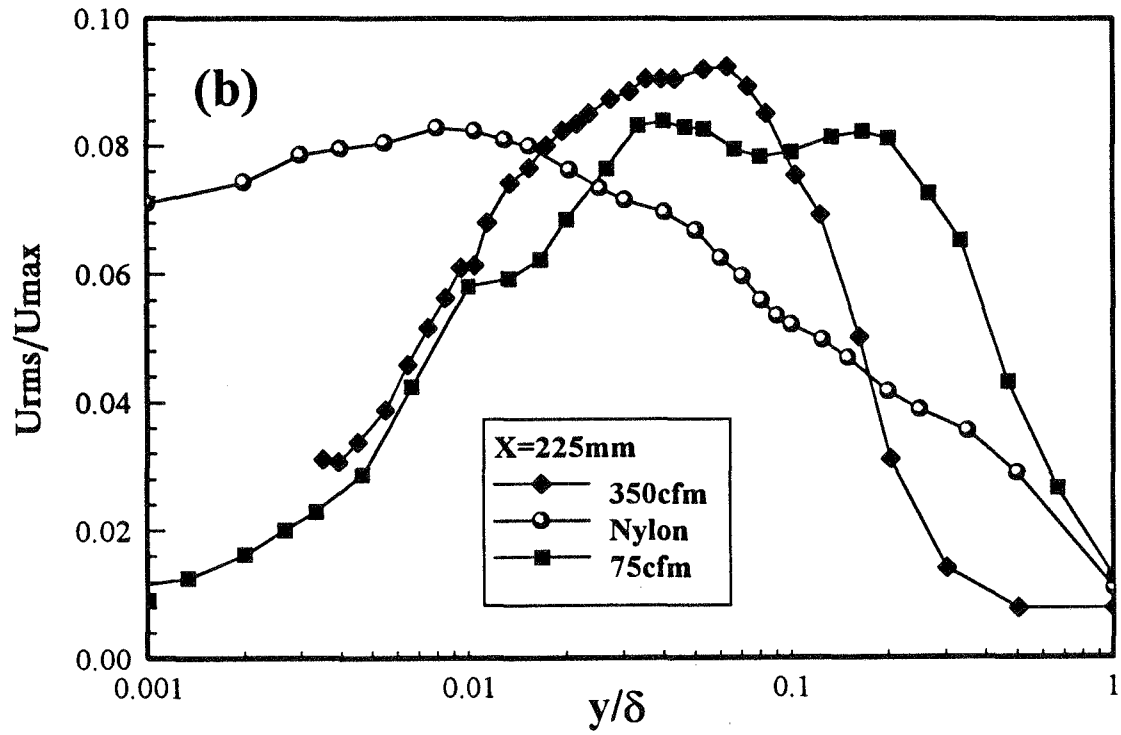

FIGURE 4.15
Turbulence intensity plot at x=225mm

Schetz also quotes experimental work which shows that the influence of roughness on the wall law plot is to shift the logarithmic portion (equation 4.7) of the smooth wall curve down and to the right, corresponding to an increase in Cf. The slope of the logarithmic region does not change. For large k^+ where the laminar sublayer disappears (k+>70) the flow is said to be fully rough and the overall effect, as confirmed by Hama (1954), can be described by,

$$u^+ = 5.6\log(y^+) + 4.9 + 5.6\log(k^+) + \Delta, \qquad (4.8)$$

where Δ is a constant and k^+ is the roughness parameter defined by,

$$k^+ = \frac{k\,u^*}{\nu}, \qquad (4.9)$$

where k is a measure of the average roughness size.

There is no definitive value for the roughness size of the dryer fabrics used in the study. Their undulating surface illustrated in Figures 4.6 and 4.7 means that roughness is quite variable due to the nature of the weave. For the purposes of the calculations a value equal to half the thickness of the dryer fabrics is taken. Given that this thickness is 2mm for both the 75cfm and 350cfm dryer felts an approximation of $k = 1mm$ has been used. This measurement was taken with the aid of the scale provided on the scanning electron micrographs.

The velocity profiles were plotted through using an appropriate value of Cf in the y^+ and u^+ calculations. Cf is selected so that the experimental results exhibit the Clauser slope in the internal wall-dominated layer. The resultant skin friction coefficients are listed in Table 4.1.

TABLE 4.1
Skin friction coefficients (C_f) and offset (Δ) for various drying felt and axial location combinations

Axial location	No felt		75 cfm		350 cfm	
x (mm)	Cf	Δ	Cf	Δ	Cf	Δ
5	0.0007	0.6	0.0015	-7.5	0.0028	-4.7
115	0.0130	-5.0	0.0190	-10.3	0.0360	-12.1
225	0.0046	1.4	0.0085	-3.1	0.0100	-12.4

Baskaran et al (1987, 1991) demonstrated the growth of an independent internal boundary layer over a curved hill. The internal layer was found to form as a result of the sharp change in surface curvature at the leading edge of the rise and was seen to control the skin friction distribution.

The streamwise pressure distributions for Baskaran et al and the geometry of this study are plotted together in Figure 4.16.

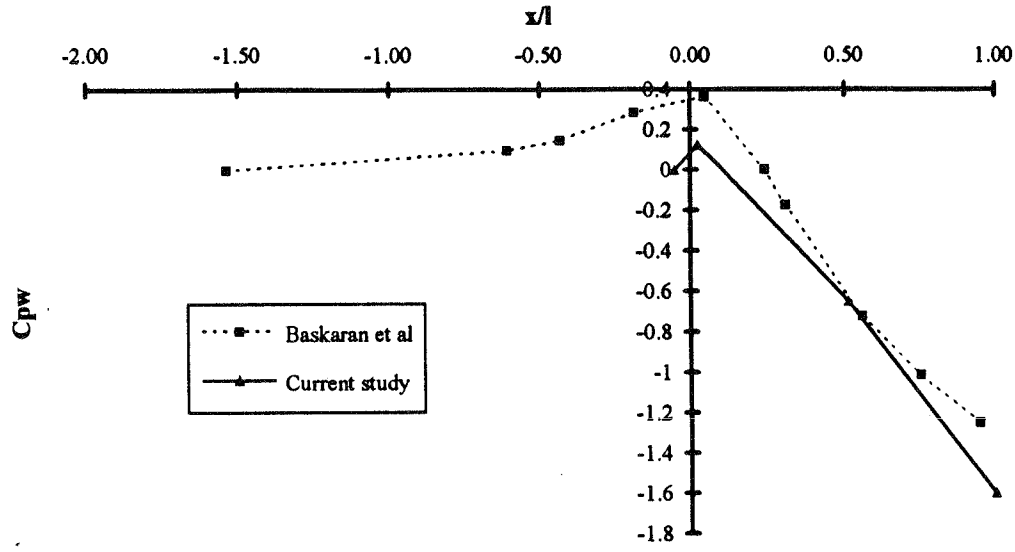

FIGURE 4.16
Wall coefficient of pressure c_{p_w} - comparison between Baskaran et al (1987) and the current study

The pressure gradient is plotted in terms of the wall pressure coefficient, c_{p_w}, which is defined as,

$$c_{p_w} = 1 - \left(\frac{U_{local}}{U_{ref}} \right)^2, \qquad (4.9)$$

where,
c_{p_w} = wall pressure coefficient,
u_{local} = local velocity [m/s],
u_{ref} = reference upstream velocity [m/s].

The related data are presented in Table 4.2.

TABLE 4.2
Variation in local velocity and wall pressure coefficient

x (mm)	x/l	U_{local} (m/s)	C_{p_w}
-12	-0.05	15.94	0.00
5	0.02	14.91	0.13
115	0.51	20.47	-0.65
225	1.00	25.72	-1.60

In Figure 4.16 and Table 4.2 *(x/l)* refers to the dimensionless streamwise coordinate, where the length, *l*, refers to the axial span of the single-sided curved hill.

It is evident that the two pressure gradient distributions are quite comparable, and this suggests that the behaviour of the outer wake region should be similar in each case. This is supported by the fact that the wake factors obtained by Baskaran et al (1987) along the upstream half of the curved hill vary from Δ=-4.8 to Δ=+1.0 in a similar fashion to those for the smooth plate in the current study which were presented in Table 4.1.

The axial variation of skin friction coefficient is generally consistent with the findings of Baskaran et al where Cf is a minimum near the leading edge of the curved hill and increases sharply to a peak at a position 1/3 the distance along the hill profile before decreasing slowly as the axial position nears the crest. The results are graphed in Figure 4.17.

The relative variation in Cf between the 75cfm felt, the 350cfm felt and the aluminium plate surface is similar at each axial location and this trend indicates that the more permeable 350cfm felt induces more drag than does the 75cfm felt. This result is not obvious from an inspection of the two materials but in hindsight can be attributed to the weave pattern. The 350cfm felt is more porous and the surface comprises a number of relatively isolated roughness elements as opposed to the denser 75cfm felt which presents a more uniform surface.

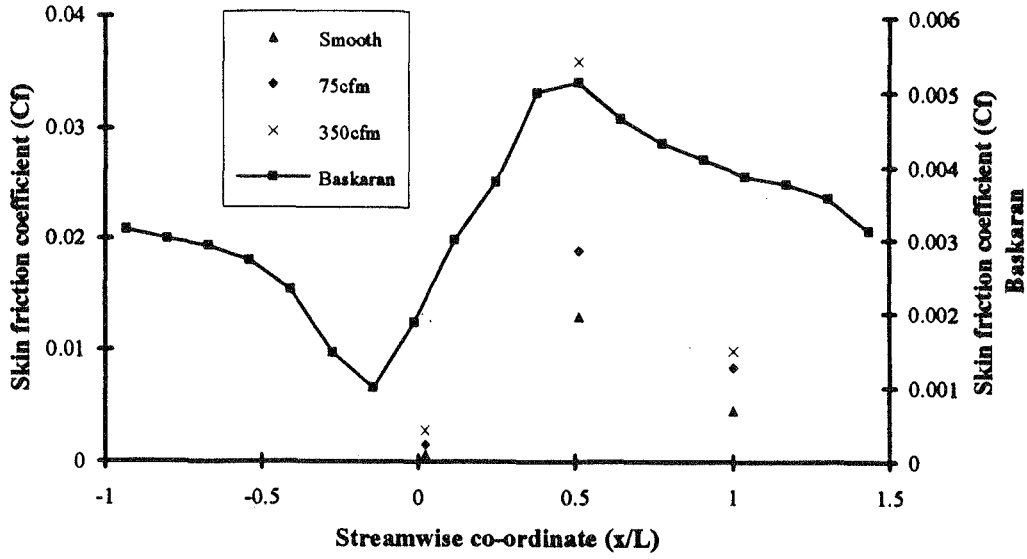

FIGURE 4.17
Skin friction coefficient between various drying fabrics and Baskaran et al's (1987) data for a smooth curved plate

The axial turbulence intensity measurements presented in Figures 4.11, 4.13 and 4.15 are useful in indicating the proximity of the probe to the rough ill-defined felt surface. Whilst a formal laminar sublayer is not identifiable due to the excessive roughness ($k^+ \cong 60$ for 350cfm felt at x = 225mm) the RMS velocity must tend towards zero at the wall. The variation of the dimensionless RMS velocity, U_{rms}/U_∞, for small values of y/δ assists in defining zero surface datum for the two rough felts studied. It should be noted that no laminar sublayer was observable in flow over the smooth aluminium hot plate surface which maintained significant turbulence to within approximately 20μm of the wall for each trial.

The turbulence intensity data can be viewed against the established literature in terms of the peak values and location of peak turbulence within the boundary layer. Schetz (1993) quotes Klebanoff's (1955) results which indicate a maximum axial turbulence intensity of 11.5% for flow over a smooth flat plate at a point which is 1% of the way from the wall to the boundary layer edge. The comparative results from the current study are shown in Table 4.3.

TABLE 4.3
Summary of turbulence intensity data for trials on a curved hill - maximum intensity and peak location

Axial location x (mm)	No felt		75 cfm		350 cfm	
	U_{rms}/U_{edge}	location (y/δ)	U_{rms}/U_{edge}	location (y/δ)	U_{rms}/U_{edge}	location (y/δ)
5	13.5%	0.04	13.5%	0.04	13.5%	0.04
115	9%	0.015	9%	0.02-0.1	9%	0.02-0.1
225	8%	0.01	8%	0.02-0.2	9%	0.03-0.06

The peak turbulence intensity values are very similar for the three different values of roughness. The location of the peaks within the boundary layers differ according to roughness. The smooth curved plate gives rise to a single identifiable peak, whereas the extremely rough dryer fabrics tend to lead to extended plateaux of high turbulence. This broader spread of the high turbulence zone is a consequence of the relatively large dimension scale introduced by the 1mm roughness elements.

The peak values of Table 4.3 are comparable with Klebanoff's 11.5% peak, although they do not occur as close to the wall. This effect is particularly prominent for the fabric-covered surfaces, which might be expected due to the excessive roughness penetration, but also mildly true for the "smooth" curved hill.

It is not possible to seek a precise comparison with Baskaran et al (1987) as their turbulence intensity data are not detailed at small values of (y/δ). However, it appears that at entry to the curved hill the peak intensity is around 10% and decreases to around 6% at the pinnacle of the hill. These values underestimate the data from the current study, but the minor differences in pressure gradients and the concave transition between the flat duct and the inclined hill would account for this.

The curved hot plate of the current study has a discontinuity at the join between the duct floor and the hill surface, whereas Baskaran et al have incorporated a smooth concave bend which results in slightly lower levels of turbulence.

Baskaran et al (1987) note that turbulence intensity should decrease in areas of favourable pressure gradient, and that the location of the maxima

will move towards the edge of the boundary layer as the strength of the pressure gradient increases. This is supportive of the comparison with Klebanoff's flat plate data for which $dp/dx=0$.

4.2.2 Temperature profile

Just as Clauser's (1956) data were used to determine the skin friction coefficient by equating gradients in the inner region so can Kader's (1981) correlation for the temperature law of the wall assist with estimating the heat flux through the surface. This will then form the basis for calculating the desired heat transfer coefficients.

Defining a heat transfer temperature, T_*, of,

$$T_* = \frac{q_w}{\rho c_p u_*}, \tag{4.10}$$

which is analogous to the friction velocity u^*, the dimensionless temperature T^+ becomes,

$$T^+ = \frac{T_w - T}{T_*}. \tag{4.11}$$

For air with a Prandtl number of 0.7 over the temperature range studied, the logarithmic region may then be expressed by (Kader),

$$T^+ = 4.88\log\left(y^+\right) + 3.73. \tag{4.12}$$

The temperature profiles ($T^+ \sim y^+$) for each of the three axial locations are illustrated in Figure 4.18. To prepare these curves requires the heat flux value at each of the sample points. As this parameter was not measured its value was obtained in the same way the earlier skin friction coefficient values were determined. Repeating the earlier analogy that the law of the wall applied in spite of differences in pressure gradient and roughness, the T^* value for each trial was manipulated so that the gradient of the internal wall dominated region matched the gradient defined by Kader's correlation expressed in equation 4.12. The heat flux, q_w, is subsequently calculated from equation 4.10 and is quoted in Table 4.4. The surface heat transfer coefficient is then determined as the ratio of the heat flux and the temperature differential between the paper surface and the free stream temperature.

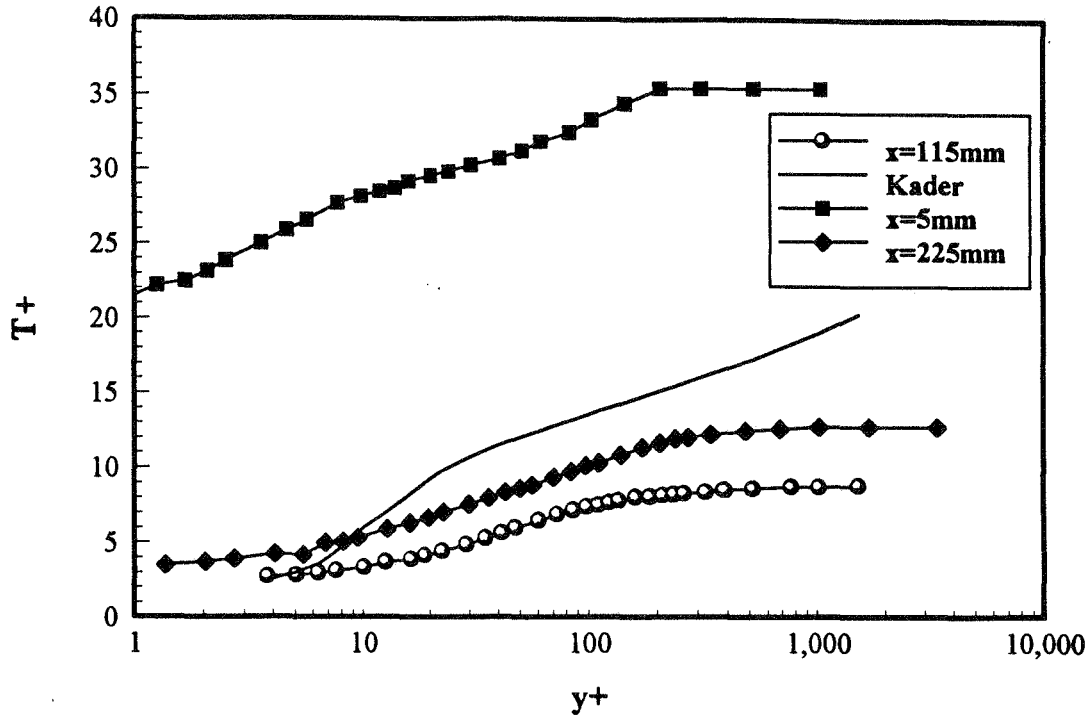

FIGURE 4.18
Temperature boundary layer profile at three axial locations for the curved hill with no drying felt. Comparison is made with Kader's (1981) flat plate correlation.

Figure 4.19 is complementary to 4.18. It shows the velocity boundary layer profile at the same three axial locations for the curved hill with no drying felt. These curves were presented in the earlier graphs of Figures 4.10, 4.12 and 4.14. These graphs grouped data from the three different drying fabrics at a single location.

Comparison between Figures 4.18 and 4.19 shows a similar trend of axial variation for the velocity and temperature boundary layer profiles over the smooth curved plate (elsewhere designated by its nylon tensioning as opposed to dryer fabric).

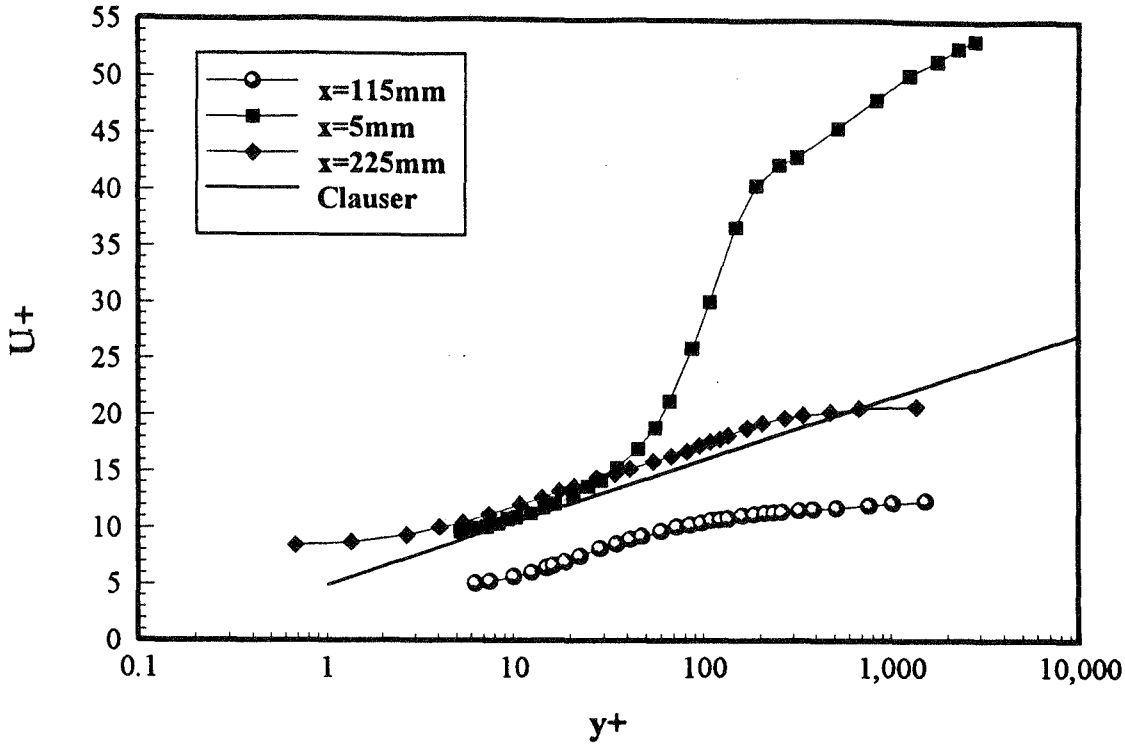

FIGURE 4.19
Velocity boundary layer profile at three axial locations for the curved hill with no drying felt. Comparison is made with Clauser's (1956) flat plate correlation.

The relativity between the boundary layer profiles at each of the three locations is maintained for both the temperature and velocity relationships. The upstream sample point at x=5mm is vertically offset above the Kader and Clauser wall-law plots. Both the middle, x=115mm, points lie below the smooth flat plate correlations, whilst the x=225mm point which represents the peak of the curved hill is closest to the theoretical models in each case. At the peak of the hill the flow is neither accelerating nor decelerating, the pressure gradient is zero. Consequently it is understandable that the velocity and temperature profiles should most closely match the zero pressure gradient, flat plate results at this point.

At the initial, x=5mm, measuring location the pressure gradient has just gone through an abrupt change due to the discontinuity between the duct floor and the leading edge of the curved hill which protrudes into the duct. This sharp favourable pressure gradient causes the large deviation between the measured profiles in Figures 4.18 and 4.19 and the flat plate ideals. For the temperature analogy the positive vertical offset is indicative of a large

differential between the wall and flow stream (T_w-T). This implies that the heat transfer will be low which is physically reasonable that the discrete interface between the duct flooring and the hill is expected to promote recirculating eddies which stifle the transfer of heat into the flow.

Surface heat transfer coefficient

The work of Colburn (1933) and Von Karman (1939) on turbulent flow over a flat plate showed the Stanton number to be directly proportional to the skin friction coefficient. The Colburn j-factor analogy, often referred to as the modified Reynolds analogy, is presented in equation 4.13.

$$\frac{c_f}{2} = St\,Pr^{2/3}, \tag{4.13}$$

where, Stanton no. $= St = \dfrac{h_s}{\rho u_e c_p}$,

Prandtl no. $= Pr = \dfrac{\mu c_p}{k}$,

and,

c_f	=	skin friction coefficient,
h_s	=	surface heat transfer coefficient [W/m^2°C],
ρ	=	air density [kg/m^3],
c_p	=	specific heat capacity of air [J/kg°C],
k	=	thermal conductivity [W/m°C],
u_e	=	air velocity at b.l. edge [m/s], and,
μ	=	absolute viscosity [m^2/s].

Expressing the Stanton number in terms of its component parameters to obtain the heat transfer coefficient gives,

$$h_s = \frac{\rho u_e c_p}{2\,Pr^{2/3}} c_f. \tag{4.14}$$

Due to the pressure gradient along the curved hot plate the velocity at the edge of the boundary layer changes at the three measuring stations. These data points were presented in Table 4.2. Inserting the skin friction coefficients and edge velocities into equation 4.14 produces the Colburn analogy prediction of surface heat transfer coefficient for the test geometry. These values are listed together with the independently derived

experimental values which were calculated as the ratio of the heat flux and the temperature differential between the paper sheet and the free stream air flow. Figure 4.20 is a graphical representation of the data under comparison.

TABLE 4.4
Heat flux and heat transfer coefficients along the centreline of the hot plate surface.

Location x(mm)	5	115	225
q_w (W/m²)	550	16610	8900
(T_w-T_{flow}) (°C)	55	67	95
$h_{surface}$ (W/m²°C) exp	10	248	94
C_f	0.0007	0.0130	0.0046
u_e	14.9	20.5	25.7
$h_{surface}$ (W/m²°C) Colburn	8.0	203.5	90.5

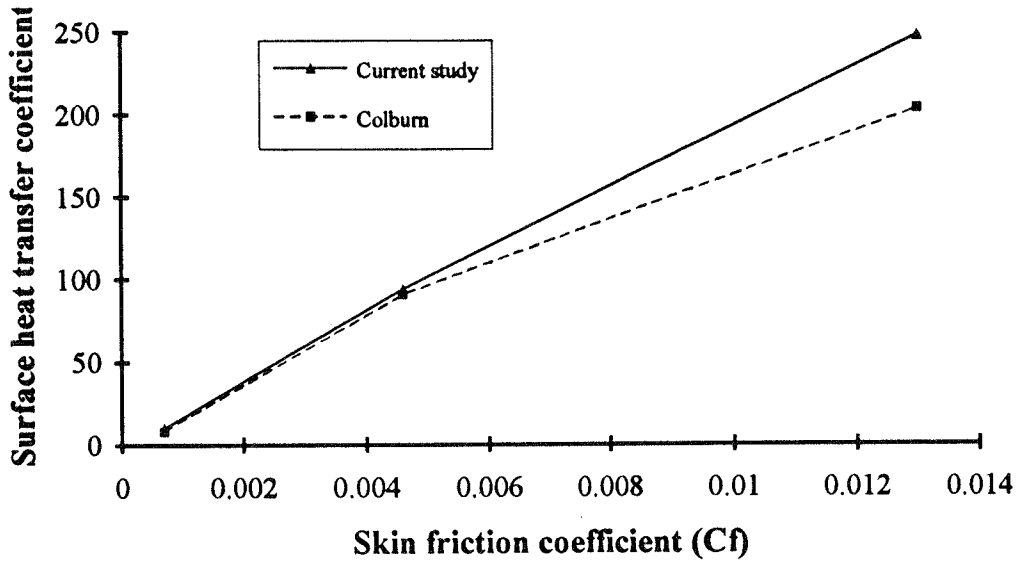

FIGURE 4.20
Linear relationship between C_f and $h_{surface}$

The comparison is relatively close, with the Colburn analogy underestimating the results of the current study by 18% when the skin

friction coeficient is high. Incropera (1985) notes whilst the Colburn analogy is only applicable for zero pressure gradients in laminar flow, in turbulent conditions the analogy is far less sensitive to non-zero pressure gradients. The data of Baskaran et al (1987) confirmed that for a similar test geometry the skin friction coefficient behaves approximately in proportion to local pressure gradient. This is demonstrated in Figure 4.21.

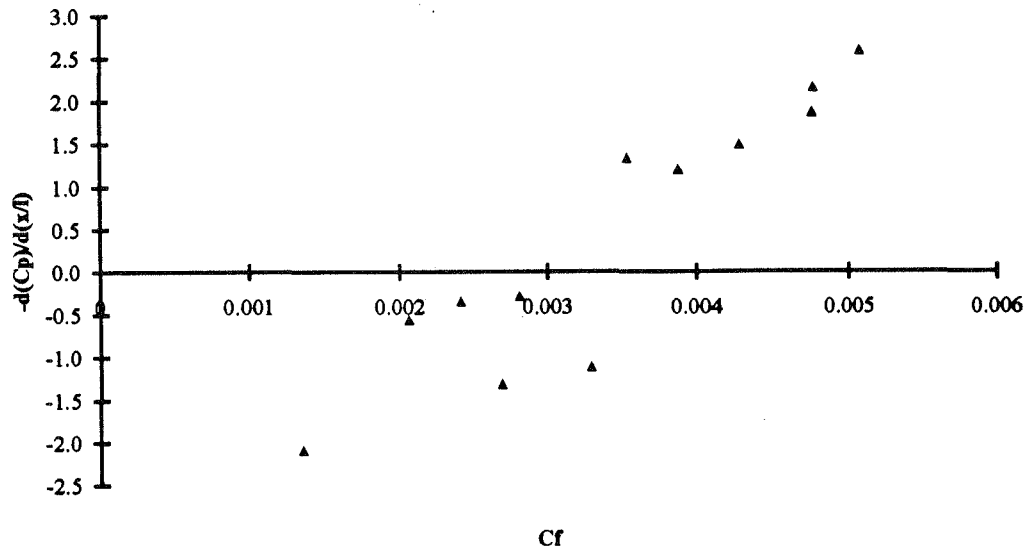

FIGURE 4.21
Relationship between pressure gradient and skin friction coefficient [Baskaran (1989)] for flow over a curved hill

Nomenclature in Figure 4.21 :

c_p - coefficient of pressure, see equation 4.9,
x - streamwise dimension, and
l - streamwise distance to peak of curved hill, and
positive values of {-d(Cp)/d(x/l)} mean the presence of a favourable pressure gradient.

The coincidence between high skin friction coefficient and large favourable pressure gradients supports the application of Incropera's philosophy to the current data and explains why Colburn's analogy is less reliable as the skin friction coefficient increases.

4.2.3 Contact heat transfer coefficient

The heat flux data generated for Table 4.4 also bear application in determining the contact heat transfer coefficient between the hot plate and the thin aluminium backing plate which is an important parameter in controlling the paper drying trials which are proceeding in parallel with this boundary layer study.

The data presented in Table 4.5 are from separate sets of measurements to those which formed Table 4.4. The contact heat transfer coefficient is calculated as the ratio of the heat flux and the temperature differential between the hot plate and the paper sheet.

The relative constancy of $h_{contact}$ at the three locations reinforces the validity of the heat flux data determined earlier with the assistance of Kader's correlation. The average value determined for the contact heat transfer coefficient between the hot plate and the paper sheet was 410 W/m^2°C.

TABLE 4.5
Contact heat transfer coefficients along the centreline of the hot plate surface.

Location x(mm)	5	115	225
q_w (W/m^2)	550	16610	8900
$T_{hot\ plate}$ (°C)	85.2	101.3	121.4
T_{paper} (°C)	83.7	61.5	101.4
$h_{contact}$ (W/m^2°C)	367	417	445

Direct comparison with contact heat transfer coefficients obtained by others for similar geometries is difficult because of the presence of the intermediate aluminium backing plate in the current series of tests. As indicated diagrammatically in Figure 4.8, the contact between the thin aluminium plate on which the paper sheet is supported and the curved hot plate adds thermal resistance to the overall heat transfer. This term is reflected in the data of Table 4.5 but is an additional component which is not present in the experimental trials of others and certainly not on actual paper machines. It is therefore anticipated that the contact heat transfer

between hot plate and paper sheet will be lower in the current trials than the results presented by other sources.

In section 5.1.1 the experimental rig is compared with that of Lee and Hinds (1983) who conducted drying tests using a similar curved hot plate geometry. Lee and Hinds used a felt tension of 700 N/m and experimentally found that the contact heat transfer coefficient between the paper and the moist sheet varied in the range from 550-580 W/m^2°C. This result is about 40% higher than the current data, in spite of using a felt tension value which was less than half of that of the current study (1.7kN/m). As explained in the previous paragraph this differential is a direct consequence of the backing plate which is not present in the tests conducted by Lee and Hinds and means that the sets of data cannot be directly compared.

It should be emphasised that the contact heat transfer coefficients derived in this section are quite different from those present on actual paper machines due to the additional interface. Section 11.2.3 uses actual paper machine data to establish appropriate values for the model simulation. The application of the data presented in Table 4.5 occurs in Chapter 5 which predicts mass transfer coefficients based on the actual model geometry.

4.3 Conclusion

The momentum and thermal boundary layer profiles of flow over a curved hot plate with and without a covering synthetic fabric were measured. The skin friction coefficients obtained from the velocity profiles demonstrated that the 350cfm dryer fabric creates significantly more drag than the 75cfm fabric and well over twice the drag of a smooth surface. This is significant from the viewpoint of predicting paper sheet disturbance from air flows caused by the motion of dryer support felts in the paper machine's dryer section.

The thermal boundary layer measurements enabled the contact heat transfer coefficient from the hot plate through the thin aluminium backing plate to the paper sheet to be determined (410 W/m^2°C). This value is required when evaluating the drying trial results in the following chapter. It is different to actual machine values for this parameter because of the additional interface between the thin aluminium backing plate and the curved hot plate.

The surface heat transfer coefficient between the paper sheet and the drying air was also calculated along the hot plate and was found to vary almost linearly with skin friction coefficient in accordance with published correlations.

5. Laboratory Tests II - Drying

The most crucial experimental data required by the mathematical model relate to the behaviour of the mass transfer coefficient. This coefficient which directly governs evaporation rates is primarily dependent upon the relative velocity between the paper sheet and drying air and the permeability of the drying fabric which supports the sheet. The variation in mass transfer coefficient is determined by a series of drying tests which monitor moisture content with time.

The experimental rig used for the drying tests is essentially as described in the previous chapter which examined the boundary layer behaviour of air flows over the curved hot plate. Facilities were provided for the monitoring of the dryer fabric tension, air temperature and humidity, hot plate surface temperature, air speed and sheet moisture content.

The normalised results (see Section 5.2) were output and a curve of best fit was generated for each trial. The exponentially-based best fit curves then enable the subsequent calculation of the mass transfer coefficient. This is done through a routine which selects the optimal value for mass transfer coefficient to match the experimental drying curve to the model prediction. The heat transfer coefficient results determined in Chapter 4 were employed in this analysis.

The mass transfer coefficient behaviour, with and without dryer fabrics, with varying felt permeability and over a range of air flows, was correlated from these experimental tests and input into the dryer model. In the dryer simulation the mass transfer coefficient varies cyclically as the paper sheet is alternately exposed to regions with and without felt support.

Through similarity relations the observed mass transfer coefficients were compared to the surface heat transfer coefficients obtained from the independent results of the previous chapter. Several comparisons were also made with the results of other investigators.

5.1 Experimentation

5.1.1 Experimental rig

The experimental rig was designed to dry 225mm×225mm handsheets of paper from an initial moisture content of approximately 5 kg_{water}/kg_{fibre} (80-85% moisture on a wet basis). The testing rig was essentially a square sectioned duct with radiant electric heating elements positioned beneath the duct floor and enclosed by a semi-circular stainless steel reflector that is thermally insulated by a combination of synthetic sheeting and loose fibreglass matting. Above the heating elements and protruding into the duct was a curved aluminium hot plate fitted with nine thermocouples embedded in its top surface. The output of these thermocouples as well as the ambient temperature and relative humidity were monitored by a datalogging computer.

A piece of dryer fabric was fastened to the leading edge of the hot plate. The fabric then covered the hot plate and was drawn out through a downstream slot in the base of the duct. This end of the dryer fabric was then connected to a fixed support by means of a ratchet and turnbuckle arrangement that allowed the fabric to be stretched to a desired tension. This tension was measured by a load cell connected in series with the fabric. The load cell output was monitored by the datalogging computer. A schematic diagram of the test set-up is shown in Figure 5.1. Photographs of the installation are provided in Figures 5.2 and 5.3.

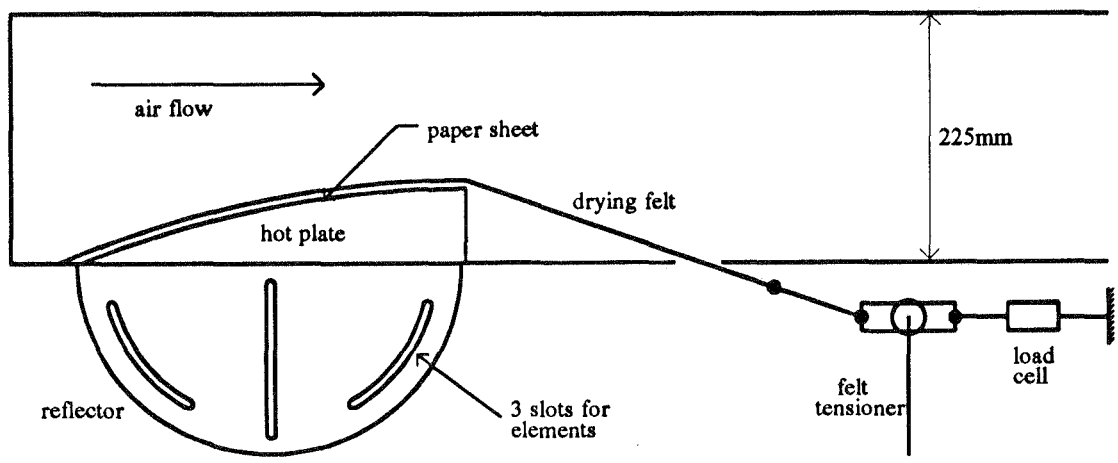

FIGURE 5.1
Schematic diagram of laboratory paper drying rig

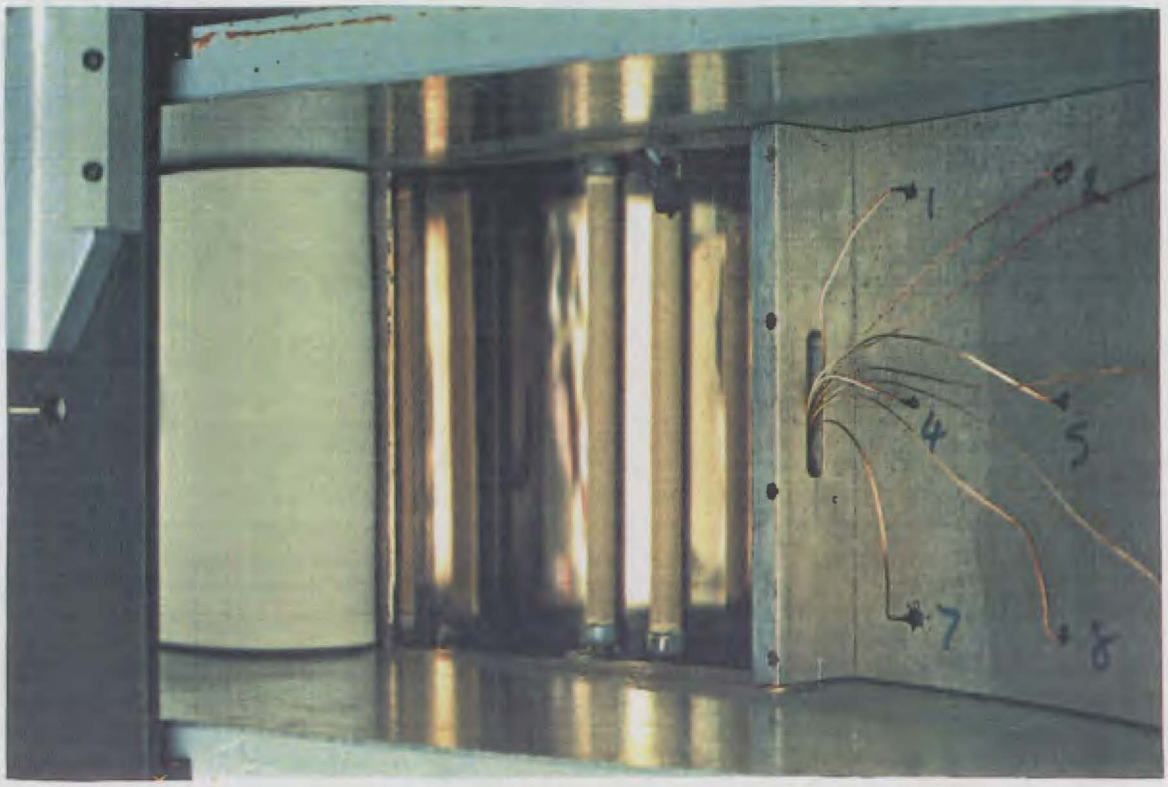

FIGURE 5.2
Photo of experimental rig used for drying paper - illustrating elements, internal surface of reflector, inverted hot plate, thermocouple locations and dryer fabric (folded back)

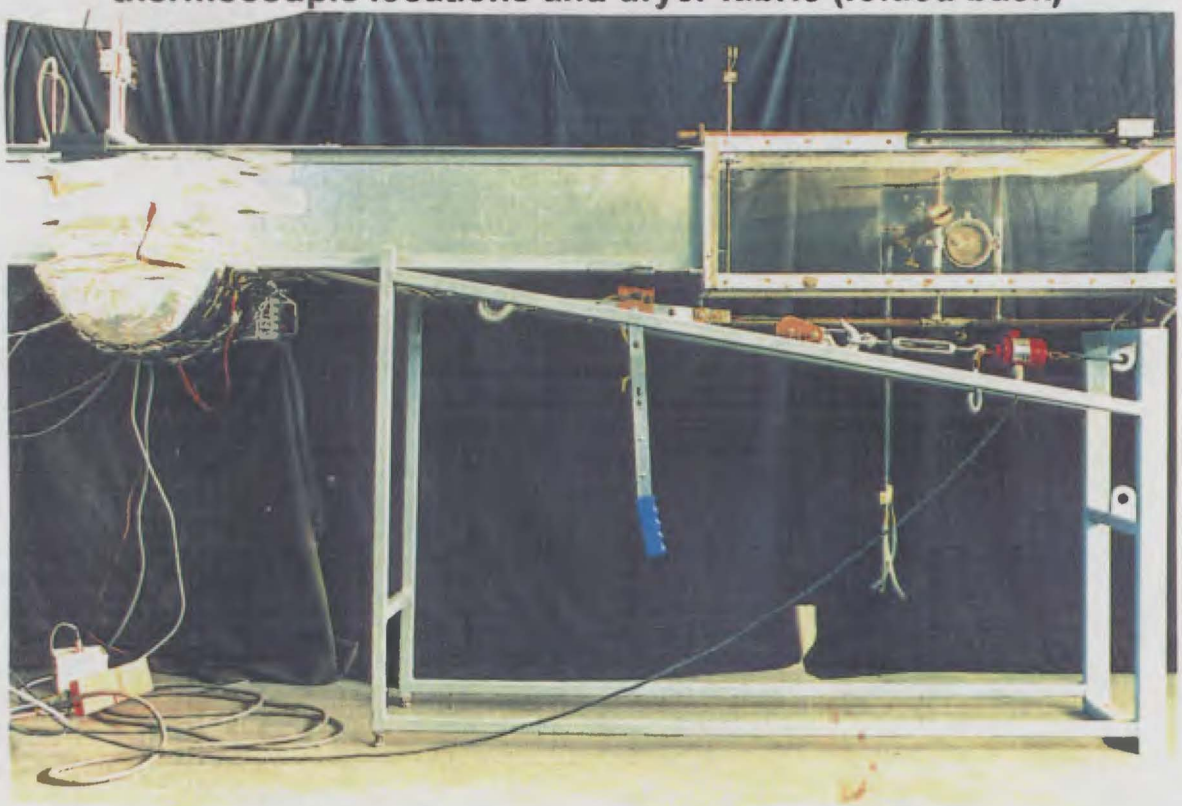

FIGURE 5.3
Photo of experimental rig used for drying paper - illustrating duct, insulated semi-circular reflector and tensioning device

The wet paper sheet was mounted onto a thin aluminium plate which was contoured to follow the curve of the hot plate surface. These two layers were then sandwiched between the hot plate and drying felt to mark the start of a drying trial. Tensioning of the dryer felt was done manually, threading it through the slot in the bottom of the duct, connecting it to the ratchet device and applying coarse tension before making the fine adjustment (in Newtons) using the turnbuckle.

The location of the heating elements is a prime factor in controlling the uniformity of heating over the aluminium hot plate. Some preliminary calculations were made to assist this design process. To allow some fine-tuning of the theoretical design positioning, slots were provided in the reflector's end caps and the elements' axes were adjusted vertically and in the streamwise direction to achieve an even temperature distribution. The optimum positioning was found to vary slightly with the magnitude of the cooling air flow over the hot plate. As the air flow passes over the curved hot plate it is heated and accelerates as a result of the contracting duct cross-section and tends to increase heat transfer towards the downstream edge of the hot plate.

The overall arrangement is quite similar to that used by Lee and Hinds (1979) in testing 20.3cm square handsheets of 600 g/m^2 basis weight. The specific geometry of this investigation was selected for several reasons :-

- a square hot plate was required to match the size of handsheet samples generated from the ANM handsheet forming equipment (225×225mm).
- a curved hot plate was necessary to allow the drying fabric (felt), which is a reasonably stiff material, to be tensioned over the hot plate whilst, a) applying an even pressure over the whole plate, and, b) laying flat at all points so as not to create a bulge which would protrude into the air flow in a different contour to that of the hot plate and paper sheet.
- the radius of curvature of the hot plate of 530mm was selected to be as close as possible to the paper machine dryer cylinder radius of 750mm whilst not compromising either of the previous two criteria.

5.1.2 Handsheet fabrication

Wet sheets of paper are required as the input specimens to the testing rig. This presents some difficulty regarding handling and dictates that handsheets must be used rather than machine-made paper. A sheet-former

is resident within the ANM research laboratory and was used to produce the handsheets required in this study. In a similar fashion to a full-scale machine the sheet-former has three distinct stages to the making of paper. Photographs of this equipment are shown in Figures 5.4 and 5.5.

Firstly, a pulp solution with a solids content of 0.15% is sprayed through a traversing nozzle onto a synthetic forming fabric lining the circumference of a drilled stainless steel drum rotating at 1000 rpm. Once the fibre mat has been laid an outlet valve is progressively opened to drain away excess water through the holes in the rotating shell. The drum speed is then increased to 1600 rpm for several minutes to centrifuge away as much free water as possible. The fibre mat is then removed from the forming drum and transferred from the forming fabric to a steel backing plate.

The wet sheet is then covered by an absorbent press felt and pressed several times at 60 psi by a pair of contra-rotating rollers. At this point the paper has a moisture content of between 5 - 6.5 kg_{water}/kg_{fibre}, the exact figure depending upon the pulp furnish used and the basis weight of the sheet.

If a dry sheet is required the sheet is passed to the third process stage, a stainless steel hot plate at 130°C. For a typical sheet, with a basis weight of 50 g/m^2, approximately seven minutes of drying time is needed to evaporate most of the moisture from the sheet. In this context the paper sheet was dried to a moisture content below the equilibrium value for ambient conditions, typically 8-10% moisture. Sheets to be tested for basis weight are dried in this way to obtain a flat sheet. It is to be noted that the intimate presence of the steel backing plate while moisture is being evaporated below the hygroscopic limit (about 0.4 kg_{water}/kg_{fibre}) will provide restraint against shrinkage and prevent wrinkles forming in the sheet. A flat sheet is critical for the area measurement needed for the basis weight calculation.

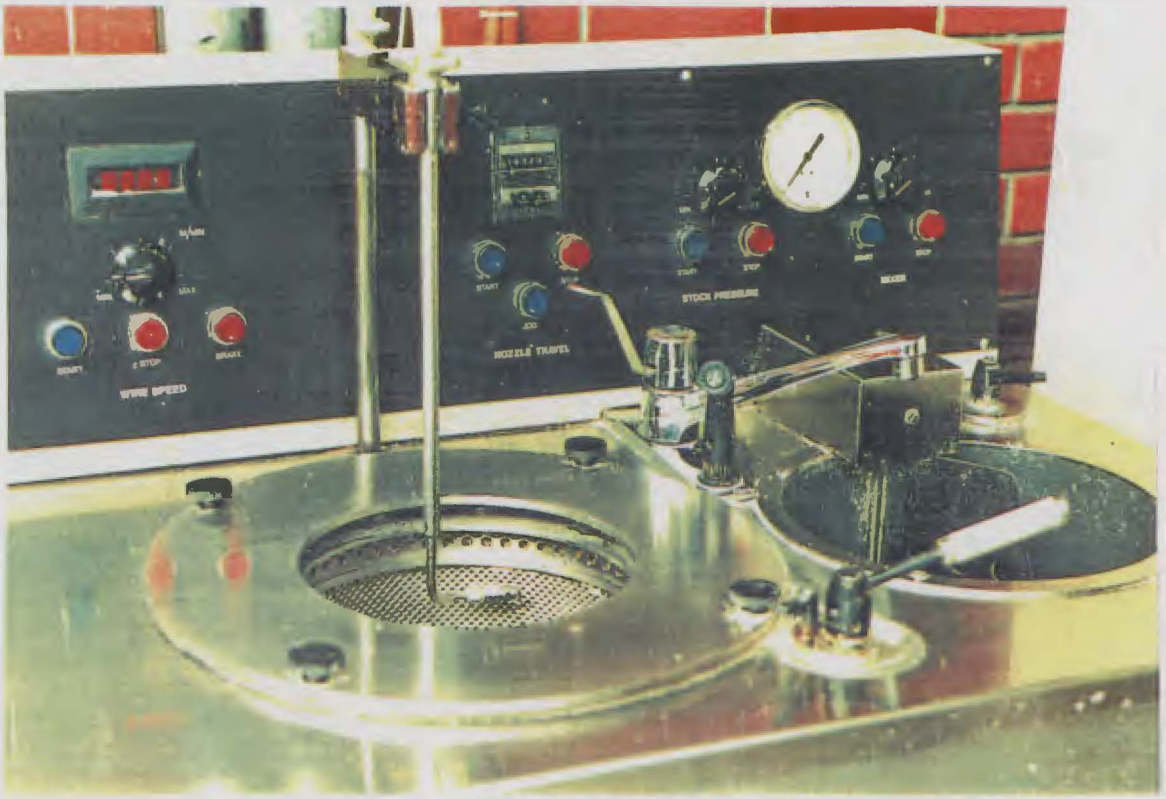

FIGURE 5.4
Photo of laboratory sheet former - illustrating the traversing pulp nozzle, the drilled forming drum on the left, the agitated pulp storage tank on the right and general instrumentation

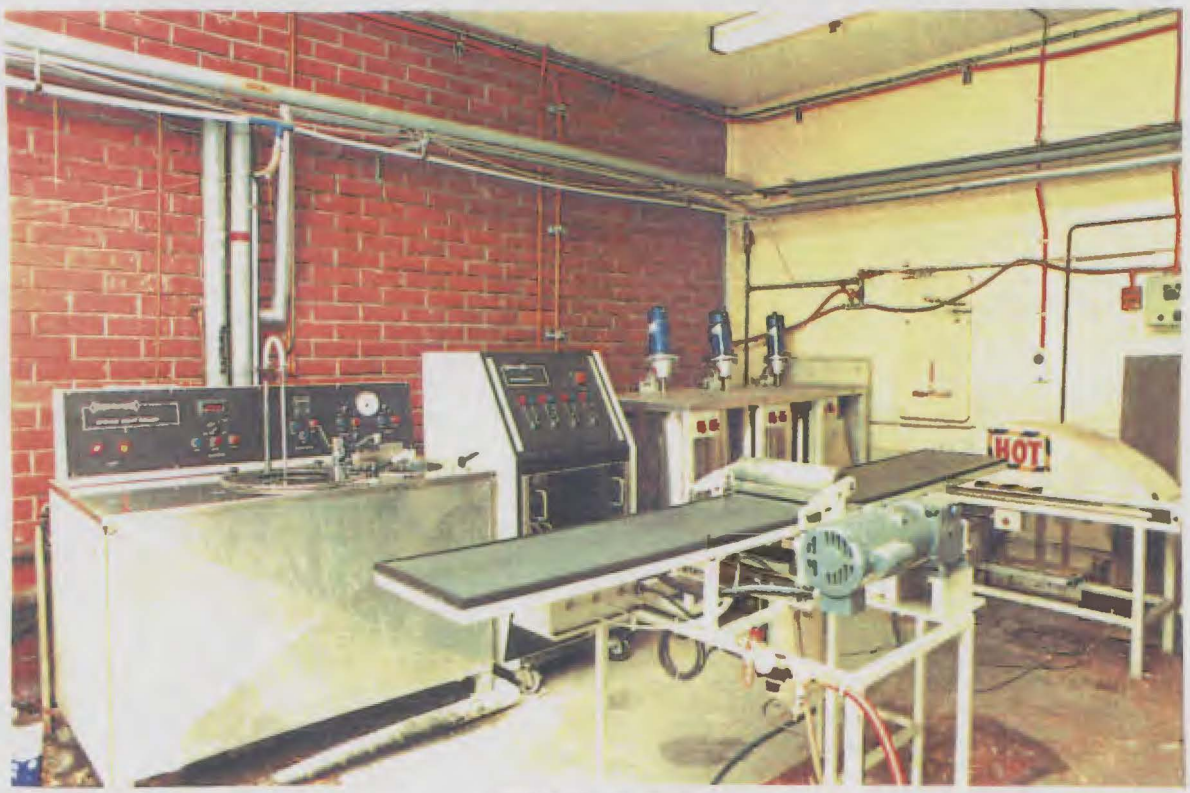

FIGURE 5.5
Photo of laboratory handsheet equipment - illustrating the sheet former (left), the pneumatic pressing table (foreground) and the curved drying hot plate (right rear)

Each handsheet formed by this process is 900mm×225mm and is divided into three wet test sheets and one dry sheet to be tested for basis weight. Each sheet is 225mm square. The three wet test sheets are not passed to the hot plate dryer but rather transferred to individual curved pieces of 0.6mm aluminium sheeting fabricated specifically for the drying tests performed in this study. The backing plates were shaped to match the contour of the thicker aluminium hot plate in the laboratory drying duct. This facilitates the handling of the very weak wet sheet. Each aluminium backing plate and wet paper sheet were sealed in a clip-lock plastic bag to prevent moisture loss. The fourth, dry, test sheet remained on the steel backing plate that it was pressed on and was transferred with this plate to a hot surface dryer. The presence of the original supporting plate provides restraint against shrinkage during the drying process when the hygroscopic moisture is removed from the sheet. The result is a very flat sample sheet that can be accurately measured for basis weight (dry fibre mass per unit area).

5.1.3 Experimental procedure

The commencement of each drying trial was marked by the removal of the thin backing plate with its attached wet paper specimen from the sealed plastic bag. The specimen plate was weighed, positioned on top of the hot plate and covered with the dryer fabric which was then loaded to the desired tension. Timing of the drying trial began at this point and continued until the fabric tension was released and the sheet removed from the duct for a second weighing (± 0.01g). At this point the trial was complete.

The remaining water in the sheet must be removed so that the dry weight of the sheet is known. This is achieved by leaving the sheet in an oven at 105°C until its mass stabilises indicating that the moisture content has reached equilibrium. For nominal room conditions of 20°C, 50% r.h. the oven relative humidity is approximately 1% and the sorption isotherms, presented in Chapter 9, predict an equilibrium 'dry' moisture content for paper of 0.0017 kg_{water}/kg_{fibre}. This is regarded as negligible in the context of the overall procedure.

During the drying trials the hot plate temperatures, air speed, air temperature, air relative humidity and fabric tension were datalogged on a personal computer. Specific software was written for this application. The software interfaced with a Singular Technology Corp. SC-1201, 12 bit Input/Output board. These values recorded were updated cyclically on a

ten second basis and stored to disk. The software calculated regression curves describing the relationship between digital PC representation of the physical parameters such as temperature, relative humidity, fabric tension and air speed. This automatic calibration facility and time-referenced storage of data provided an efficient base for the subsequent analysis of drying trials.

Each 225mm square handsheet was used just once to produce a single data point on the relevant drying curve, moisture content plotted against time. For each of the drying conditions examined between 8-16 data points were used to produce a representative drying curve. The concept of reusing a partially wet sheet in a drying test was dismissed due to the effects of the variation in initial moisture distribution and initial sheet temperature.

Tests were conducted for controlled changes in six major parameters - hot plate temperature (heating element current), duct air speed (fan input voltage), fabric tension, fabric permeability, sheet basis weight and sheet furnish composition. The test values for these variables are listed in Table 5.1 and were selected on the basis that they cover the range of values relevant to paper machine operation.

TABLE 5.1
Variable parameters used in drying tests

Parameter	Units	Values tested
heater current	A	0, 3, 4, 5, 6
fan input voltage	V	0, 100, 150, 180
fabric tension	N	50, 200, 400, 600
fabric permeability	cfm	75, 215, 350, no felt
sheet basis weight	g/m^2	50, 100
sheet furnish	-	News, TMP, Kraft, CCS

The equilibrium hot plate temperature is a function of the electric current through the elements, the duct air speed and the air temperature. The air speed is a primary function of the fan input power, whilst air temperature and the permeability of the dryer fabric, which partially blocks inlet air through the slot in the duct floor, are second order effects. Dryer fabric permeability is traditionally specified in terms of *cfm*, cubic feet per minute

of air passing through a square foot of fabric under a pressure differential of 0.5" water gauge (Rhyne, 1989). The test referred to as 'no felt' was set up by replacing the fabric by six equally spaced lengths of nylon line (0.5mm diameter) across the 225mm duct cross-section so that the contact pressure between paper and hot plate is unchanged but the mass transfer is able to occur without the impediment of the felt. This test was performed under the same applied tension as for the fabric tests.

The four sheet furnishes tested were 100% samples each of thermo-mechanical pulp (TMP), kraft pulp and cold caustic soda pulp (CCS) and a newsprint-style furnish consisting of approximately 75% TMP, 20% CCS and 5% kraft. This final mixture represented the typical composition of the newsprint actually produced on ANM's paper machines.

For the nominated values of the parameters listed above there are $5\times4\times4\times4\times2\times4 = 2560$ possible sets of drying conditions. With up to 16 data points per drying curve this would equate to over 40,000 individual drying tests. Clearly this is not feasible, so the technique adopted is to define a *standard drying test* and vary just one parameter at a time from this reference point. This gives rise to $1+4+3+3+3+1+3 = 18$ different drying conditions. The *standard drying test* selected had the operating parameters set as follows : 5A heater current, 150V fan voltage, 400N felt tension, 350 cfm felt permeability, 50 g/m^2 basis weight and the newsprint furnish.

Under most conditions ten minutes proved sufficient to dry the paper sheet fully to its equilibrium moisture content for the given conditions. A number of trials were conducted to obtain data points at intervals up to this maximum drying time. Typically 16 data points were obtained at 30 second intervals for each set of drying conditions constituting a trial. Readings of moisture content before the 30 second mark of any drying trial proved impractical due to the relatively time-consuming steps involved in removing the sheet from the duct and weighing it.

For each paper sample, corresponding to a single point on the moisture content ~ time relationship, the sheet was weighed after the designated drying time with the thin aluminium backing plate for support. This was done immediately after removal from the drying duct. The result was then differenced from each aluminium plate's standalone mass. The partially wet paper sheet was then oven-dried at 105°C in order to obtain the moisture content.

5.2 Normalisation of drying results

To integrate drying trials to form a single curve and then make comparisons between curves produced from different drying conditions, it was necessary to normalise the initial state of the paper sheets. This ensured that variations in sheet basis weight and initial moisture content were taken into account when plotting drying curves. The temperature of the hot plate also varied slightly between tests at the same nominal operating conditions. This occurred as a result of the sharp temperature drop experienced by the hot plate when the cold aluminium backing plate with accompanying wet paper sample was placed in contact with it. This upset the temperature equilibrium of the system in a manner not precisely repeated at each trial.

The mathematical model developed in Chapter 3 is too complex to describe in analytical terms the effect of the variables, basis weight, initial moisture content and hot plate temperature, on drying rate. To normalise the experimental results for such perturbations in test conditions it is necessary to define a first order approximation of the drying process. Given that the variation of these parameters from their nominally standard values is at most ±10%, the accuracy of a correction based on the following relatively straightforward drying rate equation should be satisfactory.

For temperatures below 100°C, as experienced in the laboratory tests, where the bulk flow mechanism described in Section 3.3.3 is inactive, the drying rate from the felt-covered side of the sheet is given by,

$$\dot{m} = h_m A^* (\rho_{surf} - \rho_{air}), \tag{5.1}$$

and,

$$\dot{m} = \frac{(M_{init} - M_{final})}{\Delta t} \frac{M_{init}}{M_{final}} b_{wt} A^*. \tag{5.2}$$

The duct air velocity, fluid (air) temperature and drying geometry are nominally constant throughout each individual drying test. Variations in hot plate temperature over the duration of a test are no greater than 10°C. This perturbation translates to maximum variations of Prandtl number of 0.25%, Schmidt number of 0.75% and Reynolds number of 0.75%. Thus, it is reasonable to assume that the Nusselt and Sherwood numbers are static within these tolerances over the duration of a specific test. The relative constancy of these numbers means that the respective heat and

mass transfer coefficients vary by less than 3% over the peak temperature range observed.

The following analysis takes account of these data and makes the assumption that the mass transfer coefficient remains constant throughout the drying process, $hm_{init} = hm_{final}$, and,

$$h_m = \frac{M_{init}}{M_{final}} \frac{b_{wt}}{\Delta t} \frac{(M_{init} - M_{final})}{(\rho_{surf} - \rho_{air})}, \tag{5.3}$$

where, $\dot{m}$ = evaporation rate [kg/s],
h_m = mass transfer coefficient at paper surface [m/s],
M_{init} = initial moisture content [kg_{water}/kg_{fibre}],
M_{final} = final moisture content [kg_{water}/kg_{fibre}],
ρ_{surf} = vapour concentration in air at sheet surface [kg/m^3],
ρ_{air} = water vapour concentration in air [kg/m^3],
Δt = drying time [s],

the sheet dry basis weight, b_{wt}, is expressed as,

$$b_{wt} = \frac{m_{fibre}}{A} \ [kg/m^2], \tag{5.4}$$

where, A = actual sheet area [m^2], and,
m_{fibre} = mass of dry fibre [kg],

and the active drying area, A^*, is a quantity that reduces with drying according to,

$$A^* = \frac{M_{final}}{M_{init}} A. \tag{5.5}$$

The inclusion of A^* in this drying representation is a consequence of the need to normalise the mass transfer coefficient to the available surface area for evaporation. The paper sheet is a matrix of fibres, water-filled pores and empty pores. Water evacuates preferentially from the large radii pores, leaving these pores empty and in doing so reducing the surface area available for evaporation to take place. For a constant sheet thickness, the empty pore area is proportional to the amount of moisture evaporated, and hence the wetted pore area, A^*, is proportional to the fractional amount of

moisture remaining in the sheet. The ratio, A^*/A, can be related to the Chapter 3 description of the pore radius model by,

$$\frac{A^*}{A} = \frac{M_{final}}{M_{init}} = \frac{\beta(r_{final}; a+2, b)}{\beta(r_{max}; a+2, b)} = \beta(r_{final}; a+2, b). \qquad (5.6)$$

Including the quantity, A^*, rather than actual area, A, in the defining equation (5.1) allows the mass transfer coefficient, h_m, to remain independent of moisture content and consequently act as an invariant normalising tool as expressed in equation 5.3.

The process of normalising the data involves finding a corrected value for either M_{final} or Δt, allowing h_m to remain constant when one of the three parameters in question deviates from the assumed standard value for the given drying test. The correction for each of the three parameters is performed independently.

In the three normalising equations that follow, variables with the subscript $_{std}$ refer to the corrected version of that variable under the 'standard' conditions defined for that particular test. Unsubscripted variables represent the actual drying time, moisture content, vapour density or basis weight measured during the drying trial.

5.2.1 Initial moisture content correction

From equation 5.3,

$$\frac{M_{init}}{M_{final}}(M_{init} - M_{final}) = \frac{M_{init_{std}}}{M_{final_{std}}}(M_{init_{std}} - M_{final_{std}}) = \text{constant}, \qquad (5.7)$$

whence the corrected final moisture content, $M_{final_{std}}$ can be evaluated as,

$$M_{final_{std}} = \frac{M_{init_{std}}^2}{M_{init_{std}} + \frac{M_{init}}{M_{final}}(M_{init} - M_{final})}. \qquad (5.8)$$

5.2.2 Basis weight correction

Again using equation 5.3 as a foundation it is apparent that,

$$\frac{b_{wt}}{\Delta t} = \frac{b_{wt_{std}}}{\Delta t_{std}} = \text{constant}, \tag{5.9}$$

so that,

$$\Delta t_{std} = \frac{b_{wt_{std}}}{b_{wt}} \Delta t. \tag{5.10}$$

5.2.3 Surface temperature correction

Variations in hot plate temperature manifest themselves in terms of changes in the vapour concentration gradient which is the driving potential for mass transfer from the paper sheet. With the other variables in equation 5.3 held constant the correction for surface temperature can be expressed by,

$$\frac{1}{(\rho_{surf} - \rho_{air})\Delta t} = \frac{1}{(\rho_{surf} - \rho_{air})_{std} \Delta t_{std}} = \text{constant}, \tag{5.11}$$

so that,

$$\Delta t_{std} = \frac{(\rho_{surf} - \rho_{air})}{(\rho_{surf} - \rho_{air})_{std}} \Delta t, \tag{5.12}$$

where,

$$\rho_{surf} = \frac{P_{sat}(T_{surf})}{R T_{surf}}, \tag{5.13}$$

$$\rho_{air} = \frac{\phi P_{sat}(T_{air})}{R T_{air}}, \tag{5.14}$$

T_{surf} = paper sheet surface temperature [°K],
T_{air} = drying air temperature [°K],
$P_{sat}(T)$ = saturation vapour pressure at temperature T, [Pa],
ϕ = relative humidity,
and, R = gas constant for water vapour [J/kg°K].

5.2.4 Standard drying parameters

For the purposes of displaying the drying data graphically the results are normalised to a set of standard conditions as defined by the following values :-

- basis weight, $b_{wt_{std}} = 50$ g/m^2.
- initial moisture content, $M_{init_{std}} = 5$ kg$_{water}$/kg$_{fibre}$.
- hot plate surface temperature, $T_{plate_{std}} = 65°C$.
- ambient air temperature, $T_{air_{std}} = 20°C$.
- ambient air humidity, $\phi_{std} = 0.40$.

These nominal values represent the typical operational settings used in the majority of trials. For the trials that examine the variation of drying rate with hot plate temperature and basis weight there will be different standardising values for these two parameters. Drying tests were performed with nominal hot plate temperatures of 20°C, 30°C, 45°C and 85°C. Paper sheets with basis weight of 100 g/m^2 were also trialled.

The felt tension was controlled sufficiently accurately to its nominal value of 400N that no correction needs to be made for this parameter. The same is true of the air velocity which is measured with a pitot-static tube and an inclined manometer.

5.3 Drying results

The major results from the drying tests are presented in Figures 5.6-5.11. Individual graphs show the change in drying rate with each of the six variable parameters included in the test set-up. The data points presented in these graphs have been corrected for variations in surface temperature, air temperature, air humidity, basis weight and initial moisture content according to equations 5.8, 5.10 and 5.12.

Due to the closeness of some of the sets of results the curves of best fit are not presented in Figures 5.6-5.11. The equations for these curves are quoted in Section 5.4.

The fundamental experimental input parameters are heating element current, fan voltage and felt tension. The dependent physical quantities which are useful in the actual analysis are hot plate temperature, air speed

and felt tension per unit width respectively. The relationships between the two sets of data are shown in Table 5.2 below.

TABLE 5.2
Input~resultant drying variables

Input value		Resultant value	
Heater current (Amp)	0	20	**Hot plate temperature (°C)**
	3	30	
	4	45	
	5	65	
	6	85	
Fan voltage (V)	0	0	**Velocity (m/s)**
	100	8.1	
	150	11.3	
	180	14.1	
Felt tension (N)	50	220	**Felt tension per unit width (N/m)**
	200	890	
	400	1780	
	600	2670	

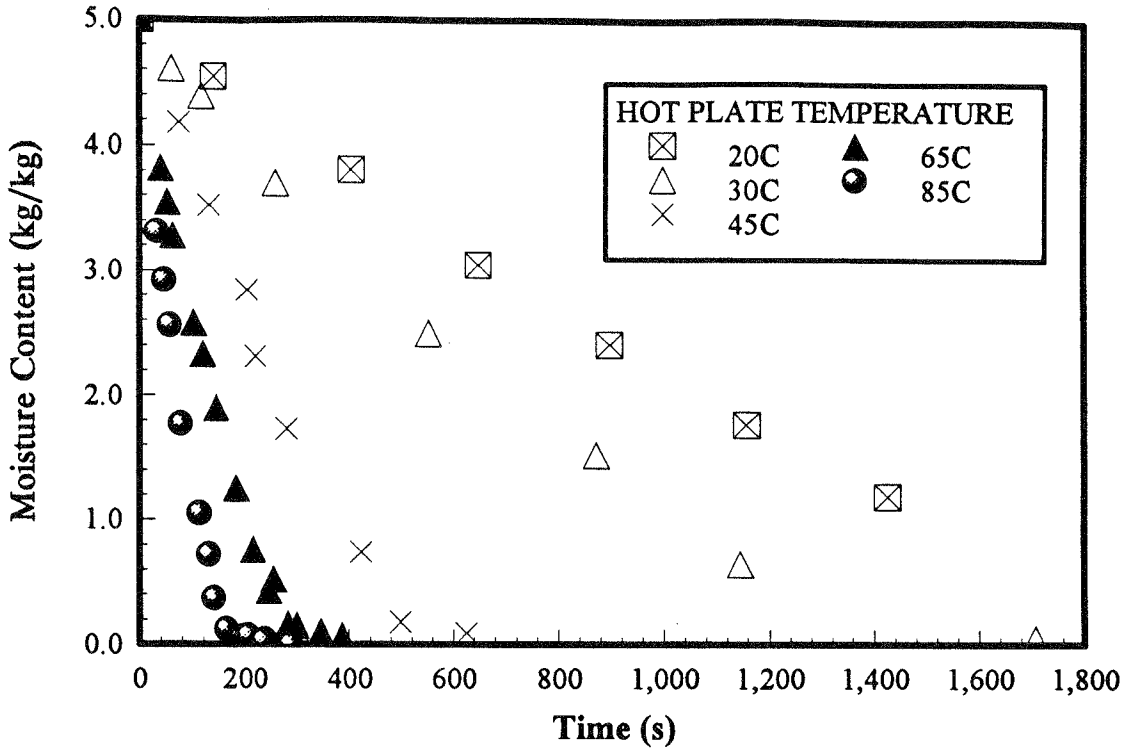

FIGURE 5.6
Drying curves for varying hot plate temperature

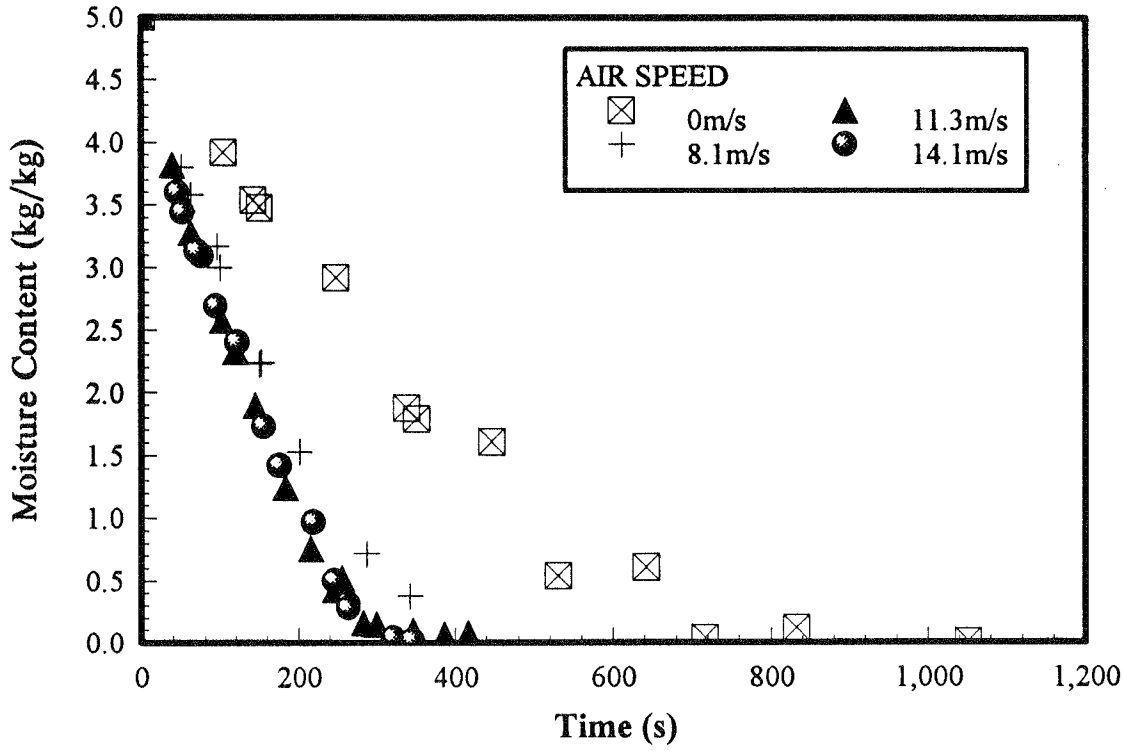

FIGURE 5.7
Drying curves for varying air flow rate

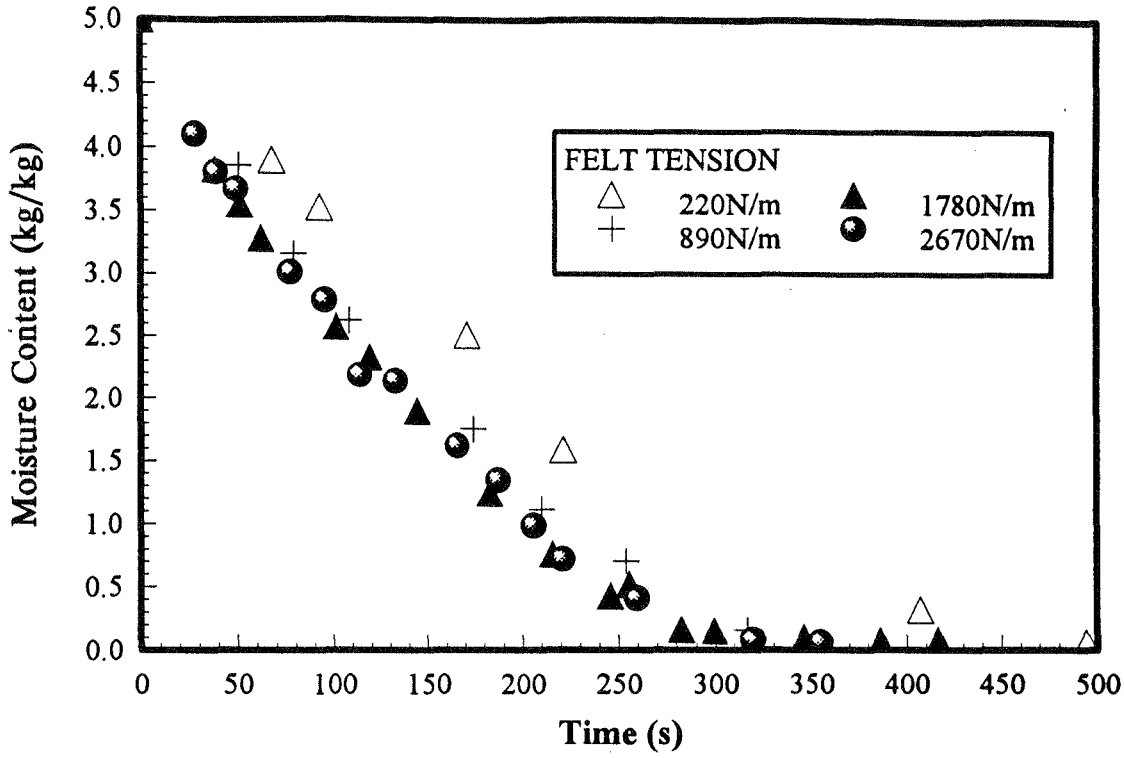

FIGURE 5.8
Drying curves for varying felt tension

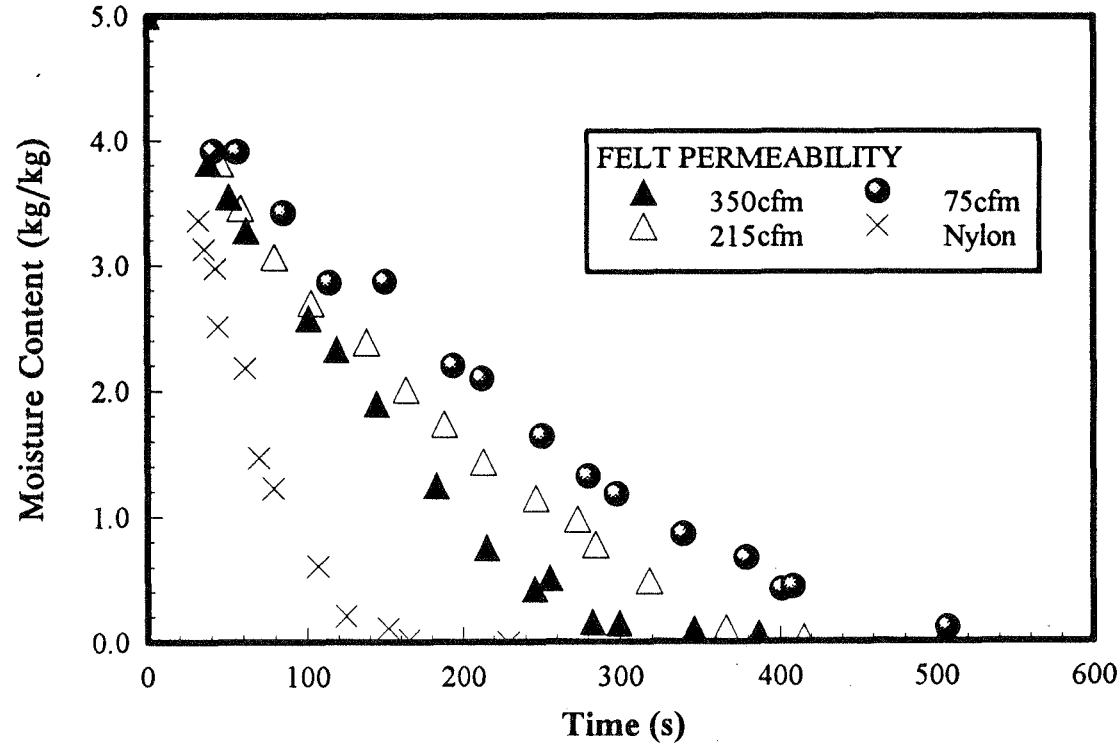

FIGURE 5.9
Drying curves for varying felt permeability

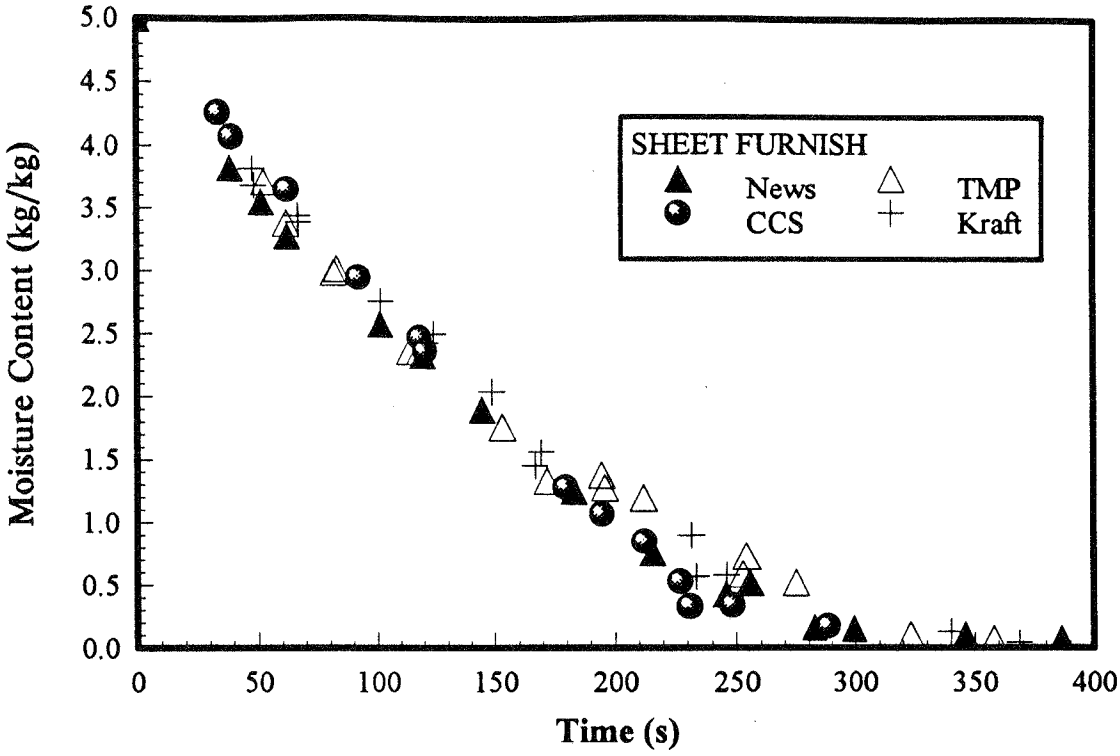

FIGURE 5.10
Drying curves for varying sheet furnish

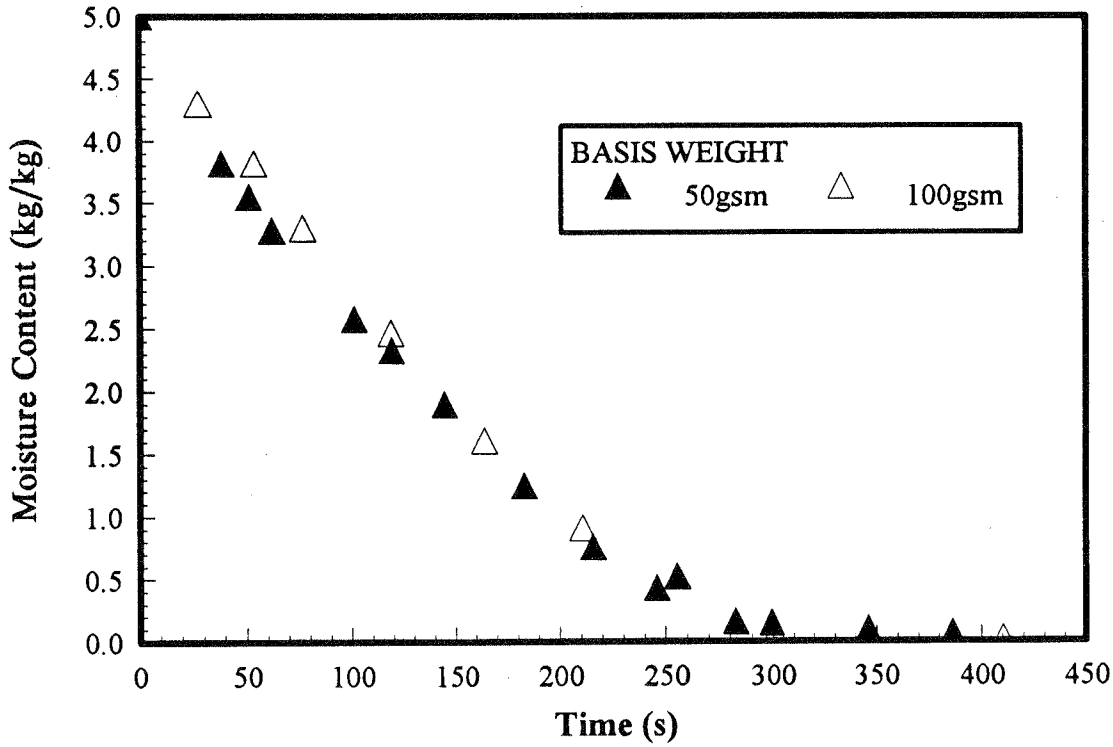

FIGURE 5.11
Drying curves for varying sheet basis weight

5.4 Analysis and discussion of drying results

Each of the 18 drying data sets presented in Figures 5.6-5.11 is represented by a best fit curve of the form,

$$M = a \exp(b(t + c)^d), \qquad (5.15)$$

where, M = moisture content on a dry basis (kg_{water}/kg_{fibre}),
t = drying time to reach moisture content M, (seconds), and,
a, b, c, d are constants chosen to achieve the best fit for each of the drying curves.

These best fit curves are generated by a least squares fit to the normalised drying data. The normalising (standard) values for temperature, relative humidity and basis weight for individual curves are different to those quoted earlier for graphical presentation. In the previous instance the intention was to standardise the data so that each curve could be compared with the others on an equivalent basis. In this case the aim is to provide coherence to the data points of each individual trial by using average values for that trial as the standardising values. Using the average values leads to less potential normalising error than using the nominal values quoted in Section 5.2.

For example, in the case of the 75cfm felt trial the relevant standardising values are $T_{plate} = 68.6°C$, $T_{air} = 22.6°C$, $\phi = 0.378$ and $B_{wt} = 51.2\ g/m^2$. These values represent the averages over the 16 points which combine to form the drying curve. These values also represent the conditions input to the theoretical model to determine the transfer coefficients for the 75cfm trial.

Thus, the smoothed version of the drying data is used to represent the experimental results and provides a comparison base for the mathematical model. The mass transfer coefficient used by the model is varied until the model's drying rate curve best matches the smoothed experimental results. This iteration procedure is employed to obtain a mass transfer coefficient for each of the drying trials.

The best fit parameters, a, b, c and d, for the 18 drying curves are quoted in Table 5.3.

TABLE 5.3
Best fit parameters for drying curves

Parameter	Value	a	b	c	d
Hot plate temperature (°C)	20	5.621	-4.142×10^{-6}	466.1	1.677
	30	5.813	-3.541×10^{-6}	400.4	1.799
	45	5.791	-2.875×10^{-7}	205.6	2.475
	65	7.899	-6.275×10^{-8}	294.7	2.791
	85	8.772	-3.904×10^{-6}	166.8	2.325
Velocity (m/s)	0	6.316	-3.296×10^{-7}	452.4	2.213
	8.1	8.340	-3.821×10^{-6}	272.1	2.112
	11.3	7.899	-6.275×10^{-8}	294.7	2.791
	14.1	7.255	-1.270×10^{-6}	209.1	2.377
Felt tension (N/m)	220	6.586	-6.583×10^{-7}	183.3	2.488
	890	8.061	-1.706×10^{-7}	263.0	2.669
	1780	7.899	-6.275×10^{-8}	294.7	2.791
	2670	7.056	-5.557×10^{-6}	217.4	2.068
Permeability (cfm)	75	6.792	-10.30×10^{-6}	208.1	1.959
	215	12.01	-4.284×10^{-7}	459.3	2.377
	350	7.899	-6.275×10^{-8}	294.7	2.791
	Nylon	7.210	-7.445×10^{-8}	149.4	3.079
Pulp furnish	News	7.899	-6.275×10^{-8}	294.7	2.791
	CCS	5.480	-7.284×10^{-7}	178.5	2.308
	TMP	9.489	-6.395×10^{-6}	230.3	2.119
	Kraft	5.885	-11.35×10^{-6}	111.1	2.067
Basis weight (g/m^2)	50	7.899	-6.275×10^{-8}	294.7	2.791
	100	5.508	-4.153×10^{-6}	169.4	1.995

5.4.1 Hot plate temperature

The first set of test results as displayed in Figure 5.6 show the variation of drying rate with hot plate temperature. The hot plate temperature is varied from the ambient value of 20°C with no electric heating, to a maximum of

85°C with a total of six amps current flowing through the three parallel resistive elements (Q_{total} = 800W). In the latter trial the hot plate temperature was initially 100°C but dropped quickly when brought into contact with the cold aluminium backing plate. This initial drop in hot plate temperature typically occurred over a period of 50-80 seconds, depending upon the individual trial conditions. The variation was monitored by the datalogger and used in analysing the drying curves. A sample graph of average plate temperature and fabric tension plotted against time is shown in Figure 5.12.

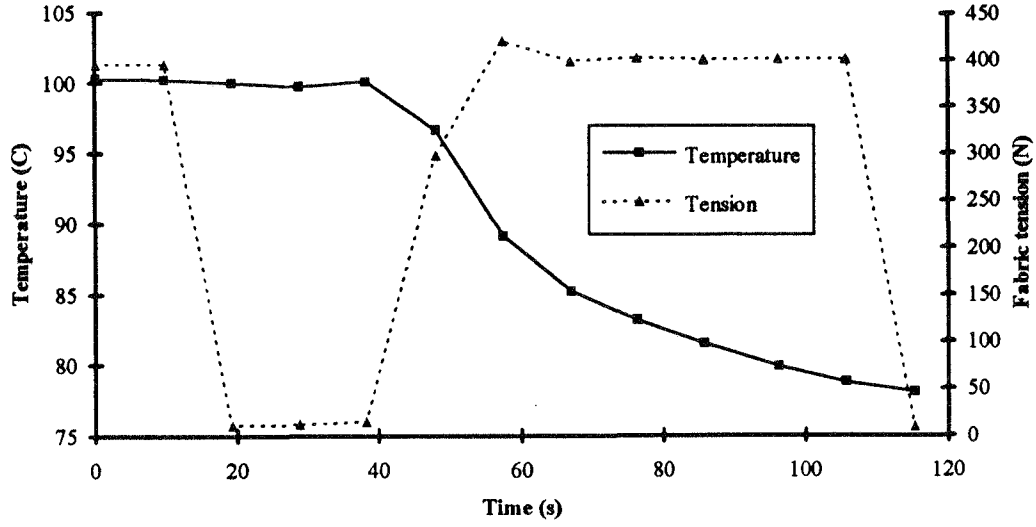

FIGURE 5.12
Sample temperature-time datalogging results for a single point on the drying rate curve of Figure 5.6

In the trial depicted in Figure 5.12 the drying time commences at the 38 second point on the x-axis. This time offset which occurs due to the datalogging procedure is corrected prior to analysis and the preparation of the graph in Figure 5.6.

Given that each data point is generated from a separate trial the scatter of each set of data points about its respective best fit curve is minimal. In the case of Figure 5.6 the maximum departure of data from the best fit curve is 0.2 kg/kg moisture with an average discrepancy of below 0.09 kg/kg.

The results demonstrate the effect of surface temperature on drying rate whilst the surface heat and mass transfer coefficients are maintained approximately constant. For each of the five hot plate temperatures tested the air speed, felt permeability and felt tension are unchanged. The hottest setting used (85°C) is sufficiently close to actual paper machine drying cylinder temperatures which are usually in the range of 90-100°C.

5.4.2 Air flow rate

The relationship between air flow and drying rate is illustrated by the graph of Figure 5.7. The four tests undertaken to generate this data set involved running the duct fan at a number of voltage levels. These voltage inputs correspond to free stream air velocities ranging from no flow through to a maximum of 14 m/s over the full duct and 18 m/s as the local peak over the curved hill of the hot plate. An air velocity of 18 m/s simulates a paper machine running at 1080 m/min. This is appropriate as the two paper machines of particular relevance to this study operate at speeds of 850 m/min through to 1100 m/min depending upon paper grade. The drying rate graphs in Figure 5.7 show a maximum departure of data from the best fit curve of 0.23 kg/kg moisture with an average discrepancy of 0.10 kg/kg. The rate of drying is observed to increase with the flow of air over the paper sheet and drying felt. The extent of this is quantified by the mass transfer coefficients calculated in Section 5.5.

5.4.3 Dryer felt tension

Figure 5.8 demonstrates quite clearly the effect of dryer felt tension on paper sheet drying rate. The range studied of 50N to 600N tension was determined as a function of the available equipment and actual paper machine conditions. The tensioning equipment within which the felt was mounted provided a minimum of 50N tension as a result of the gravitational effects. At the other end of the scale paper machine felts generally operate at 1.7kN/m$_{width}$ which for the 0.225m dryer felt under test equates to 385N. Thus 1.8kN/m (400N) was selected as one of the intermediate tension values and 2.7kN/m (600N) as an upper bound which extended the testing range whilst staying within the mechanical limits of the system. A 0.9kN/m (200N) test made up the fourth felt tension value for this study.

The resultant plots of drying rate are seen to be quite coherent with average deviations from the best fit curves of 0.08 kg/kg and a peak

deviation of 0.19 kg/kg. The results demonstrate that dryer fabric tension does influence paper drying rate through improving the contact between the hot plate and paper sheet. However, the effect of increasing fabric tension diminishes at higher values. This is evidenced by the 2.7kN/m curve drying at a comparable rate with the 1.8kN/m trial.

These results do reinforce the current mode of paper drying with a usual maximum felt tension of 1.7kN/m$_{width}$. Further increases in felt tension above this value will only place additional stress on mechanical components and the felts themselves without achieving any significant drying benefit.

5.4.4 Dryer felt permeability

The effect of dryer felt permeability on drying rate is examined in Figure 5.9. The four configurations tested include three actual paper machine drying felt samples of differing permeability and a fourth set-up where the drying felt is replaced by a series of nylon tensioning lines. This 'nylon' arrangement enables the unimpeded mass flow to be determined. The dryer fabrics are rated in terms of *cfm*, cubic feet per minute of air passing through a square foot of fabric under a standard pressure differential of $^1/_2$" water gauge. In these terms the nylon arrangement is designated ∞ cfm. The results demonstrate considerable differences in permissible drying rate. The 75cfm dryer fabric is seen to slow the drying rate to almost half of the more permeable 350cfm case. The nylon wire configuration is shown to be twice as conducive to mass flow again. The worst of the data points shows a 0.26 kg/kg deviation from the least squares fit. The average scatter for the four curves is below 0.12 kg/kg in each case.

5.4.5 Sheet composition

The effect of furnish composition on drying rate behaviour is presented in Figure 5.10. The results indicate that varying the pulp furnish has only a mild effect on drying rate. There is a degree of scatter in the results up to a maximum deviation from the best fit curves of 0.22 kg/kg. The normalised data suggest that the sheet formed by the cold caustic soda (CCS) pulp dries more quickly than either the kraft sheet or the sheet composed of a mixture of the three pulps in proportion similar to that of the paper machine newsprint mixture, 75% TMP, 20% CCS and 5% kraft. The results show the thermo-mechanical pulp (TMP) to dry marginally slower than the other pulps included in this study. It is interesting to note paper

machine operators' experience which suggests kraft is the fastest drying pulp, whilst CCS is the slowest which appears contradictory to the results presented here. This is best reconciled by consideration of the initial moisture content of the paper in each situation. In the laboratory all moisture contents are normalised to a constant value, whilst in the paper machine the moisture content at dryer inlet will vary depending upon the pressability and drainage characteristics of the paper sheet as well as general runability. Hence the appearance of slower drying for the CCS furnish is most likely due to an increased paper sheet moisture content at the juncture between press exit and dryer inlet.

5.4.6 Sheet basis weight

Figure 5.11 demonstrates the effect of basis weight on drying rate. The results indicate that the normalisation procedure satisfactorily collates data points from different trials. Whilst the 100 g/m^2 sheet physically dries in twice the time of a 50 g/m^2 sheet, when the corrections of equations 5.8, 5.10 and 5.12 are applied the two drying curves are practically indistinguishable. The two curves are relatively smooth in showing a maximum variation from best fit of approximately 0.16 kg/kg.

5.5 Calculation of mass transfer coefficients

The exponentially-based best fit curves presented in Section 5.4 encapsulate the results from the 18 distinct drying trials. These smoothed formulations become target drying profiles when input into a computerised algorithm which seeks to determine the optimal mass transfer coefficient which best matches the observed laboratory drying rate to the prediction of the mathematical model developed in Chapter 3.

A least squares criterion is used for assessing how well the calculated drying curve, generated from a given estimate of mass transfer coefficient, matches the experimentally determined curve. For each time increment used in the theoretical calculation, the square of the difference between the model predicted sheet moisture content, M_{mod}, and the moisture content generated by the best fit drying curve, M_{bf}, is added to a cumulative total. In mathematical terms,

$$\text{Sum} = \sum_1^{\text{timesteps}} (M_{mod} - M_{bf})^2, \qquad (5.16)$$

The aim of the series of calculations is to vary the mass transfer coefficient so as to minimise the sum of the errors squared. Attaining the smallest value, the least sum of squares, is the indication that the most appropriate mass transfer coefficient has been identified.

Solving for mass transfer coefficients in this way is a computationally intense procedure. Integrating the model's differential equations just once for a complete drying trial takes up to 10 minutes on a 486 based PC (33MHz) with co-processor. Searching for the optimal input value requires multiple model integrations. Hence, with such a high computational overhead it is strongly desirable to minimise the number of test calculations required to pinpoint the correct mass transfer coefficient. Thus, rather than instigating a binary search between known lower and upper limits an accelerated searching algorithm was used.

Specific computer code was developed to solve for the appropriate value of mass transfer coefficient, h_m. The Pascal program written for the implementation of the model described in Chapter 3 became the core routine of the new code. A framework was placed around this core calculation to enable multiple calculations with different input values for mass transfer coefficient.

The solving process begins with a procedure to determine a range within which the solution lies. This bracketing routine was based on that described by Press et al (1987). It begins with two values and expands the range until a minima is contained within two outer bounds. Once the function's minimum is bracketed Brent's (1973) method is used for finding it quickly. The algorithm assumes the function is smooth near the minimum and uses the technique of inverse parabolic interpolation to find the value. The function returns the minimum within an input fractional tolerance which should be larger than the square root of the computer's floating point precision. Unnecessarily small tolerances will retard the solution process without adding any meaningful precision to the final answer. Since the input data is based on smoothed drying curves with a typical average scatter of around 2% there is no justification for refining the input computational tolerance significantly beyond this limit.

Access to a Sun Workstation was obtained for this series of computations. A number of these iterative calculations for mass transfer coefficient were prepared in a batch file and the program was then set to run overnight.

Applying these algorithms to each of the 18 drying trials obtains the mass transfer coefficients set out in Table 5.4.

TABLE 5.4
Mass transfer coefficients

Parameter	Value	Mass transfer coefficient (m/s)
Hot plate temperature (°C)	20	0.0144
	30	0.0126
	45	0.0143
	65	0.0126
	85	0.0133
Air velocity (m/s)	0	0.0045
	8.1	0.0098
	11.3	0.0126
	14.1	0.0134
Felt tension (N/m)	220	0.0134
	890	0.0123
	1780	0.0126
	2670	0.0115
Felt permeability (cfm)	75	0.0078
	215	0.0104
	350	0.0126
	Nylon	0.0303
Pulp furnish	News	0.0126
	CCS	0.0135
	TMP	0.0114
	Kraft	0.0124
Basis weight (g/m^2)	50	0.01264
	100	0.01286

The six groups of results correspond to the variable parameters which feature as part of the experimental drying set-up. The mass transfer coefficients for the hot plate temperature and sheet basis weight variation should be relatively constant, whilst the other parameters will generate trends in the mass transfer coefficient. These trends will be quantified and made use of in the application of the computational model under a range of operating conditions.

5.5.1 Hot plate temperature

Variations to hot plate temperature will alter sheet temperature and hence the vapour concentration gradient between the sheet surface and drying air. This will provide a corresponding change in drying rate whilst the mass transfer coefficient should remain largely unchanged. The results in Table 5.4 demonstrate a relatively constant mass transfer coefficient of around 0.013 m/s. The small fluctuations evident are indicative of the degree of manipulation of the data required to convert the mass of a sample of wet paper at a defined time into a drying rate curve with its associated coefficient of mass transfer. To this end it must be borne in mind that drying data must first be normalised, then summarised by a best fit curve and finally matched to a theoretical drying curve. The complexity of these three mathematical manipulations will quite reasonably lead to minor fluctuations in a common calculated value.

5.5.2 Air velocity

There are many documented correlations for heat and mass transfer coefficients for flow over a flat plate or over a curved cylinder. The geometry of a curved hot plate in an enclosed duct is midway between the classical flat plate situation and that of cross flow over a cylinder. The variation of mass transfer coefficient with air velocity as depicted in Figure 5.13 supports this. The flat plate correlation used in Figure 5.13 is based on Schlicting's (1968) friction coefficient and the Chilton-Colburn (1934) analogy for heat and mass transfer. In terms of the Sherwood number the flat plate correlation is,

$$Sh_L = 0.037\,Re^{4/5}Sc^{1/3}, \qquad (5.17)$$

where, Sherwood no. $= Sh_L = \dfrac{h_m L}{D_{AB}}$,

$$\text{Reynolds no.} = Re_L = \frac{uL}{\nu},$$

$$\text{Schmidt no.} = Sc = \frac{\nu}{D_{AB}},$$

and,

h_m	=	mass transfer coefficient [m/s],
L	=	plate length [m],
D_{AB}	=	diffusivity of water vapour in air [m^2/s],
u	=	free stream air velocity [m/s], and,
ν	=	kinematic viscosity [m^2/s].

In calculating the dimensionless groups the plate length is 0.225m and the physical properties assumed for air are presented in Chapter 10. Properties are evaluated at the *film temperature*, T_f, as defined by McAdams (1985),

$$T_f = \frac{T_{plate} + T_{air}}{2}, \tag{5.18}$$

where, T_{plate} is the surface temperature of the hot plate and T_{air} the temperature of the freestream air flow.

The correlation used for the mass transfer coefficient of a cylinder in cross flow is that of Zkukauskas (1975),

$$Sh_L = 0.076 Re^{0.7} Sc^{0.37} \left(\frac{Sc_\infty}{Sc_s} \right)^{1/4}, \tag{5.19}$$

where the subscript ∞ denotes the free stream and s the surface conditions. This correlation applies for Reynolds numbers in the range from 2×10^5-10^6 and Schmidt numbers less than 10. The Schmidt number is 0.58 whilst the Reynolds number criterion is satisfied for velocities between 3 and 15 m/s.

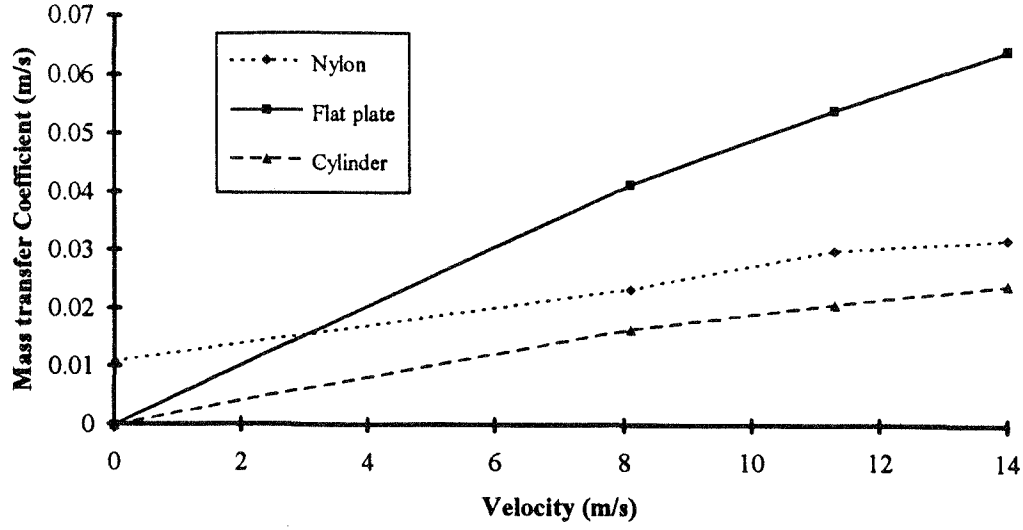

FIGURE 5.13
Mass transfer correlations for a flat plate and cylinder in cross flow compared with curved hot plate results

The correlation which describes the observed variation of mass transfer coefficient with air speed for the paper drying experimentation is,

$$h_m = 0.00159u + 0.011 \text{ [m/s]}, \qquad (5.20)$$

where, h_m = mass transfer coefficient, and,
u = free stream air velocity.

Figure 5.13 shows the comparison between equations 5.17, 5.19 and 5.20.

Others to investigate the mass transfer coefficient for the paper drying process include Nederveen et al (1991) who use a turbulent model to obtain a theoretical prediction. Nederveen predicts a value of 0.038 m/s for a paper web speed of 10 m/s with no dryer fabric present. This value corresponds to the *nylon* trial of this study which tensions the paper sheet onto the hot plate while not offering an impediment to mass transfer and predicts a mass transfer coefficient of 0.0303 m/s at a velocity of 11.3 m/s.

Nederveen also quotes the work of Lemaitre (1978) who estimated the mass transfer coefficient to be 0.014 m/s with no dryer fabric at a web speed of 0.8 m/s. This is a very similar situation to the free convection case depicted by the y-intercept on the graph of Figure 5.13 which

suggests a transfer coefficient of 0.011 m/s with zero duct flow. The agreement is quite encouraging.

Others to quote mass transfer coefficients for drying calculations include Harrmann and Schulz (1991) and Hartley and Richards (1974) who used values of 0.034 m/s and 0.0303 m/s respectively for their simulation of paper drying in the open draw regions. Machine speeds were not quoted in these cases.

Free convection

The constant term in equation 5.20 arises for the case of natural convection with zero horizontal duct velocity. This can be estimated using the correlation of Goldstein et al (1973) for mass transfer by natural convection from horizontal flat plates of various geometries. Basing Sherwood and Raleigh numbers on a characteristic length, L*, defined as,

$$L^* = \frac{A}{P}, \tag{5.21}$$

where A is the plate surface area and P is the perimeter which encompasses the area, Goldstein defined a correlation which universally applied to most flat plate geometries. Those tested included circular, square and rectangular (aspect ratio 7:1) plates. For a mass transfer Raleigh number, $Ra_m^* > 200$, the Sherwood number, Sh*, correlation based on a characteristic length, L*, was found to be,

$$Sh^* = 0.59(Ra_m^*)^{1/4}, \tag{5.22}$$

where,

$$Ra_m^* = \frac{g(\rho_w - \rho_\infty)L^{*3}}{\rho_\infty \nu^2} Sc, \tag{5.23}$$

and,

g	=	gravitational acceleration [m/s^2],
ρ_w	=	water vapour concentration at surface [kg/m^3],
ρ_∞	=	water vapour concentration in surroundings [kg/m^3],
ν	=	kinematic viscosity of air [m^2/s], and,
Sc	=	Schmidt number.

The final calculation shows that Goldstein et al's correlation predicts a free convection mass transfer coefficient of 0.014 m/s compared to the

0.011 m/s obtained from the correlation resulting from the current series of tests. The discrepancy between the experimentally observed free convection mass transfer coefficient and Goldstein's prediction arises from the geometry of the experimental hot plate set-up under test. The curved profile of the test hot plate clearly a variation on Goldstein's flat plate experimentation. Furthermore, the experimental rig of this study was designed with the principal aim of monitoring forced convection mass transfer and hence the presence of the enclosing ductwork would cause deviations from the correlations developed by others in the area of free convection.

A correlation for free convection mass transfer from an inclined plate of arbitrary angle was obtained by Fujii and Imura (1972). Their results applied to rectangular plates of 6:1 aspect ratio and the correlations developed are difficult to apply directly to the current study. However, their results do demonstrate qualitatively that an inclined plate gives rise to a lower transfer rate than does a horizontal plate. Therefore it is reasonable that Goldstein's correlation over-estimates the free convection mass transfer coefficient observed in this study in which the angle of the leading edge of the hot plate from horizontal is 12.5°.

The free convection situation discussed above represents just one of a total of 18 drying trials conducted in this survey. Whilst the key results of the current paper drying investigation are clearly not significantly affected by free convection it was of interest to compare the results with the investigations of other researchers.

The comparative calculations made in this section seek to show how the mass transfer rates of the experimental set-up of this project under varying air velocity are reasonable when considered alongside the more standard and widely repeated physical arrangements documented in the literature. This was found to apply to both forced and free convection situations.

5.5.3 Felt tension

The mass transfer coefficients obtained from the trials at four different drying fabric tensions and listed in Table 5.4 are calculated with the aid of the contact heat transfer coefficients determined in the previous chapter. Raising the felt tension improves the overall contact between the paper sheet, the thin aluminium backing plate and hot plate, thereby increasing the contact heat transfer coefficient and promoting a higher paper

temperature which in turn increases drying rate. The contact heat transfer coefficients, evaluated previously and input into the computer simulation when optimising for the appropriate mass transfer coefficient for these trials, are listed in Table 5.5.

TABLE 5.5
Contact heat transfer coefficient as a function of felt tension

Felt tension (N/m)	Contact heat transfer coefficient ($W/m^2°C$)	Mass transfer coefficient (m/s)
220	170	0.0134
890	325	0.0123
1780	410	0.0126
2670	430	0.0115

For constant external conditions, i.e. same dryer felt, air flow and air conditions, the mass transfer coefficient must remain unchanged. The results of Table 5.5 support this with a maximum variation of 9% about the nominal standard value of 0.0126 m/s for the basecase.

The contact heat transfer coefficient data provide a useful basis for analysing the effect of felt tension in a paper machine. The indication is that increased felt tension improves drying rate up to a certain threshold. After this point (400N ≡1.78kN/m) further increases provide minimal drying benefit and simply increase mechanical strain on the system. This phenomenon has been reported previously in actual paper machine operation.

The TAPPI Technical Information Sheet TIS 0404-04 (1989) recommends a dryer felt tension of 1.85 kN/m for a newsprint machine with 1.5m diameter drying cylinders operating at 1050 m/min. The document notes that beyond this level the gains in heat transfer diminish whilst the higher tensions shorten fabric life, increase bearing loads and drive loads, and cause excessive deflection of fabric rolls. The optimal felt tension is essentially the most economic one when all cost factors are included.

It should be emphasised that the TAPPI recommendation is echoed by the tension value applied at ANM and by the point of diminishing returns indicated by comparison between the 400N (1.8 kN/m) and 600N

(2.7 kN/m) felt tension tests in this study. The experimental results reinforce the TAPPI claim and the ANM practice.

5.5.4 Felt permeability

The felt permeability category provides data which relate the vapour transfer impedance provided by dryer felts of various rated permeabilities. The felts tested had notional permeabilities of 75 cfm, 215 cfm, 350 cfm and P∞ cfm, where cfm is a non-standard unit used in the industry defined as cubic feet per minute of air passing through a square foot of the fabric under a pressure differential of 0.5" water gauge. The nominal value of P∞ cfm is set up by replacing the fabric by a number of lengths of nylon line so that the contact coefficient between paper and hot plate is unchanged for a given tension but the mass transfer is able to occur without the impediment of the felt.

The results of mass transfer coefficient for different fabric permeabilities are best indicated graphically. Figure 5.14 demonstrates the variation of mass transfer coefficient under the application of the range of fabrics. The plotting of the 75, 215 and 350cfm data points is straightforward. However, the equivalent cfm value for the trial with nylon tensioning line (P∞ cfm) is not obvious. Therefore an estimate was made for the volume flow rate of air (cfm) under the standard conditions of a pressure differential of 0.5" water gauge (125Pa) at which the three fabric felts were rated. Bernoulli's energy equation for an ideal fluid represents pressure differential in terms of ,

$$\Delta p = \rho_{water} g h = \frac{1}{2} \rho_{air} v^2, \qquad (5.24)$$

where, Δp = pressure differential [Pa],
ρ_{water} = water density [kg/m^3],
g = gravitational acceleration [m/s^2],
h = pressure head water gauge [m],
ρ_{air} = air density [kg/m^3], and,
v = air velocity [m/s].

The air velocity is the ratio of the volumetric flow rate, Q [m^3/s], and the flow area, 1 ft^2. Hence, the equivalent fabric permeability of the nylon 'feltless' tensioning arrangement at 0.5" water gauge pressure drop is calculated from,

$$1000 \times 9.81 \times 0.0127 = \frac{1}{2} \times 1.2 \times \left(\frac{Q}{0.3048^2} \right)^2, \qquad (5.25)$$

whence Q = 1.34 m^3/s, or 'fabric permeability' = 2840 cfm.

This is included in Figure 5.14 along with the theoretically extrapolated zero mass transfer at zero permeability. The results indicate a diminishing increase in mass transfer coefficient with increasing permeability, or,

$$\frac{d^2(\text{mass transfer coefficient})}{d(\text{permeability})^2} < 0. \qquad (5.26)$$

Progressively more permeable felts do not yield proportionally higher drying rates. This effect is important when specifying a particular felt for a given drying duty. The other prime aspect which should also be considered is the effect of air currents passing through a given felt on the stability of the paper sheet. This is a key issue which affects the runnability of the paper machine but is beyond the scope of the current study.

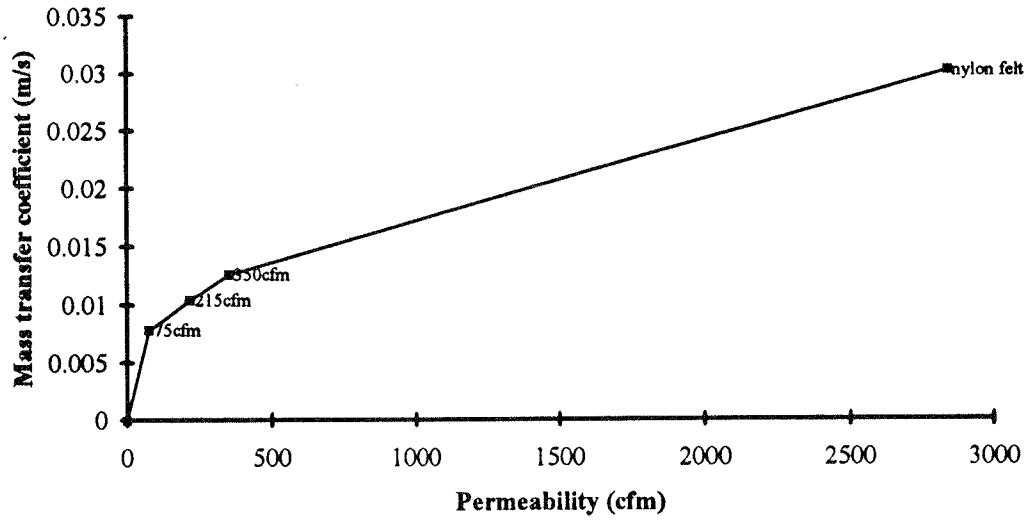

FIGURE 5.14
Variation of mass transfer coefficient with felt permeability

Within the typical range of operating felt permeability (75-350cfm) the data presents quite smoothly with a steady increase in mass transfer

potential for more permeable dryer felts. The 75cfm sample corresponds to a support felt which would be used in the early stages of the drying process. The first 6-12 dryer cylinders would be covered by a fabric of this permeability rating. The relatively thick weave fabric prevents excessive air flow from the pocket ventilating ducts being directed onto the wet paper sheet at this point and promoting a sheet break. As the paper dries and its strength increases accordingly the drying fabric permeability is increased at each felt run. This allows progressively more drying air into contact with the paper sheet and consequently improves drying rate. The final dryer sub-section felt is usually rated at around 350cfm.

The variation in mass transfer coefficients for different felt permeabilities is incorporated into the dryer model on a dryer sub-section basis. Sub-sections 1 and 2 (cylinders 1-12) employ a 75cfm fabric, sub-section number 3 uses a 215cfm fabric, and the final two sub-sections (cylinders 25-48) use 350cfm fabrics. The appropriate mass transfer coefficients from this test are input into the drying model in response to the changing machine boundary conditions which expose the paper sheet alternately to a period in contact with the fabric followed by a free draw period where the paper sheet is not in contact with a supporting fabric. This free draw phase is represented by the drying trial which employed the nylon tensioning arrangement which provided no impediment to mass flow.

Some scanning electron micrographs of a dryer fabric (felt) sample were presented in Figures 4.6 and 4.7. These photographs demonstrate the rough nature of the fabric surface. Relatively large gaps are evident between the monofilament polyester weave in the machine direction and the semi-porous cross-directional multifilament members which provide structural rigidity. These interstices allow for the passage of water vapour migrating from the paper sheet. Variations in the weave pattern, filament diameter and spacing influence the felt permeability and surface roughness, which in turn controls air flows in and amongst the dryer pockets.

The nylon tensioning trial which simulates free drying is important for the comparisons it gives with more general heat and mass transfer experimental work performed by others as well as providing information for heat and mass transfer form the open draw section of the paper machine drying run. The open draw as described in Chapter 3 is the region of paper sheet running between consecutive drying cylinders. In this region the paper sheet is not supported by the drying fabric but is exposed on both sides to drying air. This is only possible in dryer sub-sections 3,4 and

5 where the paper sheet is sufficiently dry and has enough strength to negotiate such a gap unsupported.

5.5.5 Pulp furnish

The drying rate results for the various pulp furnishes tested are difficult to predict quantitatively without an exhaustive microscopic study and theoretical simulation of fibre size, orientation and bonding characteristics with both similar and dissimilar fibres. Initially this was intended as part of the scope of the present drying study, however, the preliminary investigation undertaken as part of Chapter 6 suggested that the magnitude of work represented a complete study in itself. Consequently, it was deemed acceptable to simply measure the variation in drying rate for different pulps rather than attempt to predict it theoretically from the interaction of fibre geometries.

The consequence of this is that it is not possible to separate the effect of the sheet's internal fibre matrix on drying rate, as determined by the component pulps, from the effect of the surface mass transfer coefficient on drying rate.

The calculated mass transfer coefficients for the four pulp mixtures tested are observed to vary within a relatively small bandwidth. The small deviations between the four samples are brought about by internal drying mechanisms. The configuration of the fibre network specific to each pulp variety governs the liquid and vapour flow paths within the sheet. Such changes in sheet tortuosity and permeability do influence the drying rate and this effect is perceived as a change in mass transfer coefficient according to the algorithm defined at the start of Section 5.5. This perception arises since there is no theoretical prediction for the relationship between fibre species and pore size distribution included in the model for the reasons expressed in the preceding paragraph and expanded upon in Chapter 6.

In summary, the presence of different pulps in comparative trials changes the paper sheet's liquid permeability and vapour diffusivity and since this relationship is not modelled explicitly the calculation method which optimises for just the one variable, interprets the trials as having mildly varying mass transfer coefficients.

With these limitations in mind it is observed that the drying rates vary within a ±10% zone about the *newsprint* furnish which is a mixture of 75% TMP, 20% CCS and 5% kraft. The TMP pulp is observed to be the slowest drying of the four combinations tested. It shows a drying rate 9.5% below that of the newsprint furnish which may be regarded as the blended mean. The CCS pulp dries 7% faster than the newsprint whilst the kraft is about 1.5% slower.

ANM newsprint is typically made from a blend very similar to the recipe described above. However, other paper grades which have different strength or appearance requirements use variations on the mixture and this may be significant from the viewpoint of drying rate or drying energy per unit of product. The complicating factor in this forecasting is the differences in the way the three pulps react to the papermaking processes upstream of the dryer section. The twin-wire former and press section are essentially dewatering processes which are extremely dependent upon the structure of the paper sheet fibre network. The experiences of paper machine operators suggests that CCS makes the greatest demands on the drying energy required whilst kraft requires considerably less. Such differences are not a result of the weak variations in drying behaviour for the various pulps but rather considerable differences in the forming and pressing characteristics of these materials. For example, with all other parameters unchanged, a CCS-rich paper sheet will have a higher initial moisture content at entry to the dryer section. This increases the dryer section energy requirement and makes CCS appear to be a slow drying pulp.

The difficulty with supporting these arguments with actual paper machine drying data arises from the absence of an on-line moisture content analyser between the press and dryer sections. This means that the inlet paper sheet moisture content is logged on a monthly basis only by manual sampling prior to a planned machine maintenance shutdown. Consequently there is no real-time feedback between pulp furnish and drying behaviour. A Measurex scanner records the moisture profile of the sheet as it leaves the dryer section and this information provides the key input for dryer section control. Such scanners are very expensive and are rarely installed. Operating experience has shown them to be relatively unreliable in the hot and wet conditions prior to the dryer inlet.

To summarise, the drying rate differences evident for different pulps are firstly relatively minor with each of the individual pulps lying within a ±10% band about the typical newsprint furnish. Secondly, adjustments to

the theoretical drying rate predicted by the model can be made for variations on the pulp furnish but these calculations will only be useful if information pertaining to the initial moisture content at dryer section entry is known and input into the model.

5.5.6 Basis weight

Since basis weight is a quantity which is input to the model its variation should not affect the value of the mass transfer coefficient resulting from the model/experimental comparison. In fact for the two basis weights tested in the series of drying trials the mass transfer coefficients of 0.0126 m/s and 0.0128 m/s for the 50 g/m^2 and the 100 g/m^2 sheets respectively showed a variation of just 1.7%. This deviation may be accounted for by minor inconsistencies in the experimental procedure as well as small measurement inaccuracies.

The closeness of the two results is a validation of the normalisation process defined in Section 5.2.2. As mentioned earlier, given the equipment available, it was not possible to produce paper handsheets with identical basis weight. Hence it was necessary to apply corrections to all test data to account for variations in this parameter. This correction is important both for the analysis of individual trials as well as comparison in between trials. For example, the 8 data points which define the 100 g/m^2 drying trials have basis weights which vary between from 98.4 g/m^2 to 103.7 g/m^2. This 5% range variation from the nominal value must be corrected to bring the 8 data points into a self-consistent data set. Further to this a 50% reduction is made to drying times in accordance with equation 5.9 to allow for comparison between the 50 g/m^2 and 100 g/m^2 drying trials.

5.6 Conclusions

The surface mass transfer coefficient is one of the main first order parameters which control drying rate in the paper machine. A series of laboratory trials were carried out to determine the variation in mass transfer coefficient under changes to test variables.

Changes in air speed and dryer fabric permeability provided correlations for mass transfer coefficient against these two variables. The air speed is analogous to paper sheet speed on an actual machine and the dryer fabric permeability is a property which changes in each of the dryer sub-sections.

The mass transfer coefficient for flow over the curved hot plate was shown to lie between that for flow over a flat plate and for a cylinder in cross-flow. Basis weight, pulp furnish, felt tension and hot plate temperature were found to have no major effect on mass transfer coefficient, however these trials did confirm the validity of the normalisation procedures described in Section 5.2.2.

The results from this chapter are incorporated into the implementation of the main drying model and govern the results presented in the Chapter 12 simulations.

6. Pore Size Distribution

The pore size distribution of the paper sheet is significant in defining the liquid pressure gradient throughout the sheet during drying, in accordance with the capillary pressure equation (3.8). This gradient controls the bulk flow of liquid through the sheet and is thus responsible for the drying rate associated with one of the three major mechanisms. The pore size distribution is also used for calculating the permeability of the paper sheet which affects the internal mass transfers associated with both bulk liquid and vapour flows.

Corte (1957, 1982) acknowledges that the concept of a pore radius for the paper sheet is "a physical fiction" originating from transferring physical laws valid for annular pores to the structure of paper. He further states that, "... it is not possible to characterise porous structure numerically in such a manner that anybody receives a clear impression of a sheet of paper by these figures". In spite of this, the necessity for such a model is not doubted as there are very few other ways of describing the complex paper sheet geometry in a meaningful quantitative fashion. It must be borne in mind that the aim of the pore model is not to provide a complete description of the paper structure, but to describe its impact on fluid transfers. Consequently, it is quite adequate to use the pore radius model in this instance with the controlling parameters detailing how the fluid flow is influenced by the actual distribution - provided the limitations of the model are borne in mind.

6.1 Experimental methods

There are several approaches for attaining the pore size distribution of a paper sample. Use of the scanning electron microscope (SEM) in conjunction with suitable image processing algorithms provides a very direct way of assessing paper sheet pore size variation. Unfortunately there are difficulties associated with this method. Firstly, the nature of paper formation produces a sheet with surface structure quite different from the bulk internal structure. The surface is more dense with a higher concentration of *fines* (short fibres or fillers). This is desirable with regard to the sheet's printing characteristics as it results in a more even surface. Thus, to examine pore sizes realistically by this method it is necessary to slice the sheet across its thickness and examine the internal structure.

The *Beloit Sheet Splitter* is a device which performs this task efficiently with a minimal requirement for preparation. The split is achieved by freezing a wet paper sample simultaneously to the surfaces of two contra-rotating subcooled cylinders. Though experimentally straightforward this technique will unavoidably cause distortion of the fibre structure as fibres are wrenched apart during the split; the internal surfaces appear 'hairy'. Deforming the structure in this fashion defeats the purpose of the investigation.

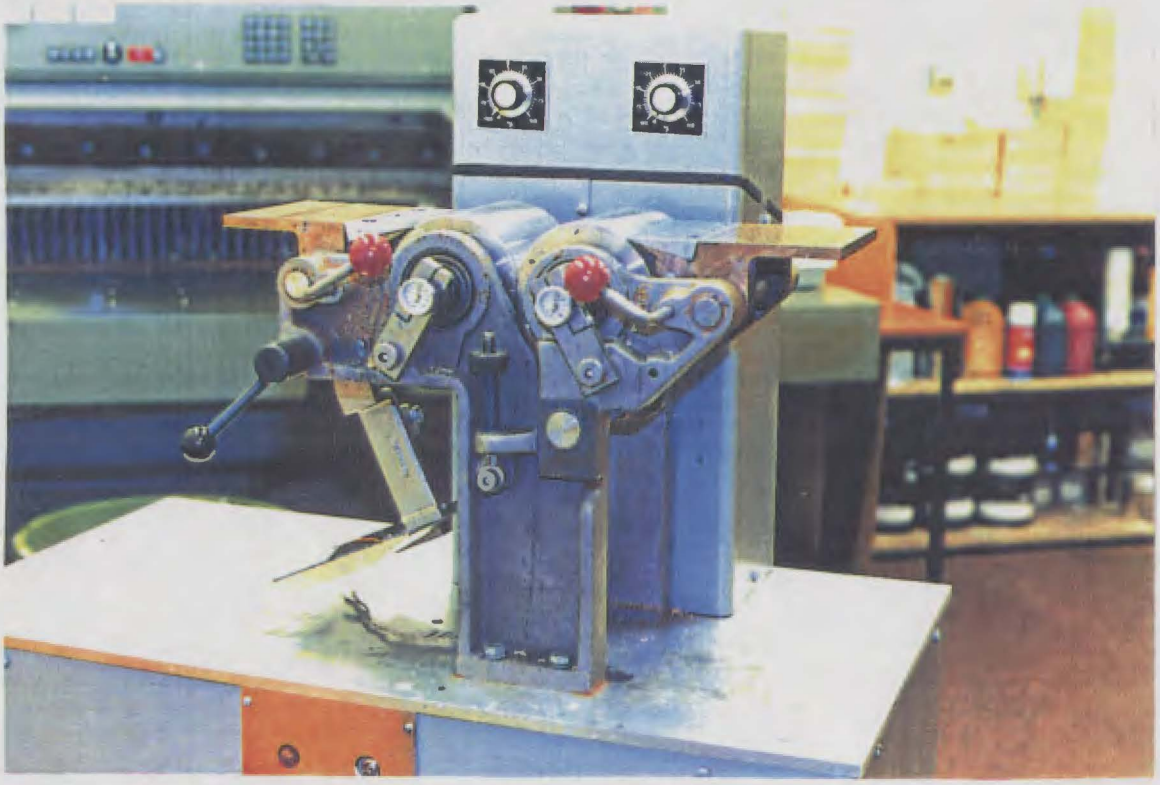

FIGURE 6.1
Beloit sheet splitter

Several trials were performed using the Beloit sheet splitter to prepare samples for viewing under a Philips SEM505 scanning electron microscope. A considerable number of the fibres were oriented vertically, indicating the deformation caused by the splitting process. Scanning electron micrographs which emphasise the differences between the internal and external structures of machine-made newsprint are shown in Figures 6.2 and 6.3. Figures 6.4 and 6.5 contrast the differences between the surface structures of machine newsprint and handsheets.

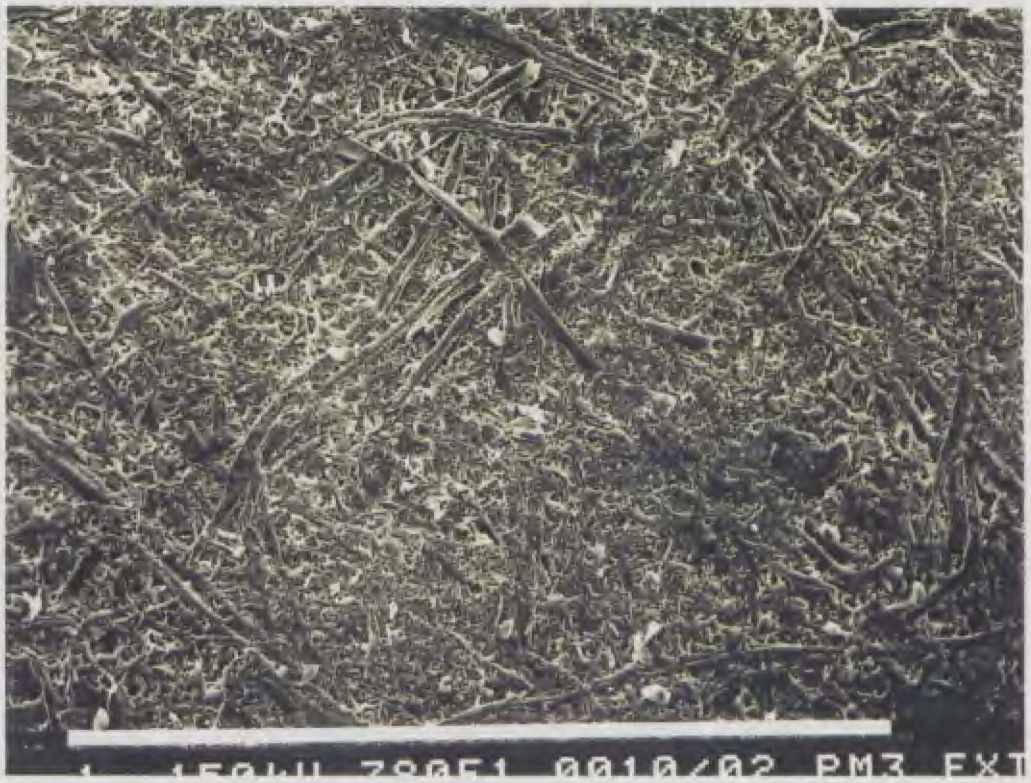

FIGURE 6.2
SEM of the external surface of machine newsprint (x110)

FIGURE 6.3
SEM of the internal surface of machine newsprint (x110)

FIGURE 6.4
SEM of the external surface of machine newsprint (x220)

FIGURE 6.5
SEM of the external surface of a laboratory handsheet (x220)

A more refined method for viewing the internal pore structure is to divide the sheet with the use of an ultra-microtome. This technique requires that the paper sheet be set firmly prior to slicing. This can be achieved by immersing the paper sheet in a resin with sufficiently low viscosity for it to permeate completely through the sheet. The next complication is that resins and cellulose have a very similar electron density since they are both essentially hydrocarbons. This makes it difficult to differentiate the two under the electron microscope. Hence it is necessary to supply an additive to the resin mixture so that the fibres can be clearly identified. Moza et al (1978) found the best mounting medium in this situation to be a mixture of Paraplex 60 resin and epoxy resin with barium methacrylate.

Despite the direct applicability of the results, this method is rarely used as a means of obtaining paper sheet pore size distribution. This is not only due to the tedious nature of the resin mixing, specimen centrifuging and microtome slicing but also to the difficult task of composing image processing software capable of coping with the intricacies of the fibrous, seemingly random paper sheet structure. Consequently, after some initial investigation with the SEM, it was decided not to proceed with these tests within the current study. The complexity of both experimental preparation and robust image processing software deemed the investigation to be a sizeable project in its own right.

It was therefore decided to obtain an approximation for the pore size distribution of the ANM newsprint sheet and laboratory handsheets tested through processing the results of the mercury porosimetry testing of similar paper samples by other researchers. The ANM newsprint sheet typically has a basis weight of 45-50 g/m^2 and is composed primarily of mechanical pulp furnish, the majority being softwood based thermo-mechanical pulp and the remainder being hardwood sourced cold caustic soda pulp. The laboratory handsheets prepared for the drying tests of Chapter 5 are considerably more bulky than the machine made product. The greater pore area is a consequence of greater sheet thickness resulting from the inability of laboratory scale formers and presses to match the mechanical dewatering and compressive performance of the equivalent machine equipment.

The method of mercury porosimetry is based upon forcing known volumes of mercury into a sample of porous paper under known pressure. Mercury is used since it has a contact angle with wood fibres of greater than 90°. Thus, a positive pressure must be applied before it will enter a capillary. As the pressure is raised stepwise the mercury is forced into progressively

smaller pores. The volume of mercury absorbed at each pressure step is obtained from the meniscus drop in a small-bored capillary measurement tube. The resultant graph of cumulative pore volume plotted against applied capillary pressure then characterises the sheet's pore size distribution.

6.2 Theoretical description

Using the assumption of a circular pore model to describe the paper structure, the pore radius can be related to the capillary pressure by the Kelvin equation,

$$P_c = -\frac{2\sigma \mathrm{Cos}\gamma}{R}, \qquad (6.1)$$

where the surface tension for mercury is generally taken as, $\sigma = 0.48$ N/m, and the contact angle as, $\gamma = 140°$.

The relationship between radius and cumulative volume can be summarised by a statistical pore size distribution. Two-parameter distributions are generally sufficiently descriptive so as to faithfully map the experimental data without providing excessive complexity when implemented theoretically. As discussed in Chapter 3 the incomplete beta function is used by this drying model to relate the range of pore radii filled with moisture to the prevailing moisture content. This relationship may be expressed from equation 3.9 as,

$$S = \beta(r; a+2, b), \qquad (6.2)$$

where, S is the fractional volumetric saturation of the paper sheet and is directly related to the moisture content, M, by equation 3.12, and the dimensionless pore radius, r, is given by, $r = R/R_{max}$.

The parameters *a* and *b* are selected so that equation 6.2 faithfully represents the experimental results. Curve fitting optimisation was performed to achieve this. Section 6.3 describes a number of sets of published experimental results describing mercury porosimetry tests on various paper samples. These data sets required fitting to an equivalent incomplete beta distribution in the form of equation 6.2. Mapping the experimental curves to analytical representations is a problem of minimisation. The parameters *a* and *b* must be adjusted simultaneously to

attain the best fit. This multi-dimensional minimisation was achieved through using the downhill simplex method of Nelder and Mead (1965) as presented by Press et al (1986). It is a very robust method which conveniently requires only function evaluations, not derivatives. Pascal computer code was developed as part of the current study to implement the downhill simplex method for two-dimensional minimisation and the values of *a* and *b* required to fit the experimental data of others to the incomplete beta function of equation 6.2 were determined.

Knowing *a* and *b* then allows the pore radius distribution function, g(r), to be expressed as :

$$g(r) = \frac{(a+b+1)!}{a!b!} r^a (1-r)^b, \qquad (6.3)$$

where g(r) is related to the incomplete beta function, β, by,

$$\beta(r;a,b) = \int_0^r g(r)\, dr. \qquad (3.10)$$

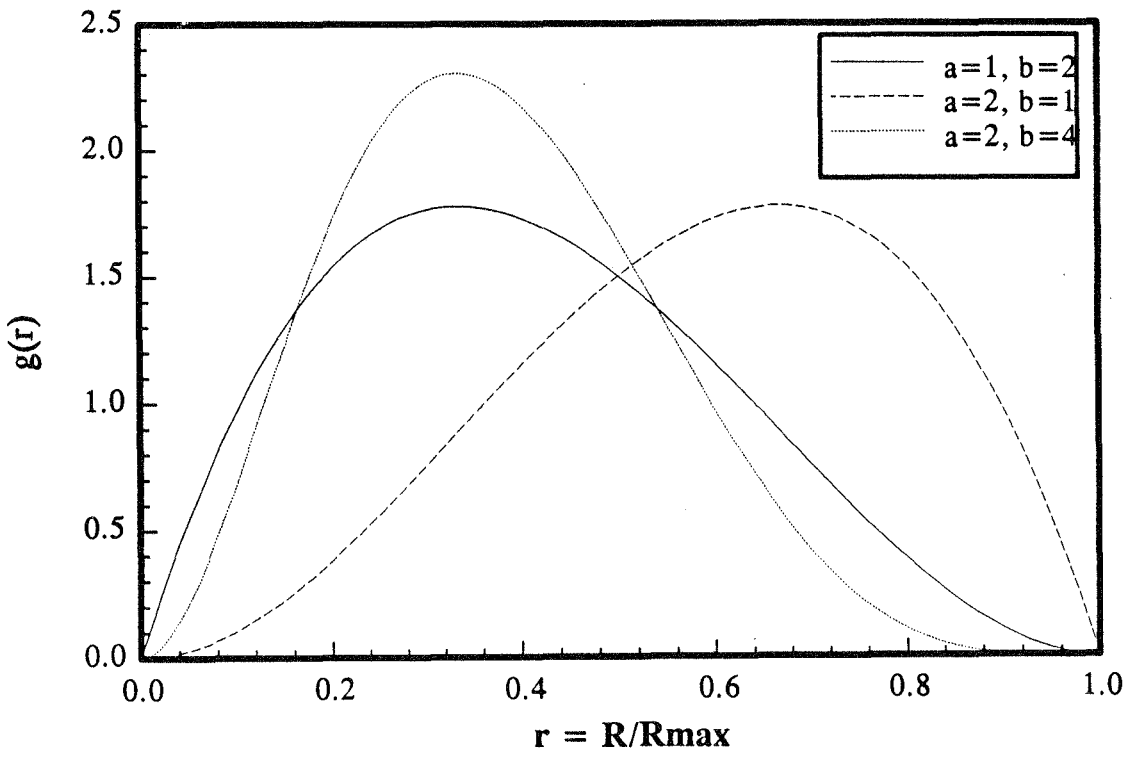

FIGURE 6.6
Pore radius distribution function g(r) for various values of a,b

Figure 6.6 shows the effects of the controlling parameters a and b. If $a>b$, the distribution is skewed towards large pore radii. As a and b are increased proportionately the distribution becomes narrower whilst the modal radius is unchanged. If $a<b$, the distribution is skewed towards smaller pore radii. Such a two-parameter distribution offers sufficient flexibility to describe all common pore structures adequately. The bimodal vegetable parchment pore radius distribution presented by Corte (1982) is not considered typical for wood fibre based paper sheets.

It is important to note that these distributions require the pore radii to be normalised against the maximum pore radius. Hence, the complete range of pore radii is represented by, $0<r<1$.

The beta function, g(r), is a frequency based distribution. The volume-weighted version of this distribution can be designated $g_v(r)$ and is calculated as,

$$g_v(r) = g(r)\, r^2, \qquad (6.4)$$

where the theoretical model assumes a number of cylindrical pores of volume $\pi R^2 l$, where R is the pore radius ($= r \times R_{max}$) and l is the sheet thickness.

6.3 Analysis of others' results

Several researchers have carried out mercury porosimetry testing on various grades of paper. Yamauchi and Kibblewhite (1988a) obtained the cumulative volume versus applied pressure relationship for handsheet samples of thermo-mechanical pulp (TMP). As TMP is the dominant pulp used in the newsprint production currently under study these results were seen as particularly useful in providing an estimate of pore size distribution for the handsheets used in the drying trials. Tests were performed on both long and short fibre fractions as well as a whole-pulp sample of TMP. It was anticipated that the whole-pulp mixture would prove the least porous and be the closest approximation to machine made paper. Indeed the mercury intrusion volume for this sample was lowest at $1.6 cm^3/g$ compared with the $3.7 cm^3/g$ registered for the long fibre fraction. However, calculation shows that machine newsprint at a typical porosity of 64% has an associated void volume of $1.15 cm^3/g$. Thus, it is to be expected that the results of Yamauchi and Kibblewhite would be biased towards larger pore radii than would be present in a newsprint sheet.

Their results as presented in Figure 6.8 indicate that most radii fall in the 0-15μm range whilst the largest radius recorded by the intrusion method was 40μm.

Tests by Yamauchi et al (1975) show a slightly narrower pore size distribution with a maximum radius of 24μm. Whilst not explicitly stated these tests are thought to be on similar samples to the TMP handsheets described earlier and later studied by Yamauchi and Kibblewhite (1988a).

Mercury intrusion results from Stone et al (1966) on black spruce sulfite pulp suggest a maximum pore radius of 20μm. The distribution as shown in Figure 6.8 is very similar to that obtained from analysis of Yamauchi's (1975, 1988) results. Typically for a pulp handsheet the radius distribution is shifted towards larger radii than would be expected in paper made commercially from the same furnish. Bristow (1986) states that the pore size distribution is influenced by operations such as calendaring, with the mean pore size becoming smaller. A similar comment would apply to machine-scale pressing compared to laboratory handsheet pressing.

Bristow (1986) presents pore radius frequency distributions for both filled and unfilled printing paper. The results, attributed to Pauler and Bergenblad, indicate that most of the pores are located in the 1-2μm range. Adding fillers such as talc, or clay, closes up the section of the distribution below the 1μm mark. Although not explicitly stated the results are indicative of a maximum pore radius of 10μm.

Corte's (1957, 1982) mercury porosimetry results are consistent with a maximum radius of 10μm and show a peak at the 2μm mark. These data are from tests performed on machine paper as opposed to a pulp sheet and are therefore more relevant to paper machine modelling than some of the other data analysed.

McKnight et al (1958) obtained mercury porosimetry data for a series of kraft paper sheets of unknown basis weight. Their volume based pore radius distribution is shown to be very similar to the results of Corte in Figure 6.8. The difference between the defining parameters a and b lies in McKnight's maximum pore radius of 6.4μm.

Figures 6.7 and 6.8 present the six aforementioned sets of pore size measurements in alternate ways. Figure 6.7 displays the results in beta

function form which is essentially a frequency distribution for normalised pore radii, R/R_{max}. The relevant values for the defining parameters *a* and *b* are quoted in the legend of this graph.

Obtaining *a* and *b* for each set of porosimetry results is a significant computational burden. In the cases of Yamauchi and Kibblewhite (1988a), Yamauchi et al (1975) and Stone et al (1966), the data are provided in the form of (radius, fractional saturation). These data sets were then matched to an equivalent incomplete beta distribution in the form of equation 6.2. Mapping the experimental curves to analytical representations with appropriate values of *a* and *b* was achieved in this study through modification of the downhill simplex method for multi-dimensional minimisation of Nelder and Mead (1965).

In the cases of Corte (1957, 1982), Bristow (1986) and McKnight (1958) their results are presented in the form of a volume based pore size distribution. Rather than demonstrate the frequency of occurrence of each pore size, this format indicates the incremental pore volume associated with pore radii in the range from R to R+dR. To standardise this it was necessary to utilise the theory developed in Chapter 3. In particular, equations 3.1, 3.4 and 3.6 can be combined to give,

$$\frac{dVol}{dR} = \varepsilon R_{max} L \frac{(a+b+3)!}{(a+2)!\ b!} r^{a+2}(1-r)^b, \qquad (6.5)$$

where, ε = porosity,
L = sheet thickness [m],
r = R/R_{max}, and,
Vol = pore volume [m^3].

For the results of Corte, Bristow and McKnight it was then necessary to use the downhill simplex method to match their experimental data to equation 6.5, rather than equation 6.2.

The downhill simplex optimisations for the six sets of data under examination produced significantly varying values for *a* and *b*. This is caused primarily by the variation in the samples tested such as basis weight, furnish composition and whether machine paper or laboratory handsheets were studied. The results, as listed in Table 6.1, were also quite sensitive to the value of the maximum pore radius assumed, and given that this parameter is defined by the final point on the tail of a

statistical distribution there is unavoidably a degree of approximation in its estimation. The final column in Table 6.1 details the modal radius for each of the recorded pore size distributions. This value, R_{modal}, represents the most probable pore radius for the paper samples under test.

TABLE 6.1
Pore radius distributions as calculated from literature and represented in Beta function [g(r)] form

Researcher	Paper type	R_{max} (μm)	a	b	R_{modal} (μm)
Kibblewhite (1988a)	TMP handsheet (150-220 g/m^2)	40	-0.079	73.39	4.0
Yamauchi (1975)	Probably TMP handsheet	25	1.14	71.96	3.2
Stone (1966)	Black spruce sulphite pulp (unknown g/m^2)	20	0.27	18.99	2.2
Bristow (1986)	Unfilled paper	10	-1.55	3.95	1.0
Corte (1957)	Machine paper	10	-0.09	25.06	1.1
McKnight (1958)	Kraft handsheet	6.4	-0.32	7.96	1.1

The calculated pore size distributions are shown in Figures 6.7 and 6.8. The first figure presents the volume-weighted pore size distribution of each set of data, defined as $g_v(r)$ in equation 6.4. The volume-weighted distribution is shown as it best illustrates the radii range in which most of the liquid to be evaporated from the paper sheet lies.

Figure 6.8 displays the same information but in a manner which is more physically meaningful. The abscissa is plotted as the actual pore radius rather than a dimensionless radius which is normalised relative to the maximum. The vertical axis is correspondingly scaled so that the area under each curve is constant :-

$$\int_0^{R_{max}} \left(\frac{g_v(r)}{R_{max}} \right) dR = \int_0^1 g_v(r)\, dr = 1. \qquad (6.6)$$

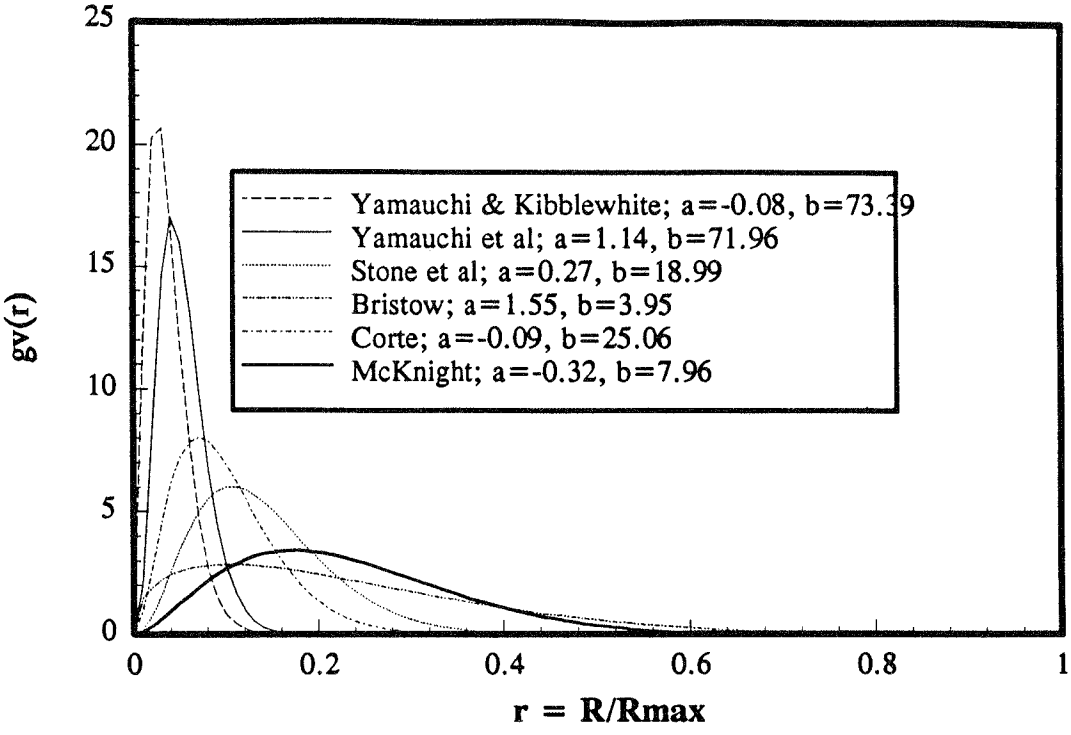

FIGURE 6.7
Incomplete beta function pore radius distribution of paper/pulp samples from a number of sources

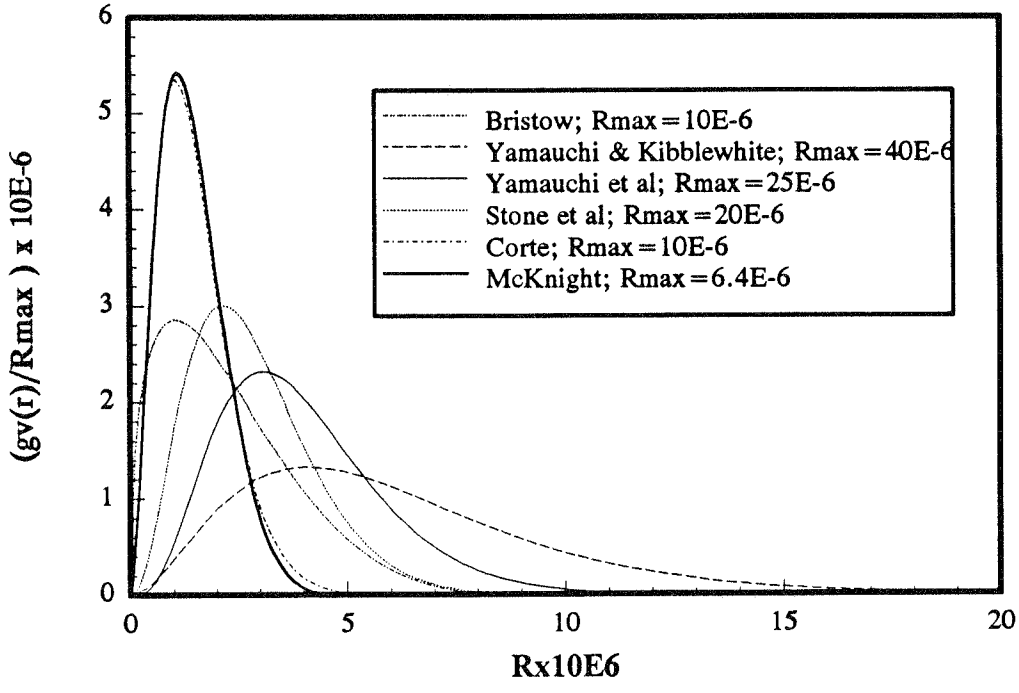

FIGURE 6.8
Normalised frequency distribution plotted against pore radius

It should be emphasised that only the distribution of Corte (1957) identifiably results from the analysis of machine paper samples as opposed to laboratory handsheets. With the exception of McKnight's (1958) data the differences between Corte's pore size distribution and the others are quite clearcut, with the results of Corte being biased towards smaller pore radii. The similarities with McKnight's findings may be due to the effect of sheet basis weight, the effect of which is demonstrated in Figure 6.9. Thus, of the six data sets analysed the description of Corte's paper samples appear to closest match the machine made newsprint of this study, and these results are therefore the ones used by the model.

In terms of the handsheets tested, those of Yamauchi and Kibblewhite (1988a) appear to best match the laboratory handsheet of this study with its high TMP concentration (75%). The documented similarity of furnish and basis weight means that this pore size distribution is used in subsequent permeability and drying calculations for handsheets in this study.

6.4 Maximum pore radii

Further guidance on pore size distribution is provided by Harrmann and Schultz (1990) who utilise a maximum pore radius of 16μm in their drying model study. This value is derived from the suction pressure curve measured by Rhodius (1980). Harrmann and Schultz further make the assumption that all pore sizes have uniform probability.

Laroque's (1937) experiments which forced oil through paper at varying pressures enabled him to calculate the maximum pore radius for a number of papers. In particular, he found that the maximum pore radius for book paper to be 5μm, and for bond paper to be 10μm.

Corte and Kallmes (1962) examined the variation of maximum pore radius with basis weight and degree of beating of the pulp. Their findings demonstrated a significant decrease in maximum pore radius with basis weight. The results of their investigation, as displayed in Figure 6.9, suggest that the maximum pore radius of a 50 g/m^2 handsheet would be approximately 22μm. The abbreviation SR, degrees Schopper Riegler, quoted in Corte and Kallmes' experiments is a measurement of pulp freeness which varies with the degree of beating; a mild form of refining which mixes pulp whilst reducing pulp freeness and consequently

narrowing the pore size distribution. This was found to have only a mild effect on maximum pore size. The relationship between maximum pore size and basis weight can be approximately expressed by the best fit hyperbolic formula,

$$R_{max} = \frac{1123}{\text{Basis Weight } [g/m^2]} \ [\mu m]. \qquad (6.7)$$

Note : Schopper Riegler (SR) is actually an alternative measurement of drainage or freeness to Canadian Standard Freeness (CSF) used in Chapter 8 which deals with permeability. The SR slowness test tends to be employed in Europe whilst the CSF freeness test tends to be utilised throughout North America.

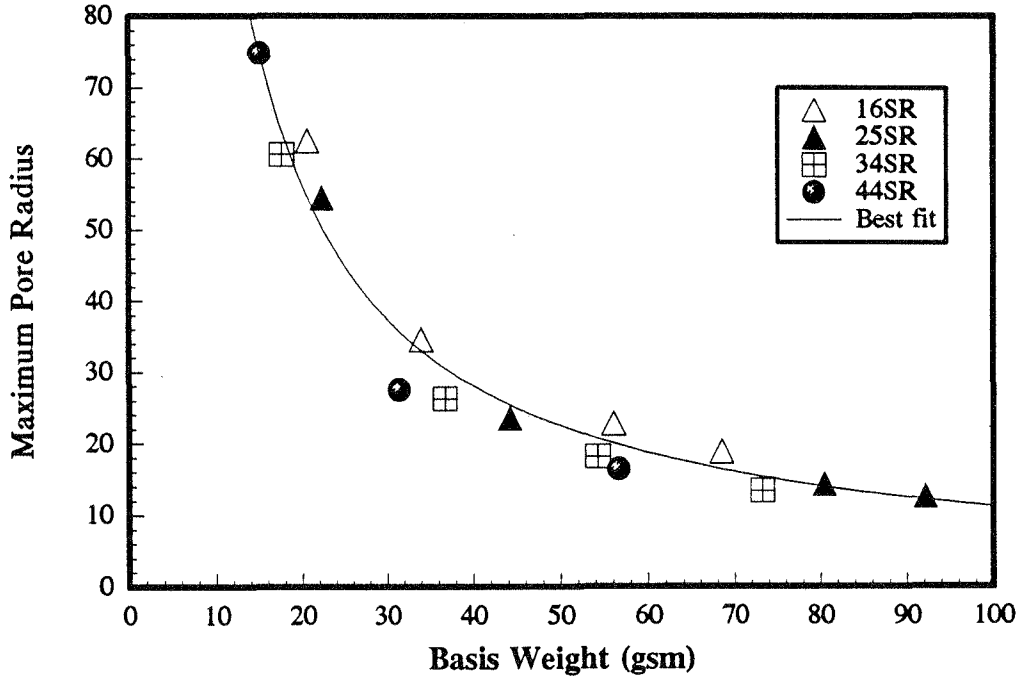

FIGURE 6.9
Variation of maximum pore radius with basis weight, Corte and Kallmes (1962)

Flyate and Kagan (1971) report maximum pore radii of 10.9μm for paper dried at 50°C and 13.7μm for paper dried at 130°C. Their tests were performed on handsheets with a porosity of 0.65.

6.5 Modal pore radii

The volume based pore size distributions in Figure 6.8 indicate the pore radii which contain the greatest quantity of liquid when the sheet is saturated. The results as tabulated in Table 6.1 demonstrate the modal pore size to fall in the range from 1-4μm. The larger values are again indicative of TMP based handsheets.

It is interesting that the most probable pore size for each of the distributions analysed is approximately 10% of the maximum pore radius. This strong bias towards smaller pores results in a much more restricted flow path than for a medium with a uniform pore size distribution. This effect is highlighted by the permeability calculations in Chapter 8.

6.6 Conclusion

Six separate sets of mercury porosimetry data applying to a range of paper grades were analysed. The beta function was used to characterise the inferred pore size distribution. The results demonstrated a diverse range of distributions. The handsheets tended to have larger pore sizes than the machine paper samples. Corte's (1957) samples were deemed to most accurately reflect the newsprint under investigation in the current study, whilst the tests by Yamauchi and Kibblewhite (1988a) on TMP handsheets best represented the handsheets used in the laboratory drying trials of this study. The following conclusions were reached :-

- Machine-made newsprint with a basis weight of 50 g/m^2 and a porosity of 65% will have a maximum pore radius of about 10μm. Laboratory handsheets with a high thermo-mechanical pulp content will typically have a maximum pore radius of about 40μm.

- Incomplete beta distribution parameters of $a = -0.09$ and $b = 25.06$ were selected for use in model calculations referring to the drying of machine paper and $a = -0.08$ and $b = 73.39$ for laboratory paper.

- The most probable pore radius was 1μm for machine made paper and 3-4μm for handsheet samples.

7. Pulp Variation

Papermills worldwide use a large variety of pulp combinations in the manufacture of equally many grades of paper. Stone groundwood, thermo-mechanical pulp, refiner mechanical pulp, cold soda pulp, unbleached and semi-bleached kraft represent the main processes which are used to convert many species of hardwoods and softwoods into pulp.

ANM uses a mixture of three different pulps in its paper products. On site the mill has two lines of thermo-mechanical pulping and two lines of cold caustic soda pulping. Some of the pulp properties from different lines but the same process do vary significantly as the lines were commissioned at different times and the equipment uses varying technologies. The main differences are in the area of strength and chemical behaviour, such as the brightness and bleachability of a pulp. Therefore it is critical that the relative usage of different pulp lines is monitored and controlled according to the preferred grade recipes.

The third type of pulp used in ANM products is kraft, a chemical pulp which is imported in both unbleached and semi-bleached form. Kraft is typically used in newsprint stock up to a maximum of around 5%. It is desirable to use more due to its superior strength properties but its cost prohibits this.

Due to the variety of pulps used in papermaking it is important to make an assessment of the effect of this diversity on the drying process. This has been partially done in the experimental work which reviewed the drying rate of a number of different handsheets made from different pulps. The laboratory results showed the drying curves of the different handsheets to fall within a ±10% band, indicating no definite trends. It should be noted that the laboratory results were all normalised for a constant initial moisture content, a condition which does not necessarily occur on a real paper machine.

On an actual machine a change of furnish will quite possibly change the moisture content of the paper sheet at the press exit or dryer inlet. This occurs because different pulps will alter both the drainage characteristics of the paper sheet which will change the amount of dewatering in the twin wire former, as well as the pressability of the paper sheet, the amount of water removal in the press section for a given nip pressure. Thus, whilst

these furnish changes need not directly affect the sheet's drying behaviour, the consequent change in the initial moisture content of the sheet will affect the drying duty directly. This effect of sheet furnish influencing initial moisture content prior to drying is one of the aspects of pulp diversity which will be examined in this chapter.

The other issue concerning the mixing of a variety of pulps is the effect on the fibre structure. This is most directly assessed by performing image processing on scanning electron micrographs. Chapter 6 explains that this was not ultimately chosen as the means of defining the pore size distribution of the paper sheet. Mercury porosimetry results which chart pore volume against pressure provide data for the pore size model in a form which is directly applicable to how the model is going to be used - in modelling drying it is not explicitly the physical pore size distribution which controls the moisture transfer rates but rather the variation of internal pressures with remaining volume.

Nonetheless, some preliminary work performed with the scanning electron microscope is also presented in this chapter. Although a detailed quantitative analysis of the images was not performed they do provide some indication of the qualitative differences between pulps.

7.1 Scanning electron microscopy on pulp furnishes

As outlined in Chapter 6 some scanning electron microscopy (SEM) work was performed on both laboratory handsheets and machine made newsprint. A Philips SEM505 was used to obtain the micrographs which are shown in Figures 7.1-7.5. The five micrographs include handsheets of TMP, CCS and Kraft pulps, a handsheet of a mixture of the three pulps and a sheet of newsprint made on PM3. The samples shown are all external surface views of the respective pulp mixtures as opposed to the internal slices described in Section 6.1 which were obtained using the Beloit Sheet Splitter available in the ANM testing laboratory.

Each of the micrographs are shown at the same magnification. The magnification level is 78x on the SEM screen and about 110x after the photos have been developed to the size presented here. The white bar at the base of each micrograph is equal to 1mm.

FIGURE 7.1
Scanning electron micrograph of a laboratory handsheet sample made from TMP (x110)

FIGURE 7.2
Scanning electron micrograph of a laboratory handsheet sample made from CCS (x110)

FIGURE 7.3
Scanning electron micrograph of a laboratory handsheet sample made from Kraft (x110)

FIGURE 7.4
Scanning electron micrograph of a laboratory handsheet sample made from 75% TMP, 20% CCS and 5% Kraft (x110)

FIGURE 7.5
Scanning electron micrograph of a newsprint sheet made on ANM's PM3 (x110)

A visual inspection of the TMP, CCS and Kraft handsheets together shows the TMP sample to be the most porous of the three. The void volume in between fibres is quite apparent in the TMP micrograph as the depth of view is quite good. The CCS fibres are seen to be considerably narrower than either the TMP or Kraft. The micrograph showing the handsheet made from a mixture of the three pulps is similar in appearance to the TMP sample but with other smaller fibres filling some of the internal voids.

The TMP and kraft pulps are both made from softwoods whilst the CCS is made from hardwood fibres. The major difference between softwoods and hardwoods is fibre length. For fully mature trees the fibre length for softwoods is approximately 4 mm whilst for hardwoods it is a little over 1 mm. As fibre length along with cell wall thickness is the most important fibre characteristic in determining paper structure it is expected that the physical differences between hardwood and softwood pulps will be significant. The field of view of the CCS micrograph is not sufficient to demonstrate the short fibre lengths but the fibre diameters are seen to be clearly narrower than those of the TMP and kraft samples. Smook (1988)

quotes typical fibre diameters of 20-40μm for hardwoods compared with 35-60μm for softwoods.

Despite the TMP and kraft both being softwood based pulps there are some significant differences between the fibre matrices formed. The fibres used for kraft preparation have a smaller cell wall thickness than those used in the TMP process. This means they collapse into flat ribbon-like structures during sheet formation. The kraft micrograph shows a number of flat areas and individual fibres do not appear to exhibit any cylindrical perspective. By contrast the TMP fibres do show some vertical perspective indicating that the fibre lumens have not collapsed. This is indicative of a thicker cell wall. Such fibres which do not collapse do not contribute to interfibre bonding to the same extent as the flattened kraft fibres. Smook (1988) states that such fibres with thicker walls tend to produce an open, absorbent bulky sheet with low burst and tensile strength but high tear resistance. The micrographs certainly support the claim that the TMP sample is more open than the kraft but the issues relating to strength were not tested.

Figure 7.4 shows the handsheet which is a mix of 75% TMP, 20% CCS and 5% kraft. This combination sheet appears similar to the TMP sheet but with less pore space brought about through the mixing of the smaller CCS fibres into the interstices. The low kraft component is not apparent in the micrograph and it is quite surprising how such a low proportion has such a significant effect on paper sheet strength and runnability.

The contrast between the combination handsheet and the machine newsprint sheet of Figure 7.5 is a striking comment on the refinement of the machine-made product and the relative coarseness of the laboratory handsheet. It should, however, be stressed that the surface of the machine newsprint sheet is considerably more uniform than the more porous internal sections. This is achieved through the relatively sophisticated performance of modern twin-wire formers which create a relatively uniform surface fibre matrix. Filler materials such as clay are sometimes used to help generate a more homogeneous surface. The calender stack, which follows the dryer section and comprises six rotating rolls in a vertical stack with alternate rolls rotating in opposite directions, guides the paper sheet through five nips which are loaded hydraulically to compress and consolidate the sheet. This also improves the surface finish of the sheet considerably and actually imparts a degree of gloss to the sheet's appearance.

With regard to assessing the drying performance of handsheets compared to machine newsprint it is necessary to change several model parameters when using the mathematical model to describe the laboratory drying of handsheets. The different parameters include :

- caliper = 150μm
- maximum pore radius, R_{max} = 40μm
- pore distribution parameters, a = -0.079, b = 73.4

The caliper value which is about twice that of machine paper of similar basis weight is determined by direct measurement whilst the pore size distribution data is obtained from Yamauchi and Kibblewhite's (1988a) mercury porosimetry experimentation on TMP handsheets. Chapter 6 outlines that Yamauchi and Kibblewhite's data are relevant because of their similarity to the pulp furnish used in the current study which is primarily TMP.

The above parameters are applied in the Chapter 5 calculations which use iterations of the mathematical model to determine the surface mass transfer coefficient for various conditions in the drying of handsheets.

7.2 Pressing tests on pulp furnishes

Drying tests performed on the three ANM pulps and a newsprint style combination handsheet in Chapter 5 showed no significant variation between the drying rates of the different furnishes when the experimental data were normalised for the differing initial moisture contents. However, anecdotal evidence from paper machine operators suggested that there were some differences between the dewatering characteristics of the three pulps in both the forming and pressing sections. In response to this some tests were carried out under the scope of the current study.

The motivation for performing these tests arises from their ability to indicate the effect of both pulp furnish and sheet basis weight on the moisture content of the paper sheet after the press section, or equivalently, the moisture content of the paper sheet at the inlet to the dryer section. The initial moisture content of the paper sheet at the start of drying is clearly a critical first order parameter in establishing the amount of moisture to be evaporated and the machine speed achievable for given drying conditions. Knowledge of some of the physical properties of the sheet which affect

this will be useful in applying the computational model to other paper grades.

A number of sets of handsheets were made using the laboratory sheet former pictured and described in Chapter 5. The wet handsheets were removed from the cylindrical former and pressed three times on the laboratory pressing table that formed Stage 2 of the same handsheet forming apparatus. The pressing table was a 25cm wide by 2.5m long bench with two 50mm diameter contra-rotating rolls at the mid-point of the bench. The rolls were electrically driven at a nip speed of 5m/s. The pressing nip was applied by pneumatic cylinders mounted to the upper pressing roll. The maximum air pressure available was 75psi (520kPa). This allowed a peak nip loading of 1.2 kN/m. The wet handsheet was mounted on a 1mm thick stainless steel sheet which was 0.25m×1m in size. A similarly sized piece of felt from an actual machine press section was then mounted on top of the paper sheet prior to feeding the three layers through the press nip.

In total six sets of trials were performed. TMP, CCS and kraft handsheets were pressed with the pneumatic pressure on the pressing roll's cylinders set first to 60psi and later 75psi (max). Eight handsheets were tested for each of the six trials. As the final moisture content, after the press, was found to vary with sheet basis weight the handsheets were made from 30-90 g/m^2 and spread relatively evenly over this range. The results are presented graphically in Figures 7.6-7.8 which show individual pulps at both 60psi and 75psi, and in Figure 7.9 which offers a comparison of the three pulps at the pressing load of 75psi.

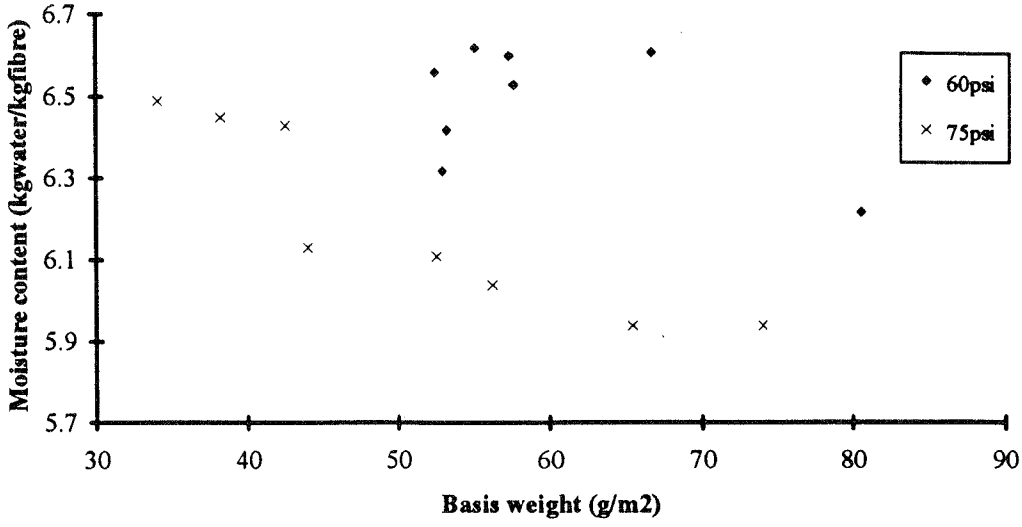

FIGURE 7.6
Moisture content after pressing plotted against basis weight for TMP handsheets

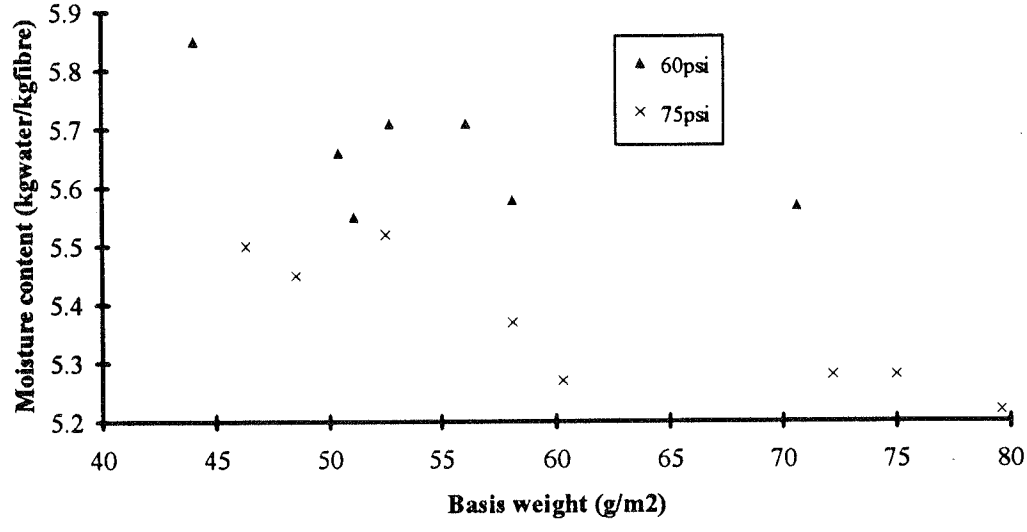

FIGURE 7.7
Moisture content after pressing plotted against basis weight for CCS handsheets

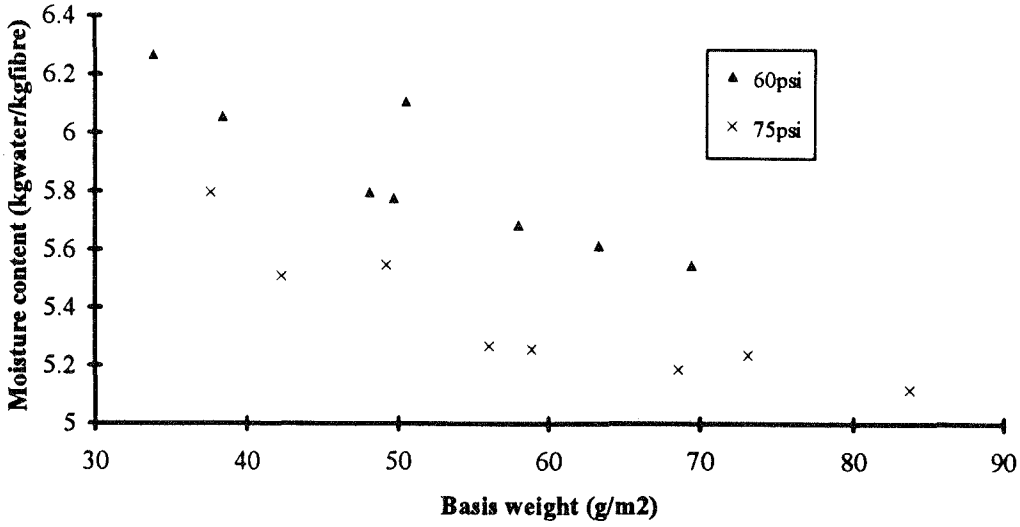

FIGURE 7.8
Moisture content after pressing plotted against basis weight for Kraft handsheets

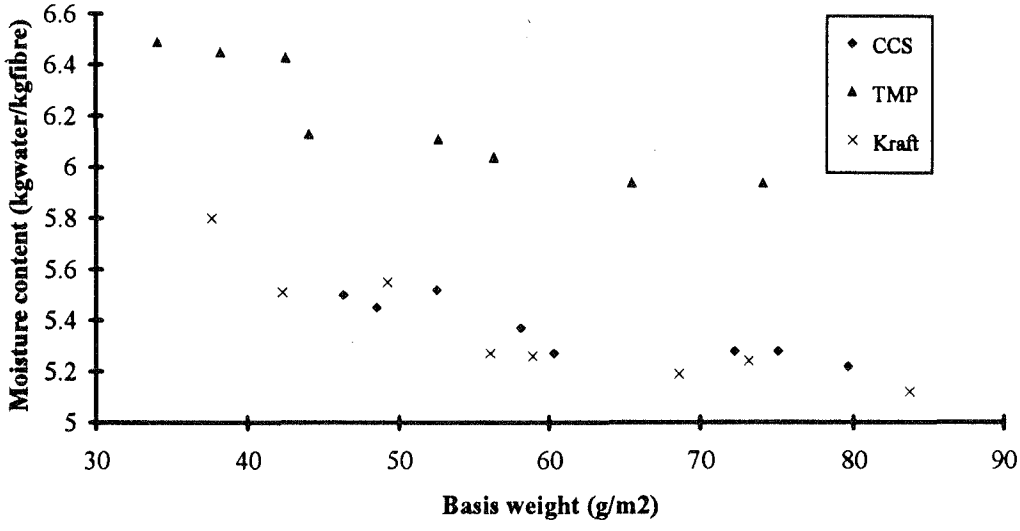

FIGURE 7.9
Moisture content after pressing (75psi) plotted against basis weight for TMP, CCS and Kraft handsheets

In each case the results from the higher press nip loading of 75psi tend to show less scatter than the 60psi data. The 75psi data exhibit a discernible linear trend between handsheet basis weight and moisture content after pressing. This negative relation is indicative of high basis weight handsheets pressing more effectively. The equations for the lines of best fit (least squares) together with their regression coefficients are shown in Table 7.1 below.

TABLE 7.1
Best fit correlations for pressing trials

Trial	Equation	Regression coeff (r)
TMP (60psi)	$M = 6.91 - 7.11b_{wt}$	-0.460
TMP (75psi)	$M = 6.96 - 15.15b_{wt}$	-0.909
CCS (60psi)	$M = 6.10 - 8.10b_{wt}$	-0.635
CCS (75psi)	$M = 5.86 - 8.17b_{wt}$	-0.891
Kraft (60psi)	$M = 6.85 - 19.18b_{wt}$	-0.894
Kraft (75psi)	$M = 6.13 - 13.06b_{wt}$	-0.895

7.2.1 Pulp effect on pressing results

In Table 7.1, M is the final moisture content after pressing in kg_{water}/kg_{fibre}, b_{wt} is the sheet basis weight in kg/m^2, and the regression coefficient r is given by,

$$r = \frac{n\sum xy - \sum x \sum y}{\sqrt{\left(n\sum x^2 - (\sum x)^2\right)\left(n\sum y^2 - (\sum y)^2\right)}}, \qquad (7.1)$$

where, n = number of data points,
x = horizontal co-ordinate, b_{wt}, and,
y = vertical co-ordinate, M.

The regression coefficient varies in the range $-1<r<1$ where $|r| = 1$ is a perfect correlation and $r = 0$ represents no correlation. In Table 7.1, r is approximately equal to -0.9 for the three 75psi tests whilst the 60psi tests have significantly lower values for $|r|$ indicating that no clear correlation exists. This suggests that the 60psi pressure in the nip between the roll and

pressing table does not remove a sufficient amount of water to generate a relationship between basis weight and moisture content which is independent of the forming process and a direct consequence of the pressing characteristics of the sheet.

The comparison in Figure 7.9 shows TMP to be the most resistant to dewatering through pressing whilst the CCS and Kraft are fairly similar and are typically 10-15% drier than the TMP at any basis weight. This is thought to be due to the relative bulkiness of the TMP sheet compared to the other two. As described in section 7.1 this is likely to be due to the thicker cell walls of the radiata pine fibres which do not collapse completely after refining thereby decreasing the fibre packing efficiency and increasing the sheet's thickness and hence bulk (specific volume). A detailed quantitative assessment of handsheet basis weight against sheet thickness was not performed but some measurements taken in conjunction with the permeability testing described in Chapter 8 suggest that at 50 g/m^2 the TMP sheet is typically 15% thicker than a CCS sheet.

Unfortunately the moisture content of the paper sheet after the press section is rarely measured on-line on paper machines and therefore there are no comparative data for these pulps. The variation of this parameter with pulp furnish is a relationship which deserves to be investigated further at higher levels of pressing intensity.

7.2.2 Basis weight effect on pressing results

With regard to the press section of an actual paper machine the relationships obtained for press moisture content varying with basis weight need to be interpreted with care. The paper machine's press section is much more intense in terms of both temperature and applied pressures compared with the laboratory version. A paper machine press section typically has 2-3 press nips which operate at loadings in the range from 50-100 kN/m whilst the paper sheet is at a temperature of 50-70°C and usually achieves an output moisture content of around 58% or 1.38 kg_{water}/kg_{fibre}. This compares with the laboratory scale version which applies a loading of just 1.2 kN/m at ambient temperature and outputs handsheets with a moisture content in the 5-6 kg_{water}/kg_{fibre} range. The lack of nip pressure means that the laboratory equipment removes only about 20% of the moisture per unit mass of dry fibre as does the machine scale version.

The machine press section squeezes the paper sheet between two porous felts which cushion the hard rolls and absorb water from the sheet. In the laboratory situation the sheet is squeezed between an absorbent felt on the top side and a steel plate on the lower side. The presence of the supporting steel plate gives rise to two effects. Firstly, dewatering can only occur in one direction because the plate is impervious to mass flow. Secondly, the presence of local contours on the nominally flat, incompressible plate means that parts of the paper sheet may not be exposed to the full nip pressure. Any misalignment of the counter-rotating pressing rolls would also lead to this occurrence. For these reasons, higher basis weight sheets which present a thicker cross-section to the laboratory nip are pressed more effectively as evidenced by the data in Figure 7.9.

On actual paper machines Busker (1980) demonstrated that basis weight is actually inversely proportional to press water removal. Busker demonstrated that pressing a 60 g/m^2 paper sheet removed 20% more water per unit dry mass than pressing a 163 g/m^2 sheet. This trend fully opposes the results of this section. Busker's findings may be explained by the shorter dewatering path for moisture in a low basis weight sheet which has a low caliper.

The imperfections in the laboratory pressing set-up are emphasised by the comparison with Busker's results. The combination of mini-contours in the steel pressing plate, misalignment of the pressing rolls and the general low intensity of conditions led to results which are not quantitatively reliable in the context of the basis weight analysis but are qualitatively applicable in the comparison between different pulp behaviour.

The usefulness of the tests also lies in the message which comes from the disparity between the laboratory scale trials and real world performance. it emphasises the potential errors which can be induced through relying entirely on laboratory data in a paper press test or a far more general environment.

The two paper machines which are the focus of this study conveniently use a relatively narrow range of furnish and sheet basis weights. Consequently, initial moisture content is assumed to be relatively constant for these machines. The figure of 58% or 1.38 kg_{water}/kg_{fibre}, as measured through manual samples on both machines during the period 1990-1992, is input into the computer dryer model and used throughout.

8. Permeability

Paper sheet permeability is an important parameter in controlling drying rate. The permeability is significant in determining the resistance to both liquid and bulk vapour flow created by the pore structure of the paper sheet. The permeability will be strongly affected by the global porosity of the sheet as well as the size distribution and shape factors of porous channels throughout the sheet. It should be noted that the intrinsic permeability of a material, which is the parameter of interest here, is solely representative of the internal structure of the given sample and is independent of both the nature of the fluid which flows amongst the pores and the size of the sample. To express this relationship definitively it is necessary to quote Darcy's law (1856) for fluid flow through a porous medium :

$$V = -\frac{\kappa A}{\mu}\frac{dP}{dy}, \tag{8.1}$$

where, V = volumetric flow rate [m^3/s],
κ = permeability (intrinsic) [m^2],
A = area of sample exposed to flow [m^2],
μ = viscosity of fluid [kg/m.s],
dP = pressure differential across sample [Pa],
and, dy = thickness of sample [m].

Darcy's Law relates the volumetric flow rate of a fluid flowing linearly through a porous medium directly to the energy loss, inversely to the length of the medium and proportional to a term referred to as the hydraulic conductivity factor or volume permeability coefficient. This proportional factor is sometimes referred to loosely as the structure's permeability, but it should be emphasised that it is dependent on the viscosity of the fluid traversing the medium. The relationship between the permeability coefficient and the medium's intrinsic permeability is given in equation 8.2.

$$\kappa = K\mu, \tag{8.2}$$

where, K = permeability coefficient [m^3s/kg].

8.1 Experimental results

Permeability data for a variety of dry paper samples was obtained through use of a Parker Print-Surf PPS78 permeability tester available at Australian Newsprint Mills Limited, Boyer, and shown in Figure 8.1 overleaf. The Parker Print-Surf is a fluidic impedance device which measures the differential pressure across the test specimen when an air flow of fixed volumetric flow rate is passed through. The manufacturers claim that this method gives improved accuracy over the more common flowmeter devices which operate at constant pressure differential. However, to conform with the output from numerous flowmeter-based devices available the PPS78 converts the measured pressure to an equivalent flow (ml/min of air) at a fixed nominal pressure of 1.47kPa. This calibrates the PPS78 to read the same as the Bendsten apparatus for permeability measurement. The information for converting between ml/min flow and permeability, m^2, for the Bendsten permeability tester is given in Annex A.2 of ISO 5636/1-1984.

For air at room temperature with a viscosity of 1.8×10^{-5} kg/ms, flowing through a standard test area of 1000×10^{-6} m^2 under a differential pressure of 1.47 kPa, equation 8.1 simplifies to :

$$\kappa = 12.245\times10^{-6}\ V\ dy. \qquad (8.3)$$

Thus, to determine the intrinsic permeability of a sample paper sheet the procedure is, 1) test the sample in the Parker Print-Surf device and convert the output in ml/min to m^3/s, 2) measure the thickness of the paper sample, and, 3) calculate permeability from equation 8.3.

Results were obtained for a number of samples including machine newsprint and handsheets made from several different pulp furnishes. The data quoted in Table 8.1 are the averages of tests on three separately sourced samples. Each sample (approximately 200mm × 200mm) was tested in nine evenly spaced positions across its area.

The sample termed "newsprint" in Table 8.1 is paper from the No. 3 ANM machine which produces exclusively 45.0 g/m^2 and 48.8 g/m^2 newsprint grades. The "handsheet" sample is made in the laboratory from a pulp mixture similar to the machine furnish; typically 75% TMP, 20% CCS and 5% kraft. The other three samples are handsheets made from 100% Kraft, TMP and CCS pulps respectively.

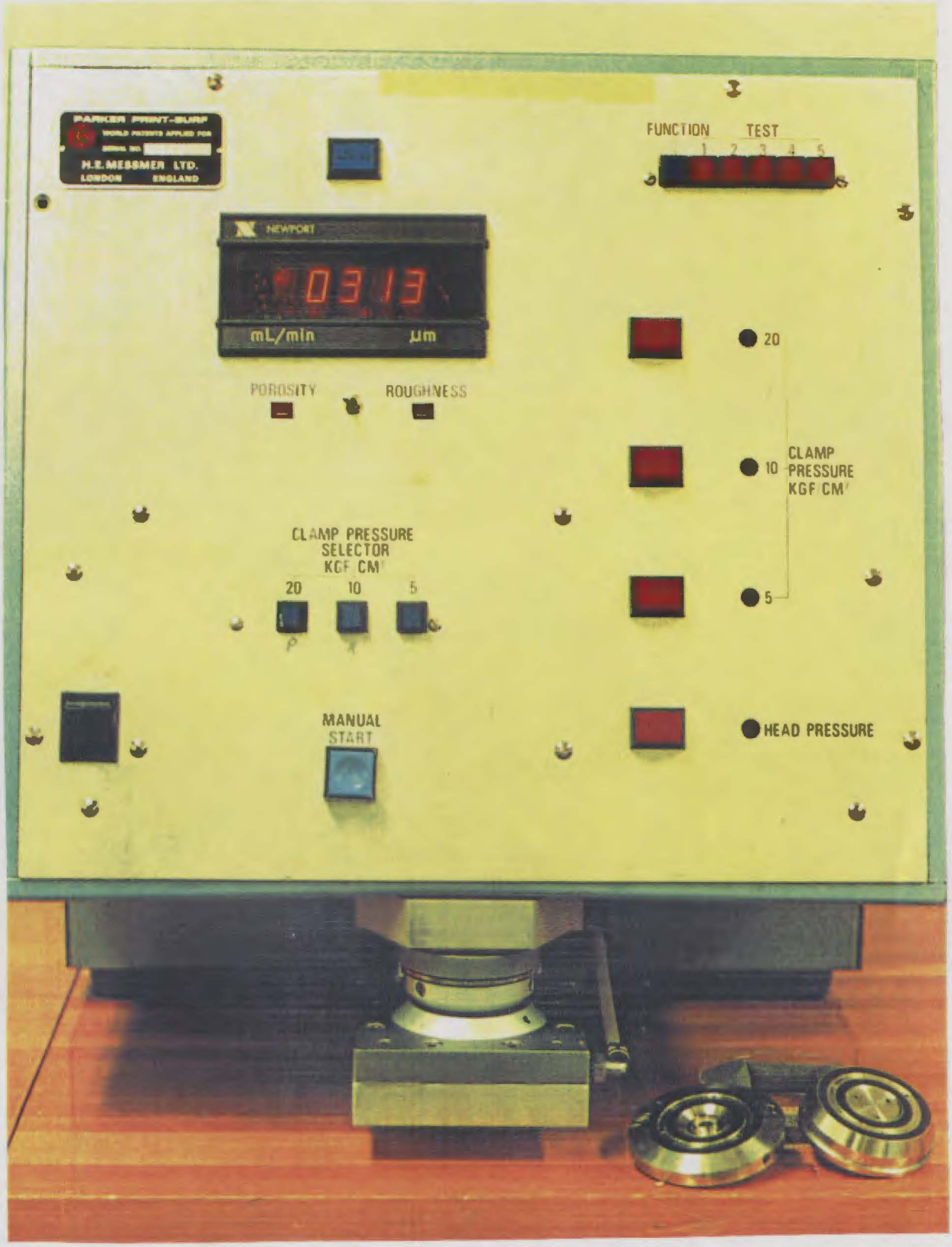

FIGURE 8.1
Parker-Print Surf tester PPS78

TABLE 8.1
Permeability (κ) test results for a number of paper samples

SAMPLE	V (ml/min)	Thickness (μm)	Basis wt. (g/m^2)	Density (kg/m^3)	Porosity	κ ($10^{-15} m^2$)
Newsprint	321	75	41	590	0.62	4.9
Handsheet	300	155	50	320	0.80	9.5
Kraft	428	133	48	250	0.84	11.6
TMP	304	173	55	330	0.79	10.7
CCS	181	147	57	450	0.71	5.4

The variation in the permeability values obtained from the Parker Print-Surf tester for individual samples differed between the homogeneous machine-made paper and the coarser laboratory handsheets. Machine newsprint showed deviations of *V(ml/min)* of no greater than 10% across an individual sample whilst thickness deviated by no more than 2% across the sample area. For handsheets, *V* varied by up to 50% from the mean value partly as a result of thickness deviations (±10%) but mainly as a consequence of variable pore structure.

The additional parameters basis weight, density and porosity are shown in this table as they are needed for making comparisons between several analogies for permeability developed later in this chapter. Basis weight is determined by weighing an oven-dried 10cm×10cm square of the sample, whilst sheet density is the ratio of basis weight to thickness. Porosity is calculated from the density of cellulose fibres which is taken as 1550 kg/m^3 (see Chapter 10). The relationship used is :

$$\text{porosity} = 1 - \frac{\text{sheet density}}{\text{cellulose density}}. \qquad (8.4)$$

The results indicate that machine grade paper is much more dense and hence less porous than the laboratory handsheets. This is due to the high pressing and calendaring nip loads employed on a full-scale paper machine which can not be easily recreated in a laboratory. The high permeability of the kraft handsheet is understandable upon consideration of the high refining freeness of that pulp; usually 500 CSF compared to the CCS and TMP pulps at about 120 CSF. The length of the kraft fibres, typically 4mm

compared to 1-1.5mm for CCS, implies that the fibre structure will be very porous as there are few short fibres to fill the interstices.

Note : Canadian Standard Freeness (CSF) is the most common method of measuring drainability, which is the resistance of fibres to the flow of water. The CSF unit is defined as the number of ml of water collected from the side orifice of the standard tester when pulp drains through a perforated plate at 0.30% consistency and 20°C. Such measurements are known as freeness. A high freeness value is indicative of a fast draining pulp and this usually relates to a dominant long fibre fraction and correspondingly high permeability (Smook, 1988).

It is also interesting to note that the weighted average of the three pulps' permeability of 9.7×10^{-15} m^2 is extremely close to the independently measured mixed handsheet permeability of 9.5×10^{-15} m^2.

The permeability readings are quite variable at different sites within each sample, particularly so for the laboratory handsheets which are less homogeneous than the machine samples. Table 8.2 gives an indication of the variability of permeability readings across the paper sample from the PPS78 testing device, where locations 1-9 refer to a 3×3 square grid across the sample.

TABLE 8.2
Typical permeability variation across individual paper samples
Volume flow rate V (ml/min)

Location	Kraft	TMP	CCS	Newsprint
1	230	280	253	346
2	251	242	169	339
3	432	202	213	341
4	401	368	157	328
5	390	392	166	321
6	728	302	152	331
7	335	324	183	304
8	339	363	172	290
9	742	263	168	286
Average	428	304	181	321
Std. dev.	186	63	32	22

The results of Table 8.2 demonstrate the variability in permeability measurements across samples of different paper grades. The key feature to notice is the relative consistency of PPS78 permeability measurements on machine-made newsprint compared to the large deviations present for laboratory prepared handsheets. Such non-homogeneity is an unavoidable part of handsheet testing. It should be emphasised, however, that the PPS78 exhibited excellent repeatability when several measurements were taken at a single location.

The permeability values quoted in Table 8.1 may be referred to as saturated permeability since the pores of the paper samples used in the air permeability test are free of water and contain air only. This becomes important when considering the concept of relative permeability later in this chapter.

8.2 Theoretical permeability calculation

Theoretical predictions for the saturated intrinsic permeability of the paper sheet can be made by extending the theory developed in Chapter 6 to describe the pore size distribution of the paper sheet. To estimate the permeability in the direction perpendicular to the sheet surface it is first necessary to define the relevant flow velocity component, v_y. Figure 8.2 illustrates the axis definitions.

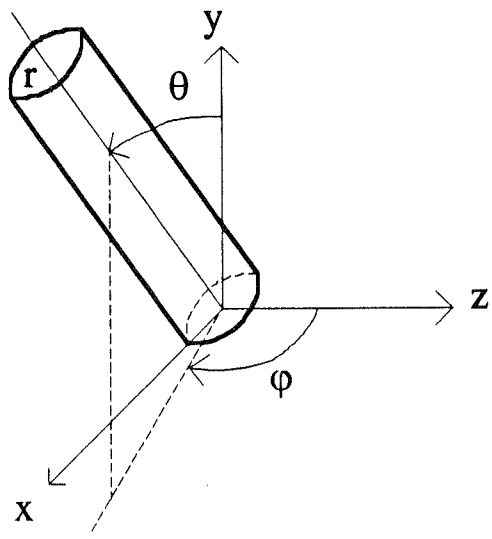

FIGURE 8.2
Axis definition for pore geometry

The paper surface is set in the x-z plane and consequently the y-axis indicates the direction of fluid evacuation from the sheet. The variables θ and φ represent the angular orientation of a pore with radius r.

From the Hagen-Poiseuille equation for incompressible viscous laminar flow through a cylindrical capillary, the velocity of the fluid through the pore is given by,

$$v = -\frac{r^2}{8\mu}\frac{dP}{dy}\cos\theta, \tag{8.5}$$

where, dP = pressure drop through pore [Pa],
μ = viscosity [kg/m.s].

The transverse y-component velocity is,

$$v_y = v\cos\theta. \tag{8.6}$$

The average velocity, $\langle V_y \rangle$, can be calculated by integrating the velocity over the range of pore sizes and orientations, $r \rightarrow r+dr$, $\theta \rightarrow \theta+d\theta$, and $\varphi \rightarrow \varphi + d\varphi$. Thus,

$$\langle v_y \rangle = -\frac{R_{max}^2}{8\mu}\frac{dP}{dy}\frac{1}{2\pi}\int_0^1 r^2 g(r)dr \int_0^{\pi/2}\cos^2\theta\sin\theta\, d\theta \int_0^{2\pi} d\varphi, \tag{8.7}$$

whence, $$\langle v_y \rangle = -\frac{R_{max}^2}{24\mu}\frac{dP}{dy}\frac{(a+2)(a+1)}{(a+b+3)(a+b+2)}, \tag{8.8}$$

where *a* and *b* are parameters from the pore size distribution function, g(r), detailed in Chapter 6, and defined in terms of the beta function as :

$$g(r) = \frac{(a+b+1)!}{a!\,b!}r^a(1-r)^b. \tag{8.9}$$

Now, Darcy's law in terms of the average pore velocity for a fluid flowing in a porous medium can be written as,

$$\langle v_y \rangle = -\frac{\kappa}{\varepsilon\mu}\frac{dP}{dy}. \tag{8.10}$$

Equating 8.8 and 8.10 results in an expression for permeability :

$$\kappa = \frac{\varepsilon R_{max}^2}{24} \frac{(a+2)(a+1)}{(a+b+3)(a+b+2)}. \qquad (8.11)$$

Substituting the values of a=-0.09, b=25.06, and $R_{max}=10\times10^{-6}\mu m$, as obtained for machine newsprint in Chapter 6, into equation 8.11 predicts a permeability of $\kappa = 5.9\times10^{-15}$ m^2. This figure is within 20% of the measured value quoted in Table 8.1 of 4.9×10^{-15} m^2. Given the strong reliance on the idealised circular pore model this comparison is very encouraging and may be regarded as a general vindication of the assumed model.

The permeability of the handsheet composed of the newsprint furnish of 75% TMP, 20% CCS and 5% Kraft was measured at 9.5×10^{-15} m^2 as presented in Table 8.1. Chapter 6 recommended pore size distribution parameters of a=-0.079, b=73.39, and $R_{max}=40\times10^{-6}\mu m$, and accordingly equation 8.11 predicts a permeability of $\kappa = 12.7\times10^{-15}$ m^2, exceeding the measured value by 34%. Again this is reasonable correlation given the diversity between the assumed theoretical model and the actual pore structure of the paper sheet.

In the implementation of the computational model the measured permeability values are used in preference to the theoretical predictions.

8.3 Kozeny-Carman permeability theory

The Kozeny-Carman equation (1927, 1937) is perhaps the most widely used theoretical tool for predicting the permeability of porous materials and as such deserves to be tested alongside the algorithm for paper sheet permeability developed in the previous section.

The Kozeny-Carman equation, as presented by Ingmanson et al (1959), may be stated as,

$$\kappa = \frac{\varepsilon^3 S_v^2}{k_c S_A^2 (1-\varepsilon)^2}, \qquad (8.12)$$

where, ε = porosity,
S_v = specific volume [m^3/kg],

S_A = specific surface area of fibres [m^2/kg], and,
k_c = Kozeny-Carman factor.

The Kozeny-Carman factor is often described by Carroll's relation as reported by Ramaswamy (1990),

$$k_c = 5 + \exp(14(\varepsilon - 0.8)). \tag{8.13}$$

The specific volume for a given paper sample is quite simply calculated as the inverse of density, so that,

$$S_v = \frac{1}{\rho} = \frac{\text{sheet thickness}}{\text{basis weight}}. \tag{8.14}$$

For ANM newsprint this value is calculated to be 1.7×10^{-3} m^3/kg ($\rho \cong 590$ kg/m^3). This compares to a typical value of 3.1×10^{-3} m^3/kg for the handsheets.

Arriving at a value for the specific fibre surface area, S_A, is not so straightforward. Due to the relatively random nature of the fibre structure this quantity must either be inferred from experimental results or estimated from a pore model. Using the circular pore model with the pore size distribution derived in Chapter 6 it is possible to estimate the specific surface area,

$$\frac{\text{fibre surface area}}{\text{unit area}} = \int_0^1 N 2\pi RL\, g(r)\, dr, \tag{8.15}$$

where,
N = number of pores per unit area [$1/m^2$],
R = pore radius [m],
r = dimensionless pore radius, R/R_{max}, [-],
L = sheet thickness [m], and,
g(r) = pore size distribution function.

Substituting equation 3.4 for N, integrating, and dividing by the sheet basis weight produces the expression,

$$S_A = \frac{2\varepsilon L}{R_{max}} \frac{(a+b+3)}{(a+2)} \frac{1}{b_{wt}}, \tag{8.16}$$

where a and b are parameters from the pore size distribution, g(r), and b_{wt} is the dry basis weight of the paper sheet.

The relevant values for the newsprint sheet tested by the PPS78 permeability tester are : $\varepsilon = 0.62$, $L = 70\mu m$, $R_{max} = 10\mu m$, $a = -0.09$, $b = 25.06$ and $b_{wt} = 0.041$ kg/m^2. Substituting these into equation 8.16 yields a specific fibre surface area of $S_A = 3100$ m^2/kg.

This can be compared with Bliesner's (1964) relationship between S_A and density for a 100 g/m^2 paper sheet. Extrapolating from just five data points gives no guarantee of accuracy. Nonetheless, it is interesting to estimate the S_A value for a density of 590 kg/m^3 corresponding to the ANM newsprint sheet. The parabolic extrapolation in Figure 8.3 suggests that the corresponding S_A value is approximately 2800 m^2/kg. This order of magnitude similarity with the model prediction of S_A=3100 m^2/kg is encouraging given the simplifying assumptions made by the model. It should be noted here that Bliesner's tests show the effect of basis weight to be less than 3% when comparing the specific surface area of a 50 g/m^2 sheet with that of a 100 g/m^2 sheet.

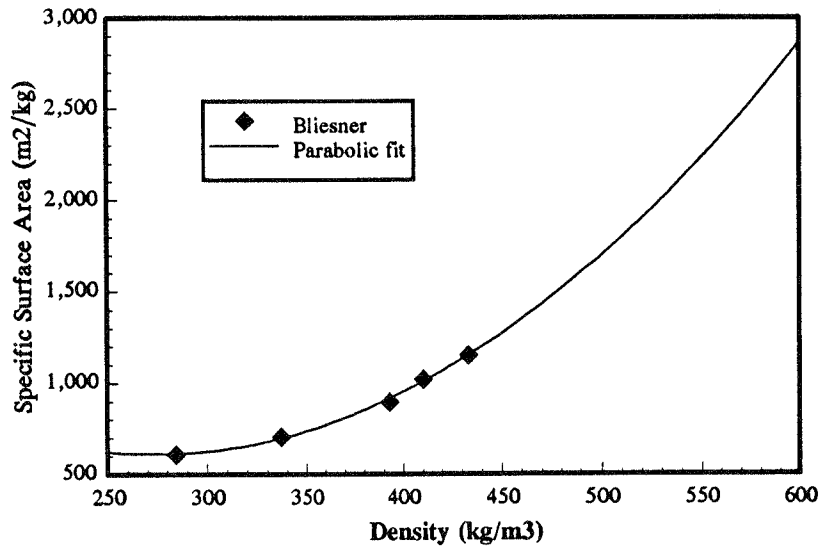

FIGURE 8.3
Extrapolation of Bliesner's results for S_A- ρ

Making use of this information it is now possible to evaluate the Kozeny-Carman permeability equation. Equation 8.13 estimates the Kozeny-Carman factor as k_c=5.08, whilst the predicted permeability from equation 8.12 is $\kappa = 98 \times 10^{-15}$ m^2. This is 20 times greater than the measured

value and illustrates the lack of applicability of the Kozeny-Carman theory to thin materials with non-uniform pore sizes.

A network combining a range of small and large pores offers more resistance to flow than one with constant diameter (and same average diameter). The results of Chapter 6, which conclude that the maximum pore radius is typically 10 times the modal pore radius, highlight that the paper structure cannot be considered as having uniform pore size.

To summarise, circumstances in which the validity of the Kozeny-Carman theory is questionable include (Murakami and Imamura, 1984) :-

- pore size is not uniform
- significant variability in pore shape
- the tortuosity ratio (= effective length of capillary / thickness of specimen) changes significantly with pore shape

Given the considerable variability of the paper sheet each of the above three situations are quite relevant and consequently it is not surprising to find the Kozeny-Carman relation predict a spurious value for paper sheet permeability.

The inability of the Kozeny-Carman theory to approximate paper sheet permeability emphasises the relative success of the theoretical development in section 8.2 which managed to replicate measured values considerably more closely.

8.4 Relative permeability

Permeability is a function of the pore arrangement of the material. Consequently, when the sample contains moisture within the pores the permeability of the material changes. This introduces the notion of relative permeability. The correlation for relative permeability will differ depending upon whether the transfer of liquid (water) or gas (air / water vapour) is being considered. Relative permeability will be maximised at a value of unity when the pore space is saturated by the relevant component. Thus, at the commencement of paper drying when the sheet is quite wet the liquid relative permeability will be larger than the water vapour relative permeability. This situation will reverse as drying proceeds and the liquid is evacuated from the pore space.

In general, if the saturated intrinsic permeability, is denoted κ_s, and the relative permeability κ_r, then the actual permeability, κ, is defined by,

$$\kappa = \kappa_r \kappa_s. \tag{8.17}$$

A description of liquid relative permeability for wood fibre mats at various saturation levels is given by Robertson (1963) and the results are shown in Figure 8.4.

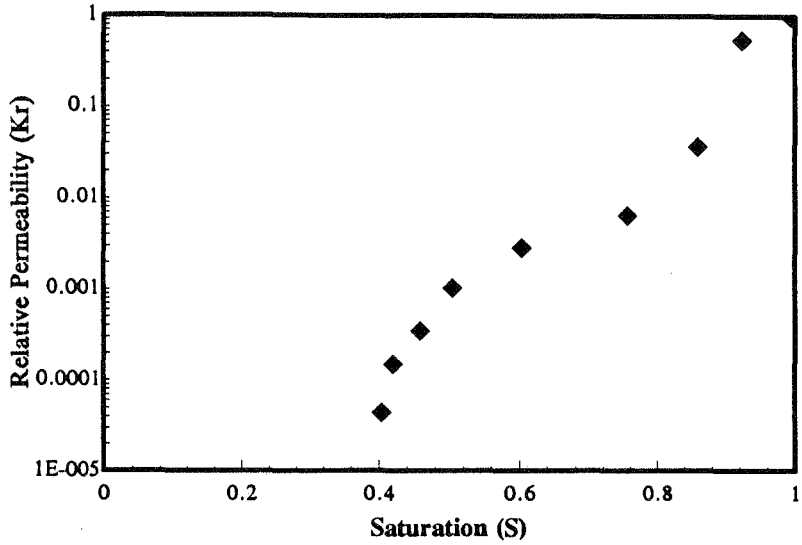

FIGURE 8.4
Robertson's (1963) liquid relative permeability data for wood fibre mats

Robertson's data illustrate a rapid drop in liquid relative permeability as the saturation falls below unity. This indicates that much of the pore network is in series and the initial removal of liquid from the fibre matrix causes several liquid path blockages which dramatically reduce the overall permeability. This contrasts with a completely parallel flow arrangement where the blockage of several paths has a comparatively minimal, approximately linear, effect on permeability.

Below a saturation level of 0.4 there are no data provided by Robertson. In this range a linear relationship is assumed from the final data point down to zero saturation. This approximation should not introduce any significant error as the liquid relative permeability is so small at these saturation levels.

There is little data to describe the variation of vapour relative permeability with saturation. Thus, it is necessary to make a similar approximation to that used by Ramaswamy (1990), namely that it changes linearly in a decreasing fashion with increasing saturation. Mathematically this may be expressed as,

$$\kappa_{r\text{vapour}} = 1 - S. \qquad (8.18)$$

Robertson's data and equation 8.18 are incorporated into the theoretical model by use of the relationship for relative permeability presented in equation 8.17.

8.5 Conclusion

Experimental results for machine-made newsprint show an intrinsic permeability of $\kappa = 4.9\times10^{-15}$ m^2. Two theoretical predictions were made to estimate this value from first principles. The pore size distribution theory developed earlier in Chapter 6 was extended and shown to predict a saturated permeability of 5.9×10^{-15} m^2. The Kozeny-Carman relation which is generally used to describe porous media was also explored and found to grossly overestimate the newsprint sheet's permeability. This was primarily due to the Kozeny-Carman's assumption of uniform pore size.

The concept of relative permeability was defined in the context of both liquid water and water vapour permeating through the porous fibrous structure.

9. Sorption Isotherms

The sorption characteristics of a material, such as paper, describe the degree of adsorption of a particular sorbate, water for example, to the surface of that material. The extent of this sorptive behaviour is essentially a measure of the strength of bonding between sorbate and surface. This sorptivity manifests itself by a reduction in the equilibrium vapour pressure for the sorbate at the prevailing temperature and also an increase in the latent heat of vaporisation required to evaporate liquid sorbate. The sorptive properties of paper therefore carry significant influence with regard to the process of machine paper drying as it is being modelled in this study.

These characteristics have a twofold effect on drying rate. The mechanism of drying by vapour transfer is retarded by the reduction in vapour pressure brought by sorption. This causes a decrease in the vapour density gradients which control the diffusion process as well as inhibiting the pressure driven bulk flow mechanism. The second effect is embodied in the latent heat of sorption, the incremental heat of vaporisation required to evaporate a unit of sorbate (water) from the paper over and above the free evaporation energy at that temperature. The latent heat of sorption becomes significant at low moisture content where this incremental evaporation requirement causes the temperature to drop and drying to slow.

Sorption effects become more dominant as drying progresses and the moisture content of the paper sheet decreases. Water within the wet sheet may be considered in two states, free and bound. Free water is defined as occupying the inter-fibre (macro) pores of the paper sheet. Bound water, often termed hygroscopic moisture, includes all liquid filling the intra-fibre (micro) pores as well as that which is attached to the fibre walls. During drying the free water evaporates first, leaving the macro-pores empty. Subsequent evaporation consumes progressively more energy per unit mass. This slows the drying process by cooling the sheet. At low moisture contents the remaining water is contained within the narrowest of fibre pores and collapsed lumens (micro-pores) and this differential heat of sorption requirement may represent up to an additional 50% vaporisation energy beyond that of an equivalent quantity of free water. The results presented later in this chapter demonstrate that this feature of the drying

process becomes significant when the moisture content falls below about 0.3 kg_{water}/kg_{fibre}.

The sorption isotherms for a given material may be determined experimentally over a considerable range of test conditions. The only requirements are a controlled environment in which temperature and relative humidity are accurately known, and a facility for measuring the weight of paper samples accurately and quickly. The need to weigh the conditioned samples quickly refers to the rapid change in the mass of a thin paper sample when it is removed from its controlled environment and exposed to the ambient conditions so that it its equilibrium moisture content can be assessed. Depending upon its test environment the paper sample will either adsorb or desorb moisture fairly rapidly when exposed to the ambient conditions of the day. The rate of this change will be proportional to the absolute humidity differential between the controlled and atmospheric regions.

The PhD thesis by Prahl (1968) suggests that the sorption isotherms of different paper samples should not be markedly different. Prahl's trial on both hardwood and softwood pulp produced by both the kraft and sulfite processes reveals practically identical isotherms at 50°C. A stone groundwood sample, however, did show a variation in its isotherm at this temperature.

Consequently, it was decided to perform a series of sorption tests for the ANM newsprint sheet under investigation and compare the results to those of Prahl to determine whether it is reasonable to use his correlations to describe the sorptive properties of the local pulps relevant to this study.

9.1 Experimental method

There are two main methods of determining equilibrium isotherms (Werling, 1978), static methods and dynamic methods. In static systems the sample can be placed in a dessicator over a saturated salt solution. Dynamic systems require air of controlled humidity to be blown over or through the material. This is a relatively fast mechanism for obtaining sorption isotherm curves.

Available equipment frequently dictates the method selected and in the current study a static test was performed. The paper samples were tested in a controlled temperature environment which consisted of a well

insulated 1.2m×0.5m×0.4m box which was heated under thermostat control by three 150W light globes. Under this configuration the temperature was able to be varied from 30°C to 65°C. Within the control volume there were supports for five sample jars. Each of the plastic sample jars was partially filled with a known saturated salt solution. The selection of each was based on handbook values which quoted the equilibrium relative humidity of air over each of the salt solutions for a range of temperatures.

Thus using the equipment available, five salt solutions were selected which covered the relative humidity range from 0-100% relatively evenly, and sorption tests were conducted for a number of temperatures. The five salts chosen, their equilibrium relative humidity in air at the temperatures of interest and an indication of their hot and cold solubility are shown in Table 9.1. The information was obtained from the *CRC Handbook of Chemistry and Physics (1991-92)* and some of the values for relative humidity were generated by interpolation.

TABLE 9.1
Solubility and relative humidity data for the five salts used in the sorption isotherm tests on paper

Salt	Symbol	ϕ%, 30° C	ϕ%, 35° C	ϕ%, 45° C	ϕ%, 65° C	g/100ml, Cold sol.	g/100ml, Hot sol.
Potassium Nitrate	KNO_3	91	89	86	81	13.3 (0°C)	247 (100°C)
Sodium Chloride	NaCl	75	75	75	75	35.7 (0°C)	39.1 (100°C)
Magnesium Nitrate	$Mg(NO_3)_2$ $.6H_2O$	52	50	47	42	125	very soluble
Potassium Carbonate	K_2CO_3	44	43	42	41	23.8 (20°C)	56.7 (100°C)
Magnesium Chloride	$MgCl_2$ $.6H_20$	33	32	31	30	167	367

Each test began with a check that the salt solution was indeed saturated for the prevailing test temperature. This was confirmed by ensuring that some solid particles remained in solution after the desired temperature was reached and the contents were well mixed. Paper samples were obtained from the paper machine reel and cut into 30cm×30cm pieces (4-5g dry).

Each sample was placed into the sealed plastic jar on an internal support which allowed for circulation of the vapour whilst preventing contact between the paper and the liquid salt solution. Each paper sample was removed and weighed daily until the mass of each sample had stabilised. Once this conditioned 'wet' mass of paper was obtained the samples were dried completely in an oven at 105°C for about a day. Weighings were conducted until moisture loss was observed to have ceased. The moisture content as a fraction of dry weight was then calculated. Masses were measured to a precision of 0.0001g.

9.2 Experimental results

The tests were performed on samples of machine newsprint made from a furnish of 75% thermo-mechanical pulp, 20% cold soda pulp and 5% kraft which had been dried once to ambient conditions and reached an equilibrium moisture content of about 0.10 kg/kg. Five relative humidity data points, corresponding to the five distinct saturated salt solutions, were obtained for each of the four temperature control points. Data from the four sorption isotherm curves are listed in Table 9.2 and graphed together in Figure 9.1.

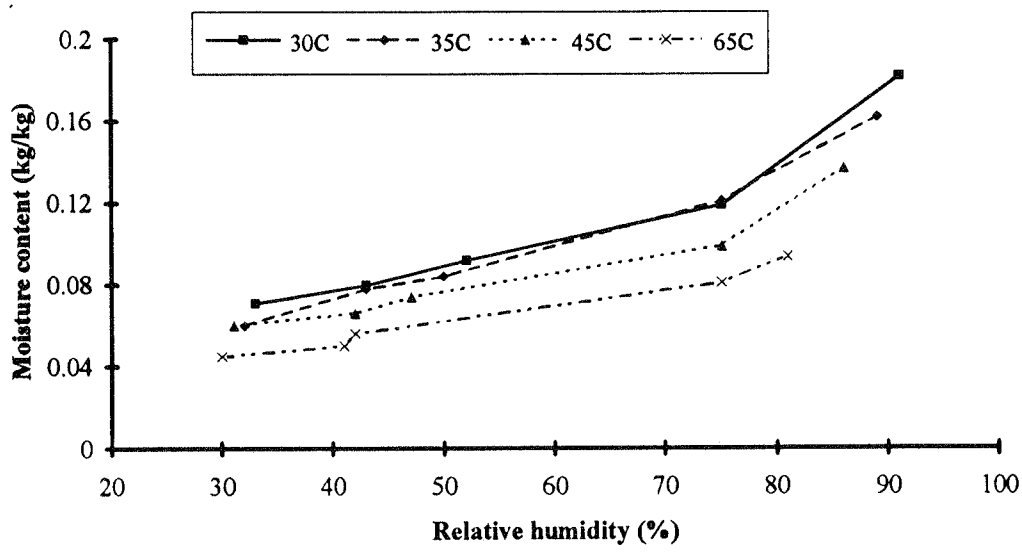

FIGURE 9.1
Graph showing sorption isotherms for machine-made newsprint (75% TMP, 20% CCS, 5% Kraft) at four test temperatures (30°C, 35°C, 45°C, 65°C)

TABLE 9.2
Results from sorption isotherm testing on newsprint

Temperature (°C)	Relative Humidity (%)	Moisture Content (kg_{water}/kg_{fibre})
30	91	0.182
30	75	0.119
30	52	0.092
30	43	0.080
30	33	0.071
35	89	0.162
35	75	0.122
35	50	0.114
35	43	0.078
35	32	0.060
45	86	0.137
45	75	0.099
45	47	0.074
45	42	0.066
45	31	0.060
65	81	0.094
65	75	0.081
65	42	0.057
65	41	0.049
65	30	0.045

Since each isotherm is composed from only five data points the resultant curves do not appear to be exceptionally smooth. Some of the scatter may be attributed to the thermostat operation which maintained control within a relatively coarse ±2°C band. This temperature control applied to the air temperature within the test volume. Temperatures within the actual

controlled relative humidity vessels within the greater test volume could be expected to exhibit some thermal inertia and experience temperature swings less than this.

With a temperature variation about nominal of up to ±2°C the results presented in Figure 9.1 may be expected to show some limited scatter about other published data. A 2°C change in ambient temperature leads to a maximum change of 2% in equilibrium moisture content. The maximum sensitivity to temperature change occurs during the high temperature test (65°C) at low relative humidities.

9.3 Comparisons with other research

The benchmark for sorption isotherm comparisons of wood pulps lies with the doctoral thesis of Prahl (1968). Prahl obtained experimentally both adsorption and desorption isotherms for 'Mobile Pine', a kraft processed softwood, for five temperatures over the range 22°C - 80°C. Prahl was able to obtain relative humidity measurements as low as 1% and as high as 99.6% but found that at these levels the paper samples took up to five days to reach equilibrium. Prahl obtained a reproducibility of 1% for adsorption tests and 2% for the desorption curves and for this reason his raw data is seen to be exceedingly smooth.

Since the current study is examining the *drying* of paper, Prahl's desorption data are used in the following analysis, as opposed to his adsorption data. Using a least squares fitting technique the current study processed Prahl's data to obtain the following relationship between equilibrium moisture content, relative humidity and temperature :-

$$\phi = \exp(b_1 T + b_2), \tag{9.1}$$

where,
$$b_1 = \exp\left(-17.255M + 0.121\sqrt{M} - 3.640\right), \tag{9.2}$$

and,
$$b_2 = -\exp\left(-14.313M - 2.167\sqrt{M} + 2.772\right). \tag{9.3}$$

Note that temperature, T, should be expressed in °K and moisture content, M, in kg_{water}/kg_{fibre}. ϕ is the fractional relative humidity.

Figure 9.2 depicts Prahl's raw desorption data for each of the five test temperatures between 22°C and 80°C. The smoothness of the curves

results from a total of 20 data points per isotherm over the range from 1%-99% relative humidity.

The shape of Prahl's isotherms is consistent with Brunauer's (1940) Type II classification for physical adsorption. Isotherms of this type are observed only in adsorbents in which there is a wide range of pore sizes. In such systems there is a continuous progression from monolayer to multilayer adsorption and then to capillary condensation.

Monolayer adsorption describes a single layer of the sorbent (water vapour) in contact with the sorbate (fibre). It may be considered that the vapour forms a hydrate with the sorbate. The attraction between the sorbent and sorbate is greater than that between the sorbent molecules themselves in the liquid state. The monolayer regime is significant at very low moisture contents, below 10%.

Multilayer adsorption occurs when several layers of the sorbent form on the sorbate. This may be regarded as a solution of the sorbent in the hydrated sorbate. The attraction of the sorbed molecules to the sorbate is small compared to the case of monolayer adsorption.

Capillary condensation is the third phase of the adsorption process and essentially involves the liquid sorbent filling the macropores of the sorbate. This refers to the sorbent generally referred to as free moisture and is outside the range of application of the sorptive behaviour of a medium.

The type II sorptive behaviour occurs as a result of the micropore structure of the material of interest. Evidence for the wide pore size distribution of paper was presented in Chapter 6. The sigmoid shape of the curves in Figure 9.2 is characteristic of all cellulosic materials.

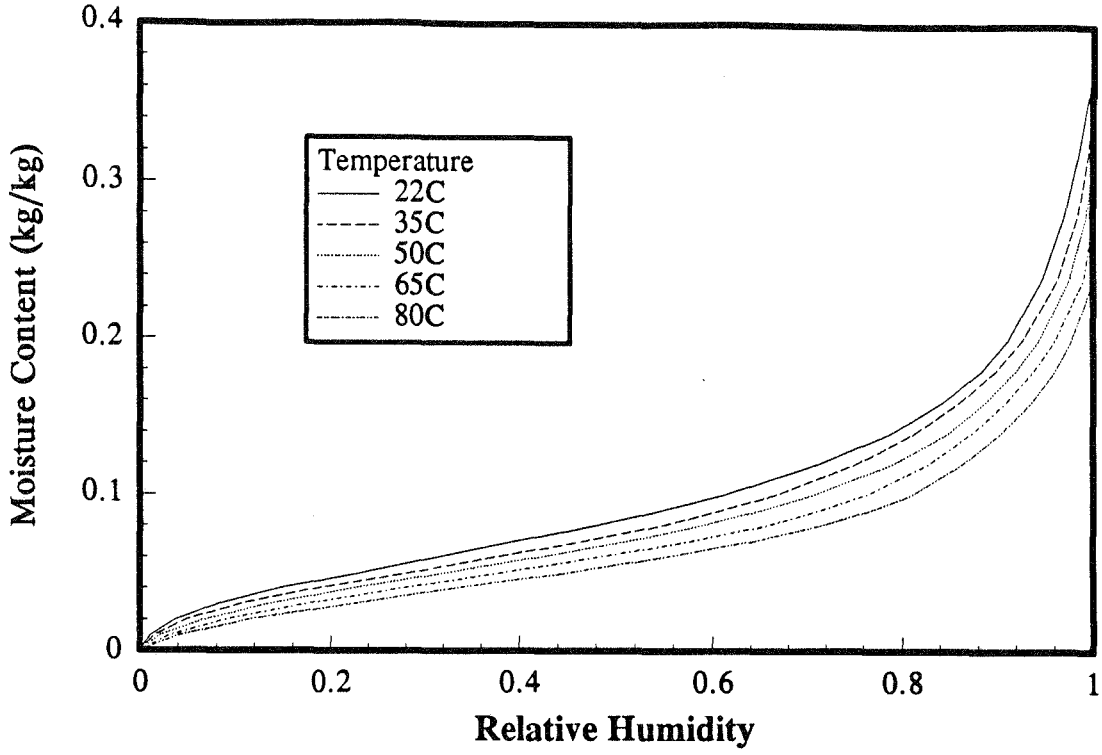

FIGURE 9.2
Prahl's desorption isotherm data for a kraft processed softwood

It is also worth noting the drop in hygroscopicity with increasing temperature. Consequently, as paper drying temperatures increase so does the sorptive effect diminish. This reduction in vapour pressure at higher temperatures is proportionately less and as a result the drying gradient and therefore drying rate increase on a normalised basis.

The sorption isotherms of Figure 9.2 give a suggestion of a *fibre saturation point (FSP)*. The FSP is the point at which the cell cavities (macropores) contain no liquid water but the fibre cell walls (micropores) are fully saturated with moisture. From a drying point of view the FSP represents a single point in a continuous range of paper sheet pore sizes. At moisture contents below the FSP the sorptive effects, such as reduced vapour pressure and increasing differential heat of sorption, gradually become significant in accordance with the data presented in this chapter. The other significance of FSP is its effect on the material's strength variation with moisture content. As moisture levels reduce below the FSP the strength of the paper sheet, or a wood sample, gradually increases as water is removed from the cell walls. This strength increase is observed in

the paper drying process by the fact that the sheet is subjected to more aggressive drying air flows in the dry end of the dryer section than in the wet end.

It is difficult to define a fibre saturation point on the basis of Prahl's results. The asymptotic nature of the curves near 100% relative humidity means it is awkward to designate a precise maximum moisture content for the hygroscopically bound water. However, the data suggest that the fibre saturation point varies from 0.24 kg_{water}/kg_{fibre} at 80°C to 0.4 kg_{water}/kg_{fibre} at 22°C

To graphically compare Prahl's results to those obtained in this study it was necessary to use equations 9.1-9.3 to interpolate Prahl's results for the four test temperatures utilised in the present study; 30°C, 35°C, 45°C and 65°C. The results of this comparison are presented in Figures 9.3-9.6. Prahl's results are represented by the continuous smooth curve, while in each case the five data points are from the current study.

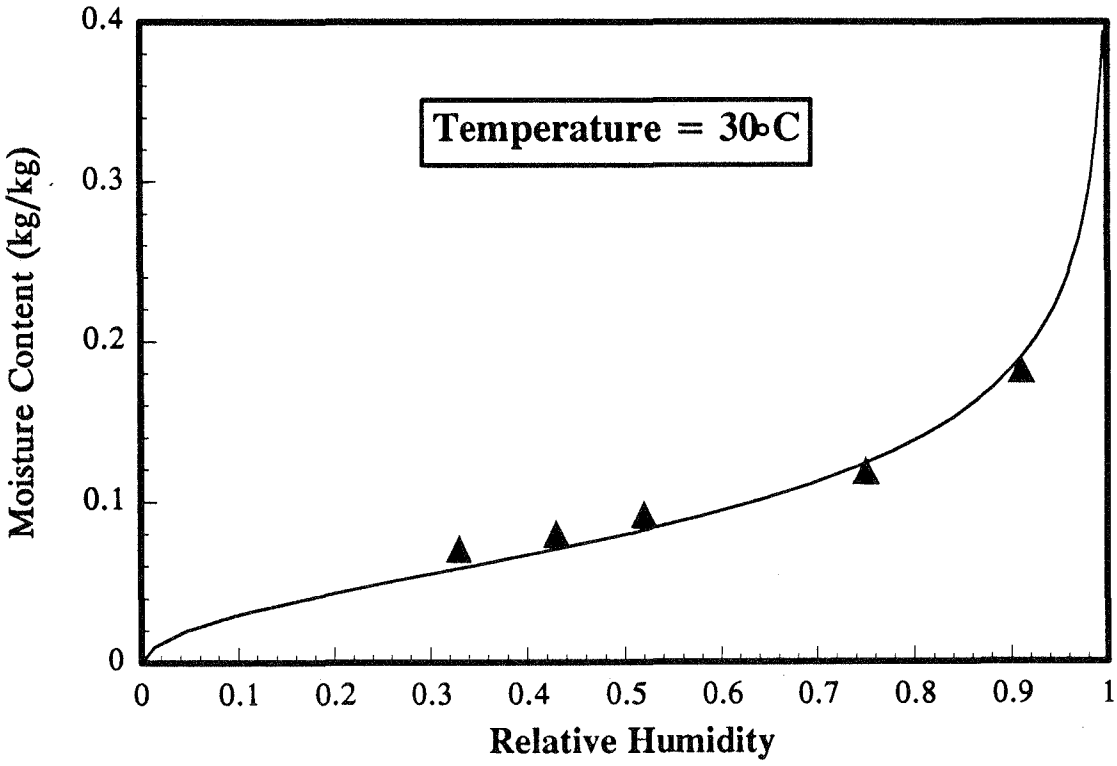

FIGURE 9.3
Comparison of sorption isotherm results of this study with those of Prahl (1968) at 30°C

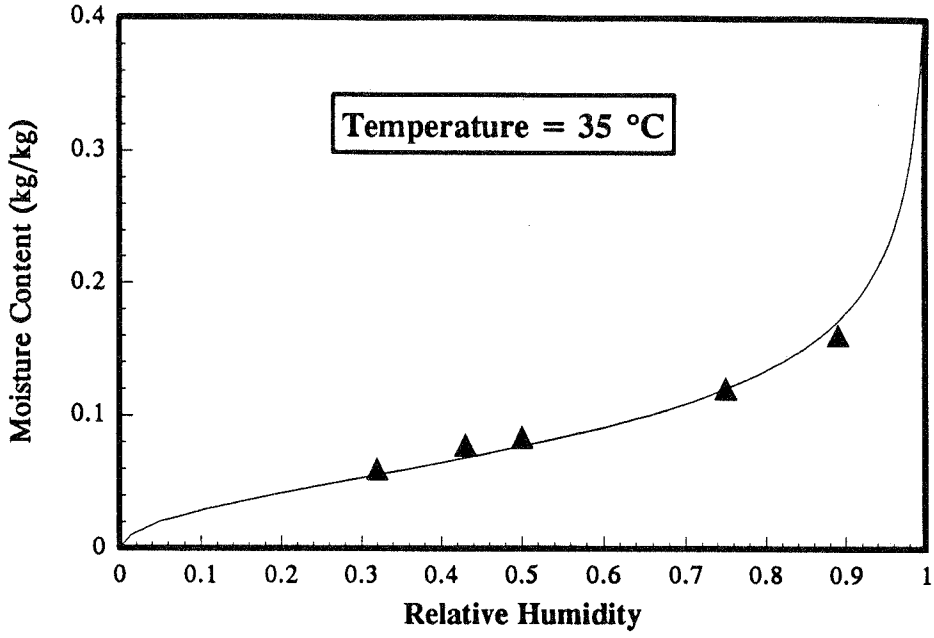

FIGURE 9.4
Comparison of sorption isotherm results of this study with those of Prahl (1968) at 35°C

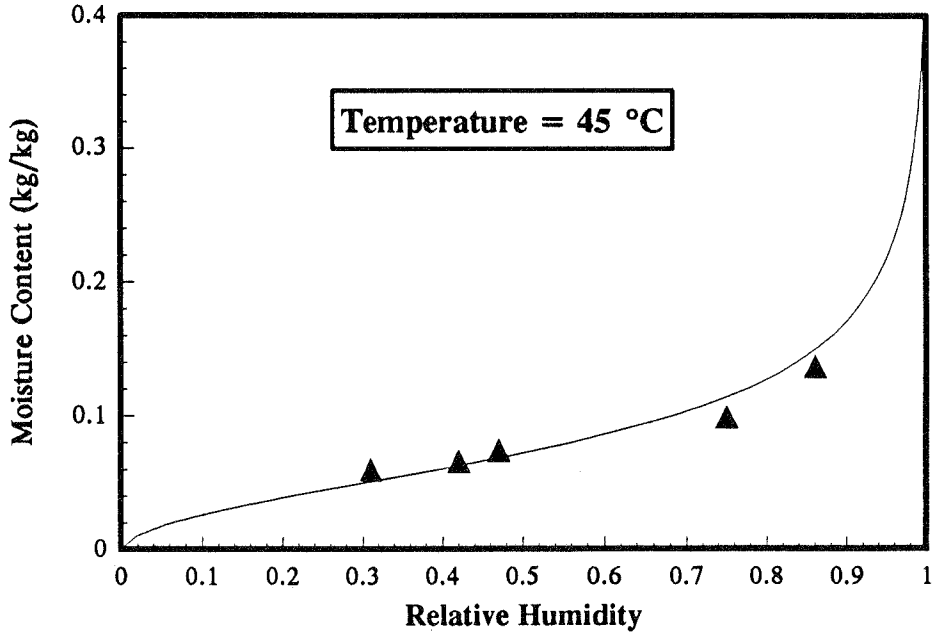

FIGURE 9.5
Comparison of sorption isotherm results of this study with those of Prahl (1968) at 45°C

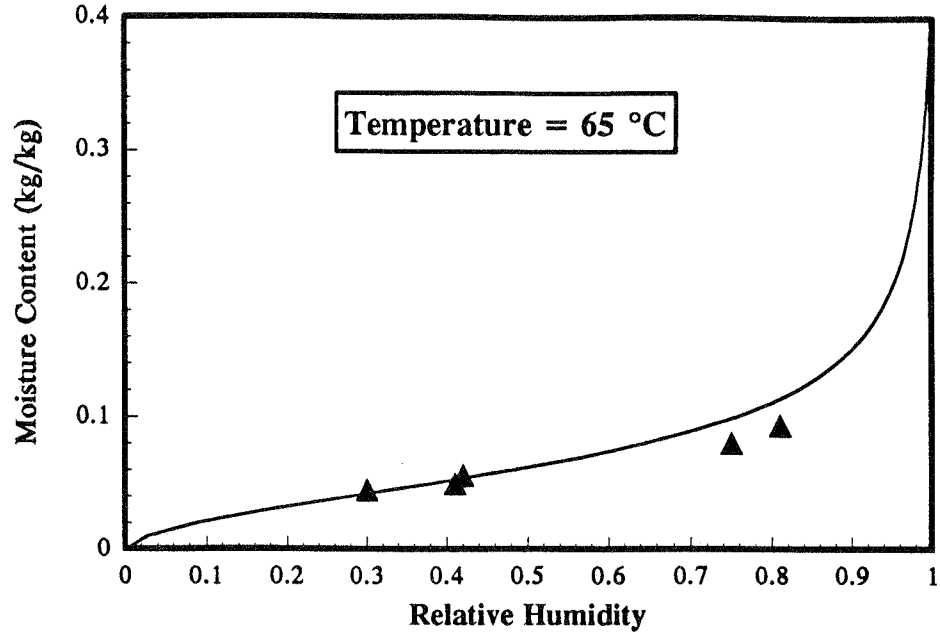

FIGURE 9.6
Comparison of sorption isotherm results of this study with those of Prahl (1968) at 65°C

The experimental results of this study are very similar to those of Prahl which is encouraging and of interest due the differences in the constituent fibres of the paper samples under study. Prahl made use of a Kraft processed softwood pulp whilst this study employed machine-made newsprint composed of 75% thermo-mechanical pulp (radiata pine), 20% cold caustic soda pulp (eucalypt) and 5% kraft (imported softwood pulp). Minor discrepancies between the two sets of data result from two sources. The earlier comment relating to coarse thermostat control on the experimental environment of this study may lead to variations in equilibrium moisture of up to 2%. The second and more significant issue relates to drying history of the paper samples.

In each of the tests performed the sample began in equilibrium with atmospheric conditions (≅ 20°C, 50% r.h., 0.085 kg/kg) and for each isotherm either gained or lost moisture depending upon the test relative humidity. Thus, low humidity measurements are obtained by desorption, whilst the high humidity readings produce equilibrium moisture contents indicative of a previously dried sample undergoing adsorption. Prahl's data demonstrated that at a given temperature and humidity the equilibrium moisture content for an desorption process will be higher than for an

adsorption process. This hysteresis tendency will therefore encourage the moisture content readings of this study at lower humidity (desorption) to be disproportionately higher than those at humidities exceeding ambient, corresponding to adsorption processes. The manner in which each set of five data points straddles the best fit correlation for Prahl's data suggests that this bias is far more significant than the temperature drift.

In summary, the sorption results generated in this study are a mixture of the adsorption and desorption curves. Notwithstanding this trend the data show close agreement with that of Prahl (1968), especially given that the fibre composition is significantly different. The correlations developed to represent Prahl's data have therefore been used in the drying model.

Other data

Another useful set of sorption isotherm data was obtained by Wink et al (1958). Their aim was to determine the desorption isotherm for paper at the high temperatures relevant to machine drying. Their particular desorption test was conducted over the range of relative vapour pressure from 0.98 to 0.20. The test was performed under a constant temperature of 200°F (93°C).

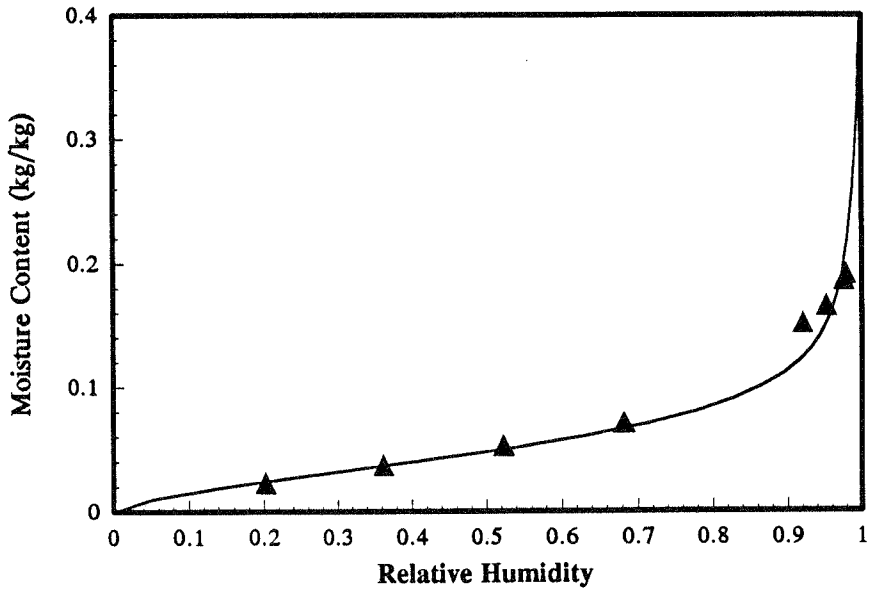

FIGURE 9.7
Data points of Wink et al (1958) for the desorption isotherm for a wood pulp furnish at 93°C plotted alongside the extrapolated prediction based on Prahl's work and calculated from equations 9.1-9.3

It is of interest to compare this set of data with the values predicted by extrapolating Prahl's results to 93°C by using equations 9.1-9.3. This is demonstrated in Figure 9.7, where the two sets of data are seen to be almost coincident, with the exception of a single point at high humidity.

The paper by Wink et al refers to 'a specific wood pulp furnish' which is not named. However, in the light of Prahl's work, and the conclusions from the previous section of this study, it appears that variations in furnish do not unduly change the sorption properties of cellulose-based materials.

The similarity of the data sets of Wink and Prahl at this temperature gives confidence for extending Prahl's results by extrapolation to the temperatures experienced within the dryer section of a paper machine, typically around 100°C.

9.4 Differential heat of sorption

Due to the bond energy associated with the physical adsorption of water to cellulose fibres there is an increase in the latent heat of vaporisation required for the water molecules to break these bonds and evaporate. This incremental energy requirement can be calculated from the Clausius-Clapeyron equation :

$$\frac{Q_s}{R_w} = -\frac{d\,Ln(\phi)}{d\left(\frac{1}{T}\right)}. \qquad (9.4)$$

where, Q_s = differential heat of sorption [J/kg],
R_w = gas constant for water [J/kg°K],
ϕ = fractional vapour pressure (Pv/Pv_{sat}), and,
T = temperature [°K].

Applying this equation to Prahl's desorption data, averaged over the five temperatures studied, allows the following correlation to be developed :-

$$Q_s = 1364 \exp\left(\frac{-19.45M}{1+M}\right) \ [kJ/kg]. \qquad (9.5)$$

Note that M represents the moisture content on a dry basis. The nature of the above relationship is illustrated graphically in Figure 9.8.

The heat of sorption data are seen to be significant below a moisture content of 0.3 kg_{water}/kg_{fibre}. As the moisture content approaches zero so does the heat of sorption approach its maximum of 1364 kJ/kg. This represents an additional 60% energy required to evaporate a quantity of water. For example, Rogers and Mayhew (1989) quote that h_{fg} = 2257 kJ/kg for free water at 100°C. Taking the extreme case as M→0, this equates to a total energy of vaporisation of 3621 kJ per kg of water in paper.

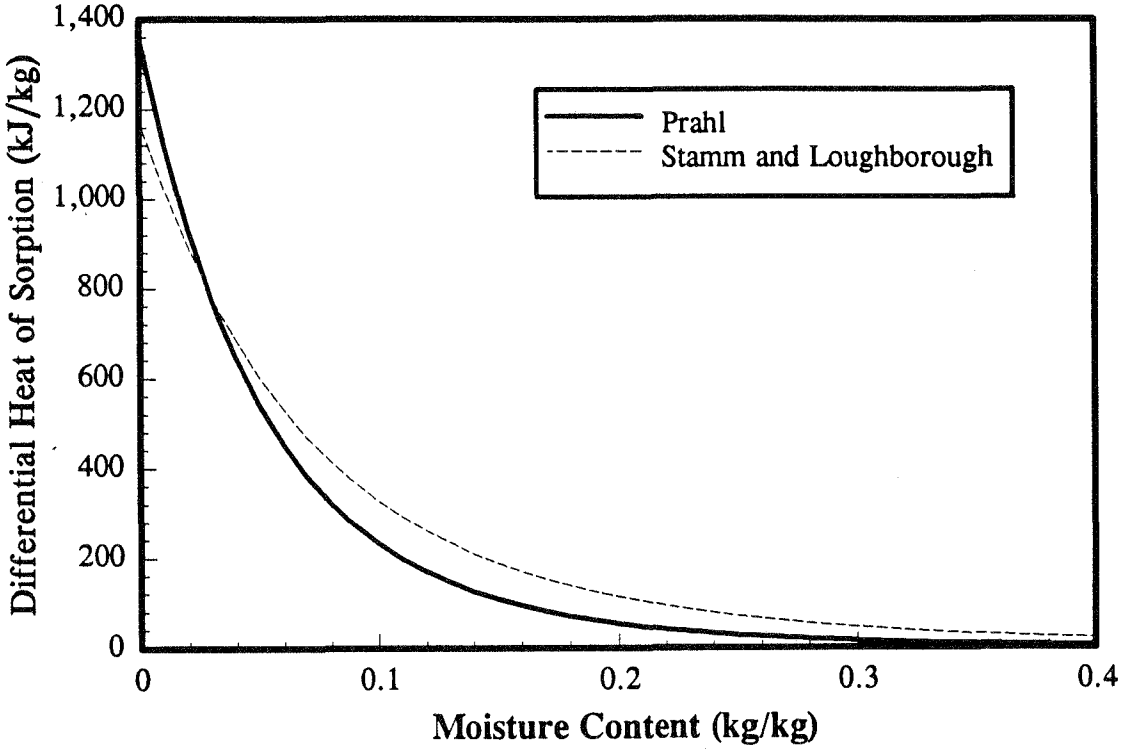

FIGURE 9.8
Correlation for differential heat of sorption computed from Prahl's desorption data together with Stamm and Loughborough's correlation

For comparison purposes it is worth noting the heat of sorption data of Stamm and Loughborough (1935) as presented by Skaar (1988). In this case the defining best fit equation is,

$$Q_s = 1172 \exp\left(\frac{-14\,M}{1+M}\right) \ [kJ/kg]. \qquad (9.6)$$

The results of Stamm and Loughborough, as shown in Figure 9.8, compare very closely with the findings of Prahl. Their data suggest that Q_s is significant up to the slightly higher moisture content of 0.4 kg/kg.

9.5 Mechanosorptive effect

Gunderson (1991) reports on the mechanosorptive properties of paper samples. Natural fibres, such as cellulose, sorb moisture under the application of mechanical stress. Given that the paper sheet in a machine dryer section is being continually stretched, as successive sub-sections run marginally quicker, the phenomenon deserves a brief comment. Gunderson's results on machine-made softwood paperboard show a moisture content gain of around 0.05% at maximum strain of 0.12%. Whilst this phenomenon is important in terms of the structural performance of paper which is subject to cyclic variations in humidity, it is not significant from the viewpoint of determining drying rates.

9.6 Conclusions

Based on the facts presented in Figures 9.1-9.7 it is fair to conclude that variation in pulp furnish makes no significant impact on the hygroscopic characteristics of a paper sample. Both the newsprint sheet composed of 75% thermo-mechanical pulp and the unspecified wood furnish of Wink et al (1958) were observed to closely follow the Prahl (1968) correlation derived from a kraft softwood pulp. Minor excursions from Prahl's data by the samples under study could be partially explained by the relatively coarse thermostat control (±2°C) available in the conditioned space and primarily by the previous drying history of the paper samples.

The sorption results generated in this study are a mixture of the adsorption and desorption curves, where the low humidity measurements are obtained by desorption and the high humidity readings produce equilibrium moisture contents indicative of a previously dried sample undergoing adsorption. This accounts for the manner in which each set of five data points straddles the best fit correlation for Prahl's data and suggests that this bias

is more significant than that induced through non-ideal temperature control.

Despite this trend the data show close agreement with that of Prahl, especially given that the fibre composition is significantly different. The correlations developed to represent Prahl's data and represented in equations 9.1-9.3 have therefore been used in the drying model.

Sorption testing by Wink et al (1958) at a temperature of 93°C was shown to closely match the correlation for Prahl's data when extrapolated to this temperature. This suggested that the relationship would be reliable at paper machine sheet temperatures which approach 100°C.

Similarly, the best fit approximation to Prahl's data was chosen to give the differential heat of desorption data over the range of temperatures encountered in paper machines. This description was quantified in equation 9.5 and is used in model calculations.

10. Other Paper Properties

To completely describe the paper drying process requires an assessment of the many diverse physical properties of the product. Permeability, pore size distribution, sorptive behaviour and drying transfer coefficients are dealt with elsewhere in this thesis. However, a number of paper properties remain to be discussed, namely, thermal conductivity, density, specific heat, fibre saturation point, shrinkage and the diffusion coefficient of vapour through the fibre structure. Consensus values determined by other investigators in these respective areas will be presented in this chapter.

The mathematical model also makes extensive use of the thermal properties of water, water vapour and air, and a summary of the constants and correlations used is presented at the end of this chapter.

10.1 Thermal conductivity

The thermal conductivity of paper, as defined by Fourier's law of conduction, is a function of the moisture content of the sheet. As the fibre, water and vapour phases which comprise the paper web transfer heat in parallel the combined thermal conductivity will be a combination of the component conductivities.

In their work on paper drying Depoy (1972) and Lee and Hinds (1981) have chosen to assume that the thermal conductivities work in parallel so that the sheet conductivity is simply the weighted sum of component conductivities. Others have estimated the sheet conductivity on the basis that the individual components are in series so the overall conductivity is calculated as the inverse of the sum of the reciprocals of the conductivities, in much the same manner as the electrical conductivity analogy works.

The parallel analogy which assumes that all fibres connect to each other and that there are no porous gaps in the direction of heat flow predicts an overall conductivity of,

$$k_I = k_f(1-\varepsilon) + k_w \varepsilon S + k_v \varepsilon(1-S), \qquad (10.1)$$

whilst the series layer model makes allowance for air/vapour gaps in between fibre and water sections and describes the overall conductivity as,

$$k_{II} = \frac{1}{\frac{1-\varepsilon}{k_f} + \frac{\varepsilon S}{k_w} + \frac{\varepsilon(1-S)}{k_v}}, \qquad (10.2)$$

where, k_f = fibre thermal conductivity [W/m²°K],
k_w = water thermal conductivity [W/m²°K],
k_v = vapour thermal conductivity [W/m²°K],
ε = sheet porosity [-], and,
S = fractional volumetric liquid saturation [-].

The parallel analogy for thermal conductivity, k_I, in equation 10.1 assumes that the fibre mass is contiguous across the sheet's thickness whilst the series model presented (k_{II}) in equation 10.2 assumes that horizontal layers of fibre, liquid and vapour apply across the sheet's thickness. A fair representation will be a combination of the two arrangements.

Nederveen et al (1991), Harmann and Schulz (1990) and Kartovaara et al (1985), proposed the use of a combination of the two structures. Kartovaara suggested that if the contribution from structure II is x and that from structure I is $1-x$, then the overall thermal conductivity of the material is,

$$k = \frac{1}{\frac{1-x}{k_I} + \frac{x}{k_{II}}}. \qquad (10.3)$$

The mixing parameter x thus diminishes as the connections formed by the solid phase between layers perpendicular to the direction of heat flow increase. Kartovaara obtained results for paper in the density range from 400-900 kg/m³ and found that x varied from 0.7 to 0.4 over this range. Analysis of Kartovaara's results shows that a mixing parameter value of $x=0.5$ is appropriate for paper with a density of 590 kg/m³ which applies to ANM newsprint. In this case equation 10.3 simplifies to,

$$k = \frac{2}{\frac{1}{k_I} + \frac{1}{k_{II}}} . \qquad (10.4)$$

The fibre thermal conductivity is considered to be independent of temperature over the relevant range. The thermal conductivity of water changes by about 7% over the temperature range from 50-120°C and a simple linear correlation for this may be applied.

Table 10.1 indicates the range of thermal conductivities for various pulp and paper products estimated by a number of authors.

TABLE 10.1
Thermal conductivity of various papers

Author	Sample	k ($W/m^2°K$)
Depoy (1972)	dry paper	0.121
Hartley & Richards (1974)	cellulose	0.335
Nakagawa & Shafizadeh (1984)	dry sulphite pulp	0.067
Soininen et al (1985)	dry paper	0.105
McAdams (1985)	unspecified paper	0.130
Kartovaara et al (1985)	solid fibre wall	0.157
Kerekes (1980)	newsprint, 8% moisture	0.169
Kirk (1972)*	bleached sulfite handsheets	0.084-0.117
Lau (1969)*	newsprint, 8% moisture	0.041
Powell (1974)*	dry newsprint	0.069

* denotes data referred to by Kerekes (1980).

The figures presented in Table 10.1 require some interpretation. The value for solid cellulose is significantly higher than the values for paper due to the effect of porosity. Several conductivities need to be corrected for moisture content to make them correspond to the other data. Most of the authors of the above conductivity values do not state the porosity of the sheets under test. Hence, it was decided to use Kartovaara's value for the solid fibre wall of $k_f = 0.157$ $W/m^2°K$.

When inserted into equation 10.4 for paper sheet conditions at dryer inlet ($M = 1.38\ kg_{water}/kg_{fibre}$) and dryer exit ($M = 0.10\ kg_{water}/kg_{fibre}$) for a sheet with porosity of 62%, the overall thermal conductivity is expected to vary from 0.37 W/m°K to 0.05 W/m°K over the course of drying.

10.2 Specific heat capacity

In a similar fashion to the handling of thermal conductivity in the previous section, the specific heat of a paper sample is also a function of the relative quantities of the constituent components. The specific heat of liquid water is widely documented as 4.19 kJ/kg°C and this is accurate to within ±0.01 kJ/kg°C over the temperature range 5-90°C (Rogers and Mayhew, 1989). For the dry fibre it is customary to use data listed for cellulose. Such data are presented in Table 10.2.

TABLE 10.2
Specific heat capacity of paper fibres

Author	Specific Heat (kJ/kg°C)
Depoy (1972)	1.34
Hartley & Richards (1974)	1.34
Nakagawa & Shafizadeh (1980)	1.17-1.34
Sutermeister (1941)	1.37
Kerekes (1980)	1.34 (dry) 1.45 (10% moisture)

Table 10.2 demonstrates that the cellulose specific heat capacity value of 1.34 kJ/kg°C is the consensus value amongst authors.

The specific heat of the paper sheet is not determined by the nature of the fibre structure but only by the relative quantities of components. For use in the computer model, the specific heat for paper is expressed as,

$$C = \frac{c_f \rho_f (1-\varepsilon) + c_w \rho_w \varepsilon S + c_v \rho_v \varepsilon (1-S)}{\rho_f (1-\varepsilon) + \rho_w \varepsilon S + \rho_v \varepsilon (1-S)}, \qquad (10.5)$$

where, C = paper sheet specific heat capacity [kJ/kg°K],
c_f = fibre specific heat capacity [kJ/kg°K],
c_w = water specific heat capacity [kJ/kg°K],
c_v = vapour specific heat capacity [kJ/kg°K],
ρ_f = fibre density [kg/m^3],
ρ_w = water density [kg/m^3],
ρ_v = vapour density [kg/m^3],
ε = sheet porosity [-], and,
S = fractional liquid saturation [-].

10.3 Density

Paper density is governed by the porosity of the sheet and the density of cellulose fibres. Values for the density of cellulose are widely documented and some quoted in Table 10.3.

TABLE 10.3
Values for cellulose density

Author	Cellulose Density (kg/m^3)
Kartovaara et al (1985)	1500
Corte (1982)	1550
Hartley & Richards (1974)	1550
Sutermeister (1941)	1560
Stone et al (1966)	1560

Stone also quotes the density of lignin, the secondary component of wood fibre, as 1440 kg/m^3. Chemical pulping is extremely effective in delignifying pulp fibres, but mechanical pulping may leave a lignin content of up to 20% according to d'A Clark (1981). The overall fibre density will be a linear combination of the two primary components and a value of 1540 kg/m^3 is substituted for use in the model.

10.4 Diffusion coefficient

The diffusion of water vapour through the paper sheet is characterised by Fick's law,

$$\dot{m}_v = -D_v \frac{\partial \rho_v}{\partial y}, \qquad (10.6)$$

where $\dot{m}_v$ = mass flow rate of vapour per unit area [kg/m^{2}s],
D_v = vapour diffusion coefficient [m^2/s],
ρ_v = vapour concentration [kg/m^3], and,
y = dimension across sheet thickness [m].

Shishido et al (1978) describe an experimental procedure for determining the diffusion coefficient of moisture within wet material. This was based on a standard drying rate arrangement with hot air blowing over the sample in a duct. The surface moisture content was measured by an infrared hygrometer and changes in the sample mass by an electronic weight transducer.

The difficulty in replicating this set-up in what is a relatively minor component of the overall paper-drying study influenced the decision to rely on other published results rather than conduct a first hand investigation into diffusion coefficient.

The effective diffusion coefficient will be a function of both the diffusion coefficient of water vapour in air and the restriction that the porous fibre structure places on vapour flows.

Incropera and Dewitt (1985) quote $D_{water\text{-}air} = 26\times10^{-6}$ m^2/s at 298°K and $D_v \propto T^{1.5}$. This value applies for unimpeded mixing of water and air over the full unit area. For the case of the paper sheet this figure will be reduced by the diffusibility, δ, a factor ($0<\delta<1$) which accounts for the tortuous flow path the vapour must engage within the web as well as area restrictions due to a porosity less than unity.

Han and Matters (1966) developed some correlations for vapour diffusibility in partially saturated fibre mats. Their correlations were quite complex and can be summarised more simply, with little loss of accuracy, by the linear relation,

$$\delta = 0.4\,\varepsilon\,(1\text{-}S), \qquad (10.7)$$

where ε is the porosity and S is the fractional volumetric liquid saturation. The $\varepsilon(1-S)$ factor in equation 10.7 deals with the area reduction whilst the 0.4 modifier is included to represent the tortuosity of the flow path.

Thus, for a newsprint sheet with a porosity of 0.62 the diffusion coefficient can be expressed as,

$$D_v = 6.45\times10^{-6}\,(1-S), \qquad (10.8)$$

and increases during drying as the liquid in the macropores evaporates and leaves more cross-sectional area for vapour transfer.

10.4 Fibre saturation point

A wet paper sheet may contain water in three forms, liquid water within the pores, water vapour within the empty pores, and water adsorbed to the surface of and within fibre walls. As discussed in Chapter 9 which deals with the sorptive behaviour of paper the liquid within the porous cavities is termed *free* water to differentiate it from the *bound* water within the fibre walls which is bonded more strongly to the fibre structure. When the sheet is dried the free water is removed first. The moment that the macro-pores are empty whilst the fibres themselves remain fully saturated (micro-pores) is designated the fibre saturation point (FSP). This point is significant in papermaking as further reductions in moisture content produce an increase in the strength of the paper sheet and consequently improve machine runnability.

Whilst the FSP is defined as a precise moisture content designating a division between micro and macro-pores in a porous fibre-based material, it does not represent a discontinuity in the overall pore structure of the medium. It is the moisture content below which hygroscopic effects such as reducing vapour pressure ratio and increasing differential heat of sorption start to become significant in the overall drying behaviour. The specific application of FSP in the drying model is detailed in the following section which describes shrinkage of the paper sheet thickness during drying.

Prahl's (1968) sorption isotherms presented in Chapter 9 are quite asymptotic for relative vapour pressures near 100%, but do suggest a relationship between FSP and temperature. Prahl's data were regressed to give the following relationship,

$$M_{fs} = 0.4575 - 0.0027 \times T \ [kg_{water}/kg_{fibre}], \qquad (10.9)$$

where the temperature, T, is in degrees Celsius.

Skaar (1988) notes that the FSP for most woods ranges between 25-30% wet basis or 0.3-0.4 kg_{water}/kg_{fibre} (dry basis). This figure is likely to be higher for papers due to the lignin removal and defibrillation associated with the pulping processes. For paper, Siau (1971) obtained an empirical relation for fibre saturation point as a function of temperature,

$$M_{fs} = 0.293 - 0.00149 \times T \ [kg_{water}/kg_{fibre}], \qquad (10.10)$$

where the temperature, T, is in degrees Celsius.

A comparison of the two correlations is shown in Figure 10.1.

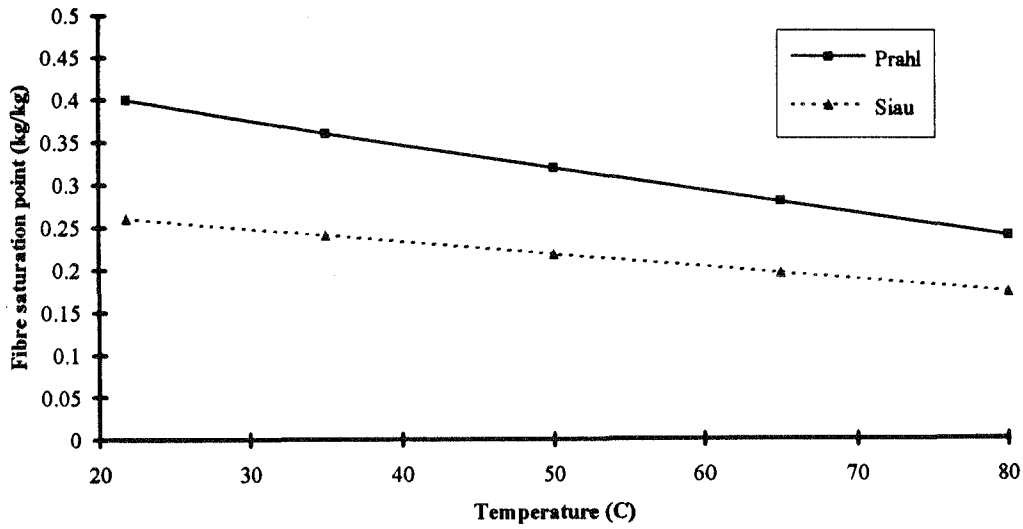

FIGURE 10.1
Comparison of FSP correlations obtained from Prahl (1968) and Siau (1971)

The composition and type of paper used by Siau was not clear and so for consistency with the previous sorption isotherm results the relationship inferred from the data of Prahl (1968) was used to define FSP for this study. Over the typical paper machine drying temperature range from 70-100°C the FSP is therefore expected to change from 0.26-0.18 kg/kg.

Both Kerttula (1984) and Eskelinen (1985) quoted a dryness content of 80% beyond which hygroscopic effects become significant. This is equivalent to claiming a fibre saturation point of 20% (wet basis) or 0.25 kg_{water}/kg_{fibre} (dry basis).

10.6 Shrinkage

The paper sheet's fibre saturation point (FSP) is useful for estimating the variation of sheet thickness throughout the drying process. Hygroscopic moisture below the FSP is primarily located within fibre micropores and causes fibres to swell as it is absorbed. This fibre swelling is translated through the fibre matrix and increases the thickness of the sheet. Thus the maximum sheet thickness is given by the swollen collective thickness of paper fibres at or above the fibre saturation point. Above FSP additional free moisture fills the macro-pore space. This can be expressed analytically as,

$$L(M) = L(0) + \text{Min}(M, FSP)\frac{b_{wt}}{\rho_w(1-\varepsilon)}, \qquad (10.11)$$

where
- L = sheet thickness (caliper) [m],
- M = moisture content [kg_{water}/kg_{fibre}],
- ρw = water density [kg/m^3],
- ε = sheet porosity [-], and,
- b_{wt} = dry fibre basis weight [g/m^2].

L(0) represents the dry caliper of the paper sheet and is determined from scanning measurements made of the paper after the dryer section. Equation 10.11 is used in the mathematical model to predict the change in sheet caliper throughout the drying process. The elemental thickness, *dy*, is therefore also a changing quantity throughout the model calculation.

McKnight et al (1958) quote the work of Pierce (1953) which shows that during drying an isotropic sheet of paper shrinks only a few percent in area, but the change in thickness may be as high as 200%. This indicates that surface tension forces generated during drying are predominantly normal to the surface and influence mainly the total void space rather than the pore size distribution. Such surface tension forces within the paper sheet are developed as a result of moisture evaporating from a pore of radius, R, in accordance with the Kelvin equation,

$$P_c(R) = -\frac{2\sigma \mathrm{Cos}\gamma}{R}, \qquad (3.8)$$

where σ is the surface tension of water and the contact angle γ is taken as 0°. The negative capillary pressure, P_c, becomes significant at small radii (micro-pores) and causes the paper web to shrink.

McKnight et al (1958) demonstrated this effect by comparing freeze-dried and air-dried samples of paper. The freeze-dried sample in which water was removed by sublimation resulted in a highly porous and bulky sheet with low strength compared with the more commonly air-dried sample. The differences were caused by the surface tension induced, capillary pressures which promote inter-fibre bonding in the air-dried sample which evaporates liquid water as opposed to subliming.

Rance (1980) presents a graph which relates lateral shrinkage to moisture content. Beginning with a paper sheet with a dry basis moisture content of 4 kg_{water}/kg_{fibre} (80% wet basis) the sheet experienced 0.5% shrinkage during drying to 1.5 kg_{water}/kg_{fibre}, a typical dryer section inlet moisture content, and a total of almost 4% lateral shrinkage in drying to 0.1 kg_{water}/kg_{fibre}. This confirms that the paper sheet surface area and hence pore size distribution is relatively unaffected by shrinkage during drying. This is convenient as it would be rather impractical to update the complex pore size distribution used in Chapter 6 for changes due to cross-directional shrinkage.

10.7 Physical properties of water

The properties of water, in both liquid and vapour form, used throughout the mathematical model are taken from Rogers and Mayhew (1989) and presented below. The values and correlations are taken to apply over the 50-100°C temperature range which is relevant to machine paper drying.

density - liquid (ρ_L) :	1000 kg/m^3
viscosity - liquid (μ_L) :	$(374\times10^{-6}\times\exp(-(T-75)/67.4))$ kg/m.s
viscosity - vapour (μ_v) :	11×10^{-6} kg/m.s
enthalpy - liquid (h_f):	$(4.19\times T)$ kJ/kg
enthalpy - vapour (h_g):	$(2635 + 1.688\times(T-75))$ kJ/kg

heat of vaporisation (h_{fg}):	(2321 - 2.508×(T-75)) kJ/kg
thermal conductivity - liquid (k_L) :	0.67 W/m/°K
thermal conductivity - vapour (k_v) :	0.022 W/m/°K
specific heat - liquid (C_{pL}) :	4.19 kJ/kg°K
specific heat - vapour (C_{pv}) :	1.94 kJ/kg°K

In the above expressions the temperature, T, is in °C.

10.8 Physical properties of air

The physical properties of air used in the analysis of laboratory test data are also taken from Rogers and Mayhew (1989) and presented below.

viscosity :	$(1.72\times10^{-5} + 4.56\times10^{-8}\times T)$ kg/m.s
kinematic viscosity :	$(1.31\times10^{-5} + 9.74\times10^{-8}\times T)$ m^2/s
thermal conductivity :	$(2.42\times10^{-5} + 7.58\times10^{-8}\times T)$ W/m/°K
diffusivity of water in air :	$2.6\times10^{-5} \times ((T+273)/298)^{1.5}$ m^2/s
specific heat :	1.005 kJ/kg°K

In the above expressions the temperature, T, is in °C.

11. Energy Consumption

The work of the model in calculating drying rate within the paper machine can quite naturally be extended to describe the energy consumption associated with given drying conditions. The detail of the model makes it possible to ascertain the implications of changes in energy input to various parts of the dryer section. For known values of energy consumption the drying efficiency can be calculated and used as the basis for comparisons between different machine operating conditions and configurations. Possible changes include the redirection of steam energy between the drying cylinders and the pocket ventilation system to obtain the most efficient balance. The impact on production and energy consumption of a change from double to single-felted drying would be another scenario which could be analysed.

11.1 Dryer section energy balance

The energy flows into and out of the dryer section are characterised by four major streams; paper fibre, steam, air, and water which enters with the paper and leaves with the exhaust air. There is also the provision for a term which expresses heat loss by radiation and natural convection from the dryer hood to the machine room. These flows are presented schematically in Figure 11.1.

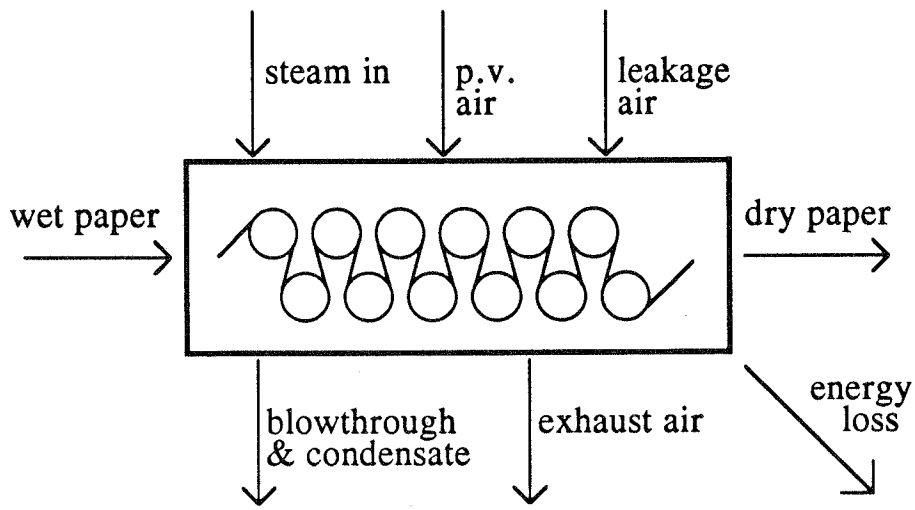

FIGURE 11.1
Energy flows through the dryer section of the paper machine

The dryer hood shown schematically in Figure 11.1 is the structural framework which encloses the entire drying region which includes the dryer cylinders, the ventilation system, the dryer fabrics and the paper sheet itself which enters with a moisture content of around 1.4 kg_{water}/kg_{fibre} and leaves with 0.1 kg_{water}/kg_{fibre}. The photographs presented in Figures 1.2 and 1.4 illustrate this arrangement.

The dryer hood operates under negative pressure. The air vented by the exhaust fans is a combination of air from the supply fans (60-80%), *pocket ventilation (p.v.) air*, and *infiltration air* (20-40%). The pocket ventilation air is so named because the duct outlets direct the drying air into the dryer pockets formed by the cylinders, the dryer fabric and the paper sheet (see Figures 3.4 and 12.4). The infiltration air leaks into the dryer hood through various access door openings and reduces the average air temperature and absolute humidity within the dryer hood. As these are counteracting effects there will be an optimal infiltration rate which aids energy efficient drying.

From this description an energy balance can be developed which enables the heat loss and dryer efficiency to be calculated. The variables used in the dryer hood energy balance are defined in Table 11.1.

TABLE 11.1
Definition of energy balance variables

Stream	Mass Flow	Temperature
paper fibre in	m_f	Tf_{in}
paper fibre out	m_f	Tf_{out}
steam in	m_s	Ts_{in}
condensate out	m_s	Ts_{out}
p.v. air in	m_{pv}	T_{pv}
leakage air in	m_{leak}	T_{leak}
exhaust air out	m_{exh}	T_{exh}
water in	$M_{in}.m_f$ $w_{leak}.m_{leak}$ $w_{pv}.m_{pv}$	Tf_{in} T_{leak} T_{pv}
water out	$M_{out}.m_f$ $w_{exh}m_{exh}$	Tf_{out} T_{exh}

In Table 11.1 the terms M_{in} and M_{out} refer to the paper sheet moisture content (kg_{water}/kg_{fibre}) at the inlet and outlet of the dryer section respectively. The variables w_{pv}, w_{leak} and w_{exh} refer to the absolute humidity of the pocket ventilation, leakage and exhaust air flows. The $m\_$ terms are mass flow rates (kg/s).

Equating energy into with energy out of the system produces the defining relation :

$$m_f cp_f(Tf_{out}-Tf_{in}) + m_s(hs_{out}-hs_{in}) + cp_{air}(m_{exh}T_{exh}-m_{pv}T_{pv}-m_{leak}T_{leak}) +$$

$$m_f cp_w(M_{out}Tf_{out}-M_{in}Tf_{in}) + (w_{exh}m_{exh}hg_{exh}-w_{pv}m_{pv}hg_{pv}-w_{leak}m_{leak}h_{gleak})$$

$$+ Q_{loss} = 0, \qquad (11.1)$$

where the c_p terms represent the specific heat at constant pressure (kJ/kg°C) for the subscripted components, h is the enthalpy (kJ/kg) of water/steam as a function of temperature and phase and Q_{loss} (kW) is the rate of heat loss from the dryer hood into the machine room.

Of the four distinct streams within the dryer section it can be said that the steam and dry paper fibre exhibit constant mass flow, mass in equals mass out, whilst the water and air flows interact with contributions from a number of sources. The relevant mass flow equations relating this interaction are, for water,

$$M_{in}m_f+w_{leak}m_{leak}+w_{pv}m_{pv} = M_{out}m_f+w_{exh}m_{exh}, \qquad (11.2)$$

and for air,

$$m_{leak} + m_{pv} = m_{exh}, \qquad (11.3)$$

Equation 11.3 allows the mass flow of the infiltration (leakage) air into the hood to be quantified using measurements of the hood air supply and exhaust flow rates. The knowledge of machine operating speed (m/s), basis weight (kg/m^2) and trim (machine width, m) implies a value for fibre mass flow and equation 11.2 then is able to determine paper sheet moisture loss and consequently sheet moisture content at the dryer inlet. This is a very useful calculation as the initial moisture content is a quantity which is rarely measured, yet clearly has a first order effect on all drying rate estimates.

11.1.1 PM3 energy balance calculation

A sample calculation for the ANM PM3 machine provides an indication of the applicability of the equations and the magnitude of the flows. At a machine speed of 1050 m/min, manufacturing newsprint of basis weight 48.8 g/m^2 and final moisture content of 8.9%, the measured air flows were $m_{pv} = 41.0$kg/s, and $m_{exh} = 73.7$kg/s. The infiltration air flow must therefore be $m_{leak} = 32.7$kg/s, and the *hood balance*, which is defined as the ratio of conditioned air input to total exhaust air, is 56%.

Using the air condition data, namely that the machine room absolute humidity is $w_{leak} = 0.015$kg/kg, the inlet pocket ventilation air is at $w_{pv} = 0.03$kg/kg, and the exhaust air has a moisture content of $w_{exh} = 0.11$kg/kg, the quantity of water evaporated from the sheet is $(M_{in}-M_{out}).m_f = 6.39$kg/s. This corresponds to an initial moisture content of 1.32 kg_{water}/kg_{fibre}.

The calculation can be extended to equation 11.1 to assess the energy loss from the dryer hood to the machine room. Given the temperatures, $Tf_{out} = 80°C$, $Tf_{in} = 50°C$, $T_{exh} = 75°C$, $T_{pv} = 40°C$, $T_{leak} = 25°C$, the steam enthalpies, $hs_{out} = 690$kJ/kg, $hs_{in} = 2771$kJ/kg, the specific heats, $c_{pf} = 1.34$kJ/kg°C, $c_{pa} = 1.005$kJ/kg°C and a dryer section steam consumption of 9.44kg/s the energy loss is $Q_{loss} = 660$kW.

The distribution between both input and output energy flows is shown in Figures 11.2 and 11.3 below. Q_{loss} is identified by the arrow.

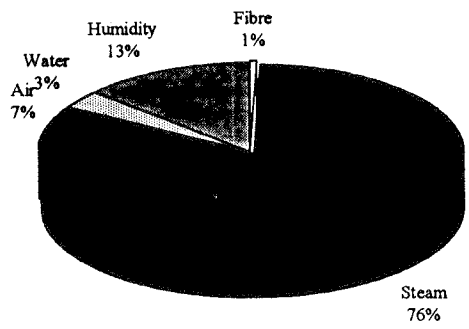

FIGURE 11.2
Input energy flows

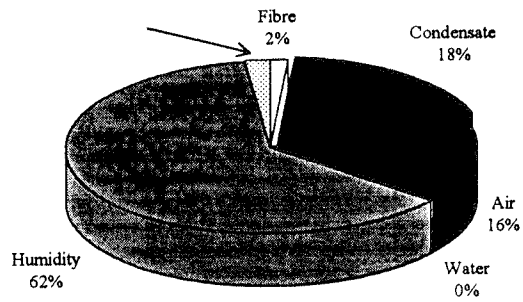

FIGURE 11.3
Output energy flows

The efficiency of the dryer section can be appraised in terms of the ratio of moisture evaporation from sheet to the steam energy expended :

$$\eta = \frac{m_f(M_{in} - M_{out})(h_{g_{exh}} - c_{p_w} T_{in})}{m_s(h_{S_{in}} - h_{S_{out}})} = 0.81. \qquad (11.4)$$

In the paper industry it is more common to quote the specific steam consumption (SSC) on either a per unit paper produced or per unit water evaporated basis. Given these definitions the figures are :

$$SSC_{water} = \frac{m_s}{m_f(M_{in} - M_{out})} = 1.5 \frac{kg_{steam}}{kg_{water\ evap}}, \qquad (11.5)$$

and,

$$SSC_{paper(reel)} = \frac{m_s}{m_f(1 + M_{out})} = 1.7 \frac{kg_{steam}}{kg_{paper}}. \qquad (11.6)$$

Similar calculations for the other ANM paper machine, PM2, producing newsprint at 880 m/min show similar results within 2%.

Although SSC_{paper} is more frequently quoted, SSC_{water} is more useful because it normalises the effect of initial moisture content and allows dryer sections to be compared equitably. When comparing these values with other paper mills caution is required as the steam consumption may only include drying cylinder steam or it may include all steam used by a machine from former to calender stack rather than the steam use of the complete dryer section.

11.1.2 Comparison of ANM machines with industry energy data

A comprehensive survey of Canadian newsprint machine dryer section energy use by Pikulik and Sayegh (1988) showed that SSC_{paper} varied from 1.2 kg/kg to 3 kg/kg with a mean of 2 kg_{steam}/kg_{paper}. The parameter SSC_{water} exhibited a range of 1 kg/kg to 2.2 kg/kg with an average value of 1.5 kg_{steam}/kg_{water}.

Comparison of the ANM machine dryer data with these values shows them to be in the lower half of the respective ranges, and equal to or below the mean values of the Canadian study. This may be due in part to the fact that the 1993 ANM data were obtained five years after Pikulik and Sayegh conducted their study. General modernisation of installed paper-making

equipment throughout the Canadian industry during this time would probably lead to a modest reduction in the specific steam consumption from those figures quoted in 1988.

The TAPPI Technical Information Sheet TIS-0404-15 (1986) presents data summarising paper machine drying rate for approximately 70 different newsprint paper machines. The results are given in terms of water evaporation per unit of cylinder drying surface ($kg_{water}/h/m^2$), which is calculated in accordance with TAPPI Technical Information Sheet TIS-0404-07 (1989), against steam temperature. This quantity is a measure of dryer section effectiveness as opposed to energy efficiency. For a given dryer section size it ranks the ability of a machine to evaporate moisture in the dryer section for a given peak steam temperature in the drying cylinders.

The specific drying rate figure for the ANM PM3 machine is 15.7 $kg_{water}/h/m^2$ for 48.8 g/m^2 newsprint produced at 1050 m/min with a peak steam pressure of 130kPag (124°C). For the ANM PM2 machine producing 48.8 g/m^2 newsprint at 880 m/min with a peak steam pressure of 110kPag (122°C) the evaporation per unit of cylinder drying surface is 14.3 $kg_{water}/h/m^2$.

The TIS-0404-15 results are used to generate Figure 11.4 which is presented below and includes reference marks to distinguish the ANM operating points.

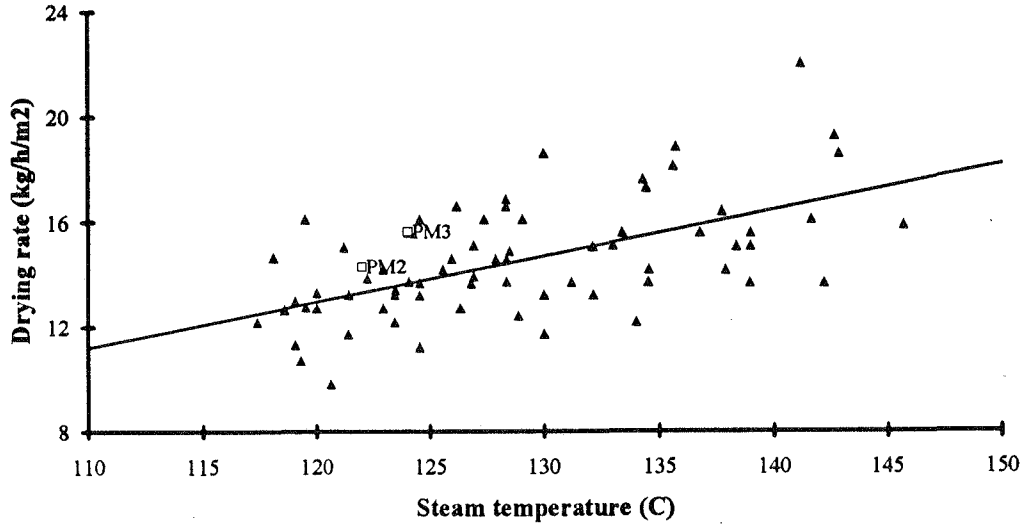

FIGURE 11.4
Paper machine drying rate data (TAPPI TIS 0404-15, 1986)

The line through the middle of the data points in Figure 11.4 is a best fit line which represents the average drying rate per unit of drying cylinder surface for each steam temperature. Data points situated above this, such as the ANM PM2 and PM3 operating points, represent above average dryer section performance. One of the key reasons for the range of values is that some paper machines may not be operating at the dryer's full potential because machine speed is limited by other sections of the paper machine, the press or forming section for example. Variations in dryer configuration, such as single versus double-felted runs, and pocket ventilation rates will also affect these values.

11.2 Heat transfer to the paper sheet

The preceding discussion concerning energy consumption can be integrated with the earlier development of the drying model. Using a calculation like the previous one as a benchmark to assign a value to Q_{loss}, the energy required for various drying configurations and operating conditions is obtained.

The dryer section energy input, $m_s.(hs_{in}-hs_{out})$, is a combination of steam into the 44-48 dryer cylinders and into the hood pocket ventilation and general air heating. The energy input to the drying cylinders, as opposed to heated ventilation, can be estimated from the heat transfer into the paper sheet. To quantify this, the heat transfer from the condensing steam through the cast iron dryer shell and into the paper sheet is,

$$\begin{aligned} Q &= h_{cond}(T_{steam} - T_{shell-int}) \\ &= \frac{k_{shell}}{dr}(T_{shell-int} - T_{shell-ext}) \\ &= h_{contact}(T_{shell-ext} - T_{paper}), \end{aligned} \qquad (11.7)$$

where the temperature drop across the dryer shell is expressed by *(Tshell-int – Tshell-ext)*, *dr* is the thickness of the dryer shell, *hcond* the heat transfer coefficient through the condensate layer, *kshell* the thermal conductivity of cast iron and *hcontact* the heat transfer coefficient between the cylinder surface and the paper sheet.

Figure 11.5 outlines the various resistances to heat flow from steam inside the cylinder to the paper sheet in a similar manner to that used by

Wiedenbeck (1989). Whilst the resistances to heat transfer are summarised by the parameters, h_{cond}, k_{shell}, and $h_{contact}$, there are a number of physical barriers which are incorporated into these coefficients and include, condensate layer thickness, condensate layer movement, non-condensable accumulation, rust or deposits on inside surface of cylinder, shell thickness, outer surface dirt or corrosion products, air boundary layer between sheet and cylinder, roughness of sheet, dryness of sheet and surface structure of sheet.

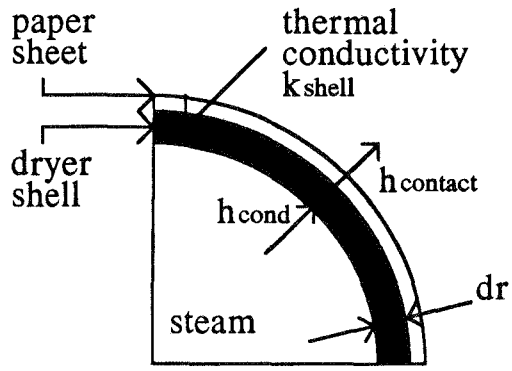

FIGURE 11.5
Drying cylinder thermal resistances

11.2.1 Condensate heat transfer coefficient

The value of the condensate heat transfer coefficient is primarily dependent upon the state of the condensate within the drying cylinder, in addition to the presence of internal scale or non-condensables. At low operating speeds the condensate may pool or cascade within the cylinder before being evacuated. However, at speeds greater than 500 m/min which are associated with newsprint production the condensate will rim the circumference of the cylinder. This stagnant layer of water produces a considerable heat transfer barrier. Thus, the internal surface of drying cylinders is often fitted with spoiler bars - rectangular, machine width bars with a cross section approximately 25mm×5mm which are spaced around the dryer periphery to promote maximum turbulence and hence improved heat transfer for the water layer. For such an arrangement, which is present on ANM machines, the condensate heat transfer coefficient has been measured by Chance (1989) as 2400 W/m^2°C, independent of machine speed once above the 500 m/min threshold. This figure will reduce as dirt and scale build up on the inner cylinder wall.

11.2.2 Shell thermal resistance

The cast iron cylinder has a thermal conductivity of 49 W/m°C and a thickness of 28.6mm ($1\,^1/_8$"). Hence, $k_{shell}/dr = 1700$ W/m^2°C.

Since the heat transfer, Q, is known from the quantity of steam condensed within the cylinder, and the saturation temperature is a function of the steam pressure, the internal shell surface temperature can be calculated. A similar calculation allows the external shell temperature to be determined. This value is then used for the cylinder contact temperature which is one of the boundary conditions in the drying model. These calculations will vary from cylinder to cylinder as the paper undergoes its cyclic temperature change and the moisture content reduces causing a corresponding drop in the paper-cylinder interface heat transfer coefficient.

11.2.3 Surface contact coefficient

Steam is directed into the dryers of ANM PM3 by a cascade arrangement on a section by section basis as illustrated in Figure 11.6. Only the high pressure steam flow rates from the main header are monitored directly and consequently separate measurements were required to determine the total steam consumption of each dryer sub-section.

This was achieved by measuring the condensing volume in the steam separator assigned to each section. Each of the five dryer sub-sections discharges blowthrough steam and condensate from the drying cylinders into a steam separator. The flash steam from the separator is recovered and cascaded to the next lowest temperature sub-section. The condensate is returned to the boiler house. To determine the rate of condensate generation the separator's condensate outlet valve was closed and the level rise over a period several minutes was measured. This was done for each of the five separators. The results give a rate of steam condensed within each group of cylinders, groups which are identified in detail in Appendix 3. This steam consumption was converted to the flow of heat, Q, into the paper sheet and this energy balance used to calculate the contact heat transfer coefficient.

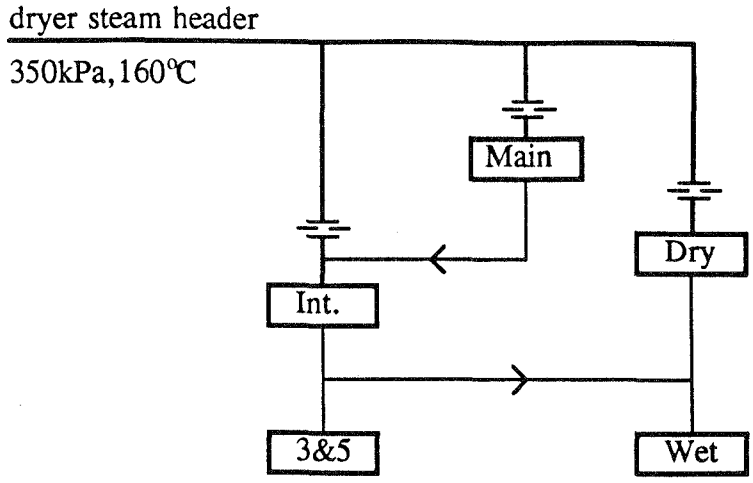

FIGURE 11.6
Cascaded steam distribution in dryer section

The heat flow, Q, is related to the contact heat transfer coefficient by the relationship,

$$Q = h_{contact}\, A_{cylinders}\, (T_{surface}-T_{sheet})\ [W/m^2°C], \qquad (11.8)$$

where $A_{cylinders}$ is the contact surface area between the paper sheet and the drying cylinders in a particular dryer sub-section, $T_{surface}$ is the dryer cylinder surface temperature in the sub-section and T_{sheet} is the paper sheet temperature.

The drying simulation model was then run iteratively for each of the five sub-sections, selecting the optimal value of $h_{contact}$ to match the machine measurement of heat transfer, Q, to the model's prediction based on an assumed contact heat transfer coefficient and model calculated instantaneous sheet temperature. The surface temperature is a constant for each sub-section, a function of the steam temperature, the condensate heat transfer coefficient and the shell thermal resistance as detailed in sections 11.2.1 and 11.2.2.

Thus, by using machine information on heat transfer from a given dryer sub-section and iteratively running the drying model a correlation was obtained for $h_{contact}$ as a function of sheet moisture content. The variation of $h_{contact}$ for PM3 is given by,

$$h_{contact} = 261M + 577\ [W/m^2°C], \qquad (11.9)$$

where M is the surface moisture content of the paper sheet at the contact surface in kg_{water}/kg_{fibre}.

ANM No. 2 paper machine (PM2) has a similar relationship given by,

$$h_{contact} = 186M + 597 \ [W/m^2°C]. \qquad (11.10)$$

Other correlations

Ng et al (1991) and Asensio et al (1991), using the same experimental apparatus, examined the thermal contact conductance of both dry and moist handsheet to metal interfaces. Asensio et al found that the interface contact heat transfer coefficient varied from 311 $W/m^2°C$ for bone-dry paper of 98 g/m^2 up to 403 $W/m^2°C$ for paper at 40% moisture content (wet basis). Tests were performed on paper sheets with basis weights of 98 g/m^2, 205 g/m^2 and 330 g/m^2 respectively, and the results quoted refer to the 98 g/m^2 tests. These data have been extrapolated down to a basis weight of 50 g/m^2 for comparison with the sheets in the current study and the estimated values for the contact heat transfer coefficient in this case are 431 $W/m^2°C$ for bone-dry paper and 504 $W/m^2°C$ for paper at 40% moisture content. Extrapolation is always an uncertain technique, but is not unreasonable in this case as the range of extrapolation is relatively small ($98 \rightarrow 50 g/m^2$) compared with the available data set ($98 \rightarrow 330 g/m^2$) and the existing data present smoothly. An exponential fit was used for the extrapolation.

Asensio et al comment that their results are a little lower than other published data and suggest that this may be due to the use of relatively rough laboratory handsheets as well as the use of higher basis weight sheets in their own study.

Hinds and Neogi (1983) obtained a relationship for the variation of contact heat transfer coefficient with the surface moisture content of the paper sheet. Their results demonstrated the coefficient to be approximately constant at moisture contents above 0.3 kg_{water}/kg_{fibre}. From this value of 580 $W/m^2°C$, it drops away sharply at very low moisture contents.

A correlation for the contact heat transfer coefficient was obtained by Depoy (1972) by using a simulation program to match actual machine drying data. The description obtained was,

$$h_{contact} = 430M + 107 \ [W/m^2°C]. \qquad (11.11)$$

Dreshfield and Han (1956) estimated that the contact heat transfer coefficient for a dry sheet of 50 g/m^2 basis weight was 765 W/m^2°C. Han and Ulmanen (1958) later estimated the contact coefficient for a 150μm paper sheet to be 790 W/m^2°C when dry and 2660 W/m^2°C when at maximum moisture content at the dryer inlet. The value for the wet sheet is considerably higher than from other correlations. The reason for this is not entirely clear but may be a result of the use of calculated temperatures which Dreshfield claimed "...may not be very accurate".

Riddiford (1969) estimated the contact coefficient using the concept of a theoretical air gap. Moisture content is not included as a parameter in this analysis, but the air conductivity may be expressed as a function of temperature :

$$h_{contact} = \frac{(0.00749T + 2.42) \times 10^{-2}}{1.5108R\left[\frac{\mu U}{F}\frac{3\pi\sqrt{2}}{4}\right]^{\frac{2}{3}}} = \frac{(0.0222T + 7.18) \times 10^{-3}}{R\left[\frac{\mu U}{F}\right]^{\frac{2}{3}}}, \qquad (11.12)$$

where,
- T = air temperature [°C],
- R = cylinder diameter [m],
- μ = air viscosity [kg/ms],
- U = paper speed [m/s], and,
- F = felt tension [N/m].

At 90°C and 1050 m/min with a felt tension of 1.7 kN/m the theoretical air gap is about 0.2mm and the heat transfer coefficient is 165 W/m^2°C. This value should be compared with the dry (M = 0) calculations of the aforementioned studies and upon doing so is found to be quite low.

Figure 11.7 demonstrates the comparison between the inferred contact heat transfer coefficient of the current study and correlations obtained by others.

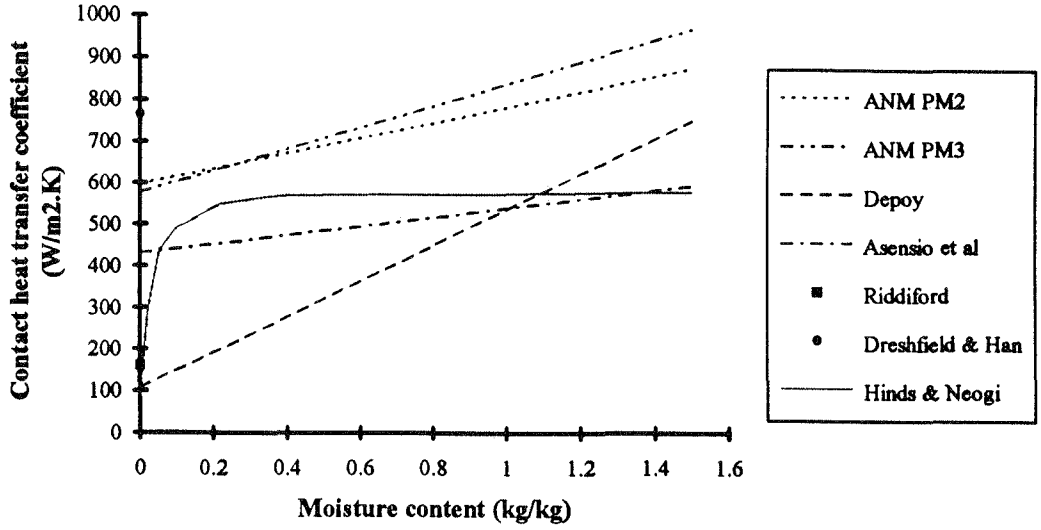

FIGURE 11.7
Correlations for $h_{contact}$ as a function of moisture content over the range of machine moisture contents from 0.1 to 1.5 kg_{water}/kg_{fibre}

Comparing the data of Asensio et al, Depoy, Han and Ulmanen, Dreshfield and Han, Hinds and Neogi, and Riddiford, shows the estimates of contact heat transfer coefficient for this study to be of a similar order of magnitude. Figure 11.7 demonstrates that there is a considerable variation in this parameter and suggests that there is an argument for customising the coefficient for each application. Some of the results are obtained from laboratory testing, some from theoretical predictions and some from machine measurements. Differences in the cleanliness of heat transfer surfaces on machines, the use of handsheets compared with machine paper, variations in sheet basis weight and dryer fabric tension will all exert an influence on the calculated contact heat transfer coefficient.

In the current study the correlations for PM2 and PM3 are used during execution of the mathematical model. This ensures that the coefficient is appropriate for the conditions encountered and also that the energy balance for the dryer cylinders is automatically achieved.

12. Model Calculations

Having developed a theoretical model to describe paper drying and conducted tests and literature reviews to obtain the appropriate physical properties for paper and transfer coefficients representative of the paper machine, it is necessary to check that the model's output is consistent with actual paper machine data. In the current context this is achieved through comparison with the ANM No. 3 paper machine (PM3) for which both moisture content data and energy consumption information are available.

Secondly it is desirable to run a series of calculations with it to develop correlations which relate drying performance to operating parameters. These trends will prove extremely useful in establishing the optimal energy efficient control strategy for operating the dryer section.

The other useful function of the mathematical model is its ability to forecast the effect of configuration changes to the dryer section. Several examples of the model's ability to assist with design related issues are presented at the end of the chapter.

12.1 Confirming model accuracy

The model developed in Chapter 3 must be tested against actual paper machine data to ascertain its accuracy and establish its relevance as a tool for analysis of the various operating parameters within the dryer section.

To make this comparison requires a means of assessing paper machine operation and obtaining relevant and accurate information from it. The main parameter of interest is that of moisture content. Sheet temperature is also of interest but is much more sensitive to rapid and local variations due to the low thermal capacitance of the thin paper sheet.

The complexity, high running speeds, low clearances and intense heat of a paper machine dryer section make it physically difficult to obtain useful paper sheet data from it. The hot, humid environment (85°C, 50% r.h.) impairs the operation of most electronic moisture measuring devices. The high running speeds (17-18 m/s) of rotating drums and tail threading ropes and the high temperatures of gear cases pose a safety threat to manual attempts at obtaining a wet sheet sample.

However, despite these inconveniences it was possible to measure three moisture contents on the ANM PM3 machine.

- Moisture content at the dryer inlet is obtained by grabbing a paper sheet sample at the exit from the press section. As the paper sheet is very wet at this point (around 1.4 kg_{water}/kg_{fibre}) small amounts of moisture evaporation between sampling and weighing will not influence the result significantly.

- After dryer cylinder No. 38 out of 48 total, there is a 5.2 metre gap before cylinder No. 39 where the paper sheet runs horizontally. This is a space which was previously used as a *breaker stack*, a process which was intended to perform some preliminary calendering of the paper sheet whilst it was still moist. Removal of the breaker stack some years ago generated the access to grab samples of partially dry paper at this point. The moist paper samples were placed into a sealed clip-lock plastic bag immediately, weighed in the wet state and dried in an oven prior to weighing a second time. The difficulty with this method was that it results in a paper sheet break and potential loss in production. Thus, such a moisture sample could only be obtained in the lead-up to a planned machine maintenance shutdown, an event which occurs five weekly. Even so, the fine timing required to grab a sample after the pulp feed is stopped but before the sheet runs out or is broken elsewhere meant that only six samples per year could be obtained.

- After exiting the dryer section the paper sheet passes through a Measurex scanner. This is a device which measures and controls key paper sheet parameters including moisture content. The scanning machine is calibrated regularly and is accurate to within 0.1% moisture.

The three moisture content values for PM3 were logged over a period of three years. The full data record is shown in Appendix 4 and a summary of results for typical paper machine operating conditions is shown in Table 12.1.

With the typical machine operating conditions, as outlined in the top section of Table 12.1 input into the dryer model, comparison was then made with the two paper sheet moisture contents which were recorded on a number of occasions during the period 1990-1992.

TABLE 12.1
ANM PM3 moisture contents and operating conditions

Speed (m/min)	1050
Basis weight (g/m^2)	48.8
Sheet caliper (μm)	80
Dryer cylinder steam (t/h)	19.3
Temperature of cyls. 3&5 (°C)	95
Temperature of cyls. 7-14 (°C)	110
Temperature of cyls. 15-23 (°C)	116
Temperature of cyls. 24-38 (°C)	122
Temperature of cyls. 39-48 (°C)	120
Make up air temperature (°C)	73
North PV air temperature (°C)	98
South PV air temperature (°C)	107
Moisture content at dryer inlet (kg_{water}/kg_{fibre})	1.38
Moisture content after dryer No. 38 (kg_{water}/kg_{fibre})	0.306
Moisture content at dryer exit (kg_{water}/kg_{fibre})	0.100

The dryer model output may be usefully expressed in terms of either moisture content or drying rate with time. The former is preferable for establishing a comparison with actual paper machine data whilst the latter is necessary to illustrate the cyclic drying variation with time. Both of these curves are generated for the case of the "standard" PM3 conditions defined in Table 12.1 and are presented in Figure 12.1.

Figure 12.2 shows the variation in drying rate and sheet temperature over a brief period of drying, approximately one second. During this time the paper sheet contacts five drying cylinders and so experiences five cyclic boundary condition changes.

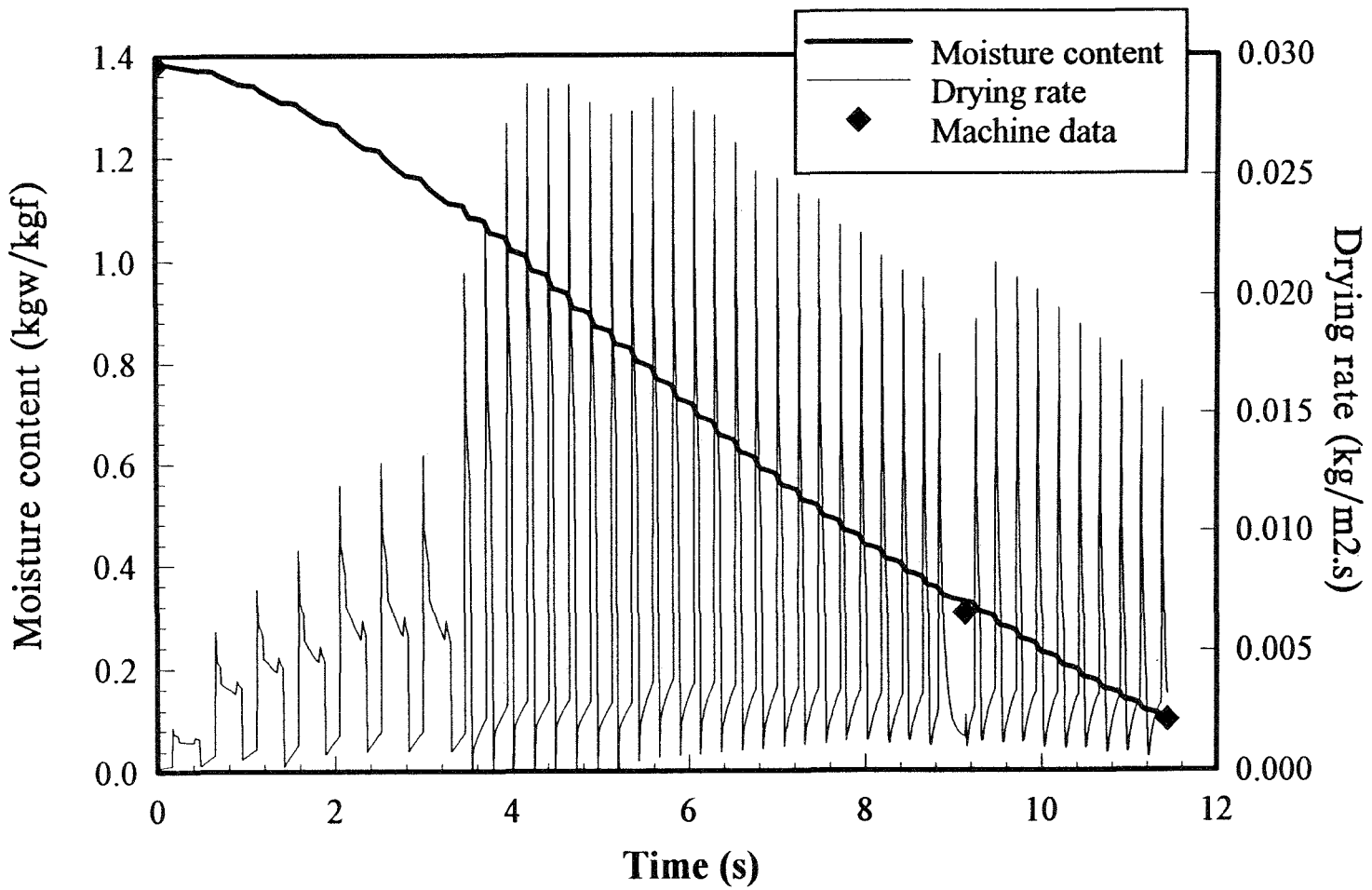

FIGURE 12.1
Variation of drying rate and moisture content with time

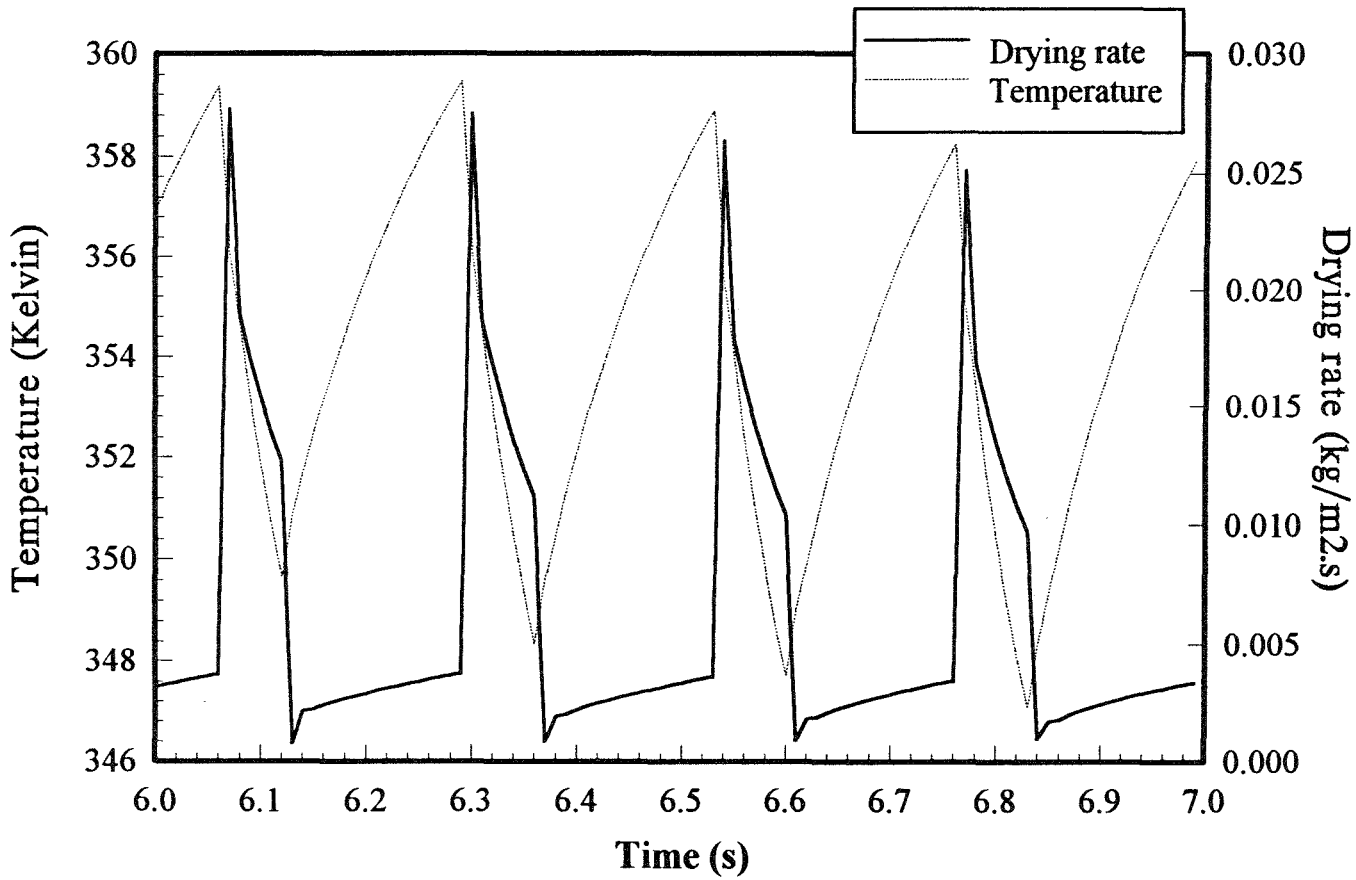

FIGURE 12.2
Paper sheet temperature and drying rate over a one second period

The variation of moisture content against time as displayed in Figure 12.1 is essentially an exponential relationship which approaches an equilibrium value with time. The equilibrium moisture content is determined by the dryer air conditions and the paper's sorption characteristics. With the final dryer sub-section operating at a temperature of 85°C and a relative humidity of 30.5% the equilibrium moisture content of paper is 0.0354 kg_{water}/kg_{fibre}. However there is no point in drying the paper sheet to this moisture content as the ambient storage conditions for the sheet imply a higher equilibrium value. For paper sheet storage at 20°C and 50% relative humidity the equilibrium moisture content is 0.084 kg_{water}/kg_{fibre} as calculated from Prahl's sorption isotherm correlation. In practice the paper sheet is dried to about 0.10 kg_{water}/kg_{fibre}. The exact value depends upon the anticipated storage conditions. It should be noted that an excessive difference between the final moisture content from the dryer section and the storage moisture content will result in shrinkage or expansion of the paper sheet on the roll and result in a sub-standard product at the printing press.

The three paper machine moisture content values obtainable are superimposed on the graph of the model moisture content prediction. The theoretical and actual values compare extremely closely and this is emphasised in Table 12.2.

TABLE 12.2
Comparison of theoretical prediction and paper machine data

Position (cylinder)	Time (s)	Machine moisture content (kg_{water}/kg_{fibre})	Model moisture content (kg_{water}/kg_{fibre})
0	0	1.381	1.381
38	9.13	0.306	0.328
48	11.43	0.100	0.099

A similar comparison is made on ANM's No. 2 paper machine (PM2). An intermediate value can not be obtained in this case but the final moisture content is measured after the dryer section by the Measurex scanner. The model prediction is a final moisture content of 0.0854 kg_{water}/kg_{fibre} whilst the measured value at a speed of 880 m/min is 0.0876 kg_{water}/kg_{fibre}. The

slightly lower equilibrium moisture content is due to the different paper grade produced on PM2.

Figure 12.2 shows the drying rate curve over a one second drying period. Sheet temperature is overlaid on the same plot. Four boundary condition cycles are shown, with the sheet alternately in contact with the cylinder and drying fabric followed by a shorter time in the open draw. Figures 12.3 and 12.4 are useful references when following a single cycle.

Consider the cycle beginning at t = 6.12s. The sheet begins contact with the drying cylinder which is at a surface temperature of 105°C (378K). The sheet temperature increases from 76.6°C to 86.5°C during this 0.17 second phase. This is represented by Phase I in Figure 12.4. The drying rate initially drops as the sheet is covered by the supporting felt which impairs mass transfer. As the sheet heats up the drying rate slowly increases from 0.0007 kg/m^2.s to 0.0037 kg/m^2.s. At t = 6.29s the sheet leaves the drying cylinder and the confines of the felt disappear. Vapour is driven from the sheet and the drying rate increases sharply to 0.0275 kg/m^2.s. This marks the beginning of Phase II from Figure 12.4. The drying rate falls away in the open draw as the latent heat of vaporisation causes the sheet temperature to drop. The lower sheet temperature causes a drop in the vapour concentration gradient which controls surface mass transfer and the drying rate decays until the next cylinder is reached when the process repeats itself at t = 6.36s.

The cycle length from one cylinder to the next is typically 4.13m on PM3. At a machine speed of 1050 m/min this corresponds to a single cycle duration of 0.24 seconds. With 48 drying cylinders in the whole drying section the elapsed drying time is just under 12 seconds at this machine speed.

It is notable that the first six cycles on the drying rate curve in Figure 12.1 are considerably wider than the subsequent ones. The first twelve drying cylinders form two single-felted drying runs. Cylinders 1-6 represent the first single-felted dryer sub-section and this arrangement is shown schematically in Figure 12.3. The key feature is that the paper sheet is only heated by every second drying cylinder, the upper cylinders. On the lower cylinders the paper sheet is insulated from the hot surface by the relatively thick drying fabric (felt). This configuration is repeated with a separate felt for cylinders 7-12. As there are fewer bursts of heating in this region the drying rates are proportionately lower.

Cylinders 13-24, 25-38 and 39-48 are all part of double-felted drying runs as depicted in Figure 12.4. In these sub-sections heating is achieved from both the upper and lower rows of cylinders.

Single-felted drying sections thereby lead to lower drying rates than do the double-felted sections. Their advantage lies in the additional support they give the paper sheet in the region between cylinders. The single-felted drying runs are placed at the beginning of the dryer section as the paper sheet is at its wettest and weakest at this point.

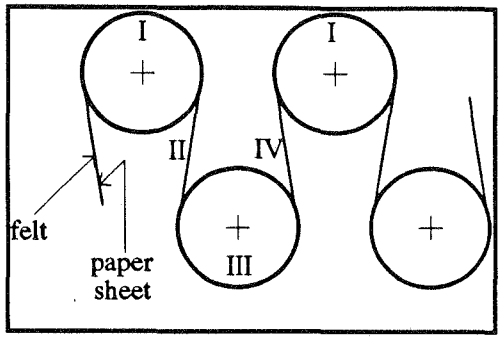

FIGURE 12.3
Single-felted dryers

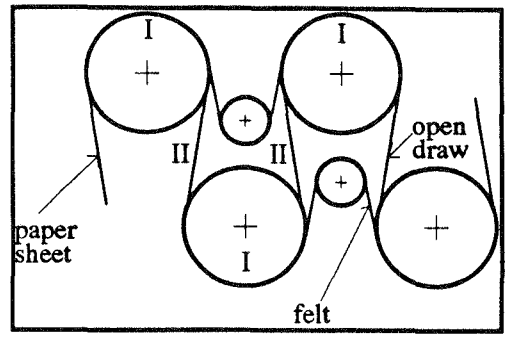

FIGURE 12.4
Double-felted dryers

In each of the five dryer sub-sections the paper sheet is exposed to differing drying conditions, which are listed in detail in Table 12.1 and at the beginning of Section 12.2. The machine's heat and mass transfer coefficients consequently also change throughout the sheet's passage through the various sub-sections. These values derived in earlier chapters are input into the model at this stage. This includes correlations described previously which relate the transfer coefficients to machine speed, paper sheet moisture content and dryer fabric permeability.

12.2 Steam consumption predictions

Historical data over the period from September 1990 to November 1992 of typical paper machine operating parameters were recorded for the purpose of checking the model moisture content predictions. These data, as presented in Appendix 4, also include metered steam consumption information for the variety of paper grades and machine operating speeds encountered. This provides an ideal opportunity for comparing the model forecasts of steam consumption against actual machine results.

Since the machine data were logged over a relatively long period of time (2 years) there are variations in the machine drying characteristics which will manifest themselves in the form of scatter on the summary graphs. These perturbations are due to a number of factors :

- Pulp is sourced from five separate processes at the mill and consequently there were variations in physical properties.
- Machine runnability is a relatively unpredictable combination of pulp quality, feed temperature and a mixture of other subtle physical and chemical factors. Therefore a paper grade with its given basis weight is not always produced at the same machine speed because of such runnability factors which cause production to be slowed. Consequently there is no consistently repeatable relationship between sheet basis weight and observed operating speed despite a general trend for heavier sheets to be dried at slower machine speeds.
- Local drying effects within the hood will necessitate air dampers and moisturising sprays acting as moisture control units across the machine width. The spray nozzles are located at 10-15cm intervals and direct a hot water and air mixture onto the surface of the paper sheet. This enables specific bands of the paper sheet's width to be precisely controlled for moisture content.
- In paper machines operating at speeds in excess of 500 m/min the condensate within the drying cylinder forms into a rim of uniform thickness due to the centrifugal force. This condensate is removed through a syphon assembly which collects condensate from the cylinder's internal surface and channels it out of the cylinder through the rotating steam joint. Drying cylinders with malfunctioning syphons can not evacuate condensate satisfactorily, thereby allowing the thickness of the rimming condensate layer to build up and consequently providing lower heat transfer to the paper sheet than would be the case under ideal conditions. Scale build-up on both the internal and external surfaces of the dryer cylinder also reduces heat transfer.
- Drying felts are replaced periodically and their performance changes considerably during a life cycle ($\approx$ 12 months). Permeability of these fabrics may be reduced considerably below the rated value prior to replacement.
- Inlet moisture content on the machine over an extended period will be quite variable and will be a key factor in determining specific steam consumption.

- Dryer pocket ventilation settings are subject to mild variations periodically. This will cause small perturbations to the pocket humidities and temperatures in each of the five drying zones.

Figure 12.5 demonstrates the trends indicated by both theoretical and actual machine data with respect to specific steam consumption variation with basis weight.

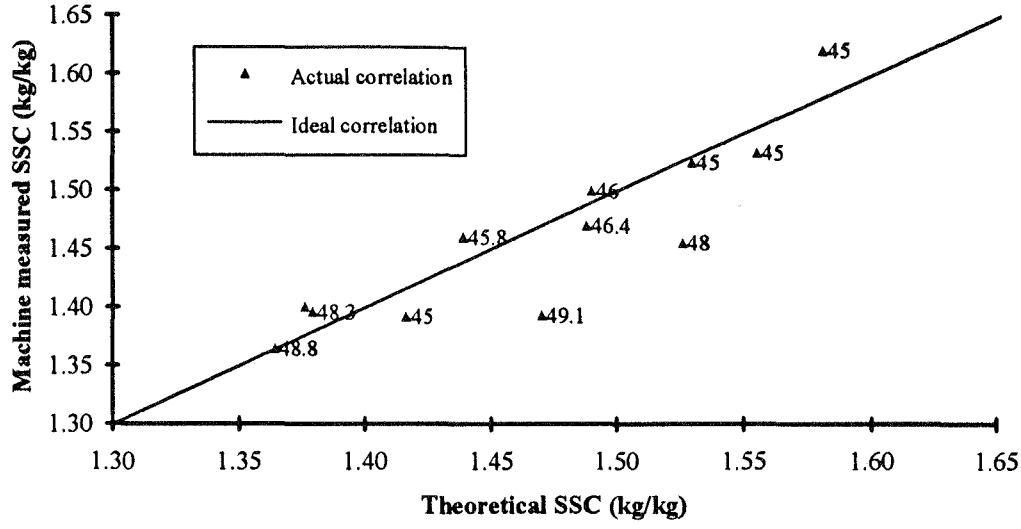

FIGURE 12.5
Comparison between machine measured specific steam consumption (SSC) data and model prediction of SSC for a number of monitored paper machine operating conditions between (1990-1992). The sheet basis weight (g/m^2) is shown with each data point.

The relationship between machine specific steam consumption and the model prediction can be expressed through the linear regression calculation of equation 12.1 :-

$$SSC_{machine} = 0.91 \times SSC_{model} + 0.123, \qquad (12.1)$$

where the data have a regression coefficient of 0.78.

The mild scatter in the data occurs for the reasons described previously which are changes in machine operation which are not able to be monitored in a straightforward manner.

Given these factors the correlation observed is a solid reinforcement of the realistic behaviour of the model.

12.3 Exploring model predictions - operation

Having established the reliability of the model there are a number of paper sheet and paper machine parameters which can be analysed. In doing this it is necessary to establish a base-case from which changes in specific parameters can be assessed.

The key paper sheet conditions and their nominal standard (base-case) values are :-

- inlet moisture content - 1.38 kg_{water}/kg_{fibre} (58% wet basis)
- sheet caliper - 70μm
- basis weight - 44.4 g/m^2 (0% moisture, equivalent to a nominal basis weight of 48.8 g/m^2 at the reel)
- inlet temperature - 50°C

Paper machine control conditions which can be infinitely varied by the model and their standard values for each of the five dryer sub-sections are listed below for PM3. These data are as presented in Table 12.1 and represent the base-case conditions.

- dryer cylinder temperatures - 95°C, 110°C, 116°C, 122°C, and 120°C
- dryer pocket temperatures - 55°C, 65°C, 78°C, 80°C, and 85°C
- dryer pocket humidity - 65%, 65%, 55%, 52%, and 30%
- machine speed - 1050 m/min

The key production data of interest from any analysis are the achievable machine speed for a given set of conditions and the resultant specific steam consumption (SSC). The SSC represents the mass ratio of drying steam used for each unit of paper produced by the machine. It is the paper industry's measure of dryer energy efficiency.

The achievable machine speed for a given set of drying conditions and initial conditions is that speed which brings the paper sheet to a fixed final moisture content, taken as 9% or 0.10 kg_{water}/kg_{fibre} for the paper machine under study, immediately after the final drying cylinder.

To demonstrate the drying model the following sub-sections (12.3.1-12.3.3) will use it to analyse the operation of the paper machine dryer section from a number of perspectives to determine :-

1. The effect of paper sheet properties (initial moisture content, sheet caliper, basis weight and initial temperature) on achievable machine speed and specific steam consumption.
2. The effect of different drying conditions (cylinder temperatures, pocket air temperatures and pocket air humidity) on achievable machine speed and specific steam consumption.
3. The optimal change in drying conditions from an energy efficiency (SSC) viewpoint to counteract a change in paper sheet grade or properties whilst maintaining constant production speed.

These series of calculations will summarise the scope of the model application from an operational perspective. The relationships developed are important because they indicate the most effective way to manage the operation of the dryer section. Interpretation of the results allows energy consumption to be minimised in this part of the paper machine. The subsequent section of this chapter (12.4) will address the model's ability to be used as a design tool in assessing the overall geometry and configuration of the dryer section.

The changes to dryer section operating conditions recommended by these calculations need to be assessed within the physical limits of a particular paper machine. They would need to be examined on a case by case basis but typical limitations which may be significant include :-

- Drive capacity of the machine. This sets a maximum achievable operating speed (m/min).
- Ability of other machine components such as twin wire former and press section to cope with higher speeds. Press roll vibrations or drainage limitations in the former may prevent the machine from operating at a speed which matches the dryer section's full capacity.

- Strength (runnability) of the paper sheet. This relates to the occurrence of sheet breaks where it is necessary to reduce the machine operating speed to obtain stable production.
- Pressure rating of the drying cylinders. This will govern the maximum achievable cylinder surface temperature.
- Need for cross-machine moisture control. Re-moisturising sprays which ensure that the paper sheet has a constant moisture content across its width may be necessary for quality control.
- Capacity of supply and exhaust fans. This will limit the maximum quantity of pocket ventilation air able to be fed into the dryer section.
- Maximum humidity prior to the onset of local condensation. Non-uniform air flows in the dryer section may cause specific regions to have higher humidities than others. Controlling dryer humidity to an average value may therefore lead to local areas with potentially saturated air and this may lead to condensation. Condensation drops are problematic because they can cause sheet breaks if they fall on the sheet.
- Ability of the dryer hood to control infiltration air. The condition of air within the dryer hood is a function of the heated pocket ventilation air blown into the hood and the degree of infiltration air leaking into the hood through gaps in the dryer section external structure. An excess of infiltration air, at 25°C, from the machine room may make high dryer air temperatures unattainable.
- Paper sheet quality considerations which may lead to a maximum allowable cylinder surface temperature. If cylinder temperatures are increased substantially the surface of the paper sheet tends to stick to the cylinder causing considerable quality problems. This is particularly significant at the wet end of the dryer section.
- Turbulence caused by pocket ventilation air which may result in sheet instability or wrinkles. Increasing the amount of pocket ventilation air may cause excessive movement of the sheet (flapping) which could result in a sheet break or the sheet folding causing wrinkles.
- Production requirements may demand specific quantities of paper at various times. It will rarely be economic for a paper mill to operate at the most energy efficient setting. The financial benefits of increased production quantities will usually mean that the machine must run at the highest speed possible for stable production. It is then necessary to determine the most efficient dryer settings at *this speed.*

12.3.1 Effect of paper sheet properties

This first analysis assumes the standard paper sheet inlet and dryer section control conditions and calculates the achievable operating speed and the required energy input in terms of specific steam consumption [kg_{steam}/kg_{paper}] under the constant drying conditions defined earlier. This calculation is done for four sets of conditions by varying one of the paper sheet initial conditions - initial moisture content, caliper, basis weight, initial temperature - each time over its likely operational range. This gives rise to the graphs presented in Figures 12.6-12.9.

The parameters investigated here are independent of the drying section control regime. They are properties of the paper sheet grade or press section operation which influence the drying behaviour but are outside the control of the dryer section itself. Sub-section 12.3.2 will analyse the effect of the controllable dryer section conditions.

Throughout this section the best fit equations used to describe the relationship between both achievable machine speed and specific steam consumption and the relevant initial sheet condition have been set in the form :-

$$\text{Speed}, SSC = A\, e^{B \times \text{InitCond}} + C \ , \qquad (12.2)$$

where A, B and C are constants chosen to minimise the square of the error between the correlation and the data points output from the model. Whilst some of the relationships could have been described with a linear approximation without any significant loss of accuracy the exponential form of equation 12.2 has been used in each case to ensure a unified approach.

12.3.1.1 Initial moisture content

The moisture content of the paper sheet leaving the press section is a first order parameter in controlling achievable drying rate for a given set of drying conditions. The moisture content is directly representative of the drying load - the quantity of water to be evaporated in the dryer section. Figure 12.6 demonstrates this relationship and highlights the importance of an efficiently operating press section. Water that is not removed mechanically in the press section must be removed at added cost in the dryer section. The *cost* of extra dryer inlet moisture for given operating

conditions is a decrease in production speed and an increase in dryer energy consumption.

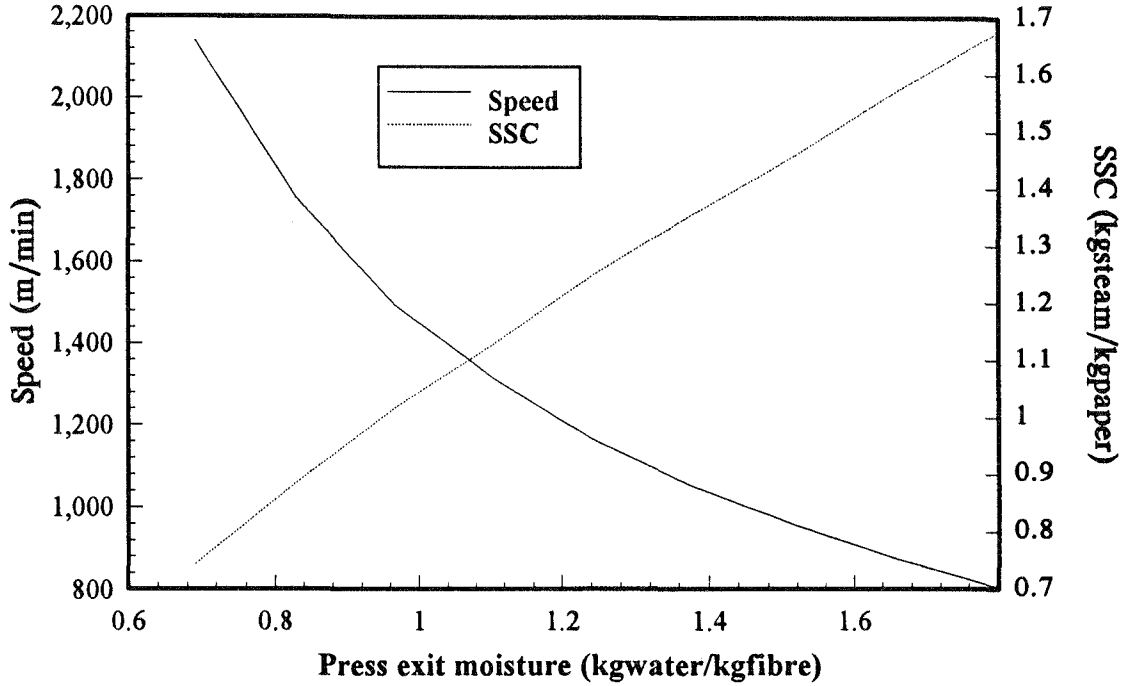

FIGURE 12.6
Variation of paper sheet drying rate and dryer steam consumption with initial moisture content

Figure 12.6 demonstrates that *under constant drying conditions* an increased initial moisture content will lead to a decrease in production speed and an almost linear increase in steam consumption per unit of dry paper produced. The resultant curves can be regressed to give the following exponential best fit equations :-

$$\text{Speed} = 5723e^{-1.97M_{init}} + 658 \quad \text{(m/min), and} \qquad (12.3)$$

$$\text{SSC} = 183.25e^{0.0045M_{init}} - 183.05 \quad (kg_{steam}/kg_{paper}). \qquad (12.4)$$

About the base-case of 1.38 kg_{water}/kg_{fibre}, it can be shown that a 10% increase in initial moisture content will lead to an 8.6% reduction in machine speed and an 8.5% increase in specific steam consumption. These data highlight the importance of an efficient press section.

It is quite understandable that the specific steam consumption shows an almost linear relationship with initial moisture content. An increment in initial moisture content brings about a proportional increase in the quantity of water to be evaporated. The evaporation of more water per unit mass of dry fibre will result in the use of a proportional increase in the amount of steam per unit mass of dry fibre.

12.3.1.2 Sheet caliper

The paper sheet thickness is a parameter which varies for different paper grades depending upon the desired basis weight and porosity of the final product. For a fixed basis weight, which is specific to paper grade, the effect of caliper on drying is to alter the diffusion and permeability paths through which vapour and liquid moisture must pass to reach the sheet surface and in so doing dry the paper sheet. The sheet dry caliper which has been assumed for the 'standard dry sheet' is 70μm. The effect of changing this value on drying rate and specific steam consumption, under the fixed drying conditions defined earlier, is illustrated in Figure 12.7.

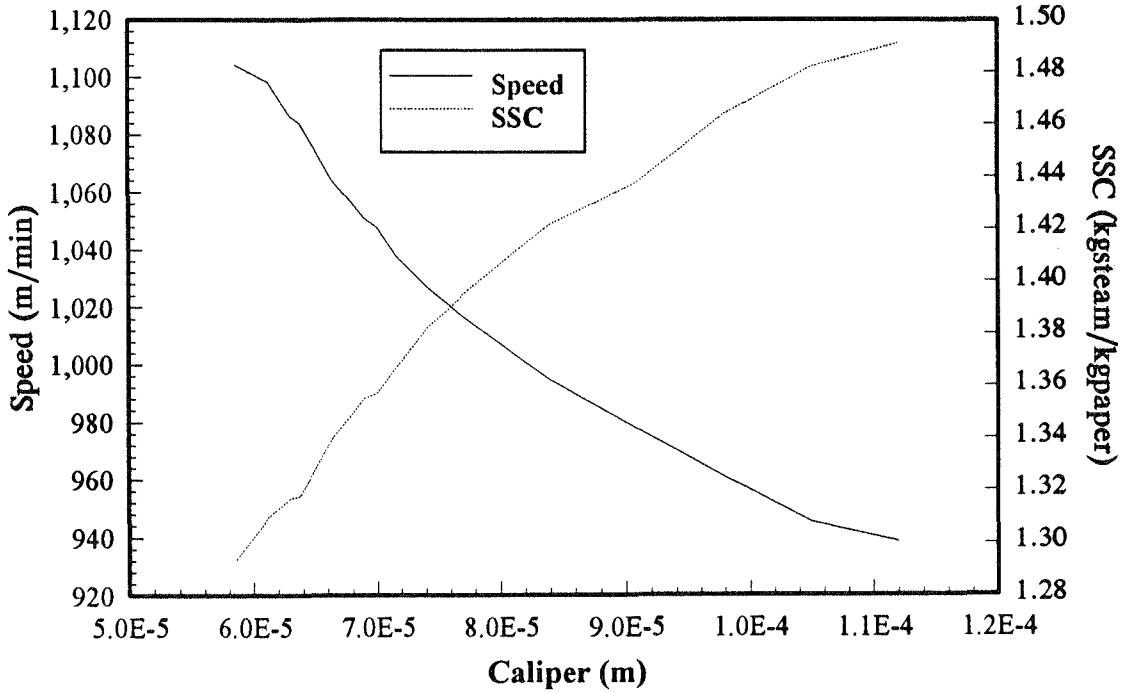

FIGURE 12.7
Variation of paper sheet drying rate and dryer steam consumption with sheet caliper

For a constant sheet basis weight, increasing the sheet caliper makes the sheet more bulky, increases the amount of void space and increases the distance moisture must travel to exit the sheet. An increase in caliper also decreases the thermal conductance of the sheet and results in a lower average temperature through the sheet. Consequently this change is accompanied by a reduction in achievable drying rate for constant operating conditions. Hence the paper machine speed must be lowered in order to dry the sheet and this sees additional steam per unit of reel-dry paper consumed.

Figure 12.7 demonstrates that under constant drying conditions an increased sheet caliper will lead to a decrease in production speed and a corresponding increase in steam consumption per unit of dry paper produced. This increase occurs because a larger caliper means the evaporating moisture has to travel further to reach the surface of the paper sheet. This increased distance reduces both the liquid and vapour pressure gradients within the web and brings about a corresponding drop in drying rate.

The resultant curves were regressed to give the following exponential best fit equations :-

$$\text{Speed} = 1295e^{-30666L_{init}} + 896 \ \text{(m/min), and} \qquad (12.5)$$

$$\text{SSC} = -1.21e^{-25372L_{init}} + 1.56 \ (kg_{steam}/kg_{paper}). \qquad (12.6)$$

About the base-case of $L_{init} = 70\mu m$, it can be shown that a 10% increase in sheet caliper will lead to a 2.8% reduction in machine speed and a 2.4% increase in specific steam consumption. These data show that whilst sheet caliper is a significant parameter in controlling drying it is less dominant than the initial moisture content of the paper sheet. During actual paper machine operation the sheet caliper is governed by the grade of paper and basis weight.

12.3.1.3 Basis weight

The paper sheet basis weight is the key parameter which identifies each product. Telephone directory paper is 36-40 g/m^2, newsprint is 45-49 g/m^2 and higher quality paper suitable for four colour offset printing is produced in the 52-55 g/m^2 range. Variation in the sheet basis weight changes the fibre density per square metre. For the same initial moisture content the

quantity of water per square metre of paper will change directly with the basis weight. This change will be accompanied by a proportional change in production rate for a given set of conditions. The predicted change to drying rate and specific steam consumption resulting from a variation in sheet basis weight is shown in Figure 12.8.

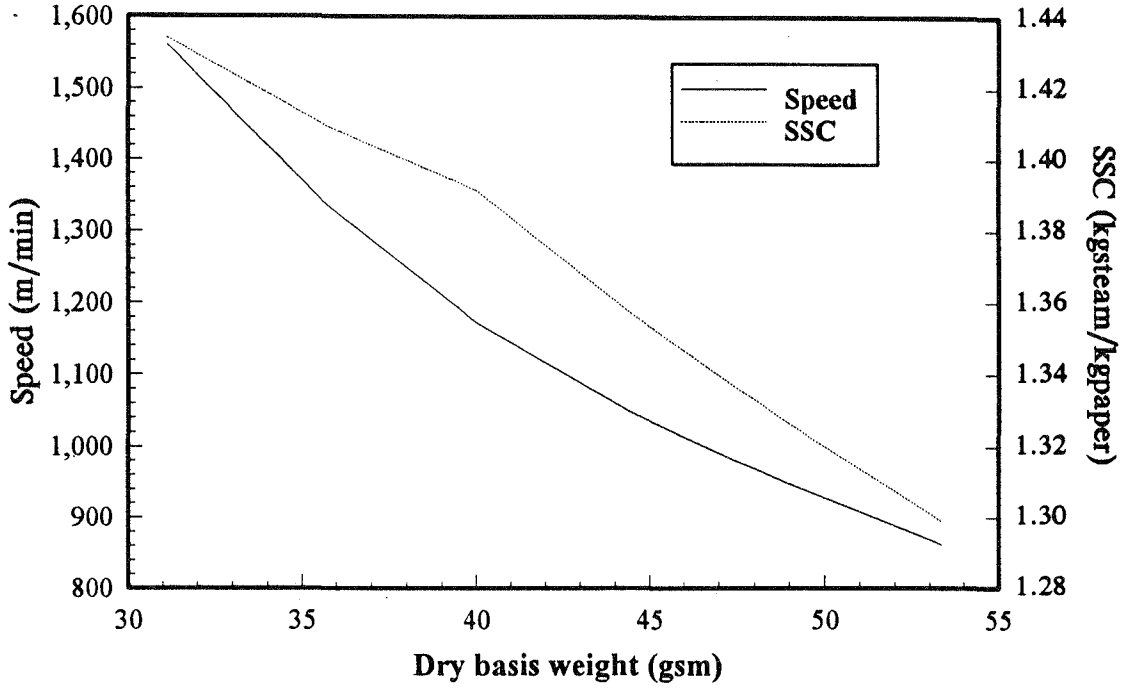

FIGURE 12.8
Variation of paper sheet drying rate and dryer steam consumption with sheet basis weight

Figure 12.8 demonstrates that under constant drying conditions an increased sheet basis weight will lead to a decrease in production speed as well as a decrease in steam consumption per unit of dry paper produced. The resultant curves can be regressed to give the following exponential best fit equations :-

$$\text{Speed} = 5731e^{-57.3b_{wt}} + 597 \quad \text{(m/min), and} \qquad (12.7)$$

$$\text{SSC} = 7.03e^{-0.91b_{wt}} - 5.39 \quad (\text{kg}_{\text{steam}}/\text{kg}_{\text{paper}}). \qquad (12.8)$$

About the base-case of $b_{wt} = 44.5\times10\text{-}^3$ kg/m^2, it can be shown that a 10% increase in sheet basis weight will lead to a 9.7% reduction in machine speed and a 2.0% decrease in specific steam consumption. These data

show that basis weight is almost inversely proportional to machine speed. This is understandable as increasing basis weight means a corresponding increase in the water removal requirement for a fixed initial moisture content. The decreasing SSC with increasing basis weight is a more interesting phenomenon. This suggests that drying heavier sheets at slower speeds is a more efficient means of drying a quantity of newsprint. The analysis predicts this relationship because the variation in basis weight is done at constant sheet caliper. This increase in basis weight whilst maintaining constant sheet thickness means that the fibre and water matrix is much more densely packed and the dewatering path is therefore much shorter than in a more bulky sheet. The shorter dewatering path reduces the overall resistance to moisture movement within the sheet and allows moisture to evacuate much more easily.

12.3.1.4 Initial temperature

The paper sheet initial temperature is determined by the pressing operation prior to the dryer section. Most press sections include a *steambox* which passes a stream of live steam over the wet web to heat the sheet. High temperatures in the press section lower the water's viscosity and assist the process of mechanical dewatering. Hence a high initial temperature is often associated with a lower initial moisture content entering the dryer section. In isolation the initial sheet temperature is likely to affect drying rates to a limited degree due to the lack of thermal mass of a given area of paper. The effect of initial temperature on speed and steam consumption is shown in Figure 12.9.

Figure 12.9 demonstrates that under constant drying conditions an increased initial sheet temperature will lead to an increase in production speed and a corresponding decrease in steam consumption per unit of dry paper produced. The resultant curves were regressed to give the following exponential best fit equations :-

$$\text{Speed} = 975e^{0.00146T_{init}} + 0.003 \quad \text{(m/min), and} \qquad (12.9)$$

$$\text{SSC} = 0.72\,e^{-0.0029L_{init}} + 0.74 \quad (kg_{steam}/kg_{paper}). \qquad (12.10)$$

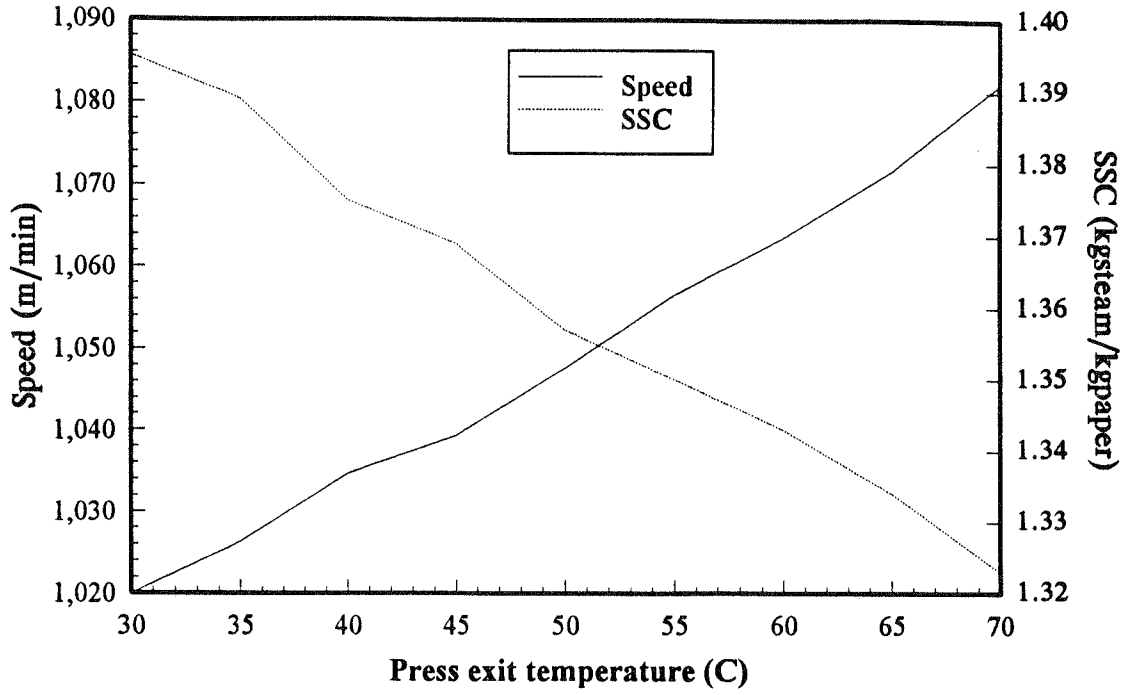

FIGURE 12.9
Variation of paper sheet drying rate and dryer steam consumption with initial sheet temperature

About the base-case of T_{init} = 50°C, it can be shown that a 10% increase in initial temperature will lead to a 0.8% increase in machine speed and a 0.7% decrease in specific steam consumption. This demonstrates that the overall drying process is relatively insensitive to this parameter. This occurs because the relatively light basis weight paper sheet has very little thermal storage. Increasing the sheet's initial temperature is a very small energy input in the overall dryer energy balance. The data in Chapter 11 demonstrate that the enthalpy associated with the wet paper sheet entering the dryer section at 50°C represents just 5% of the total energy input into the dryer section.

12.3.2 Effect of machine drying conditions

The previous sub-section (12.3.1) dealt with the effect of paper sheet properties and initial conditions on drying rate and energy efficiency at constant drying conditions. This section investigates the effect of varying drying conditions whilst the parameters described in 12.3.1 are held constant. The variation in achievable machine speed and specific steam consumption is monitored as each of the three drying control parameters are varied in turn. The controllable drying conditions to be examined are :-

- cylinder steam temperature which is controlled by the steam pressure for the given dryer sub-section,
- pocket air temperature which is controlled by the steam flow through the air heating coils, and,
- pocket air humidity which is governed by the quantity of dry air circulated through the dryer hood for a given evaporation rate.

These calculations are significant because they demonstrate how the dryer section's energy efficiency is influenced by changes in operating conditions. This concept will be developed further in Section 12.3.3 to indicate the optimal means of controlling the dryer section in response to given changes in sheet grade or initial conditions.

On a paper machine the cylinder steam temperature, pocket air temperature and pocket air humidity are varied in each of the five sub-sections which constitute the overall dryer section. Thus, each of these five groups of 6-16 drying cylinders expose the paper sheet to the same nominal drying conditions.

When investigating a change in one of these three parameters it is therefore necessary to acknowledge that each parameter is set at a different value depending upon the position within the dryer section. Hence, for the purposes of analysis a *change* in one of the three controlling parameters means that the value in *each* of the five sub-sections changes by a corresponding amount. This will be explained further for the specific cases examined in the following sections.

12.3.2.1 Cylinder steam temperature

The cylinder steam temperatures are controlled by the pressure of the steam input into the cylinders. The steam pressure relates to a specific saturation temperature. The magnitude of heat transfer coefficients from steam to the cylinder itself and through the cast iron cylinder's shell governs the surface temperature to which the paper sheet is exposed.

The nominal steam temperatures for the five dryer sub-sections are :-

- 95°C, 110°C, 116°C, 122°C, and 120°C.

These values are varied over the range ±10°C and the achievable machine speed, as limited by drying capacity, and the resultant specific steam

consumption are calculated. This is done by iterating the drying model with different machine speeds to determine the speed which will bring the sheet to a moisture content of 9% or 0.10 kg_{water}/kg_{fibre} at the exit from the final drying cylinder.

As an example, a change of $\Delta T_{cyl} = +5°C$ in the cylinder steam temperatures would lead to the following values :-

- 100°C, 115°C, 121°C, 127°C, and 125°C.

The results of these calculations are presented in Figure 12.10.

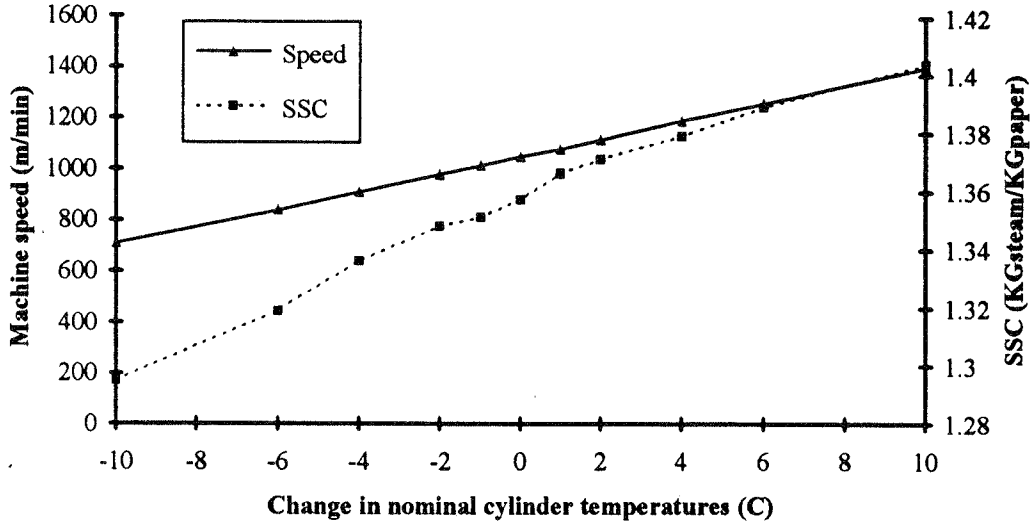

FIGURE 12.10
Variation of machine drying rate and dryer steam consumption with changes in cylinder steam temperature

The speed and SSC can be correlated by the following equations :-

$$\text{Speed} = 34.8\,\Delta T_{cyl} + 1050.6 \quad \text{(m/min), and} \qquad (12.11)$$

$$SSC = -9.4 \times 10^{-5}\,\Delta T_{cyl}^2 + 0.0056\,\Delta T_{cyl} + 1.36 \ (kg_{steam}/kg_{paper}). \qquad (12.12)$$

The results demonstrate that the dryer section operates more efficiently at lower cylinder temperatures, although this will naturally slow production speeds. For example, a 10°C increase in all cylinder temperatures leads to a 34% increase in drying speed and a 3.5% increase in specific steam

consumption. This demonstrates that drying capacity is particularly sensitive to the cylinder steam temperature. The practical limitation may come in the form of :-

- pressure rating of the cylinders.
- the paper sheet sticking to the cylinders if the contact temperature is too high.

It is noted at this point that the cylinder temperatures within each of the dryer sub-sections can be changed one at a time, and the computational model is quite able to handle this analysis. However, for the sake of clarity in the presentation of results the numerous permutations are not explored at this point.

12.3.2.2 Pocket air temperature

The temperatures of the pocket ventilation air throughout the dryer section are controlled by the pressure of the steam fed to the heat transfer coils which heat the incoming air. The amount of steam controls the temperature of air input into the dryer hood and consequently the temperature of the mixed drying air adjacent to the paper sheet in the dryer pockets.

The nominal temperatures of the drying air for the five dryer sub-sections are :-

- 55°C, 65°C, 78°C, 80°C, and 85°C.

In the following calculations these values are varied over the range ±20°C and the achievable machine speed, as limited by drying capacity, and the resultant specific steam consumption are calculated. This is done by iterating the drying model with different machine speeds to determine the speed which will bring the sheet to a moisture content of 9% or 0.10 kg_{water}/kg_{fibre} at the exit from the final drying cylinder.

As an example, a change of $\Delta T_{pock} = +10°C$ in the pocket air temperatures would lead to the following values :-

- 65°C, 75°C, 88°C, 90°C, and 95°C.

The results of these calculations are presented in Figure 12.11.

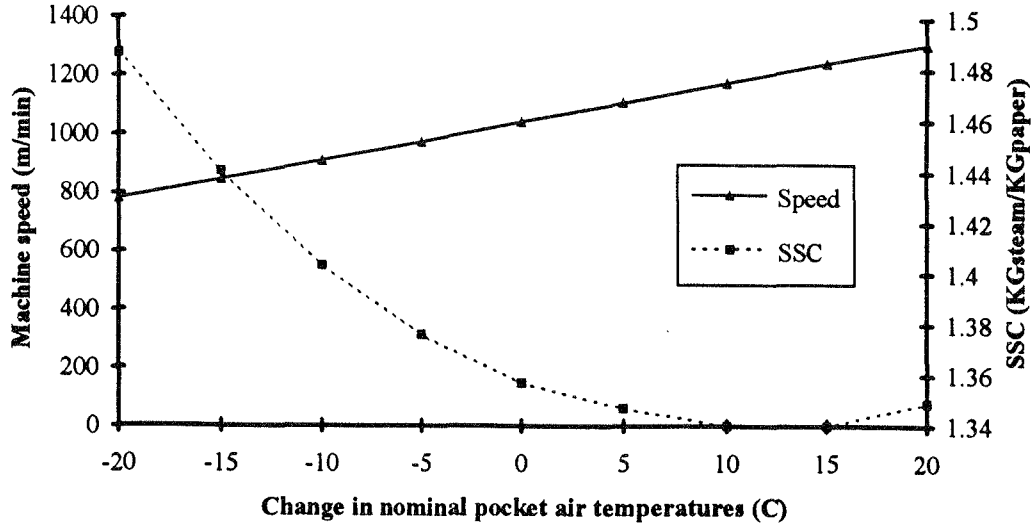

FIGURE 12.11
Variation of paper sheet drying rate and dryer steam consumption with changes in pocket air temperature

The speed and SSC can be correlated by the following equations :-

$$\text{Speed} = 13.3\Delta T_{pock} + 1047.2 \quad \text{(m/min), and} \qquad (12.13)$$

$$SSC = 1.5 \times 10^{-4} \Delta T_{pock}^2 - 0.0033\Delta T_{pock} + 1.36 \ (kg_{steam}/kg_{paper}). \qquad (12.14)$$

The results demonstrate that the dryer section operates most efficiently when the pocket air temperatures throughout the whole dryer section are all increased by 11°C. This change leads to a 1.4% decrease in specific steam consumption and a 14% increase in drying speed. This demonstrates that better drying performance can be achieved without compromising production speed through increasing the temperature of the pocket ventilation air. Practical limitations may come in the form of :-

- the ability of the hood to minimise infiltration air from the machine room which dilutes the conditioned air input into the dryer section and lowers the temperature in the drying pockets.
- the maximum heat transfer available from the heat transfer coils at the given air flow.

It is noted at this point that the pocket air temperatures within each of the dryer sub-sections can be changed one at a time by varying the steam into the heating coils. The computational model can handle such changes but

for the sake of clarity in the presentation of results the numerous permutations possible are not developed further here.

12.3.2.3 Pocket air humidity

The pocket air humidity is controlled by the volume of air injected into the dryer hood for a given drying (evaporation) rate. The air flow is controlled by both the supply and exhaust fans. The hood is maintained at a slight negative pressure by ensuring the capacity of the exhaust fans exceeds that of the supply fans. Air is supplied into individual pockets through the double-felted parts of the dryer section, and by more general ducting arrangements in the single-felted parts at the wet end.

The nominal pocket relative humidity values for the five dryer sub-sections are :-

- 65%, 65%, 55%, 52%, and 30%.

In terms of absolute humidity these values may be represented as :-

- 0.0697, 0.1186, 0.1927, 0.1994, and, 0.1282 kg_{water}/kg_{air}.

These absolute humidity values are varied over the range ±50% and the achievable machine speed, as limited by drying capacity, and the resultant specific steam consumption are calculated. This is done by iterating the drying model with different machine speeds to determine the speed which will bring the sheet to a moisture content of 9% or 0.10 kg_{water}/kg_{fibre} at the exit from the final drying cylinder.

As an example, a change of +25% to the absolute humidity of the pocket air, or $W_{factor} = 1.25$, would lead to the following values :-

- 0.0871, 0.1483, 0.2409, 0.2493, and, 0.1603 kg_{water}/kg_{air}.

The results of these calculations are presented in Figure 12.12.

The speed and SSC can be correlated by the following equations :-

$$\text{Speed} = -593.5 W_{factor} + 1664.9 \ \text{(m/min), and} \qquad (12.13)$$

$$\text{SSC} = 2.40\, e^{-3.85 W_{factor}} + 1.305 \ (kg_{steam}/kg_{paper}). \qquad (12.14)$$

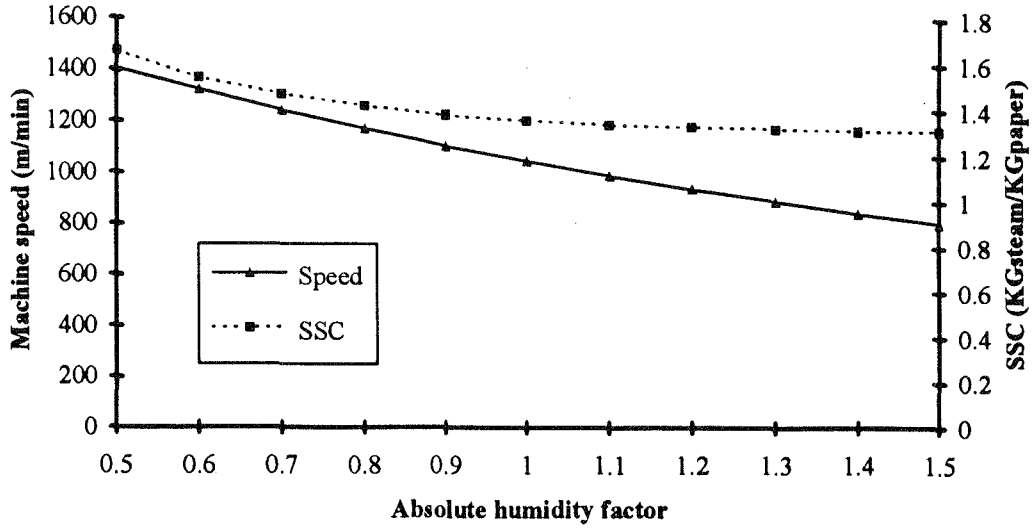

FIGURE 12.12
Variation of paper sheet drying rate and dryer steam consumption with changes in pocket air absolute humidity

The results demonstrate that the dryer section operates more efficiently at higher humidities, although this comes at the expense of drying capacity. For example, a 20% increase in all pocket absolute humidities leads to a 10.2% decrease in drying speed and a 2% decrease in specific steam consumption. It is noted that above a 40% increase in absolute humidity there are no further gains in energy efficiency.

Practical limitations to changes in the pocket humidity may come in the form of :-

- local condensation caused by increases in humidity.
- low humidities may require air flows which exceed either the supply fan capacity or the stability limit for the paper sheet which is exposed to this air movement.

It is noted at this point that the pocket humidity within each of the dryer sub-sections can be changed one at a time and this can be analysed conveniently by the computational model. The potentially excessive number of calculations prohibits this being presented in a compact, methodical way and it is preferable to investigate specific changes as they become relevant.

12.3.3 Controlling changes in sheet properties with changes to drying conditions at constant machine speed

This series of calculations combines the results of the previous sections 12.3.1 and 12.3.2. The calculations analyse the effect of initial sheet conditions on paper drying but differ from section 12.3.1 in assuming a constant machine speed, and then solve in turn for the change required in each of the control parameters, cylinder temperature, pocket temperature and pocket humidity, to bring the sheet to the required final moisture content of 9%. This is particularly significant in paper machine operation. It is applicable to circumstances where the paper grade is changed or conditions upstream of the dryer section change whilst the production speed is required to remain constant.

Each of the four paper sheet initial conditions identified (initial moisture content, sheet caliper, basis weight and initial temperature) are varied in turn across their typical range. The machine speed is maintained constant, at the base-case figure of 1050 m/min. The variation in specific steam consumption is then monitored as each of the three drying control parameters are varied. The controllable drying conditions to be examined are :-

- cylinder steam temperature which is controlled by the steam pressure for the given dryer sub-section,
- pocket air temperature which is controlled by the steam flow through the air heating coils, and,
- pocket air humidity which is governed by the quantity of dry air circulated through the dryer hood for a given evaporation rate.

12.3.3.1 Sheet initial moisture content

The initial sheet moisture content is governed by the operation of the press and forming sections. Its variation needs to be compensated for by a change in drying conditions in order to maintain a constant production speed. The model calculations as presented in Figures 12.13-12.15 indicate the impact of such control changes on drying energy efficiency.

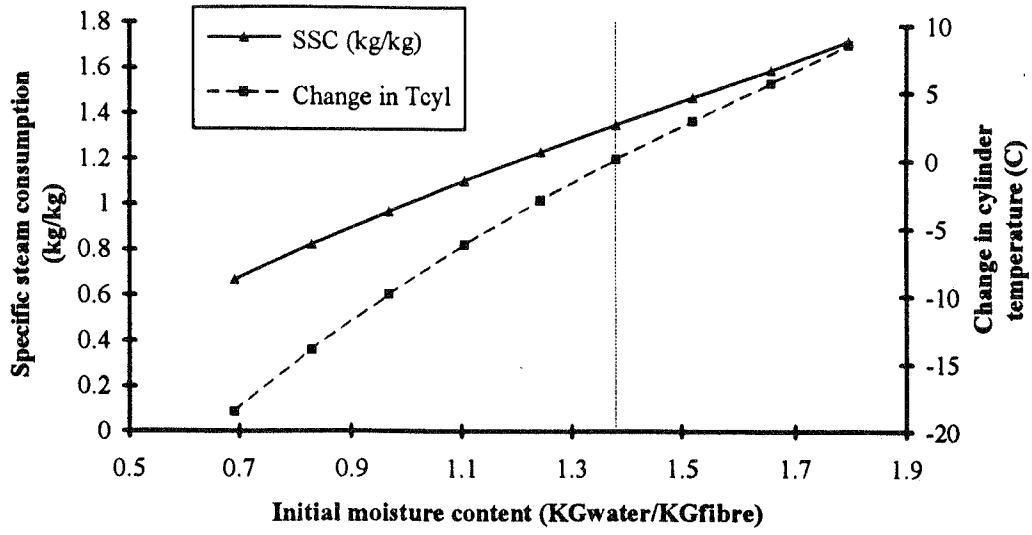

FIGURE 12.13
Variation of specific steam consumption with ΔT_{cyl} varied to maintain a constant production speed (1050m/min) in response to changes in initial paper sheet moisture content

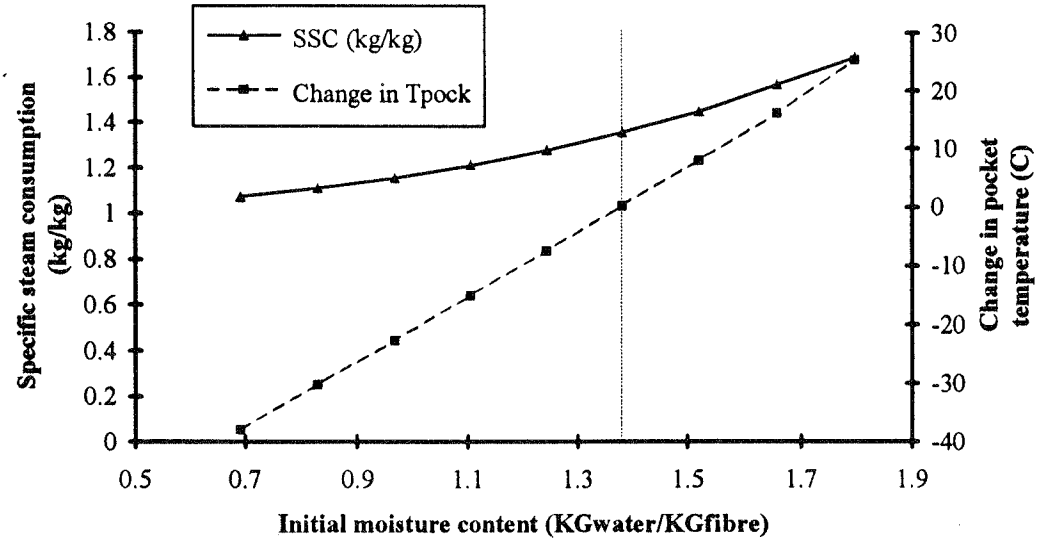

FIGURE 12.14
Variation of specific steam consumption with ΔT_{pock} varied to maintain a constant production speed (1050m/min) in response to changes in initial paper sheet moisture content

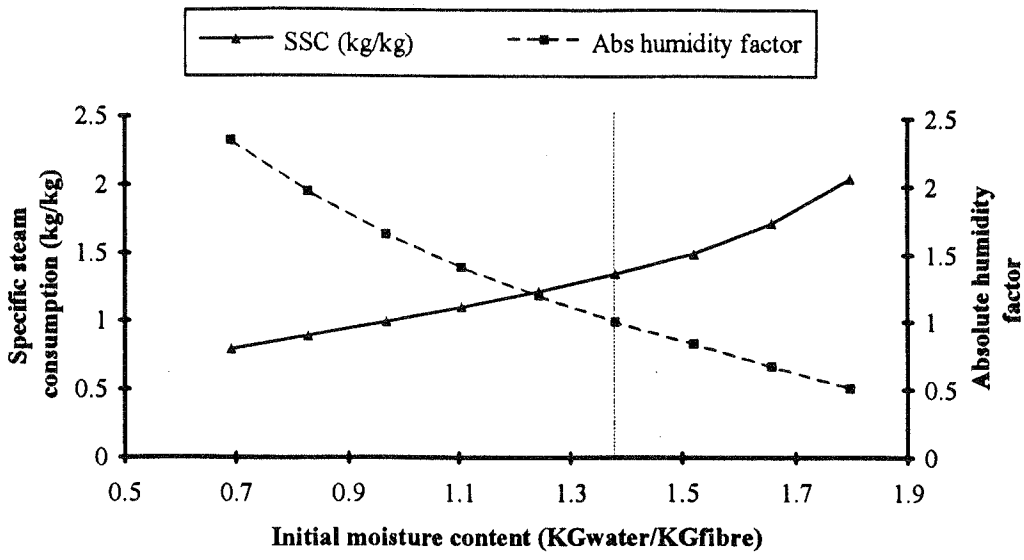

FIGURE 12.15
Variation of specific steam consumption with W_{factor} varied to maintain a constant production speed (1050m/min) in response to changes in initial paper sheet moisture content

Figures 12.13-12.15 show the most energy efficient means of handling a change in the sheet's moisture content at dryer inlet. Increases in the sheet's initial moisture content which lead to an increase in the required drying rate can be handled in three main ways : increase cylinder temperature by controlling steam pressure, increase pocket air temperature by increasing steam flow through heating coils, or, decrease pocket humidity by increasing the fresh air flow into the dryer hood. The graphs therefore demonstrate the optimal control changes to make in response to perturbations in the paper sheet's moisture content about the usual value of 1.38 kg_{water}/kg_{fibre} (58% wet basis) whilst maintaining a constant production rate.

In general terms the graphs demonstrate that increases in the sheet moisture content should be controlled by increasing the pocket air temperature in accordance with Figure 12.13. Decreases in the sheet moisture content below the nominal basecase value of 1.38 kg_{water}/kg_{fibre} are most efficiently controlled by reducing the cylinder steam temperatures as described by Figure 12.14.

As an example, if improved pressing efficiency results in a reduced initial moisture content of 1.2 kg_{water}/kg_{fibre}, then, for a fixed production speed,

the input energy to the dryer can be minimised by reducing the pocket air flow which will in turn allow the pocket relative humidities to rise. For this example the specific steam consumption drops to 1.189 kg_{steam}/kg_{paper} from the usual value of 1.358 kg_{steam}/kg_{paper}. This is achieved through increasing the relative humidities in all pockets by 25.5% of their initial values. Alternative control strategies for this change in press moisture content are listed in Table 12.3.

TABLE 12.3
Control options for a change of initial moisture content from 1.381 kg_{water}/kg_{fibre} to 1.20 kg_{water}/kg_{fibre}

Parameter	Change	SSC (kg_{steam}/kg_{paper})
Steam temperature	-4.0 °C	1.196
Pocket temperature	-9.9 °C	1.258
Pocket abs. humidity	+25.5 %	1.189

Further it should be noted that the above analysis does not include any combinational changes of the four control parameters. This is simply because of the large number of potential permutations created by considering the drying response to, changes in machine speed *and* cylinder temperature, changes in cylinder temperature *and* pocket humidity, etc. Consideration of such combinations is within the bounds of the analytical infrastructure set up to produce the current set of data, but would detract from the clarity of the results.

12.3.3.2 Sheet caliper

Sheet caliper is a parameter which is indicative of the paper grade being produced. Given a constant production speed, changes in caliper can be addressed by altering the controlled conditions of the cylinder temperatures, pocket air temperatures or pocket air humidities. These relationships are illustrated in Figures 12.16-12.18.

For the range of paper grades under production at ANM, Boyer, the caliper would generally vary by no more than ±10% of the standard value. This narrows the important region of the graphs to the 60-80μm range.

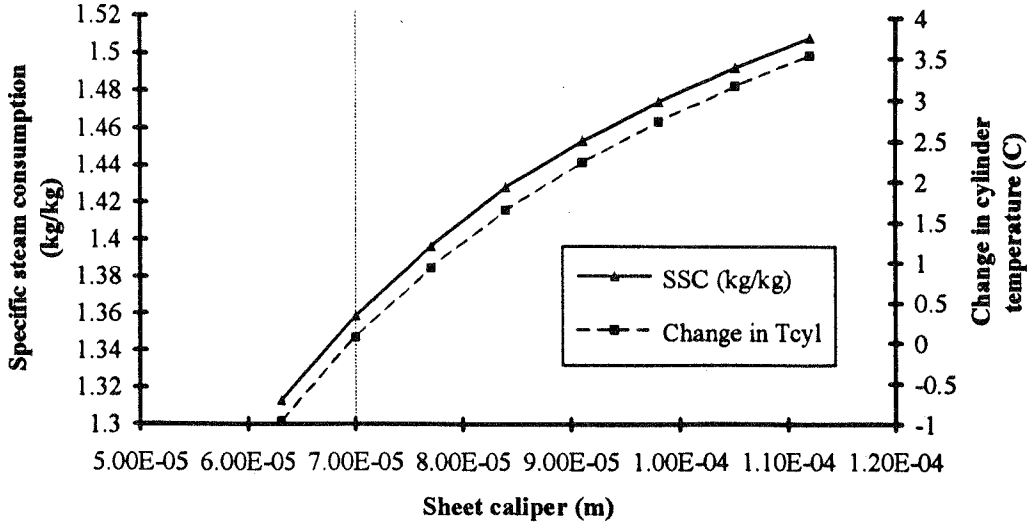

FIGURE 12.16
Variation of specific steam consumption with ΔT_{cyl} varied to maintain a constant production speed (1050m/min) in response to changes in sheet caliper

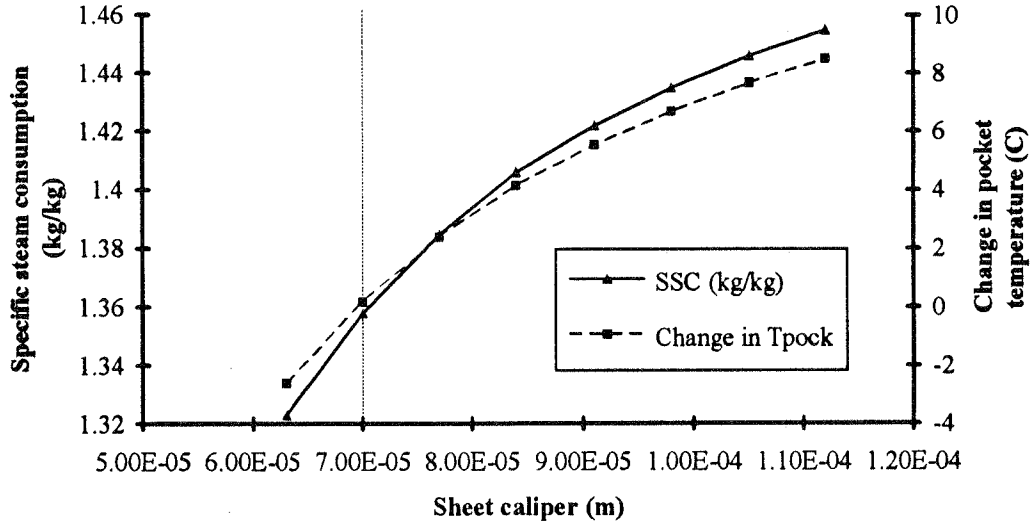

FIGURE 12.17
Variation of specific steam consumption with ΔT_{pock} varied to maintain a constant production speed (1050m/min) in response to changes in sheet caliper

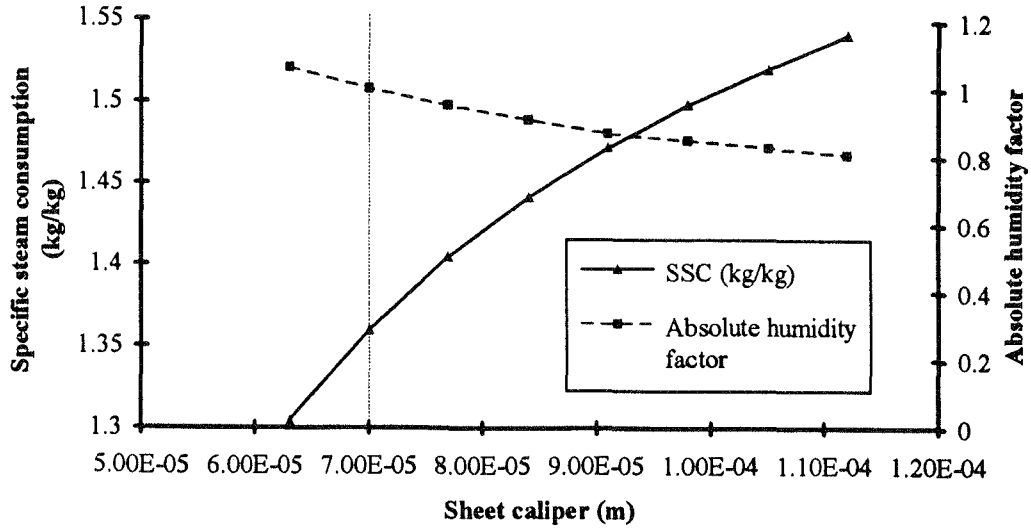

FIGURE 12.18
Variation of specific steam consumption with W_{factor} varied to maintain a constant production speed (1050m/min) in response to changes in sheet caliper

The key conclusion from Figures 12.16-12.18 is that the optimum technique for maintaining drying rate as sheet caliper increases is through increasing the pocket air temperature. For example, for a 100μm thick paper sheet the most energy efficient adjustment to the standard settings, compared to drying a 70μm sheet is to increase the pocket air temperature by 7°C in all dryer sub-sections. An outline of other control options for this particular example is shown in Table 12.4 below.

TABLE 12.4
Control options for a sheet caliper change from 70 to 100μm

Parameter	Change	SSC (kg_{steam}/kg_{paper})
Steam temperature	+2.85 °C	1.480
Pocket temperature	+6.95 °C	1.438
Pocket abs. humidity	-15.6 %	1.505

12.3.3.3 Sheet dry basis weight

The next series of results presented in Figures 12.19-12.21 shows the changes to dryer sections conditions required to maintain a constant machine speed whilst the basis weight varies. The optimal control measure is indicated by the option which leads to the minimum specific steam consumption.

The conclusion from these graphs is that low basis weights are best managed, from an energy efficiency viewpoint, by dropping the cylinder steam temperatures or increasing the pocket humidity through reducing air flow. At higher basis weights the best control option is to increase the pocket temperatures to maintain drying rate and machine speed.

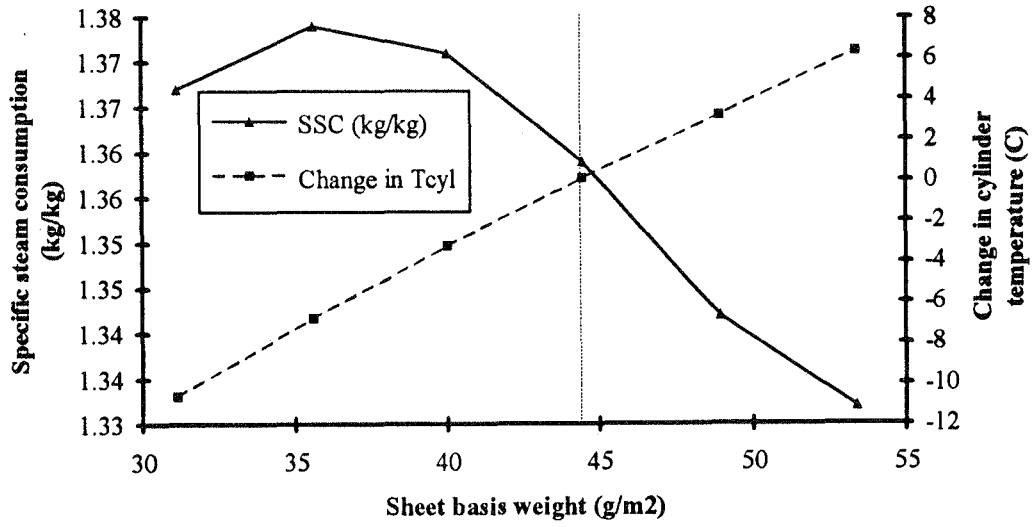

FIGURE 12.19
Variation of specific steam consumption with ΔT_{cyl} varied to maintain a constant production speed (1050m/min) in response to changes in sheet basis weight

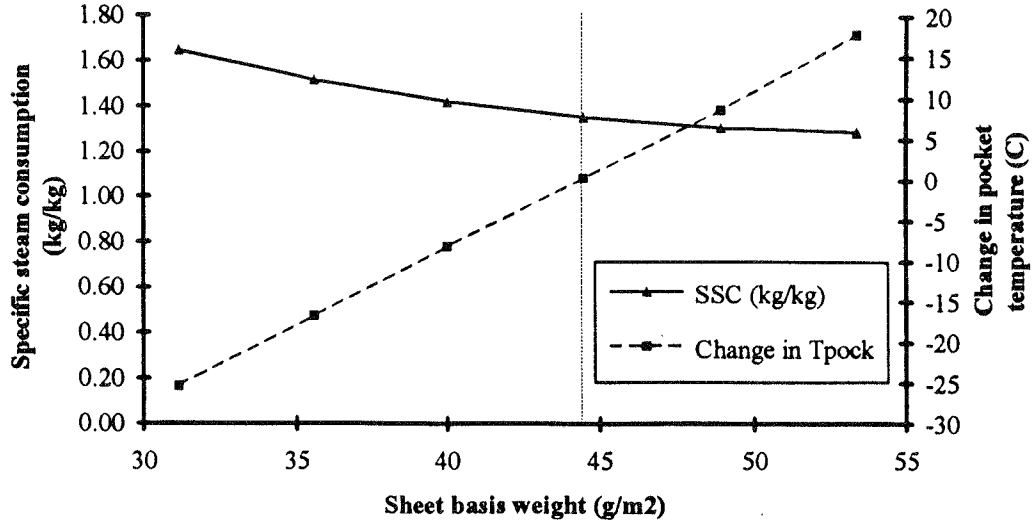

FIGURE 12.20
Variation of specific steam consumption with ΔT_{pock} varied to maintain a constant production speed (1050m/min) in response to changes in sheet basis weight

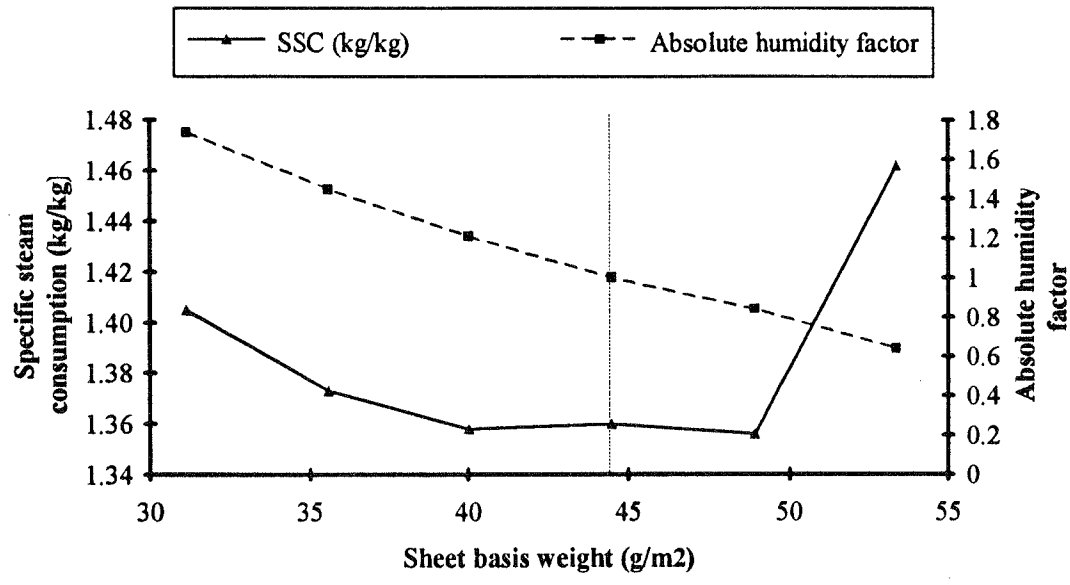

FIGURE 12.21
Variation of specific steam consumption with W_{factor} varied to maintain a constant production speed (1050m/min) in response to changes in sheet basis weight

As an example, 50 g/m^2 dry basis weight paper will dry most efficiently by increasing the air pocket temperatures by 11°C compared with drying conditions for the basecase 44.5 g/m^2. This is summarised in Table 12.5.

TABLE 12.5
Control options for a change in dry basis weight from 44.5g/m^2 to 50g/m^2

Parameter	Change	SSC (kg_{steam}/kg_{paper})
Steam temperature	+3.94 °C	1.340
Pocket temperature	+10.86 °C	1.310
Pocket humidity	-21.9 %	1.382

12.3.3.4 Sheet initial temperature

Three sets of control strategies for maintaining constant speed during a change in sheet initial temperature are presented in Figures 12.22-12.24.

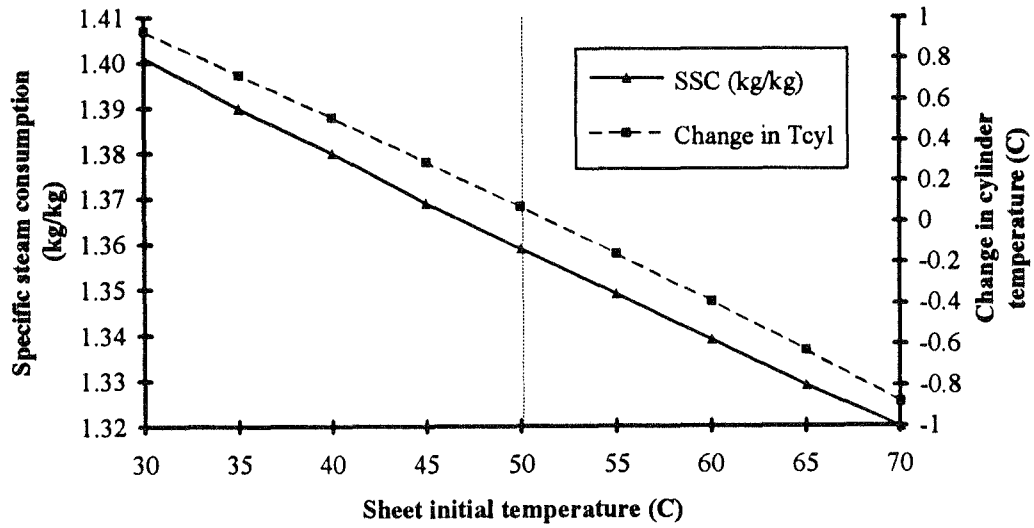

FIGURE 12.22
Variation of specific steam consumption with ΔT_{cyl} varied to maintain a constant production speed (1050m/min) in response to changes in sheet initial temperature

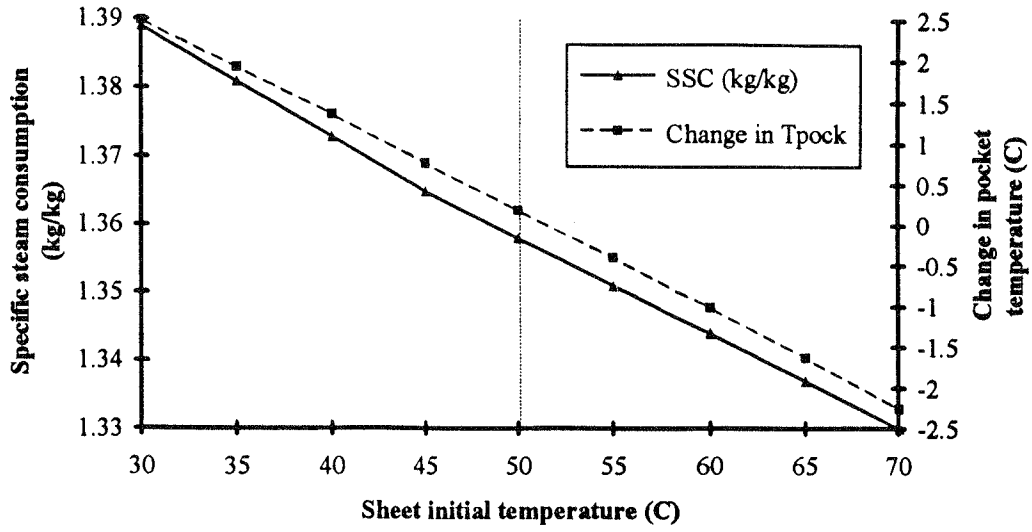

FIGURE 12.23
Variation of specific steam consumption with ΔT_{pock} varied to maintain a constant production speed (1050m/min) in response to changes in sheet initial temperature

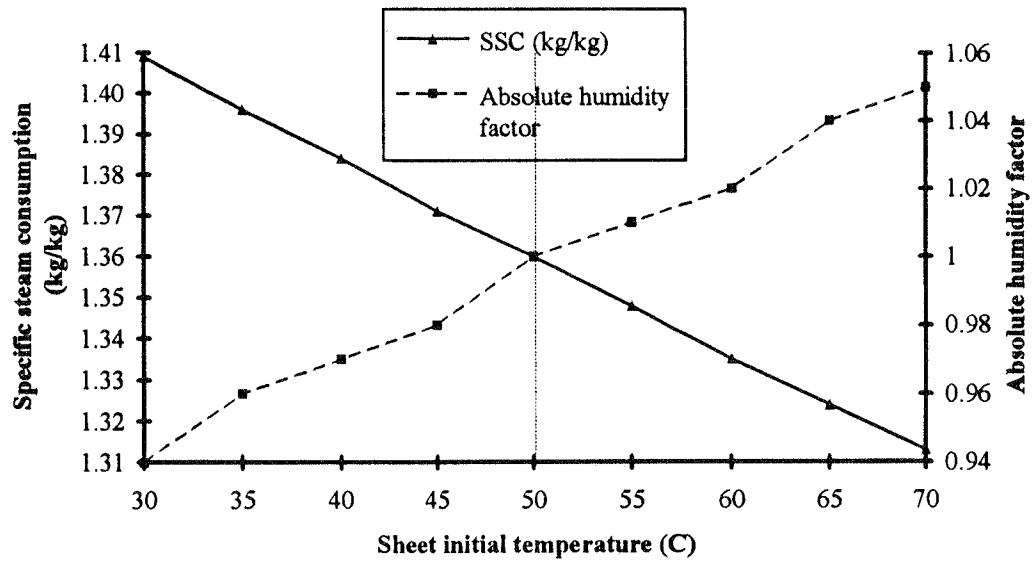

FIGURE 12.24
Variation of specific steam consumption with W_{factor} varied to maintain a constant production speed (1050m/min) in response to changes in sheet initial temperature

The graphs show that increases in initial sheet temperature are best handled by adjustments to the pocket air humidity. Decreases in sheet temperature are most energy efficiently dealt with by increasing the pocket air temperature.

By way of example consider a drop in sheet temperature at dryer section inlet from 50°C to 40°C. A 1.35°C increase in all pocket temperatures would allow the machine to maintain a constant 1050 m/min in spite of this 10°C temperature drop. The alternative control options are presented in Table 12.5.

TABLE 12.5
Control options for changing initial sheet temperature from 50°C to 40°C

Parameter	Change	SSC (kg_{steam}/kg_{paper})
Steam temperature	+0.51 °C	1.380
Pocket temperature	+1.35 °C	1.373
Pocket humidity	-3.0 %	1.384

These results further demonstrate that the drying process is relatively insensitive to initial temperature.

12.4 Exploring model predictions - design

The theoretical drying model was intended to assist with optimising the dryer section's performance both in terms of operational settings as well as hardware configuration. The previous section discussed the control strategy application whilst the ensuing examples will demonstrate the model's relevance in examining the effects of major structural changes to the dryers on either of the ANM machines.

12.4.1 Design review of PM3 dryer section configuration

The mathematical drying model has applications as a design aid when recommending optimal configurations for paper machine dryer sections. Whilst it would not be economic to redesign an entire paper machine dryer section in terms of cylinder locations and length of the open draws simply

from the viewpoint of energy efficiency, it is of interest to assess the current configuration from this perspective. This provides an opportunity to demonstrate the capability of the model and compare it with the design tools employed by the paper machine manufacturer in the 1960s when the machine was built. It should be noted that the design tools used by such manufacturers generally fall within the bounds of *proprietary knowledge* and consequently it is difficult to assess their degree of sophistication.

As described in Appendix 3, the PM3 dryer section has 48 drying cylinders. The first twelve cylinders compose two single-felted dryer sub-sections whilst the remaining three sub-sections are double-felted drying runs. The typical sheet wrap per drying cylinder is 2.968m whilst most of the free draws are 1.159m long. These figures vary marginally at the changeover between sub-sections.

An interesting theoretical consideration lies in the question of the optimal balance between cylinder wrap and open draw for a dryer section. The length of cylinder wrap governs the amount of heat which can be input into the paper sheet to provide energy for the evaporation of moisture. The open draw offers a considerably higher mass transfer coefficient where the evaporating moisture is not impeded by the close contact of the drying fabric. Thus an over-abundance of cylinder wrap will maintain a hot sheet which cannot freely vent moisture whilst an excessive amount of free draw will allow the sheet's temperature to drop dramatically so that insufficient energy remains for further evaporation after an initial period.

ANM PM3 has a 70% : 30% split between cylinder wrap and free draw length throughout its dryer section. To analyse the suitability of this mix a series of calculations were devised whereby the total length of paper run throughout the dryer section (200.039m) was held constant and the balance between cylinder wrap and free draw varied. The balance was changed by adding/subtracting a fixed incremental distance to each of the 48 lengths of cylinder wrap throughout the dryer section and subtracting/adding the same distance to the 48 free draw lengths throughout the dryer section.

For each of these dryer section geometries the paper sheet speed required to bring the sheet to standard dryness, 8.9% or 0.0988 kg_{water}/kg_{fibre} was calculated. Constant drying conditions such as cylinder temperature and dryer pocket air temperature and humidity were used throughout all calculations.

The machine speed calculated is governed by drying capacity, a phenomenon which is not necessarily the case on actual paper machines, where the runnability of a paper sheet, or its degree of resistance to breaks, may require the operator to reduce the machine speed to increase production reliability. Given the constant drying conditions assumed, the drying capacity is a direct function of the structural geometry input into the model. The optimal configuration will be the one which predicts the highest attainable machine speed.

The results presented in Figure 12.25 show the variation of paper machine speed with a variable referred to as *offset*, which is defined as the incremental length added to the cylinder wrap components of the dryer section. Thus a positive value for *offset* means that the cylinder wrap is being increased and the free draw decreased. Similarly a negative value for *offset* means that each free draw section has been lengthened whilst reducing the contact with the heated cylinder to maintain the overall length constant.

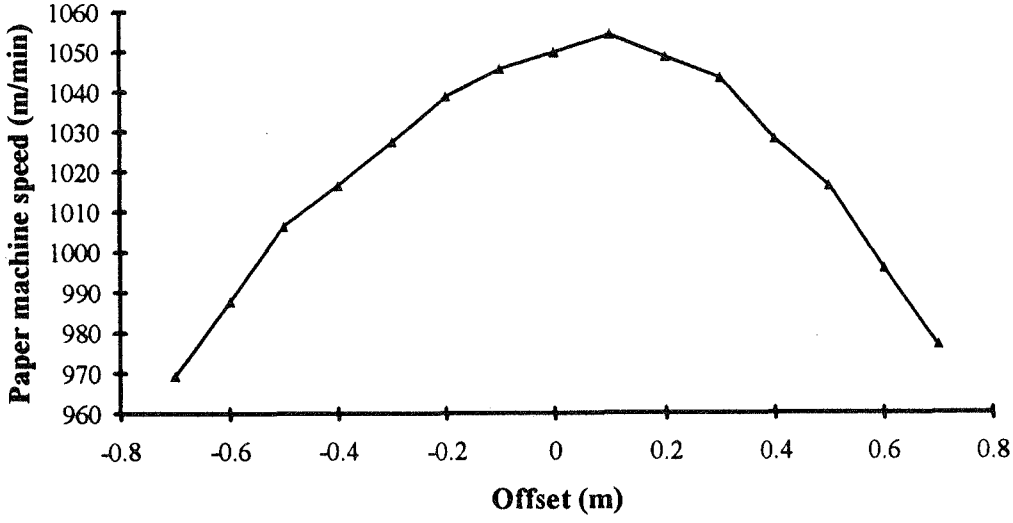

FIGURE 12.25
Attainable operating speed on PM3 with cylinder wraps increased by *offset* and free draws reduced by *offset*

Figure 12.25 indicates that the optimal value for *offset* is +0.1m. This implies that cylinder wraps would be increased to 3.07m and the free draws reduced to 1.06m. Given this change the achievable machine speed under constant drying conditions would increase by 0.5% to 1055 m/min.

This is a modest performance increase and demonstrates that the initial design of the dryer section geometry of this paper machine was well-founded. However, the calculation very succinctly emphasises the usefulness of the computer-based model for resolving a wide range of performance issues related to dryer section operation.

12.4.2 PM2 conversion to a single-felted wet section

The ANM PM2 machine is about 10 years older than the wider PM3 and generally runs at 880 m/min when producing 48.8 g/m^2 newsprint. In order to improve the runnability of the paper sheet through the dryer section as well as drying capacity one proposal that has been considered is to revise the initial single-felted dryer sub-section.

All drying cylinders in PM2 (and PM3) are 1.52m (5') diameter. The cylinder-sheet contact area can be increased by installing larger diameter cylinders. 2.13m (7') cylinders are available and could be retrofitted as the upper cylinder row in the wet single-felted region. The number of cylinders would be reduced in this case from twelve to ten - corresponding to five 2.13m cylinders along the upper row. Consequently, the change in achievable drying rate for a given set of drying conditions will be influenced by the new balance between cylinder wrap and open draw in the wet end sub-section and also the reduction in cylinder number. A diagram of the proposed arrangement and the key dimensional variables is presented in Figure 12.26.

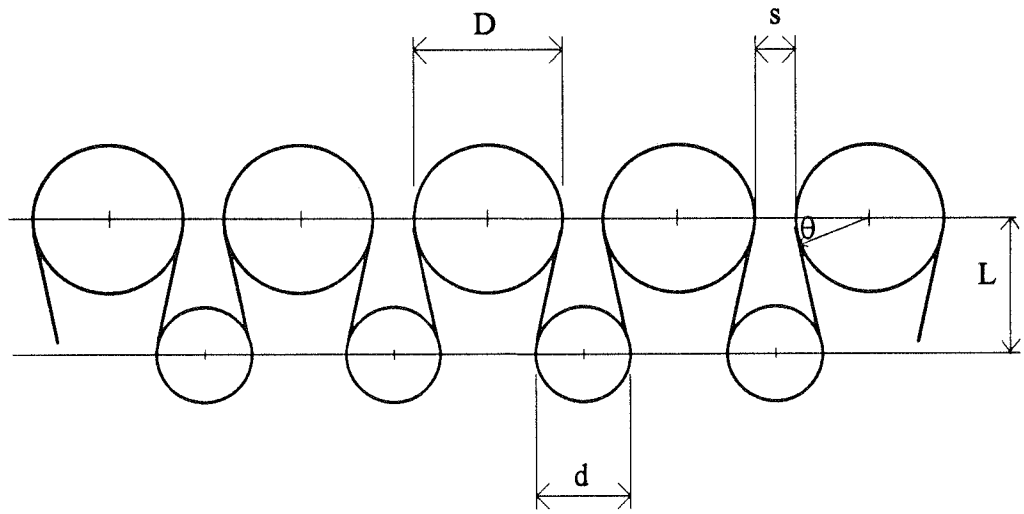

FIGURE 12.26
Diagram of potential PM2 single-felted drying run with 2.13m diameter upper cylinders

The diagram defines the variables *s*, representing the offset distance between upper cylinders, *D* and *d*, being the diameters of the upper and lower cylinders respectively, *L*, the vertical distance between upper and lower cylinder centres, and θ, the angle of contact arc between paper and the heated cylinder in excess of 180°.

Some relatively straightforward geometry shows that,

$$D + d = 2L\sin\theta + (D + s)\cos\theta. \qquad (12.11)$$

As mentioned earlier *D* is to be set to 2.13m. The horizontal separation distance *s* is typically 0.45m on most paper machines and it appears impractical to reduce the clearance below this value. The lower cylinder diameter *d* may be either 0.45m if new turning rolls are specified or 1.52m if the existing 5' cylinders are re-used in this location - note that this option would retain the flexibility to put some heat into the lower cylinders even though they are insulated from the paper sheet by the drying felt. Thus, given the vertical separation *L* equation 12.11 can be solved for θ. Then the contact arc and free draw can be determined from,

$$\text{cylinder wrap} = \frac{D}{2}(\pi + 2\theta), \text{ (top cylinder), and,} \qquad (12.12)$$

$$\text{free draw} = \left(L - \frac{D + d}{2}\sin\theta\right) / \cos\theta. \qquad (12.13)$$

With these relations for cylinder wrap and free draw as functions of *L* the infrastructure is set up to predict achievable machine speed under the new drying configuration for varying values of vertical separation between upper and lower rolls. The results are presented in Figure 12.27 both for the case of *d=0.45m* and *d=1.52m*.

The results of Figure 12.27 show clearly that selecting the lower cylinder with the 1.52m diameter gives considerably more drying capacity than the smaller 0.45m diameter turning roll would. This is partly because of the increased overall dryer section run which leads to a longer residence time for mass transfer to occur, but primarily because the larger lower roll promotes a greater contact angle on the upper heated roll and this allows more heat to be transferred into the sheet.

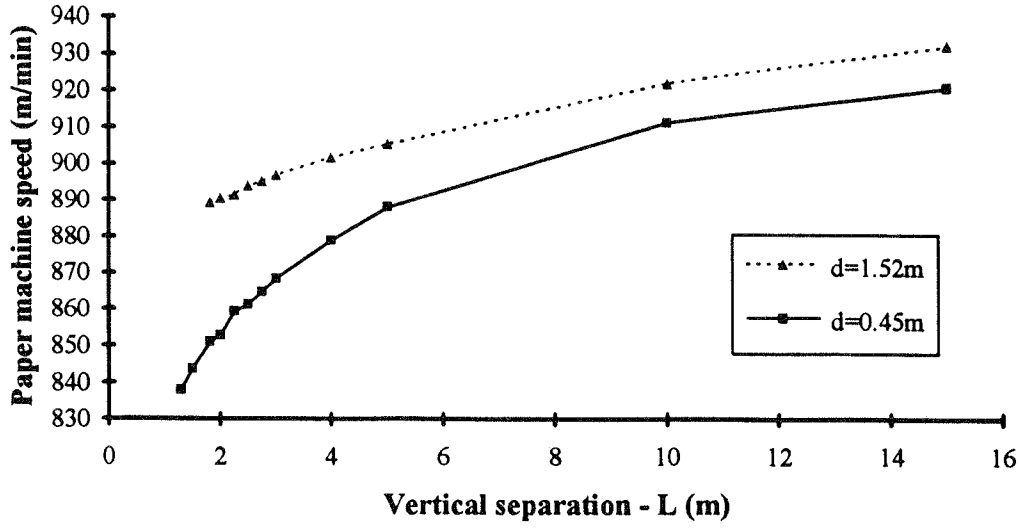

FIGURE 12.27
Paper machine production for a number of potential paper machine geometries

The selection of the optimal L is limited by physical considerations. This distance must be greater than the sum of the radii of upper and lower cylinders, 1.825m and 1.29m for the case of the large and small lower rolls respectively. The maximum distance is limited primarily by space considerations and the allowable increase in unsupported sheet length. It is unlikely that an L value beyond 3m would be considered.

Comparing the results for $L=3m$ shows a machine speed of 897 m/min for the 1.52m lower cylinder case and 868 m/min 0.45m case. These values should be compared with the achievable speed under the existing geometry which is 880 m/min. On this basis the new values represent a 2.2% increase and a 1.4% decrease in production rate respectively. The potential 2.2% improvement may not be considered sufficient to justify the rebuild unless other factors such as improved paper sheet runnability were taken into account.

It should be emphasised that the preceding calculations have assumed constant drying conditions. The new dryer section geometries considered may allow more intense drying conditions to be employed beyond those currently used in which case these effects should be factored into a future calculation.

12.4.3 Other useful model applications

The calculations presented in Sections 12.4.1 and 12.4.2 demonstrate the applicability and relevance of the model to a number of issues relating to the paper machine's dryer operation. There are clearly many other situations which can be examined by the model. Several of these are listed below.

- In recent times many newsprint manufacturers have considered the move to supercalendered papers. These are a high gloss, high quality paper grade which are eligible for a premium price. The supercalender itself is larger than the usual machine calender stack and in some cases necessitates removal of some drying cylinders. In these situations the model could be used to predict the loss of drying performance resulting from a reduction in the number of drying cylinders.
- The breaker stack area on ANM PM3 machine was previously described as the region where samples of paper for moisture content testing were obtained. The impact of the installation of a non-productive drying area such as this, or the restoration of such an area to full drying capacity could be explored by the computer model.
- The current trend towards higher speeds of paper production highlights the property of sheet runnability - the ability of a paper sheet to run for extended periods of time without breakage. Single-felted dryer section runs provide support for the sheet and reduce the incidence of breaks. Converting the third sub-section of ANM's two machines' dryer sections from double-felted to single-felted runs would assist runnability and therefore increase sheet speed significantly. However, the drawback is the reduction in drying capacity brought about through rendering all affected lower cylinders redundant from a heat transfer perspective. Under these circumstances it would be necessary to consider various means of increasing drying capacity per m^2 of drying surface. A number of permutations of increased cylinder steam or pocket air temperatures can be evaluated by the model for effect and practicality.

The potential application of the model to dryer section changes is enormous. The number of potential combinations of model input parameters is quite vast and some customisation may be necessary to cater for specific situations. For many future projects the model can be a useful screening tool which will highlight the impact on drying capacity, and in doing so pass comment on the viability or urgency of many proposals.

13. Conclusion

The outcome of this study is a complete description of the paper drying process which relates initial sheet conditions, paper sheet properties, drying conditions and dryer section configuration to the variation of the moisture content and temperature in the paper sheet. This relationship is ultimately used to predict unit energy consumption.

There have been three major stages in the course of the study. The first stage was developing a mathematical model which could be implemented by computer. Stage two required the physical parameters describing the system to be defined. These fall into two categories - machine specific parameters and paper sheet properties. The final phase of the study was to apply the model, complete with its physical description of the ANM paper grades, to the two ANM machines to demonstrate firstly that the model was accurate and secondly that it was relevant in a production environment.

Model development

The theoretical model was based on mass and energy balance equations about a slice of paper composing pulp fibres, free and bound water, water vapour and air. Time-varying boundary conditions, corresponding to the movement of the paper sheet over the 40-50 drying cylinders, were assigned and the equations were converted to finite difference form and solved by computer using standard linear algebra methods. Despite the equations being relatively cumbersome when fully expanded, the full dryer section integration could be done with reasonable accuracy (5%) on a desktop personal computer in about one minute using a time step of 0.01 seconds and five slices across the sheet's thickness. Accuracy to within 1% of the asymptotic drying curve was obtained in ten minutes of computer time using an integration time step of one millisecond.

Physical parameters

Definition of the physical parameters employed by the model was a crucial phase of the project as these values directly dictate the accuracy of the model when applied to an actual paper machine. The heat and mass transfer coefficients which control evaporation rates in the dryer section were investigated experimentally.

The skin friction coefficients for the drying fabrics and the smooth aluminium hot plate were determined using a hot wire probe and boundary layer analysis. The drag coefficient, Cf, was found to vary along the length of the curved surface in a similar fashion to the results of Baskaran et al (1987). The frictional drag of the 350cfm dryer fabric was significantly greater than that of the less permeable 75cfm dryer fabric. This has great importance in terms of the paper sheet's runnability in the dryer section. This relates to the extent to which air flows entrained by the dryer fabric create sheet instability which can lead to wrinkles or breaks. This was not pursued further under the current scope of work but is a worthy subject for a future study. The surface heat transfer coefficient was determined independently by measurement of the thermal boundary layer and shown to vary linearly with the skin friction coefficient in a manner corresponding to that expected from Colburn's analogy.

The contact heat transfer coefficient for the laboratory drying trials was investigated through analysis of the thermal boundary layer and found to be 410 $W/m^2°C$. This was found to be somewhat lower than other researchers, such as Lee and Hinds (1983) proposed, but was explained on the basis of the additional interface between the hot plate and the thin aluminium supporting plate. This value was used later in the series of model calculations which iterated for the mass transfer coefficient for individual drying trials.

Eighteen drying trials were carried out to define the effect of a number of parameters on drying rates. This enabled the variation of the mass transfer coefficient to be determined. For each of the parameters investigated, hot plate temperature, air velocity, felt tension, felt permeability, pulp furnish and sheet basis weight, the model was used to determine the mass transfer coefficient required to give the observed rate of drying. The trial examining mass transfer coefficient as a function of relative air velocity over the dryer felt resulted in the most important correlation. The experimental relationship predicted a mass transfer coefficient midway between those expected for a flat plate (Chilton-Colburn, 1934) and for a cylinder in cross flow (Zkukauskas, 1975).

The felt permeability trials quantified the influence of the different dryer fabrics on drying behaviour. The results showed that the drying rate for the case of the nylon tensioning lines which offered no resistance to evaporation occurred was about 2½ times greater than the rate of drying through even the most permeable felt (350cfm). Obtaining both these data was essential as the paper sheet is exposed to both situations during drying

on an actual machine. Felt tension was shown to affect drying rate through increasing the contact heat transfer coefficient. However, the results showed that increasing the tension beyond 1.8 kN/m did not assist the drying rate further and this finding agreed with TAPPI's technical information sheet (1989) on the subject.

Trials performed on a range of different pulp handsheets showed very little variation in their drying behaviour. The three individual pulps, TMP, CCS and kraft, all dried at rates within ±10% of the blended 'newsprint' mixture. This subtle difference suggested that the variation due to different fibre structures was fairly minimal and machine operation will be influenced more by the draining and pressing characteristics of the furnish.

The drying tests which examined the effects of hot plate temperature and sheet basis weight showed a constant mass transfer coefficient. This supported the normalisation procedure used to correct for perturbations in sheet basis weight, initial moisture content and hot plate temperature.

A number of *paper sheet properties* were investigated as part of the study. The pore size distribution of the sheet which exerts influence over the liquid capillary pressure distribution within the sheet was defined in terms of the beta distribution and subsequently a relationship between moisture content and the maximum pore radius filled with free water was developed. Literature suggested that the maximum pore radius within a typical newsprint was 10μm whilst for a handsheet a value four times larger was likely.

The newsprint's permeability was measured as 4.9×10^{-15} m^2 and theoretically predicted to be 5.9×10^{-15} m^2. This calculation, based on the pore size distribution described previously, was found to be considerably more reliable than the Kozeny-Carman theory which is not suited to media with non-uniform pore sizes and predicted 98×10^{-15} m^2.

Measurements were also made of the sorption isotherms for machine made newsprint. This set of data quantifies the reduction in vapour pressure during drying due to the hygroscopic characteristics of wood fibres as well as the differential heat of sorption. Both of these factors combine to slow the drying rate at low moisture contents. The results were found to exhibit close similarity with Prahls' (1968) tests on 'Mobile Pine', a kraft processed softwood. This demonstrated that sorptive characteristics do not change significantly between different pulps.

Other paper properties correlated from literature for the purposes of this study included thermal conductivity, for which a combination series-parallel representation was described, specific heat capacity, density, fibre saturation point, diffusibility and shrinkage.

Model application - operation

Developing a theoretical foundation and researching parameters for use in a model are essential preparatory steps before a drying model becomes useful. Applying the model to the two ANM paper machines is the culmination of the study and the calculations presented demonstrate the breadth of the model application.

The first drying rate calculation was a comparison with actual machine moisture content values and showed the model's prediction of moisture change during drying to cylinder No. 38 on PM3 to be 2% less than actual and 0.1% more than actual by the exit from the drying cylinder. These results were obtained by iterating for the contact heat transfer coefficient along the length of the dryer section to give an energy balance with steam measurements taken on the individual sub-sections. On PM2 no intermediate measurement was possible but the overall moisture change between dryer inlet and exit differed only by 0.2% between theoretical and actual.

In terms of predicting energy consumption of the paper machine a 91% correlation was obtained. This was a comparison of the theoretical estimate and actual machine data monitored over a three year period. Subtle changes in the machine characteristics over such a long timeframe are invisible to the model and will lead to small distortions between the forecast and actual values.

A series of simulations were performed to demonstrate the effect of the paper sheet condition on drying, specifically, initial moisture content, sheet thickness, sheet basis weight and initial temperature. These graphs provided a useful insight into the effect on achievable machine speed and specific steam consumption as a function of such variables.

A second set of calculations was carried out to examine the effect of drying conditions, namely, cylinder temperatures, pocket air temperatures and pocket air humidity, on achievable machine speed and specific steam consumption. The results showed that lower cylinder temperatures, higher pocket ventilation temperatures and higher pocket absolute humidity will

all lead to more efficient drying operation. The effect of these changes on machine speed was defined.

An alternative perspective on the analysis was to specify the machine speed as constant, as often occurs in a production environment, and determine the necessary change in each of the drying parameters pocket temperature, pocket humidity and cylinder temperature to maintain this speed in response to changes in the paper sheet properties. The energy efficiency of each option was monitored in terms of the specific steam consumption. In each case, increases in the drying duty were best served by increasing the temperature of the pocket ventilation air. On occasions when the drying duty was reduced, a lower initial moisture content for example, the preferred control option was to reduce either the dryer cylinder temperatures, a function of steam pressure, of reduce the quantity of ventilating air, subject to the avoidance of local condensation in the cooler areas of the dryer section.

Model application - design

One of the most useful applications of the mathematical dryer model is its ability to investigate the effect of configuration changes to machine dryer sections. As structural rebuilds are extremely capital intensive the benefits of forecasting the effect of changes on drying capacity and energy efficiency are significant. Two scenarios were considered. The first examined the dryer section geometry from the perspective of an optimal design, an exercise relevant to a paper machine manufacturer. The results showed the optimal case to be an extension of each cylinder wrap by 10cm, whilst maintaining a constant total sheet length within the dryer section, which would lead to a 5 m/min speed increase under constant conditions. This is relatively small and suggests that ANM PM3 was well designed in this regard.

The second prospective change examined was that of PM2's conversion to an initial dryer sub-section with seven foot diameter cylinders, in a bid to improve heat transfer and hence drying rate and also improve runnability in this critical wet section. The simulation predicted that this would lead to a production increase of almost 20 m/min, just over 2%. This suggests the project would not be feasible on the basis of increased drying rate alone but would need to be co-justified by other factors.

A comparison of the ANM PM3 machine with other paper manufacturers worldwide showed it to be in the upper echelon in terms of drying rate per unit dryer section surface area and also specific steam consumption.

Conclusion

Numerous variables have been researched and the mathematical model has been tested against actual machine data and found to predict moisture content within several percent. Energy predictions have been made against a scattered data set within 10%. These results are very positive given the strong reliance on fundamental physical data to generate the model characteristics.

Overall the results generated by this study, and the general infrastructure which supports it, are unique from the viewpoint that the model considers all relevant paper and dryer section characteristics. These range from scanning electron microscopy to assist in determining the pore size distribution and differences between pulps to specification of the drying cylinder steam pressures required to dry the paper sheet sufficiently.

The benefits of this approach are evident from the diversity of calculations that can be handled by the model and the computational infrastructure. Throughout this analysis instantaneous drying rates, moisture contents and temperatures are calculated as well as key production data which are relevant in the environment of the machine room itself, such as maximum machine speed and specific steam consumption. The usage of actual paper machine control parameters in the analysis makes the model a practical tool which can be gainfully applied to optimise the performance of a given dryer section. The model's ability to review the impact of design configuration changes is a feature which has enormous application and is not discussed in the literature by paper machine manufacturers, possibly because of the barrier of proprietary information and possibly because the detail required for the implementation of such a model is so immense.

The model performs precisely what it set out to achieve when the project was initiated in 1990, and does so to a high level of accuracy and in a manner which is extremely relevant and accessible to the industry.

14. References

AHRENS, F., KARTSOUNES, G. and RUFF, D., *A Laboratory Study of Hot-Surface Drying at High Temperature and Mechanical Loading*, Pulp and Paper Magazine of Canada, Vol. 85, No. 3, 1984, pp 93-98.

ALLAN, R.J., GHOSH, A.K. and HARRIS, D.J., *Simulation of Web Drying in a Paper Machine - an Optimising Tool*, 1988 Appita Conference, Hobart, Tasmania, April 1988, pp A5.1-A5.20.

ASENSIO, M.C., SEYED-YAGOOBI, J., NG, K.H., FLETCHER, L.S. and PULKOWSKI, J.H., *Thermal Conduct Conductance of a Moist Paper Handsheet/Metal Interface*, American Society of Mechanical Engineers, 1991.

ATTWOOD, D., *The Mechanism of Drying Paper on Heated Cylinders*, Pulp and Paper Magazine of Canada, December 1964, pp T533-T536.

BANHAM, P.W. and COX, R.E., *Comparative Properties of Albury and Boyer TMP*, Research Report No. 89-19, Australian Newsprint Mills Limited, November 1989, pp 7-9.

BASKARAN, V., SMITS, A.J. and JOUBERT, P.N., *A turbulent flow over a curved hill. Part 1. Growth of an internal boundary layer*, J. Fluid Mech., Vol. 182, 1987, pp 47-83.

BASKARAN, V., SMITS, A.J. and JOUBERT, P.N., *A Turbulent Flow over a Curved Hill. Part 2 : Effects of Streamline Curvature and Streamwise Pressure Gradient*, Journal of Fluid Mechanics, Vol. 232, 1991, pp 377-402.

BERGER, D. and PEI, D.C.T., *Drying of Hygroscopic Capillary Porous Solids - a Theoretical Approach*, International Journal of Heat and Mass Transfer, Vol. 16, No. 2, February 1973, pp 293-302.

BLIESNER, W.C., *A Study of the Porous Structure of Fibrous Sheets Using Permeability Techniques*, Tappi Journal, Vol. 47, No. 7, July 1964, pp 392-400.

BRENT, R.P., *Algorithms for Minimisation without Derivatives*, Prentice-Hall, New Jersey, 1973, Chapter 5.

BRISTOW, J.A., *Paper - Structure and Properties*, Marcel Dekker, New York, 1986, Chapter 9.

BRUNAUER, S., DEMING, L.S., DEMING, W.E. and TELLER, E.J., Journal of the American Chemistry Society, Vol. 62, 1940, p1723.

BUSKER, L.H., *Wet Press Water Removal over a Wide Parameter Range*, Paper Technology and Industry, Vol. 21, No. 3, April 1980, pp91-96.

CARMAN, P.C., Transactions of the Institution of Chemical Engineers (London), Vol. 15, 1937, pp 150-166.

CHANCE, J.L., *Overview of the Dryer Section*, 1989 Practical Aspects of Pressing and Drying, pp 121-137.

CHILTON, T.H. and COLBURN, A.P., *Mass Transfer (Absorption) Coefficients - Prediction from Data on Heat Transfer and Fluid Friction*, Industrial and Engineering Chemistry, Vol. 26, 1934, pp 1183-1187.

CLAUSER, F.H., *Advances in applied mechanics - Vol. IV*, Academic Press, New York, 1956.

COLBURN, A.P., *A Method of Correlating Forced Convection Heat Transfer Data and a Comparison with Fluid Friction*, Transactions of the American Institute of Chemical Engineers, Vol. 29, 1933, pp 174-210.

CORTE, H., *The Porous Structure of Paper*, Fundamentals of Papermaking Fibres, edited by F. Bolam, Cambridge, 1957, pp 301-331.

CORTE, H., *Handbook of Paper Science, Volume 2 : The Structure and Physical Properties of Paper - Chapter 6 : The Porosity of Paper*, edited by H.F.Rance, Elsevier Scientific Publishing Company, 1982, pp 1-70.

CORTE, H. and KALLMES, O.J., *The Formation and Structure of Paper*, Transactions of the Fundamental Research Symposium, Oxford, 1962, pp 351-368.

CRC Handbook of Chemistry and Physics, edited by Rhide, D., 1991-92, 72nd edition.

d'A CLARK, J., *Pulp Technology and Treatment of Paper*, Miller Freeman Publications, San Francisco, 1981, pp 135-144.

DARCY, H., *The Public Fountains of the City of Dijon*, Dalmont, Paris, 1856. (original not seen)

DEPOY, J.A., *Analog Computer Simulation of Paper Drying : A Workable Model*, Pulp and Paper Magazine of Canada, Vol. 73, No. 5, May 1972, pp 67-74.

DOE, P.E., *Fundamental Aspects of Convective Evaporation and Drying*, Doctoral Thesis, University of Tasmania, 1970.

DRESHFIELD, A.C., and HAN, S.T., *The Drying of Paper*, Tappi, Vol. 39, No. 7, July 1956, pp 449-455.

ESKELINEN, P.J., *How to Improve the Paper Machine Performance by Combining Dryer Section Survey and Computer Simulation*, Drying Technology, Vol. 3, No. 2, 1985, pp 255-269.

FAGERHOLM, L., *Thermodynamical Properties of Dryer Fabrics for High Speed Paper Machines*, 1990 Tappi Engineering Conference, pp 165-174.

FLYATE, D.M. and KAGAN, M.R., Bumazh. Prom., Vol. 9, 1971, pp 7-8.

FUJII, T. and IMURA, H., *Natural Convection Heat Transfer from a Plate with Arbitrary Inclination*, International Journal of Heat and Mass Transfer, Vol. 15, 1972, pp 755-767.

GOLDSTEIN, R.J., SPARROW, E.M. and JONES, D.C., *Natural Convection Mass Transfer Adjacent to Horizontal Plates*, International Journal of Heat and Mass Transfer, Vol. 16, 1973, pp 1025-1035.

GREENKORN, R.A., *Flow Phenomena in Porous Media*, Marcel Dekkar Inc., 1983, Chapter 1.

GUNDERSON, D.E., *Method for Measuring Mechanosorptive Properties*, Journal of Pulp and Paper Science, Vol. 17, No. 2, March 1991.

HAMA, F.R., *Boundary Layer Characteristics for Smooth and Rough Surfaces*, Trans. Soc. Nav. Arch. Mar. Eng., Vol. 62, 1954, pp 333-358.

HAN, S.T., *Heat and Mass Transfer in Hot-Surface Drying of Fibre Mats*, Pulp and Paper Magazine of Canada, December 1964, pp T537-T549.

HAN, S.T. and MATTERS, J.F., *Vapour Transport in Fibre Mats During Drying*, Tappi, Vol. 49, No. 1, January 1966, pp 1-4.

HAN, S.T. and ULMANEN, T., *Heat Transfer in Hot-Surface Drying of Paper*, Tappi, Vol. 41, No. 4, April 1958, pp 185-189.

HARING, R.E. and GREENKORN, R.A., *A Statistical Model of a Porous Medium with Nonuniform Pores*, AIChE Journal, Vol. 16, No. 3, May 1970, pp 477-483.

HARRMANN, M. and SCHULZ, S., *Convective Drying of Paper Calculated with a New Model of the Paper Structure*, Drying Technology, Vol. 8, No. 4, 1990, pp 667-703.

HARTLEY, F.T. and RICHARDS, R.J., *Hot Surface Drying of Paper - the Development of a Diffusion Model*, Tappi Journal, Vol. 57, No. 3, March 1974, pp 157-164.

HINDS, J.A. and NEOGI, A.N., *The Dynamic Computer Simulation of a Paper Machine Dryer*, Tappi Journal, Vol. 66, No. 6, June 1983, pp 79-82.

IIDA, K., *The Computer Simulation of Web Drying in a Paper Machine Dryer Section*, 1985 Pulp and Paper Technology Conference, Tokyo, October 1985, pp 115-127.a

IIDA, K., *The Computer Simulation of Web Drying in a Papermachine Dryer Section. Part I : Modeling of Web Drying in a Dryer Section*, Japan Tappi, Vol. 39, No. 5, 1985, pp 35-42.b

IIDA, K., *The Computer Simulation of Web Drying in a Papermachine Dryer Section. Part II : Simulation of Web Drying in a Dryer Section*, Japan Tappi, Vol. 39, No. 6, 1985, pp 58-68.c

INCROPERA, F.P. and DEWITT, D.P., *Fundamentals of Heat and Mass Transfer*, John Wiley and Sons, 1985, pp 334-335 and 777.

INGMANSON, W.L., ANDREWS, B.D. and JOHNSON, R.C., *Internal Pressure Distributions in Compressible Mats under Fluid Stress*, Tappi Journal, Vol. 42, No. 10, October 1959, pp 840-849.

ISO 5636/1-1984, Annex A.2.

KADER, B.A. , *Temperature and concentration profiles in fully turbulent boundary layers*, Int. J. Heat Mass Transfer, 24, pp 1541-1544, 1981.

KARLSSON, M. and SOININEN, M., *The Influence of the Hygroscopic Properties of Paper on the Transient Phenomena during Contact Drying of Paper Webs*, Internal Publication, Abo Akademi, Turku, Finland.

KARLSSON, M., *Results from On-line Investigations of Paper Contact Drying Process*, Drying '80, Volume 2 : Proceedings of the Second International Symposium, Montreal, July 1980, edited by A.S. Mujumdar, Hemisphere Publishing Corporation, pp 322-329.

KARTOVAARA, I., RAJALA, R., LUUKKALA, M. and SIPI, K., *Conduction of Heat in Paper*, Papermaking Raw Materials : Transactions of the Eighth Fundamental Research Symposium, Volume 1, Oxford, September 1985, pp 381-412.

KEEY, R.B., *Drying : Principles and Practice*, Pergamon Press, 1972, Chapters 2 and 7.

KEREKES, R.J., *A Simple Method for Determining the Thermal Conductivity and Contact Resistance of Paper*, Tappi Journal, Vol. 63, No. 9, September 1980, pp 137-140.

KERTTULA, R., *How to Increase and Optimise the Capacity of the Paper Machine Dryer Section Using Simulation Model*, 70th Annual Meeting of the Technical Section of the Canadian Pulp and Paper Association, Montreal, February 1984, pp B115-B119.

KIBBLEWHITE, R.P. and BROOKES, D., *Dimensions and Collapse Behaviour of Kraft and Bisulphite Fibres in Wet Pulps and 'in situ' in Handsheets*, Appita, Vol. 31, No. 2, September 1977, pp 111-118.

KISAKÜREK, B and GEBLIZLIOGLU, O., *Capillary Mechanism in Drying*, Proceedings of the 1st International Drying Symposium, Montreal, August 1978, edited by A.S.Mujumdar, Science Press, pp 59-65.

KOZENY, J., *Akad. Wiss. Wien.*, Math-Nat. Kl. 36 (Abt IIa), 1927, pp 271-306. (original not seen)

LAROQUE, G.L., Pulp and Paper Magazine of Canada, Vol. 38, No. 2, 1937, pp 77-84.

LEE, P.F. and HINDS, J.A., *A Technique for Measuring the Drying Characteristics of Fiber Webs*, Tappi Journal, Vol. 62, No. 4, April 1979, pp 45-48.

LEE, P.F. and HINDS, J.A., *Measurements of Heat and Mass Transport within a Sheet of Papermaking Fibers during Drying*, Drying '80, Volume 2 : Proceedings of the Second International Symposium, Montreal, July 1980, edited by A.S. Mujumdar, Hemisphere Publishing Corporation, pp 523-528.

LEE, P.F. and HINDS, J.A., *Modeling Heat and Mass Transfer within a Moist Sheet of Paper or Board*, Tappi Journal, Vol. 64, No. 12, December 1981, pp 39-44.

LUDWIEG, H. and TILLMANN, W., *Investigation of the Wall Shearing Stress in Turbulent Boundary Layers*, NACA TM 1285, 1950. (original not seen)

McADAMS, W.H., *Heat Transmission*, McGraw-Hill, 1985.

McCABE, W. and SMITH, J., *Unit Operations of Chemical Engineering*, McGraw-Hill, 1976, pp 328-337.

McCONNELL, R.R., *A Literature Review of Drying Research in the Pulp and Paper Industry*, Drying '80, Volume 2 : Proceedings of the Second International Symposium, Montreal, July 1980, edited by A.S. Mujumdar, Hemisphere Publishing Corporation, pp 330-337.

McKNIGHT, T.S., MARCHESSAULT, R.H. and MASON, S.G., *The Distribution of Pore-Sizes in Wood-Pulp Fibres and Paper*, Pulp and Paper Magazine of Canada, February 1958, pp 81-88.

MEISEL, R.M., *Analog Computer Simulation of Paper Drying*, Tappi Journal, Vol. 60, No. 1, January 1977, pp 160-162.

MOZA, A., STRICKLER, D.W. and AUSTIN, L.G., *A Mounting Medium for Coal Particles*, Scanning Electron Microscopy, Vol. 1, 1978, pp 289-291.

MURAKAMI, K. and IMAMURA, R., *Handbook of Physical and Mechanical Testing of Paper and Paperboard, Volume 2 - Chapter 17 : Porosity and Gas Permeability*, edited by R.E. Mark, Marcel Dekkar Inc., 1984, pp 57-101.

NAKAGAWA, S. and SHAFIZADEH, F., *Handbook of Physical and Mechanical Testing of Paper and Paperboard, Volume 2 - Chapter 23 : Thermal Properties*, edited by R.E. Mark, Marcel Dekkar Inc., 1984, pp 242-279.

NEDERVEEN, C.J., VAN SCHAIK-VAN HOEK, A.L., and DIJKSTRA, J.J.F.M., *Present Theories on Multi-Cylinder Paper Drying*, Paper Technology, November 1991, pp 30-35.

NELDER, J.A. and MEAD, R., Computer Journal, Vol. 7, 1965, p308.

NG, K.H., SEYED-YAGOOBI, J., ASENIO, M.C. and FLETCHER, L.S., *Thermal Contact Conductance of a Bone-Dry Paper Handsheet / Metal Interface*, National Heat Transfer Conference, Minneapolis, July 1991.

NISSAN, A.H. and KAYE, W.G., *An Analytical Approach to the Problem of Drying of Thin Fibrous Sheets on Multicylinder Machines*, Tappi Journal, Vol. 38, No. 7, July 1955, pp 385-395.

NISSAN, A.H. and HANSEN, D., *Heat Transfer and Water Removal in Cylinder Drying : I. Unfelted Cylinders*, Tappi Journal, Vol. 43, No. 9, September 1960, pp 753-756.

NISSAN, A.H., GEORGE Jnr., H.H. and HANSEN, D., *Heat Transfer and Water Removal in Cylinder Drying : II. Felted Cylinders*, Tappi, Vol. 45, No. 3, March 1962, pp 213-218.

NORDON, P. and BAINBRIDGE, N.W., *An Analysis of the Process of Through Drying of Wet Textile Materials*, Applied Polymer Symposium No. 18, John Wiley & Sons, 1971, pp 1111-1129.

PANCHAPAKESAN, B., *Optimisation of Dryer Hood and Pocket Ventilation Systems*, 1990 Tappi Engineering Conference, pp 933-937.

PIERCE, C., Journal of Colloid Chemistry, Vol. 57, 1953, p 149ff. (original not seen)

PIKULIK, I.I. and SAYEGH, N.N., *Improving Energy Efficiency of Paper Machine Dryer Sections*, US Dept. of Energy Final Report, DOE/CE-9021253, December 1988.

POUNDER, J.R. and AHRENS, F.W., *A Mathematical Model of High Intensity Paper Drying*, Drying Technology, Vol. 5, No. 2, 1987, pp 213-243.

PRAHL, J.M., *Paper Fiber and Water Mixtures*, Doctoral Thesis, Harvard University, Cambridge, Massachusetts, 1968.

PRESS, W.H., FLANNERY, B.P., TEUKOLSKY, S.A. and VETTERLING, W.T., *Numerical Recipes - The Art of Scientific*

Computing (Pascal), Cambridge University Press, 1986, Chapters 2,3,4,6,9 and 10.

RAMASWAMY, S., *Analysis of Heat and Mass Transfer During Drying of Paperboard Under Conventional and High Intensity Conditions*, Doctoral Thesis, State University of New York, May 1990.

RANCE, H.F., *The Raw Materials and Processing of Papermaking*, Elsevier Scientific Publishing Company, 1980, pp 258-267.

REARDON, S.A., *Cogeneration in the Paper Industry*, Institution of Engineers, Australia, Annual Conference, Hobart, April 1991, pp 191-195.

REARDON, S.A., *A Mathematical Model for the Drying of Paper*, 4th International Symposium on Transport Phenomena in Heat and Mass Transfer, Sydney, July 1991, pp 559-570.

REARDON, S.A., *Paper Industry Energy Usage*, International Mechanical Engineering Congress - Conference IV - Energy, Sydney, July 1991, pp 47-51.

REARDON, S.A., *Boundary Layer Development on Paper Drying Felts*, 11th Australasian Fluid Mechanics Conference, Hobart, December 1992, pp 833-836.

RHODIUS, D., *Über die Konvektions - und Mehrzylinder-trocknung von Papier im Hinblick auf die Trocknungsleistung*, Dissertation Universität Darmstadt, 1980. (original not seen)

RHYNE, M., *Modern Dryer Fabric Design and Application*, 1989 Practical Aspects of Pressing and Drying, pp 161-169.

RIDDIFORD, A.W., *Airflow Between a Paper Web and a Dryer Surface*, Tappi, Vol. 52, No. 5, 1969, p939.

ROBERTSON, A.A., Svensk Paperstidning, Vol. 66, No.12, June 1963, pp 477-497. (original not seen)

ROGERS, G.F.C. and MAYHEW, Y.R., *Thermodynamic and Transport Properties of Fluids - SI Units*, Basil Blackwell Ltd., 1989.

ROHSENOW, W.M. and CHOI, H., *Heat, Mass and Momentum Transfer*, Prentice-Hall, 1961, pp 414-419.

RUTHVEN, D.M., *Principles of Adsorption and Adsorption Processes*, John Wiley & Sons, 1984, Ch. 2.

SCALLAN, A.M., *The Accommodation of Water within Pulp Fibres*, Symposium on Fibre-Water Interactions in Paper-Making, Oxford, September 1977, The British Paper and Board Industry Federation, pp 9-27.

SCHETZ, J.A., *Foundations of boundary layer theory for momentum, heat and mass transfer*, Prentice-Hall, Englewood Cliffs, N.J, 1984.

SCHLICTING, H., *Boundary Layer Theory*, 6th ed., McGraw-Hill, New York, 1968.

SHISHIDO, I., SUZUKI, M. and OHTANI S., *Determination of the Diffusivity of Moisture within Wet Material*, Proceedings of the 1st International Drying Symposium, Montreal, August 1978, edited by A.S. Mujumdar, Science Press, pp 30-35.

SIAU, J.F., *Flow in Wood*, Syracuse University Press, New York, 1971.

SIAU, J.F., *Transport Processes in Wood*, Springer-Verlag, Berlin, 1984.

SINGULAR TECHNOLOGY CORPORATION, *Singular SC-Series Analog Input/Output Board User Manual*, 1989.

SKAAR, C., *Wood-Water Relations*, Springer-Verlag, 1988, Chapter 1-2.

SMITH, G.D., *Numerical Solution of Partial Differential Equations : Finite Difference Methods*, Oxford University Press, 1978, Chapter 2.

SMOOK, G.A., *Handbook for Pulp and Paper Technologists*, TAPPI and CPPA, 1988.

SNOW, R.H., *Computer Modelling of Drying in Paperboard Machines*, Proceedings of the Technical Association of the Pulp and Paper Industry, 1980 Annual Meeting, pp 243-257.

SOININEN, M. and NURMINEN, J., *An Orientation to the Pocket Ventilation Design in a Drying Section with Open Mesh Fabrics*, Paperi ja Puu, Vol. 4a, 1974.

SOININEN, M., *A Mathematical Model of the Contact Drying Process*, Drying '80, Volume 2 : Proceedings of the Second International

Symposium, Montreal, July 1980, edited by A.S. Mujumdar, Hemisphere Publishing Corporation, pp 315-321.

SOININEN, M., *The Physics of Paper Machine Sheet Flutter*, 1982 International Water Removal Symposium, pp 85-86.

SOININEN, M., HEIKKILÄ ,P., KARLSSON, M. and SARA R., *Computer Simulation of Web Drying in a Paper Machine Dryer*, 1985 Pulp and Paper Technology Conference, Tokyo, October 1985, pp 205-209.

STONE, J.E., SCALLAN, A.M. and ABERSON, G.M.A., *The Wall Density of Native Cellulose Fibres*, Pulp and Paper Magazine of Canada, May 1966, pp T263-T268.

STONE, J.E. and SCALLAN, A.M., *The Effect of Component Removal upon the Porous Structure Of the Cell Wall of Wood*, Pulp and Paper Magazine of Canada, June 1968, pp T288-T293.

SUTERMEISTER, E., *Chemistry of Pulp and Paper Making*, John Wiley & Sons, 1941, pp 24-35.

SZENTGYÖRGYI, S. and MOLNÁR, K., *Calculation of Drying Parameters for the Penetrating Evaporation Front*, Proceedings of the 1st International Drying Symposium, Montreal, August 1978, edited by A.S. Mujumdar, Science Press, pp 92-99.

TAKEDA, G. and YAKEBE, M., *Analysis of Drying Mechanism on Paper Machine*, 1981 Papermaking Conference, Tokyo, pp 183-192.

TIS 0404-04, *Recommended Tensions in Dryer Felts*, Tappi Technical Information Sheet, 1989.

TIS 0404-07, *Paper Machine Drying Rate*, Tappi Technical Information Sheet, 1989.

TIS 0404-15, *Paper Machine Drying Rate (Newsprint)*, Tappi Technical Information Sheet, 1986.

TIS 0404-17, *Recommended Minimum Dryer Pocket Air Requirements*, Tappi Technical Information Sheet, 1984.

VAN BRAKEL, J. and HEERTJES, P.M., *On Period of Constant Drying Rate*, Proceedings of the 1st International Drying Symposium, Montreal, August 1978, edited by A.S. Mujumdar, Science Press, pp 36-41.

VENNARD, J.K. and STREET, R.L., *Elementary Fluid Mechanics*, John Wiley and Sons, 1982, Chapter 2.

VON KARMAN, TH., *The Analogy between Fluid Friction and Heat Transfer*, Trans ASME, Vol. 61, 1939, pp 705-710.

WERLING, K., *Adiabatic Drying of Hygroscopic Materials*, Proceedings of the 1st International Drying Symposium, Montreal, August 1978, edited by A.S. Mujumdar, Science Press, pp 36-41.

WIEDENBECK, R.D., *Steam Heated Dryers*, Tappi Seminar Notes - 1989 Practical Aspects of Pressing and Drying, pp 173-181.

WINK, W,A, BOBB, F.C. and VAN DEN AKKER, J.A., *Equilibrium Moisture Content Determination at High Temperature*, Tappi Journal, Vol 41., No. 11, November 1958, pp 643-646.

YAMAUCHI, T. and KIBBLEWHITE, R.P., *Pore Structure of Paper Webs from Radiata Pine Thermomechanical Pulp*, Appita, Vol. 41, No. 1, January 1988, pp 37-42.a

YAMAUCHI, T. and KIBBLEWHITE, R.P., *Pore Structural Organisation and Behaviour During the Consolidation of TMP Paper Webs*, Appita, Vol. 41, No. 5, September 1988, pp 383-388.b

YAMAUCHI, T., MURAKAMI, K., and IMAMURA, R., *The Porous Structure of Paper, analytical research on the behaviour of mercury penetration and retraction*, Japan Tappi, Vol. 29, No. 9, 1975, pp 492-297. (in Japanese - original not seen)

YOUNG, B.W., *The Reformulation of BW Offset - Report 1*, Research Report No. 89-12, Australian Newsprint Mills Limited, August 1989, p17.

ZHUKAUSKAS, A., *Heat Transfer from Tubes in Cross Flow*, Advances in Heat Transfer, Vol. 8, Academic Press, New York, 1975.

APPENDIX 1 - Nomenclature

a	dimensionless parameter in beta distribution	-
b	dimensionless parameter in beta distribution	-
b_{wt}	sheet basis weight	kg/m^2
c_f	skin friction coefficient	-
cp_f	specific heat capacity of pulp fibres	J/kg°K
cp_w	specific heat capacity of liquid water	J/kg°K
cp_v	specific heat capacity of vapour	J/kg°K
C	specific heat capacity of paper sheet	J/kg°K
D_v	vapour diffusion coefficient	m^2/s
h_c	contact heat transfer coefficient	$W/m^2°K$
h_s	surface heat transfer coefficient	$W/m^2°K$
h_m	surface mass transfer coefficient	m/s
H_f	enthalpy of pulp fibre	J/kg
H_L	enthalpy of liquid water	J/kg
H_v	enthalpy of saturated water vapour	J/kg
k	thermal conductivity	W/m°K
k	roughness size	m
k^+	roughness parameter, ku^*/ν	-
k_c	Kozeny-Carman factor	-
L	sheet thickness	m
m_L	liquid mass flux through capillaries	kg/m^2s
m_v	vapour mass flux through porous region	$kg/m^2/s$
M	moisture content (dry basis)	kg_{water}/kg_{fibre}
M_{fs}	fibre saturation moisture content	kg_{water}/kg_{fibre}
N	number of pores per unit area	$1/m^2$
P_v	partial vapour pressure	Pa
P_c	capillary liquid pressure	Pa
P_{sat}	saturation vapour pressure	Pa
Q_s	differential heat of sorption	J/kg
Q	heat flux	W/m^2
r	normalised pore radius	-
R	pore radius	m
R_{max}	maximum pore radius	m
R_w	gas constant for water vapour	J/kg°K
S	fractional volumetric saturation of pores	-
S_v	specific volume	m^3/kg
S_A	specific surface area	m^2/kg

t	time	s
T	temperature	°K
T_c	steam-heated cylinder temperature	°K
T_{air}	dryer hood air temperature	°K
T_w	wall temperature	°K
T^*	heat transfer temperature	°K
T^+	dimensionless temperature	°K
u	local velocity	m/s
u^*	friction velocity	m/s
u^+	dimensionless velocity, u/u^*	-
U_∞	free stream velocity	m/s
U_{rms}	root mean square velocity	m/s
V	volumetric flow rate	m^3/s
x	streamwise coordinate	m
y	co-ordinate across thickness of sheet	m
y^+	dimensionless transverse coordinate, yu^*/ν	-
β	incomplete beta function	-
δ	boundary layer thickness	m
ε	porosity	-
ϕ	relative vapour pressure (humidity)	-
γ	contact angle	°
κ_L	liquid permeability	m^2
κ_v	vapour permeability	m^2
μ_L	liquid water viscosity	kg/ms
μ_v	water vapour viscosity	kg/ms
ν	kinematic viscosity	m^2/s
ρ_f	fibre density	kg/m^3
ρ_L	liquid water density	kg/m^3
ρ_v	vapour concentration	kg/m^3
σ	surface tension	N/m
τ_w	wall shear stress	Pa

APPENDIX 2 - Glossary

ANM - Australian Newsprint Mills Limited is a newsprint manufacturer with two mills in Australia. One is situated in Boyer, Tasmania, whilst the other is in Albury, New South Wales. The Boyer Mill is a sponsor of this study and the characteristics of its operations are the focus of much the theoretical and experimental work performed.

APPITA - Australian Pulp and Paper Industry Technical Association

Basis weight - Weight per unit area of paper

Break - Tear or rupture of the paper during manufacture. A break stops production until the paper sheet is re-established.

Caliper - Thickness of a paper sheet.

CCS - Cold caustic soda pulp is a grade manufactured by ANM, Boyer. The regrowth eucalypt chips are impregnated with caustic soda prior to mechanical refining.

Cellulose - A polymer composed of glucose monomers which is the main constituent of paper fibres.

CFM - cubic feet per minute of air passing through a square foot of dryer fabric under a pressure differential of ½" water gauge.

Consistency - weight percentage of pulp in a pulp and water mixture

CPPA - Canadian Pulp and Paper Association

CSF - Canadian Standard Freeness. This is the North American method of defining drainability, the resistance of fibres to the flow of water. CSF is the number of ml of water collected from the side orifice of the standard tester when pulp drains through a perforated plate at 0.30% consistency and 20°C.

Double-felted - Region of a dryer section where separate drying felts support the sheet along each of the top and bottom rows of cylinders.

Dryer fabric - An open mesh synthetic fabric which supports the paper sheet in the dryer section and ensures close contact between the sheet and hot drying cylinder. Also known as *dryer felt*.

Dryer felt - see *dryer fabric*.

Dryer hood - The enclosed region surrounding the drying cylinder run which prevents the mixing of ambient air from the machine room with conditioned air fed into the dryer region through the pocket ventilation system.

Free draw - Transfer of an unsupported sheet from one drying cylinder to the next (double-felted region only).

Furnish - The blend of pulps which compose the paper sheet, often referred to as stock.

Kraft - A chemical pulping process which cooks wood chips in a mixture of sodium hydroxide and sodium sulphide. The kraft process produces a very strong pulp at a yield of around 50-60%.

Nip - Line of contact between two rolls, such as press or calender rolls. The 'line' is actually a narrow band due to the compressibility of the web, felt and/or roll covers.

Open draw - see *free draw*.

PM2 / PM3 - Paper machines No 2 and 3 respectively at ANM's Boyer plant. These paper machines are the main focus of this study. The parameters used relate to these machines specifically, but adjustments can be made to reflect different geometries, grades or conditions on other machines.

Pocket ventilation (p.v.) - Conditioned drying air input to the dryer section between drying cylinders. The 'drying pocket' refers to the region enclosed by the paper sheet and the felt turning roll in a double-felted drying sub-section.

Porosity - Volumetric fraction of air voids in a paper sheet.

Runnability - The ability to produce paper without the incidence of sheet breaks. Good runnability is indicative of a strong paper sheet and is essential for high productivity.

Single-felted - Region of a dryer section where a single drying felt supports the paper sheet along both the top and bottom rows of cylinders. The felt (fabric) is in constant contact with the sheet within each sub-section.

SR - The Schopper-Riegler slowness test is the principal drainage measurement used in Europe. Has an inverse scale to CSF which is the measure of freeness.

SSC - Specific Steam Consumption is the quantity of drying steam required per unit of paper produced. SSC should refer to steam within the drying cylinders as well as steam used by the pocket ventilation system. It is usually expressed in terms of kg_{steam} per kg_{paper}.

TAPPI - Technical Association of the Pulp and Paper Industry (North America)

TMP - Thermo-Mechanical Pulp is a grade manufactured by ANM, Boyer. The radiata pine chips are impregnated with steam prior to mechanical refining.

Trim - Width of the paper sheet.

Web - An alternative term for the paper sheet which refers to the fibre matrix at any point in the papermaking process.

Wrap - The section of sheet travel in contact with the drying cylinders.

Yield - The fractional weight of pulp output from a pulping process per unit weight of wood input. Chemical pulping processes dissolve lignin, and some hemi-cellulose and cellulose and result in a yield of around 50-60%. Mechanical pulping processes have yields of around 95% where the losses are accounted for by the rejects from the screening stages.

APPENDIX 3 -
Paper Machine Configurations

The two ANM Boyer paper machines, PM2 and PM3, are considerably different both in terms of production capacity and dryer section configuration. Although both machines have undergone rebuilds since their initial construction, PM3 remains a wider, faster machine which produces about 25% more tonnage than PM2. The number 3 machine runs with 48 drying cylinders divided into five sub-groups whilst the PM2 dryer section consists of 44 drying cylinders and four control groups. Both machines employ both single and double-felted dryer sections.

The theoretical work developed in this study is of course relevant to both paper machines. Consequently it is necessary to make available the geometrical characteristics of both machine dryer sections to define the time-varying boundary conditions experienced by the paper sheet. With regard to this thesis, PM3 calculations are performed in Chapter 12 for comparison with moisture content measurements taken from the machine dryer section. Calculations on PM2 are carried out at the end of Chapter 12 for a proposed change in configuration of the early drying cylinders and a 'before and after' situation is presented.

Typical operating conditions for both machines are presented in Table A3.1. It should be noted that both machines produce a range of paper grades over a wide range of speeds with varying pulp furnish. The figures detailed in the table are chosen to represent production of 48.8 g/m^2 newsprint at a sustainable operating speed.

In this context "typical" describes observed machine operating conditions on occasions the machine was running at its nominal operating speed. Those who are familiar with the papermaking industry will understand that the production speed is more frequently driven by *runability*, the ability of the sheet to run at as specified speed without breaking, rather than drying limitations. Hence, the nominal speeds selected of 880 m/min for PM2 and 1050 m/min for PM3, represented the highest reliably achievable machine speeds towards the end of 1992. Drying conditions and steam usage of the machines at these speeds were recorded at this time and used in model calculations.

TABLE A3.1
Operating parameters for both PM2 and PM3

Parameter	Units	PM2	PM3
basis weight	g/m2	48.8	48.8
speed	m/min	880	1050
machine width	m	5.9	6.6
reel moisture	% (w.b.)	8.9	8.9
sheet caliper (reel)	µm	80	80
main steam	t/hr	29	30
aux. steam	t/hr	not applicable	10.8
header pressure	kPa	210	350
header temperature	°C	150	160
dry end flow pressure condensate flow	t/hr kPa	96	6.3 120
main flow pressure condensate flow	t/hr kPa	113	9.5 130
intermediate flow pressure condensate flow	t/hr kPa	91	3.8 97
wet end flow pressure condensate flow	t/hr kPa	67	0 65
initial flow pressure condensate flow	t/hr kPa	49	0 0
p.v. air temperature absolute humidity	°C kg/kg	-	100 0.01
exhaust temperature relative humidity	°C %	-	65 40
hood air temp. relative humidity	°C %	-	85 35

Note that the final three quantities, p.v. air temperature and humidity, exhaust temperature and humidity, and hood air temperature and humidity, do vary throughout the dryer hood. Typical mean values are shown in Table A3.1. Some machine operating conditions logged whilst obtaining moisture content samples from PM3 are presented in Appendix 4. PM2 values are not measured on the machine.

In Table A3.1 the terms "dry end flow", "main flow" etc refer to the live steam flow into the nominated dryer sub-section. The corresponding parameter "pressure" is the steam pressure, after throttling, into the drying cylinders. The "condensate flow" is the total steam consumed by the particular dryer sub-section and will be considerably different to the fresh steam input. The relationship between the two is,

$$\text{condensate} = \text{live steam} + \text{cascade steam} - \text{blowthrough}, \quad \text{(A3.1)}$$

where the term blowthrough refers to steam which passes through the drying cylinder without condensing. This additional steam is required to help evacuate the condensate from the drying cylinder through the syphon. It is the blowthrough steam from the main and dry end sub-sections which passes to the wet and intermediate sections as cascade steam. The separation of dryer sections into control sub-groups is defined for each paper machine in Table A3.2.

TABLE A3.2
Dryer section sub-groups

Sub-group	PM2 cylinders	PM3 cylinders
initial	2,4,6	3,5
wet end	5,7,8,9,10,11,12,13	7,9,11,13,14,16
intermediate	14-24	15,17-23
main	25-44	24-38
dry end		39-48

The boundary conditions for the dryer simulation are defined by the alternate cylinder wrap and open draw. As discussed in Chapter 3 it was decided to restrict the boundary condition variation to a two zone per cylinder representation rather than the four zone version suggested by

Nissan and Kaye (1955). The disparity lies in the recognition of the short region of the double-felted run where the paper sheet wraps the drying cylinder but its open surface is not in contact with the felt. As PM2 has 44 drying cylinders the lengths of 88 zones must be defined. Similarly PM3's dryer section requires 96 zones to be specified. These data are presented in Table A3.3. The geometry of the dryer section is repetitive with the deviations from this pattern occurring at the transition between separate drive sections. The drive sub-sections are generally similar but not necessarily identical to the control sub-sections which govern steam pressure into a given group of cylinders.

TABLE A3.3
Boundary condition variation for both PM2 and PM3

Cylinder No.	PM2 wrap	PM2 open draw	PM3 wrap	PM3 open draw
1	2.998	1.175	2.968	1.159
2	2.998	1.175	2.968	1.159
3	2.998	1.175	2.968	1.159
4	2.725	1.615	2.968	1.159
5	2.725	1.175	2.920	1.228
6	2.998	1.175	2.920	1.159
7	2.998	1.175	2.968	1.159
8	2.998	1.175	2.968	1.159
9	2.998	1.175	2.968	1.159
10	2.998	1.175	2.968	1.159
11	2.998	1.175	2.968	1.159
12	2.725	1.615	2.968	1.159
13	2.725	1.175	2.968	1.159
14	2.998	1.175	2.968	1.159
15	2.998	1.175	2.968	1.159
16	2.725	1.615	2.968	1.159
17	2.725	1.175	2.968	1.159
18	2.998	1.175	2.968	1.159
19	2.998	1.175	2.968	1.159
20	2.998	1.175	2.968	1.159

Cylinder No.	PM2 wrap	PM2 open draw	PM3 wrap	PM3 open draw
21	2.998	1.175	2.968	1.159
22	2.998	1.175	2.968	1.159
23	2.998	1.175	2.920	1.228
24	2.725	1.615	2.920	1.159
25	2.725	1.175	2.968	1.159
26	2.998	1.175	2.968	1.159
27	2.998	1.175	2.968	1.159
28	2.998	1.175	2.968	1.159
29	2.998	1.175	2.968	1.159
30	2.998	1.175	2.968	1.159
31	2.998	1.175	2.968	1.159
32	2.998	1.175	2.968	1.159
33	2.998	1.175	2.968	1.159
34	2.998	1.175	2.968	1.159
35	2.998	1.175	2.968	1.159
36	2.998	1.175	2.968	1.159
37	2.998	1.175	2.968	1.159
38	2.998	1.175	1.933	5.226
39	2.998	1.175	1.933	1.159
40	2.998	1.175	2.968	1.159
41	2.998	1.175	2.968	1.159
42	2.998	1.175	2.968	1.159
43	2.998	1.175	2.968	1.159
44	2.998	1.175	2.968	1.159
45			2.968	1.159
46			2.968	1.159
47			2.968	1.159
48			2.968	1.159

Note that all dimensions are expressed in metres.

Dryers 1-12 of each paper machine are single-felted whilst the remainder are double-felted. The distinction between the two regimes is depicted in Figures A3.1 and A3.2.

Single-felted dryers provide support for the sheet at all times during drying. This enables the sheet to be run at higher speeds with less breaks. The disadvantage of single-felted dryers is that only half of the drying cylinders provide heating due to the insulating effect of the felt. For this reason the lower cylinders are not heated with steam. As the sheet dries and its strength increases it is possible to move to double-felted sub-sections where the sheet is unsupported in the open draw but higher drying rates are possible due to cylinder contact from both sides of the sheet.

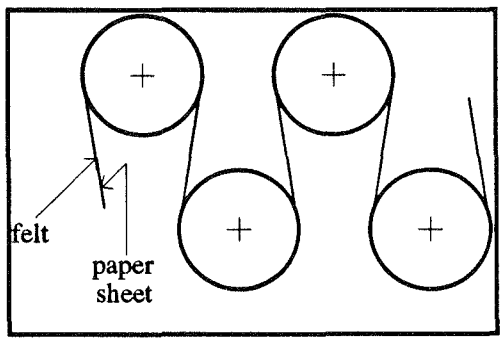

FIGURE A3.1
Single-felted dryers

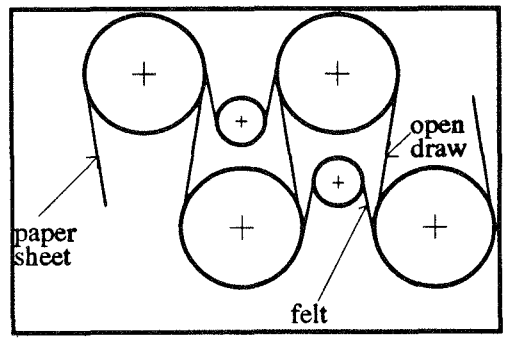

FIGURE A3.2
Double-felted dryers

APPENDIX 4 -
ANM Moisture Content Samples

During the period from 1990-1992 a number of paper samples were taken from ANM's PM3 machine to assist with assessing the applicability of the mathematical model. The paper machine does not have moisture monitoring equipment either before or in the dryer section and hence a physical sample must be grabbed to determine paper sheet moisture content. As described in Chapter 12 there were some difficulties with obtaining these samples. These stemmed primarily from the fact that the sheet had to be broken to obtain a sample. Paper machine productivity relies on sheet continuity as sheet breaks can take anywhere from 5 minutes to 1 hour to recover from.

Obtaining paper sheet samples within the dryer section is limited from two perspectives. As alluded to above, samples can not be obtained upon demand but rather in the lead up to a planned machine maintenance shutdown. This gives rise to a five weekly sheet sample at best. Many operational occurrences can combine to render an attempted sample grab ineffective.

The second limitation arises from the operating environment of the paper machine dryer section. The enclosed region is at temperatures of 80°C near the centre and the paper sheet together with all rotating machinery runs at 17-18 m/s. The tail threading ropes on one side of the machine and the hot gear cases on the other side combine to make access to the paper sheet awkward. Fortunately, there is one clear region 80% of the way through the 200m drying section run which was previously used as a breaker stack for preliminary paper sheet calendering. Samples were able to be obtained safely and consistently from this access point.

The table presented on the following pages lists the key paper machine operating parameters at the time each moisture sample was taken from PM3. Occasions where the moisture content is not listed are indicative that the sample grab was unsuccessful. Generally this was due to the paper machine running out of stock, in a bid to empty the feed chests prior to maintenance, or the paper sheet being broken elsewhere by chance or another testing officer.

Moisture Samples from PM3

Date	26/9/1990	18/2/91	27/2/91	22/5/91	1/92	17/3/92	15/4/92
Basis Weight (g/m^2)	49.1	45	45.0	48.8	45.8	46.0	48.3
Speed (m/min)	1015	1045	1060	1050	1065	999	1041
Reel Moisture %	8.9	8.9	8.9	8.9	8.9	8.9	8.9
Caliper ($10^{-6}m$)	71.7	71.7	76.2		70	70.9	91
Main Steam (t/hr)	35	32.7	36	35	30	27	27
Aux. Steam (t/hr)		10	10.8		10.7	10.7	
Supply Pressure (kPa)	350		358		360	350	367
Temperature (^oC)	160		160		167.5	166	160.3
Dry Flow (t/hr)	5.7	5.7	5.1	6.3	6.36	5.4	6.33
Pressure (kPa)		107	105	100		92	
Main Flow (t/hr)	9.3	9.4	9.6	9.0	9.0	8.5	8.6
Pressure (kPa)		125	118	113		106	
Intermed Flow (t/hr)	3.8	5.1	4.5	4.2	3.65	3.2	4.3
Pressure (kPa)		94	85	80		73	
Wet Flow (t/hr)	0	0	0	0	0	0	0
Pressure (kPa)		60	53	45		58	45
#5 Pressure (kPa)			15	14			
#3 Pressure (kPa)				6			
Moisture Content (%)		-		34.3 (wb)	-	22.3	-
	30.5		17.7	28.2		16.7	

Moisture Samples from PM3 (continued)

Date	13/5/92	20/5/92	24/6/92	12/8/92	9/9/92	7/10/92	13/11/92
Basis Weight (g/m^2)	46.4	45.0	48.0	45.0	45.0	47.6	48.3
Speed (m/min)	1003	981	1030	1060	1040	1015	1100
Reel Moisture %	9.0	8.9	8.9	8.9	8.9	9.1	8.8
Caliper ($10^{-6}m$)	86.2	74.0	79.8	77.0	75.0	80.8	88
Main Steam (t/hr)	27.5	23	29.5	27.7	25.5	29.5	29
Aux. Steam (t/hr)	10.5	10.8	10.8	10.7	10.8	10.8	10.8
Supply Pressure (kPa)	350		350	350	350	350	
Temperature (^oC)	161		155	160	160	160	
Dry Flow (t/hr)	5.1	4.0	6.3	5.0	5.6	5.7	6.4
Pressure (kPa)	97		116	101	88	88	110
Main Flow (t/hr)	8.3	8.2	9.5	9.0	8.7	8.9	9.8
Pressure (kPa)	109		132	115	98	99	121
Intermed Flow (t/hr)	3.8	3.8	3.8	2.0	1.8	2.9	4.0
Pressure (kPa)	76		97	81	65	67	87
Wet Flow (t/hr)	0	0	0	0	0	0	0
Pressure (kPa)	44		65	50	35	36	60
#5 Pressure (kPa)	12			3.5	-1.2	0.2	1.7
#3 Pressure (kPa)				-15	-16.2	-16	-22
Moisture Content (%)	23.7(wb) 21.8	22.3(x2) (wb)	26.3(Me wb) 22.2(Me wb)	21.7(x2) (wb)	22.8(Me wb) 24.0(Me wb)	21.7(wb) 21.5(wb)	-

The following miscellaneous parameters relating to the drying section were also noted on a number of occasions :

- Wet end make up air input at 80°C and pocket ventilation air at 100°C
- 20/5/92 : 8.9% moisture average - 10.6% max (centre), 5.6% min (edges)
- 24/6/92 : 8.9% moisture average - 9.9% max (centre), 7.8% min (edges)
- 24/6/92 : hood exhaust 65°C and 40%
- Vacuum receiver : 50°C.
- Machine sheet trim : 6.66m
- Fan currents : Make up - 40A, PV1 - 120A, PV2 - 130A, Exhaust1 - 20A, Exhaust2 - 20A, Exhaust3 - 20A, Exhaust4 - 15A
- 12/8/92 : South PV - 110°C, North PV - 83°C
- 9/9/92 : South PV - 107°C, North PV - 98°C, Make up - 73°C.
- 9/9/92 : Exh1 : 61.4°C and 46%, Exh2 : 69.3°C, Exh3 : 72.0°C and 40% rh
- 7/10/92 : steam cylinder differential pressures : dry-27kPa, main-38kPa, int-28kPa, wet-30kPa, #5-30kPa

APPENDIX 5 -
Finite Difference Expansion

The intention of this Appendix is to provide the full expansions for the defining mass and energy equations, 3.22 and 3.25, using only the primary variables moisture content, M, temperature, T, and vapour pressure, P_v. The third of the simultaneous equations required for solution is a relation between the local vapour pressure and slice temperature.

The three equations are converted into finite difference form, organised into a matrix system and solved by LU decomposition followed by back substitution using subroutines presented by Press et al (1986). LU decomposition refers to the following expression for a matrix, A,

$$A = L\,U, \tag{A5.1}$$

where L is a lower triangular matrix and U is upper triangular. Having obtained L and U for a given matrix A the solution of,

$$A\,\mathbf{x} = \mathbf{b}, \tag{A5.2}$$

is trivially obtained using back substitution.

Mass and energy equation expansion

Recalling from Chapter 3 the differential equation (3.22) defining mass transfers within the paper sheet,

$$\frac{\partial M}{\partial t} = \frac{\rho_L \kappa_L}{\mu_L}\frac{\partial^2 P_L}{\partial y^2}\delta y + D_v\frac{\partial^2 \rho_v}{\partial y^2}\delta y \left(+ \frac{\rho_v \kappa_v}{\mu_v}\frac{\partial^2 P_v}{\partial y^2}\delta y \right). \tag{A5.3}$$

The corresponding energy differential equation (3.25) is,

$$\frac{\partial CT}{\partial t} = k\frac{\partial^2 T}{\partial y^2} + \frac{\rho_L \kappa_L}{\mu_L}H_L\frac{\partial^2 P_L}{\partial y^2} + D_v(H_v + Q_s)\frac{\partial^2 \rho_v}{\partial y^2}$$

$$\left(+ \frac{\rho_v \kappa_v}{\mu_v} (H_v + Q_s) \frac{\partial^2 P_v}{\partial y^2} \right), \qquad \text{(A5.4)}$$

where the all symbols are as defined in Chapter 3.

There a number of terms in the above two equations which require further expansion so that a solution can be implemented, namely, liquid capillary pressure, P_L, vapour density, ρ_v, and vapour pressure, P_v.

The *liquid capillary pressure,* P_L, can be expressed in terms of the moisture content, M, by virtue of the chain of relationships :

$$P_L = f_1(r), \quad r = f_2(S), \quad S = f_3(M). \qquad \text{(A5.5)}$$

Capillary pressure and pore radius are related by equation 6.1,

$$P_L = -\frac{2\sigma \mathrm{Cos}\gamma}{r R_{max}}. \qquad \text{(A5.6)}$$

Pore radius is a rather more complicated function of the fractional saturation, S. This is defined according to the pore size distribution theory developed in Chapter 3, making use of the incomplete beta function :

$$\beta(r\,;\, a+2,\, b) = S. \qquad \text{(A5.7)}$$

To simplify finite difference implementation and prevent time-consuming repetitive calculations equation A5.6 is approximated by a piecewise linear representation. This is achieved by pre-calculating r for a number of S values over the range from 0 to 1, and forming the results into a look-up table. Intermediate values of r can be obtained by interpolating linearly between the two boundary values,

$$r = c_k S + d_k, \qquad \text{(A5.8)}$$

where c_k and d_k are the relevant linear interpolation coefficients for $S_k<S<S_{k+1}$.

Moisture content is directly proportional to the fractional saturation, S. Given an initial moisture at the start of drying of M_{init} and S_{init} respectively,

$$S = \frac{S_{init}}{M_{init}} M. \tag{A5.9}$$

Combining equations A5.6, A5.8 and A5.9 leads to the following relationship between capillary pressure, P_L, and moisture content, M,

$$P_L = \frac{-2\sigma \, Cos\gamma}{R_{max}\left(c_k \frac{S_{init}}{M_{init}} M + d_k\right)}. \tag{A5.10}$$

The second derivative of this term with respect to the transverse dimension, y, is then given by :

$$\frac{\partial^2 P_L}{\partial y^2} = \frac{-2\sigma}{R_{max}} \frac{c_k}{M_{init} r^2} \left\{ \frac{2c}{M_{init} r} \left(\frac{\partial M}{\partial y} \right)^2 - \frac{\partial^2 M}{\partial y^2} \right\}, \tag{A5.11}$$

where the contact angle, γ, is taken to be zero, and dimensionless radius, r, may be expanded to,

$$r = c_k \frac{M}{M_{init}} + d_k. \tag{A5.12}$$

The next term in equation A5.3 which requires expanding is the *vapour density*, ρ_v. This is assumed to follow the ideal gas law, an assumption which can be shown to be quite reasonable for water vapour :

$$\rho_v = \frac{P_v}{R_v T}, \tag{A5.13}$$

where R_v is the gas constant for water vapour (462 J/kg°C).

Again it is the second derivative of the density which is required for the mass balance differential equation :

$$\frac{\partial^2 \rho_v}{\partial y^2} = \frac{D_v dy}{R_v}\left\{\frac{1}{T}\frac{\partial^2 P_v}{\partial y^2} - \frac{2}{T}\frac{\partial T}{\partial y}\frac{\partial P_v}{\partial y} - \frac{2P_v}{T^3}\left(\frac{\partial T}{\partial y}\right)^2 - \frac{P_v}{T^2}\frac{\partial^2 T}{\partial y^2}\right\}, \tag{A5.14}$$

where *dy* is the thickness of the incremental paper slice.

Since the *water vapour pressure,* P_v, is a non-linear function of temperature and the mass-energy equations are already quite complex it was decided to introduce this as a third simultaneous equation rather than an expansion of the existing two. To fit within the framework of the linear differential equation matrix system it is necessary to express the vapour pressure as a piecewise linear function of temperature in a similar fashion to the pore radius - fractional saturation relationship of equation A5.8, i.e.,

$$P_{v\,sat} = a_k T + b_k, \tag{A5.15}$$

where a_k and b_k are the relevant linear interpolation coefficients for $T_k < T < T_{k+1}$.

Now due to the hygroscopicity of paper the local vapour pressure is the product of the saturated water vapour at the given temperature with the sorption isotherm relative humidity for the existing moisture content. Hence the third simultaneous equation becomes,

$$P_v = \phi(M,T)\,(a_k T + b_k), \tag{A5.16}$$

where $\phi(M,T)$ is the sorption isotherm function for paper and is discussed in Chapter 9.

Finite difference implementation

As it is clearly not possible to solve the defining equations analytically it is necessary to engage a numerical method. The finite difference method divides the paper sheet into a number of equal slices and converts the problem from a continuous one to a discrete one. The solution is in the form of values for moisture content, temperature and vapour pressure at a finite number of locations across the paper web.

As mentioned in Chapter 3 a fully implicit method is used in conjunction with central differencing. In the following equations the subscipt i denotes position in the y direction and the subscript j denotes the time variable. If there is no i subscript quoted then the i^{th} position is assumed. Similarly, the default value of the j subscript is the $j+1^{th}$ time.

The finite difference expansion for the mass balance equation is shown below, in two stages :

$$\frac{M_{i,j+1} - M_{i,j}}{\delta t} =$$

$$\frac{\rho_L \kappa_L}{\mu_L} \frac{2\sigma}{R_{max}} \frac{c\delta y}{M_{init} r^2} \left\{ \frac{M_{i+1} - 2M_i + M_{i-1}}{\delta y^2} - \frac{c}{2r M_{init}} \left(\frac{M_{i+1} - M_{i-1}}{\delta y} \right)^2 \right\} +$$

$$\frac{D_v \delta y}{R_v T} \left\{ \frac{Pv_{i+1} - 2Pv_i + Pv_{i-1}}{\delta y^2} - \frac{1}{T} \frac{(T_{i+1} - T_{i-1})(Pv_{i+1} - Pv_{i-1})}{2\delta y^2} \right\} +$$

$$\frac{D_v \delta y}{R_v T} \left\{ -\frac{Pv}{T} \frac{T_{i+1} - 2T_i + T_{i-1}}{\delta y^2} - \frac{Pv}{T^2} \frac{(T_{i+1} - T_{i-1})^2}{2\delta y^2} \right\} +$$

$$\frac{\kappa_v \delta y}{R_v \mu_v T} \left\{ Pv \frac{Pv_{i+1} - 2Pv_i + Pv_{i-1}}{\delta y^2} + \frac{(Pv_{i+1} - Pv_{i-1})^2}{4\delta y^2} \right\} +$$

$$\frac{\kappa_v \delta y}{R_v \mu_v T} \left\{ -\frac{Pv}{T} \frac{(Pv_{i+1} - Pv_{i-1})(T_{i+1} - T_{i-1})}{4\delta y^2} \right\} \qquad \text{(A5.17)}$$

Collecting up the coefficients of each of the M, T, P_v terms produces the final version required for implementation :

$$\left\{ M_{i-1} \left[-b_{wt} \frac{\rho_L \kappa_L}{\mu_L} \frac{2\sigma}{R_{max}} \frac{c}{M_{init} r^2} \left\{ 1 + \frac{c}{2r M_{init}} (M_{i+1,j} - M_{i-1,j}) \right\} \right] +$$

$$M_i\left[2\,b_{wt}\frac{\rho_L\kappa_L}{\mu_L}\frac{2\sigma}{R_{max}}\frac{c}{M_{init}r^2}+b_{wt}\frac{\delta y}{\delta t}\right]+$$

$$M_{i+1}\left[-b_{wt}\frac{\rho_L\kappa_L}{\mu_L}\frac{2\sigma}{R_{max}}\frac{c}{M_{init}r^2}\left\{1-\frac{c}{2r\,M_{init}}\left(M_{i+1,j}-M_{i-1,j}\right)\right\}\right]+$$

$$T_{i-1}\left[\frac{\kappa_v}{R_v\mu_v T^2}\left\{-Pv\frac{Pv_{i+1,j}-Pv_{i-1,j}}{4}\right\}\right.$$

$$\left.+\frac{D_v}{R_v T^2}\left\{-\frac{Pv_{i+1,j}-Pv_{i-1,j}}{2}-\frac{Pv}{T}\frac{T_{i+1,j}-T_{i-1,j}}{2}+Pv\right\}\right]+$$

$$T_i\left[\frac{D_v}{R_v T^2}\{-2Pv\}\right]+$$

$$T_{i+1}\left[\frac{\kappa_v}{R_v\mu_v T^2}\left\{Pv\frac{Pv_{i+1,j}-Pv_{i-1,j}}{4}\right\}\right.$$

$$\left.+\frac{D_v}{R_v T^2}\left\{\frac{Pv_{i+1,j}-Pv_{i-1,j}}{2}+\frac{Pv}{T}\frac{T_{i+1,j}-T_{i-1,j}}{2}+Pv\right\}\right]+$$

$$Pv_{i-1}\left[\frac{\kappa_v}{R_v\mu_v T}\left\{-Pv+\frac{Pv_{i+1,j}-Pv_{i-1,j}}{4}\right\}+\frac{D_v}{R_v T}\{-1\}\right]+$$

$$Pv_i\left[\frac{\kappa_v}{R_v\mu_v T}\{2Pv\}+\frac{D_v}{R_v T}\{2\}\right]+$$

$$Pv_{i+1}\left[\frac{\kappa_v}{R_v\mu_v T}\left\{-Pv-\frac{Pv_{i+1,j}-Pv_{i-1,j}}{4}\right\}+\frac{D_v}{R_v T}\{-1\}\right]\frac{\delta t}{\delta y}$$

$$=b_{wt}M_{i,j} \qquad \text{(A5.18)}$$

The expansion of the energy equation follows a similar pattern to the mass equation expansion presented above (A5.18). The major difference is the addition of the Fourier term to describe heat conduction. The final finite difference form of the energy equation is presented below :

$$\left\{M_{i-1}\left[-b_{wt}\frac{\rho_L\kappa_L}{\mu_L}\frac{2\sigma}{R_{max}}\frac{c}{M_{init}r^2}\left\{1+\frac{c}{2rM_{init}}(M_{i+1,j}-M_{i-1,j})\right\}H_L\right]+\right.$$

$$M_i\left[2b_{wt}\frac{\rho_L\kappa_L}{\mu_L}\frac{2\sigma}{R_{max}}\frac{c}{M_{init}r^2}H_L+\varepsilon\rho_L c_L T_{i,j}b_{wt}\frac{S_{init}}{M_{init}}\frac{\delta y^2}{\delta t}\right]+$$

$$M_{i+1}\left[-b_{wt}\frac{\rho_L\kappa_L}{\mu_L}\frac{2\sigma}{R_{max}}\frac{c}{M_{init}r^2}\left\{1-\frac{c}{2rM_{init}}(M_{i+1,j}-M_{i-1,j})\right\}H_L\right]+$$

$$T_{i-1}\left[-k+\frac{\kappa_v}{R_v\mu_v T^2}(H_v+Q_s)\left\{-Pv\frac{Pv_{i+1,j}-Pv_{i-1,j}}{4}\right\}\right.$$

$$\left.+\frac{D_v}{R_vT^2}(H_v+Q_s)\left\{-\frac{Pv_{i+1,j}-Pv_{i-1,j}}{2}-\frac{Pv}{T}\frac{T_{i+1,j}-T_{i-1,j}}{2}+Pv\right\}\right]+$$

$$T_i\left[\sum\varepsilon\rho c_p\frac{\delta y^2}{\delta t}+2k+\frac{D_v}{R_vT^2}(H_v+Q_s)\{-2Pv\}\right]+$$

$$T_{i+1}\left[-K+\frac{\kappa_v}{R_v\mu_v T^2}(H_v+Q_s)\left\{Pv\frac{Pv_{i+1,j}-Pv_{i-1,j}}{4}\right\}\right.$$

$$\left.+\frac{D_v}{R_vT^2}(H_v+Q_s)\left\{\frac{Pv_{i+1,j}-Pv_{i-1,j}}{2}+\frac{Pv}{T}\frac{T_{i+1,j}-T_{i-1,j}}{2}+Pv\right\}\right]+$$

$$Pv_{i-1}\left[\frac{\kappa_v}{R_v\mu_v T}(H_v+Q_s)\left\{-Pv+\frac{Pv_{i+1,j}-Pv_{i-1,j}}{4}\right\}+\frac{D_v}{R_vT}(H_v+Q_s)\{-1\}\right]+$$

$$Pv_i\left[\frac{\kappa_v}{R_v\mu_v T}(H_v+Q_s)\{2Pv\}+\frac{D_v}{R_vT}(H_v+Q_s)\{2\}\right]+$$

$$Pv_{i+1}\left[\frac{\kappa_v}{R_v\mu_v T}(H_v+Q_s)\left\{-Pv-\frac{Pv_{i+1,j}-Pv_{i-1,j}}{4}\right\}+\frac{D_v}{R_v T}(H_v+Q_s)\{-1\}\right]\frac{\delta t}{\delta y^2}$$

$$=\sum\varepsilon\rho c_p T_{i,j}+\varepsilon\rho_L c_L T_{i,j}\frac{S_{init}}{M_{init}}b_{wt}M_{i,j}. \qquad \text{(A5.19)}$$

The bulk flow terms which appear in parenthesis in equations A5.3 and A5.4 are controlled by a binary mask, the value of which varies depending upon the local temperature. For temperatures below 100°C the the multiplying mask is set to zero, whilst for larger temperatures the total pressure will exceed atmospheric and the bulk flow mechanism is activated by setting the mask to unity.

Boundary conditions

The boundary equations which describe mass and energy transfers across the exterior surfaces of the paper sheet must also be represented by finite differences. Beginning with the side of the sheet in contact with the heated drying surface, denoting this interface with the subscript $_0$, and making use of equations 3.26-3.29 the boundary conditions are :

$$T_{-1}=T_1+\frac{2h_c\delta y}{k}(T_c-T_0), \qquad \text{(A5.20)}$$

$$Pv_{-1}=Pv_1\frac{T_{-1}}{T_1}, \qquad \text{(A5.21)}$$

$$M_{-1}=M_1, \qquad \text{(A5.22)}$$

and,

$$Ptot_{-1}=Ptot_1. \qquad \text{(A5.23)}$$

The boundary conditions on the side of the sheet exposed to the ventilating air are derived from equations 3.30-3.33. The subscript $_n$ represents the outer surface where there are n slices through the sheet.

$$T_{n+1}=T_{n-1}-\frac{2h_s\delta y}{k}(T_n-T_{db}), \qquad \text{(A5.24)}$$

$$Pv_{n+1} = \left\{ \frac{Pv_{n-1}}{T_{n-1}} - \frac{2 h_m \delta y}{D_v} \left(\frac{Pv_n}{T_n} - \frac{P_{pock}}{T_{db}} \right) \right\} T_{n+1}, \qquad \text{(A5.25)}$$

$$M_{n+1} = \frac{\left(\frac{c}{2} M_{n-1} + 2d M_{init}\right) M_n + \left(\frac{c}{2} M_n - d M_{init}\right) M_{n-1}}{2c M_{n-1} - c M_n + d M_{init}}, \qquad \text{(A5.26)}$$

and,

$$Ptot_{n+1} = 2 Ptot_n - Ptot_{n-1}. \qquad \text{(A5.27)}$$

APPENDIX 6 -
Z Direction Profiles

The issue of moisture content and temperature profiles across the paper sheet, in the Z direction, has not been dealt with extensively in the thesis proper despite the clear ability of the mathematical model to calculate these data. This is for two key reasons :

1. As stated (p42) there is "very little variation in moisture content and temperature across the web", and consequently there are no significantly interesting results to emerge from an extended examination of these data.
2. The intent of this joint venture industry study has been to generate results which can be correlated against actual paper machine performance to add value to the existing process through, 1) increased production speeds, 2) improved drying energy efficiency, and/or 3) better controllability leading to a more uniform paper product. Therefore reduced effort has been invested in the analysis of more esoteric issues arising from the study.

An important distinction needs to be drawn between the context of this study and others which have preoccupied themselves with Z direction moisture and temperature profiles. The paper sheet under study has been 49 g/m^2, 80μm newsprint. This is clearly an order of magnitude different in terms of bulk to the 600 g/m^2 paperboard investigated by Lee and Hinds (1980), and the 457 g/m^2 paperboard studied by Ramaswamy (1990), both of whom devote some effort to the analysis of cross-directional profiles.

This Appendix is included for completeness and presents two graphs which verify that the variation of moisture content and temperature across the very thin paper sheet is indeed limited. The two curves in Figure A6.1 represent the fractional variation of sheet moisture content from the centre of the sheet to each surface, at successive time intervals for ANM PM3. Although drying is bilateral, the terms "underside" and "topside" are used to distinguish the two sheet surfaces. The lack of symmetry is a result of the single-felted dryer section where only the underside of the sheet is exposed to the hot cylinder surfaces. This leads to the underside being generally drier in this region, as the topside is shielded by the thick dryer fabric at all times.

Figure A6.2 is a similar graph to describe temperature fluctuations within the sheet. Again the absence of symmetry is a result of the single-felted dryer section for cylinders 1-13. This leads to the underside being generally hotter in this region, as the topside is continuously insulated by the thick dryer fabric.

Whilst the trends are of interest, the magnitude of variation is seen to be minimal. The maximum excursions of surface values from those of the sheet centre are listed in Table A6.1.

TABLE A6.1
Extremes of internal sheet moisture content and temperature fluctuations for PM3

	Moisture variation	Temperature variation
Underside minimum	-0.375 %	-0.275 %
Underside maximum	0.049 %	0.435 %
Topside minimum	-0.374 %	-0.263 %
Topside maximum	0.122 %	0.330 %

It is undisputed that z-direction profiles are a vital source of insight in assessing the drying of paperboard sheets. However, with newsprint the variations of both temperature and moisture content are limited to extremes of ±0.5%, and are therefore not worthy of extensive review.

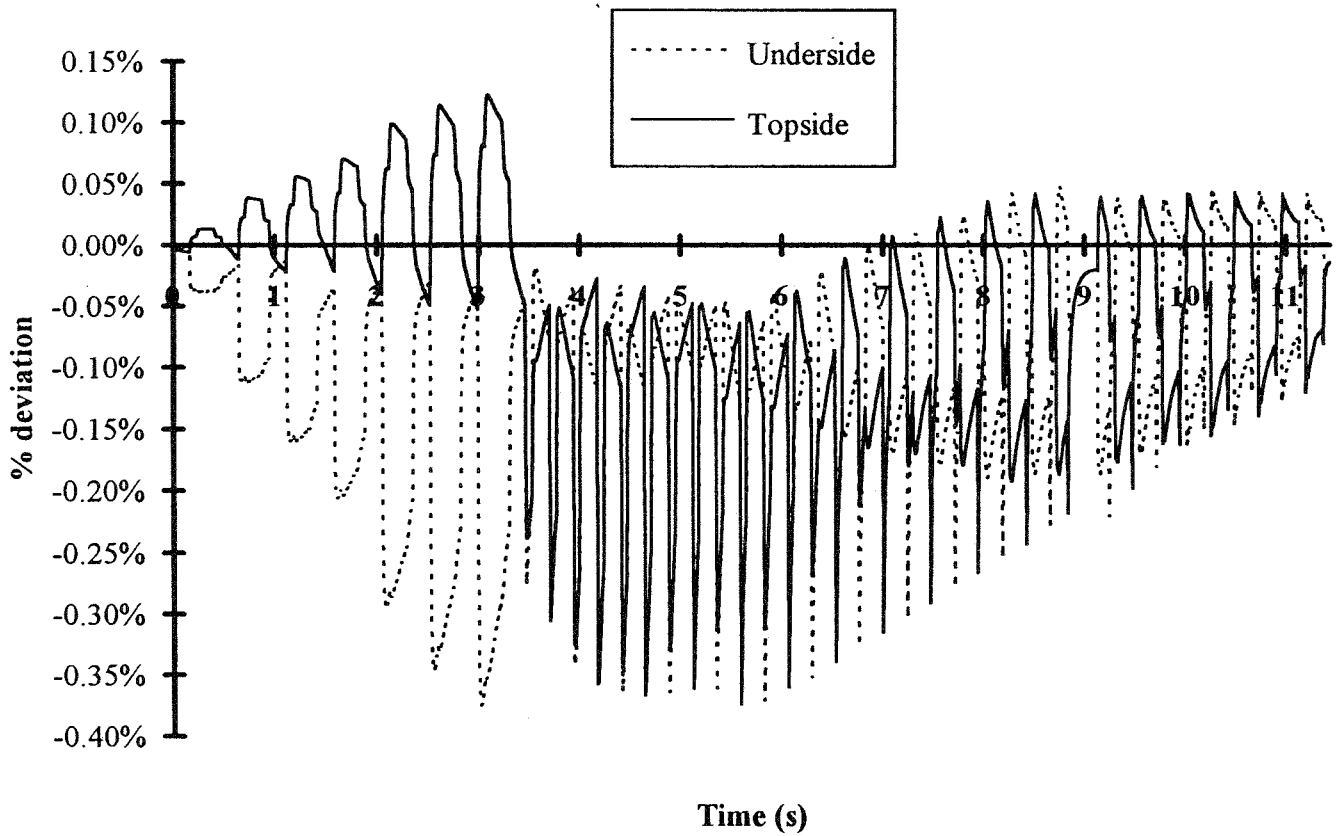

FIGURE A6.1
Z Direction Moisture Content Variation - % Deviation from Centre to Surface

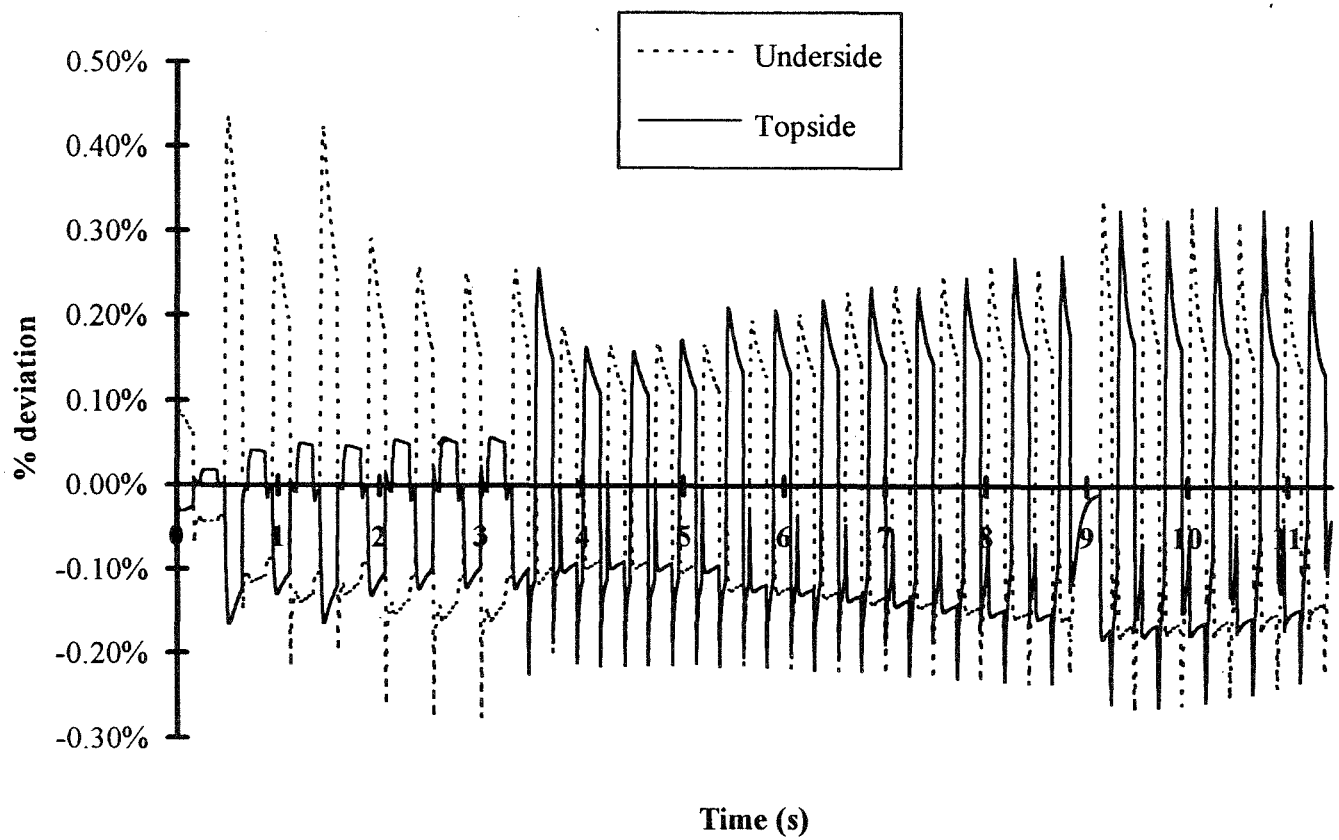

FIGURE A6.2
Z Direction Temperature Variation - % Deviation from Centre to Surface

APPENDIX 7 -
Listing of Drying Program

The drying program is written in Turbo Pascal, Version 6.0, and the source code is presented in the following pages. The main routines are included in *Drying.pas* whilst a number of numerical support routines are collated as a separate Pascal *Include* file, *Suncrun.pas*. This is presented at the end of the main program.

A summary of the program structure is presented in the flow chart overleaf. The modular procedure-based nature of Pascal means that the particular routines can be readily identified within the code.

The program was generally run, compiled and debugged on a 486DX, 33MHz personal computer. This was quite satisfactory in terms of processing speed for time increments down to 1ms. However, for iterative operations of the model, e.g. solving for laboratory mass transfer coefficients, or conducting the predictive perturbation analysis of Chapter 12, a Sun Workstation was used. This required several extremely minor modifications to the source code to suit the resident Pascal compiler, which exhibited some subtle differences to the Turbo Pascal PC version.

The physical constants and process values presented in this listing of the program represent those typically used for newsprint production on PM3. Whilst a large number of parameter permutations were tested on the computational model, the intention is that the values included in this listed version are consistent with those quoted for typical paper machine operation throughout the thesis and appendices.

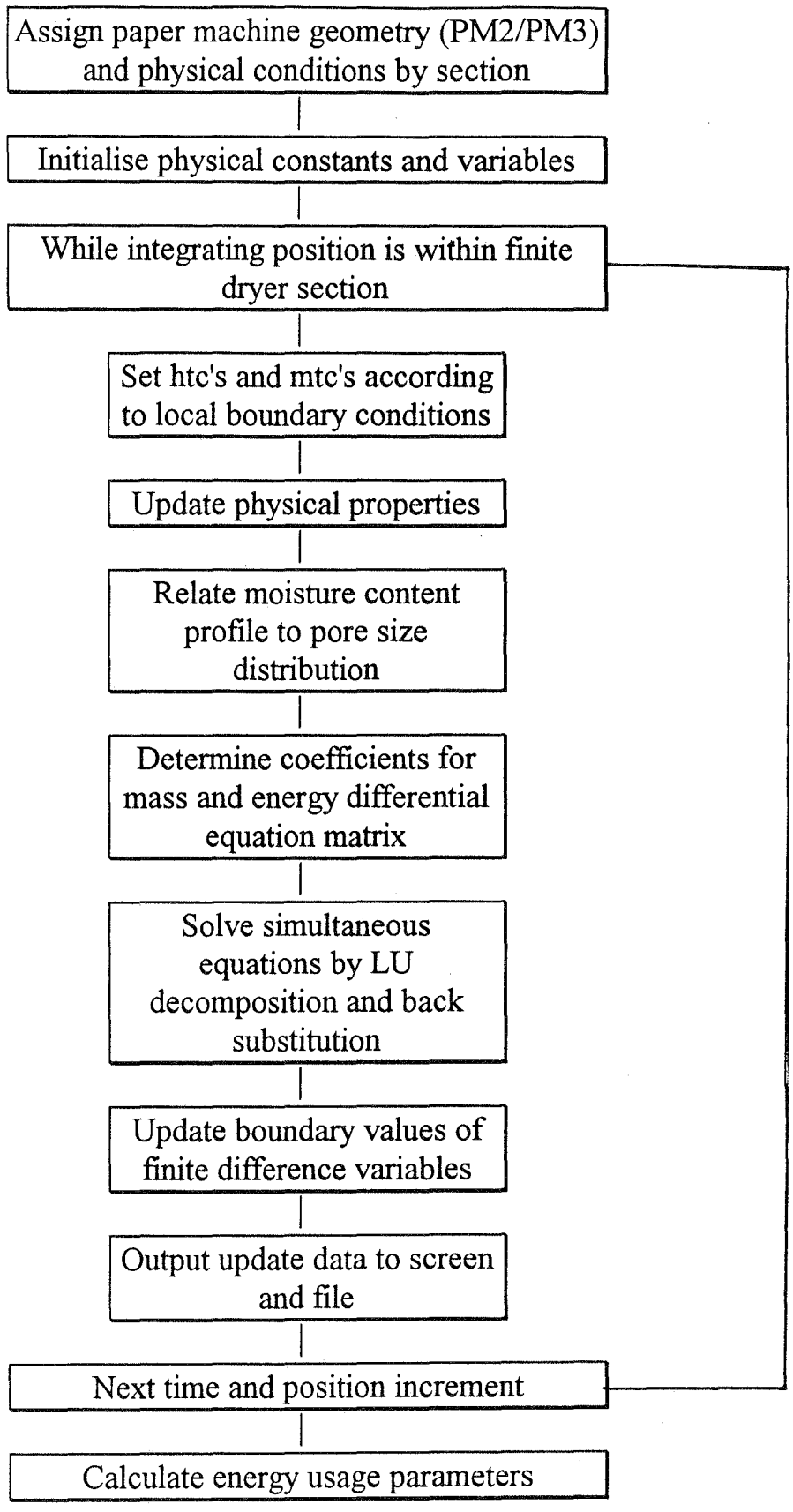
Assign paper machine geometry (PM2/PM3) and physical conditions by section
Initialise physical constants and variables
While integrating position is within finite dryer section
Set htc's and mtc's according to local boundary conditions
Update physical properties
Relate moisture content profile to pore size distribution
Determine coefficients for mass and energy differential equation matrix
Solve simultaneous equations by LU decomposition and back substitution
Update boundary values of finite difference variables
Output update data to screen and file
Next time and position increment
Calculate energy usage parameters

Main Program - DRYING.PAS

```
PROGRAM HeatMass;
{Taken from DRY1.PAS -
 Simple drying rate calculation for PM2 or PM3 - 1 pass}

USES Crt;

CONST
  pressmoisture = 0.58/(1-0.58);        {kgwater/kgfibre}
  drycaliper = 70E-6;                   {70+10 = 80}
  drybasiswt = 44.4568E-3;              {48.8 at 8.9%}
  Rmax = 15E-6;
  steps = 5;
  aa = -0.09;
  bb = 25.06;
  Rw = 8314/18;
  pi = 3.141592654;

TYPE
  glnarray = array[1..20] of double;
  LUglnarray = array[1..3*(steps+1)] of double;
  glindx = array[1..3*(steps+1)] of integer;
  glnpbynp = array[1..3*(steps+1),1..3*(steps+1)] of
double;
  matrix = array[0..3*steps+2,0..3*steps+2] of double;
  vector = array[0..3*steps+2] of double;
  integcase = (volume);

VAR
  M,Pv,S,T,R : array[-1..steps+1] of double;
  Hmfelt,distancepointer,Tdb,RHpock,Ts : array[0..96] of
double;
  Mevap : array[0..96,0..3] of double;
  pocket : array[1..48] of double;
  lookup : array[0..200] of double;
  k,Dv,Hl,Hv,Hfg,permV,permL : array[-1..steps+1] of
double;

Wfinal,trim,sigma,viscV,viscL,Mmax,perm,Ppock,DL,Dfibre,d
t,x,dy,fibsat : double;

Hm,Hs0,Hs5,Hm0,Hm5,T0,T5,hotsurfdry,opendrawdry,Wav,drypo
rosity : double;

speed,Pamb,Sinit,caliper,length,dlength,porosity,gcoeff,R
2av,maxliq : double;

Sfeltlimit,sectnum,samples,sampl_air,glit,bcpointer,bc,nu
mcyl : integer;
  Q,w,Tpock,Tsteam,ActualQ,Qhood : array[1..5] of double;
  section : array[0..5] of double;
  MM : matrix;
```

```
  fff : text;
  PM3 : boolean;
  Tpockoffs,Tsteamoffs,wfactor : double;
  Wavprev : double;
{-------------------------------------------------------
--------------------}
{$I sr\suncrun.pas}
{-------------------------------------------------------
--------------------}

PROCEDURE INITVAR;

VAR
  Dpaper,presstemp,Pvap,RHS,kozeny,SSA : double;
  i : integer;

BEGIN

  Dfibre := 1550;                          {density of fibre,
kg/m3}
  Dpaper := drybasiswt/drycaliper;         {density of final
sheet}
  DL := 1000;                              {density of water}
  fibsat := 0.4;                           {fibre saturation
point}
  presstemp := 273+50;                     {Kelvin}
  x := 0;                                  {longitudinal co-
ordinate}
  dt := 1E-2;                              {time increment,
seconds}
  viscV := 11E-6;
  viscL := 400E-6;
  sigma := 0.073;
  dlength := speed*dt;
  bcpointer := 0;
  hotsurfdry := 0;
  opendrawdry := 0;
  Wav := pressmoisture;

  R2av := (aa+1)*(aa+2)/(aa+bb+2)/(aa+bb+3);
  dryporosity := 1 - Dpaper/Dfibre;
  caliper := drycaliper + fibsat*drybasiswt/(DL*(1-
dryporosity));
  porosity := 1 - (1-dryporosity)*drycaliper/caliper;
  dy := caliper/steps;
  SSA :=
2*porosity*drycaliper/Rmax*(aa+bb+3)/(aa+2)/drybasiswt;
  kozeny := 5 + exp(14*(porosity-0.8));
  perm := POWER(porosity,3)/(kozeny*SQR(SSA*Dpaper*(1-
porosity)));

  Gcoeff := FACTORIAL(aa) * FACTORIAL(bb);
  Gcoeff := FACTORIAL(aa+bb+1)/Gcoeff;
```

```
  RHS :=
pressmoisture*drybasiswt*R2av/(porosity*caliper*DL);

  Sinit := RHS/R2av;
  Mmax := pressmoisture*drybasiswt/steps;
  Pamb := Psat(373);
  Pvap := Psat(presstemp);
  maxliq := R2av/RHS*Mmax;

{  FOR i := 0 TO 200 DO
    lookup[i] := SOLVE(0,1,R2av*i/200,0);}

  FOR i := -1 TO (steps+1) DO                    {store
initial values}
  BEGIN
    T[i] := presstemp;
    Pv[i] := Pvap;
    M[i] := Mmax;
    S[i] := Sinit;
  END;

  FOR i := 1 TO 5 DO BEGIN
    ActualQ[i] := 0;
    Qhood[i] := 0;
  END;

  FOR i := 0 TO 2*numcyl DO BEGIN
    Mevap[i,0] := 0;
    Mevap[i,1] := 0;
    Mevap[i,2] := 0;
    Mevap[i,3] := 0;
  END;

  FOR i := 1 TO numcyl DO
   pocket[i] := 0;

END;    {INITVAR}


PROCEDURE PM3BC;

CONST
  contactarc = 2.968;
  freerun = 1.159;

VAR
  i : integer;
  Tshell_int : double;
  Hmsect,ro : array[1..5] of double;

BEGIN
  Sfeltlimit := 28;

  FOR i:= 1 TO 48 DO
```

```
  BEGIN
    distancepointer[2*i - 1] := contactarc;
    distancepointer[2*i] := freerun;
  END;
  {exceptions}
  distancepointer[0]  := 0;
  distancepointer[09] := 2.920;
  distancepointer[10] := 1.228;
  distancepointer[11] := 2.920;
  distancepointer[45] := 2.920;
  distancepointer[46] := 1.228;
  distancepointer[47] := 2.920;
  distancepointer[75] := 1.933;
  distancepointer[76] := 5.226;
  distancepointer[77] := 1.933;

  FOR i:= 1 TO 96 DO
    distancepointer[i] := distancepointer[i-1] +
distancepointer[i];

  length := distancepointer[96];
  numcyl := 48;
  trim := 6.6;

  section[0] := distancepointer[0]+1E-6;
  section[1] := distancepointer[12];
  section[2] := distancepointer[30];
  section[3] := distancepointer[46];
  section[4] := distancepointer[76];
  section[5] := distancepointer[96];

  Hmsect[1] := 452.6E-6*speed+3.471E-3;      {0.0114}
  Hmsect[2] := 452.6E-6*speed+3.471E-3;      {0.0114}
  Hmsect[3] := 564.4E-6*speed+4.328E-3;      {0.0142}
  Hmsect[4] := 705.4E-6*speed+5.410E-3;      {0.0178}
  Hmsect[5] := 705.4E-6*speed+5.410E-3;      {0.0178}
  Hm := 2.619E-3*speed+20.08E-3;             {0.0660}

  Tsteam[1] := 95;
  Tsteam[2] := 110;
  Tsteam[3] := 116;
  Tsteam[4] := 122;
  Tsteam[5] := 120;

  Q[1] := 17000;
  Q[2] := 17076;
  Q[3] := 15384;
  Q[4] := 16950;
  Q[5] := 17000;

  Tpock[1] := 328;
  Tpock[2] := 338;
  Tpock[3] := 351;
  Tpock[4] := 353;
```

```
  Tpock[5] := 358;

  w[1] := 0.07;
  w[2] := 0.12;
  w[3] := 0.19;
  w[4] := 0.20;
  w[5] := 0.13;

  FOR i := 1 TO 5 DO BEGIN
    Tpock[i] := Tpock[i] +Tpockoffs;
    Tsteam[i] := Tsteam[i] + Tsteamoffs;
    w[i] := w[i] * wfactor;
  END;

  ro[1] := w[1]*101.3E3/(w[1]+0.622)/Rw/328;
  ro[2] := w[2]*101.3E3/(w[2]+0.622)/Rw/338;
  ro[3] := w[3]*101.3E3/(w[3]+0.622)/Rw/351;
  ro[4] := w[4]*101.3E3/(w[4]+0.622)/Rw/353;
  ro[5] := w[5]*101.3E3/(w[5]+0.622)/Rw/358;

  sectnum := 1;

  FOR i := 1 TO 96 DO BEGIN
    IF (distancepointer[i]>section[sectnum-1]) THEN BEGIN
      Tshell_int := 273+Tsteam[sectnum] -
Q[sectnum]/2400;
      Ts[i] := Tshell_int - Q[sectnum]/1700;
      Hmfelt[i] := Hmsect[sectnum];
      Tdb[i] := Tpock[sectnum];
      RHpock[i] := ro[sectnum]*Rw*Tdb[i]/Psat(Tdb[i]);
      sectnum := sectnum+1;
    END
    ELSE BEGIN
      Ts[i] := Ts[i-1];
      Hmfelt[i] := Hmfelt[i-1];
      Tdb[i] := Tdb[i-1];
      RHpock[i] := RHpock[i-1];
    END;

  END;
  Ts[1] := Tpock[1];
  sectnum := 0;
END;


PROCEDURE PM2BC;

CONST
  contactarc = 2.998;
  freerun = 1.175;

VAR
  i : integer;
  Tshell_int : double;
```

```
  Hmsect,ro : array[1..5] of double;

BEGIN
  Sfeltlimit := 24;

  FOR i:= 1 TO 44 DO
  BEGIN
    distancepointer[2*i - 1] := contactarc;
    distancepointer[2*i] := freerun;
  END;

  {exceptions}
  distancepointer[0] := 0;
  distancepointer[07] := 2.725;
  distancepointer[08] := 1.615;
  distancepointer[09] := 2.725;
  distancepointer[23] := 2.725;
  distancepointer[24] := 1.615;
  distancepointer[25] := 2.725;
  distancepointer[31] := 2.725;
  distancepointer[32] := 1.615;
  distancepointer[33] := 2.725;
  distancepointer[47] := 2.725;
  distancepointer[48] := 1.615;
  distancepointer[49] := 2.725;
  distancepointer[71] := 2.725;
  distancepointer[72] := 1.615;
  distancepointer[73] := 2.725;

  FOR i:= 1 TO 88 DO
    distancepointer[i] := distancepointer[i-1] +
distancepointer[i];

  length := distancepointer[88];
  numcyl := 44;
  trim := 5.9;

  section[0] := distancepointer[0]+1E-6;
  section[1] := distancepointer[12];
  section[2] := distancepointer[26];
  section[3] := distancepointer[48];
  section[4] := distancepointer[72];
  section[5] := distancepointer[88];

  Hmsect[1] := 452.6E-6*speed+3.471E-3;      {0.0101}
  Hmsect[2] := 452.6E-6*speed+3.471E-3;      {0.0101}
  Hmsect[3] := 564.4E-6*speed+4.328E-3;      {0.0126}
  Hmsect[4] := 705.4E-6*speed+5.410E-3;      {0.0158}
  Hmsect[5] := 705.4E-6*speed+5.410E-3;      {0.0158}
  Hm := 2.619E-3*speed+20.08E-3;             {0.0590}

  Tsteam[1] := 100;
  Tsteam[2] := 118;
  Tsteam[3] := 120;
```

```
  Tsteam[4] := 124;
  Tsteam[5] := 123;

  Q[1] := 17000;
  Q[2] := 19000;
  Q[3] := 15840;
  Q[4] := 17640;
  Q[5] := 15820;

  Tpock[1] := 323;
  Tpock[2] := 338;
  Tpock[3] := 348;
  Tpock[4] := 353;
  Tpock[5] := 353;

  w[1] := 0.10;
  w[2] := 0.15;
  w[3] := 0.19;
  w[4] := 0.20;
  w[5] := 0.20;

  ro[1] := w[1]*101.3E3/(w[1]+0.622)/Rw/323;
  ro[2] := w[2]*101.3E3/(w[2]+0.622)/Rw/338;
  ro[3] := w[3]*101.3E3/(w[3]+0.622)/Rw/348;
  ro[4] := w[4]*101.3E3/(w[4]+0.622)/Rw/353;
  ro[5] := w[5]*101.3E3/(w[5]+0.622)/Rw/353;

  sectnum := 1;

  FOR i := 1 TO 88 DO BEGIN
    IF (distancepointer[i]>section[sectnum-1]) THEN BEGIN
      Tshell_int := 273+Tsteam[sectnum] -
Q[sectnum]/2400;
      Ts[i] := Tshell_int - Q[sectnum]/1700;
      Hmfelt[i] := Hmsect[sectnum];
      Tdb[i] := Tpock[sectnum];
      RHpock[i] := ro[sectnum]*Rw*Tdb[i]/Psat(Tdb[i]);
      sectnum := sectnum+1;
    END
    ELSE BEGIN
      Ts[i] := Ts[i-1];
      Hmfelt[i] := Hmfelt[i-1];
      Tdb[i] := Tdb[i-1];
      RHpock[i] := RHpock[i-1];
    END;

  END;

  sectnum := 0;

END;


PROCEDURE BCONDS;
```

```
CONST
  Hcfelt = 5;
  Hs = 60;

VAR
  Hc,Tamb,RH : double;

BEGIN

  x := x + dlength;

  IF PM3 THEN
     Hc := 261*M[0]*steps/drybasiswt + 577
  ELSE
     Hc := 186*M[0]*steps/drybasiswt + 597;

  IF (x>distancepointer[bcpointer]) THEN
    bcpointer := bcpointer+1;

  IF (x>section[sectnum]) THEN BEGIN
    sectnum := sectnum+1;
    samples := 0;
    sampl_air := 0;
  END;

  IF (x<length) THEN BEGIN
    bc := bcpointer MOD 4;
    Tamb := Tdb[bcpointer];
    RH := RHpock[bcpointer];
    Ppock := Psat(Tamb) * RH;

    IF (bc = 1) THEN  BEGIN
      Hs0 := Hc;
      Hs5 := Hs;
      Hm0 := 0;
      Hm5 := Hmfelt[bcpointer];
      T0  := Ts[bcpointer];
      T5  := Tdb[bcpointer];
    END
    ELSE
      IF (bc = 3) THEN BEGIN
        Hs0 := Hs;
        Hs5 := Hc;
        Hm0 := Hmfelt[bcpointer];
        Hm5 := 0;
        T0  := Tdb[bcpointer];
        T5  := Ts[bcpointer];
      END
      ELSE BEGIN    {bcpointer is even}
        Hs0 := Hs;
        Hs5 := Hs;
        Hm0 := Hm;
        Hm5 := Hm;
```

```
        T0  := Tdb[bcpointer];
        T5  := Tdb[bcpointer];
      END;

    IF (bcpointer<Sfeltlimit+1) THEN            {single
felted}
        IF (bc = 3) THEN BEGIN
          Hs5 := Hcfelt;
          Hm0 := Hm;
        END
        ELSE
          IF NOT(ODD(bcpointer)) THEN         {bcpointer
is even}
            Hm5 := Hmfelt[bcpointer];

  END;
END;


PROCEDURE PROPERTIES;

VAR
  W,Kr,RHS,b1,b2 : double;
  i : integer;

BEGIN
  caliper := drycaliper +
MIN(fibsat,Wav)*drybasiswt/(DL*(1-dryporosity));
  porosity := 1 - (1-dryporosity)*drycaliper/caliper;
  dy := caliper/steps;
  RHS :=
pressmoisture*drybasiswt*R2av/(porosity*caliper*DL);
  Sinit := RHS/R2av;

  FOR i := -1 TO (steps+1) DO BEGIN
    W := M[i]*(steps/drybasiswt);
    k[i] := 1.731*(0.07+0.375*W)/(1+W);
    k[i] := (1-porosity)*0.12 + porosity*S[i]*0.65 +
porosity*(1-S[i])*0.022;
    b1 := exp(-2.20987*W+3.88563*sqrt(W)-5.4288);
    b2 := -exp(-0.64962*W+0.10628*sqrt(W)+1.31179);
    k[i] := exp(b1*(T[i]-273)+b2);
    Dv[i] := 2.5E-5*POWER(T[i]/298,1.5)*porosity*(1-
S[i]);
    Hl[i] := 4190*(T[i]-273);
    Hv[i] := 2634700 + 1688*(T[i]-273-75) + Qs(W);
    Hfg[i] := (2320800 - 2508*(T[i]-273-75));
    permV[i] := perm*(1-S[i]);
    Kr := 1.896*EXP(7.54*POWER(S[i],7.113) - 8.19);
    permL[i] := perm*Kr;
  END;
END;
```

```
PROCEDURE FINDR(f : double; VAR c,d,R : double);
{0<f<1}
VAR
  base : integer;
  interp : double;

BEGIN
  base := TRUNC(200*f);
  interp := 200*f-base;
  R := (1-interp)*lookup[base] + interp*lookup[base+1];
  c := (lookup[base+1]-lookup[base])/(1/200);
  d := lookup[base] - c*base/200;
END;


PROCEDURE MASSENERGY;

CONST
  Cpf = 1340;
  Cpv = 1688;
  Cpl = 4190;

VAR
  i,j,n : integer;
  MM : matrix;
  RHS : vector;
  BLU : LUglnarray;
  term : array[1..14] of double;
  mask : array[-1..steps+1] of integer;

EPC,E,F,G,H,phi,Mfactor,Pfactor,c,d,tt,pp,ppb,denom0,deno
m5 : double;
  P1,P2,a,b : double;
  flashoff : double;
  Ml,Mvdiff,Mvbulk : array[0..steps] of double;

PROCEDURE SUBPROC;
BEGIN
    term[1] := G*(-Pv[i]/SQR(T[i])*ppb/4);
    term[2] := F*(-2/SQR(T[i])*pp/4 -
2*Pv[i]/POWER(T[i],3)*tt/4 + Pv[i]/SQR(T[i]));
    term[3] := F*-2*Pv[i]/SQR(T[i]);
    term[4] := G*(Pv[i]/SQR(T[i])*ppb/4);
    term[5] := F*(2/SQR(T[i])*pp/4 +
2*Pv[i]/POWER(T[i],3)*tt/4 + Pv[i]/SQR(T[i]));

    term[6] := G*(-Pv[i]/T[i]*mask[i-1] + ppb/4/T[i]);
    term[7] := F*-1/T[i];
    term[8] := G*2*Pv[i]/T[i]*mask[i];
    term[9] := F*2/T[i];
    term[10] := G*(-Pv[i]/T[i]*mask[i+1]-ppb/4/T[i]);
    term[11] := F*-1/T[i];

    term[12] := -E*(1+c/2/R[i]/maxliq*(M[i+1]-M[i-1]));
```

```
    term[13] := E*2;
    term[14] := -E*(1-c/2/R[i]/maxliq*(M[i+1]-M[i-1]));

    IF (((bc<>3)AND(i=steps)AND(mask[i+1]=1)) OR
((bc<>1)AND(i=0)AND(mask[i-1]=1))) THEN BEGIN
      term[6] := term[6] + G*Pv[i]/T[i]*mask[i-1];
      term[8] := term[8] - 2*G*Pv[i]/T[i]*mask[i];
      term[10] := term[10] + G*Pv[i]/T[i]*mask[i+1];
    END;

    Mvdiff[i] := term[2]*T[i-
1]+term[3]*T[i]+term[5]*T[i+1]+term[7]*Pv[i-
1]+term[9]*Pv[i]+term[11]*Pv[i+1];
    Mvbulk[i] := term[1]*T[i-
1]+term[4]*T[i+1]+term[6]*Pv[i-
1]+term[8]*Pv[i]+term[10]*Pv[i+1];
    Ml[i]     := term[12]*M[i-
1]+term[13]*M[i]+term[14]*M[i+1];

    IF (i=0) THEN BEGIN
      IF (bc=1) THEN BEGIN
        MM[j,j]   := 1 + term[13];
        MM[j,j+3] := term[14]+term[12];
      END
      ELSE BEGIN
        MM[j,j]   := 1+term[13] +
term[12]*(c/2*M[1]+2*d*maxliq)/denom0;
        MM[j,j+3] := term[14] + term[12]*(c/2*M[0]-
d*maxliq)/denom0;
      END;
      MM[j,j+1] := term[3] -
(term[1]+term[2])*2*Hs0*dy/k[i];
      MM[j,j+4] := term[4]+term[5]+term[1]+term[2];

      IF (bc=1) THEN BEGIN
        MM[j,j+2] := term[8]+term[9] -
term[7]*2*Hm0*dy/Dv[i]*T[i-1]/T[i];
        MM[j,j+5] := term[10]+term[11] + T[-
1]/T[1]*term[7] + term[6];
      END
      ELSE BEGIN
        MM[j,j+2] := term[8]+term[9] -
2*Hm0*dy/Dv[i]*T[i-1]/T[i]*term[7] + 2*term[6];
        MM[j,j+5] := term[10]+term[11] + T[-
1]/T[1]*term[7] - term[6];
      END;

      RHS[j] := RHS[j] -
(term[1]+term[2])*2*Hs0*dy/k[i]*T0 -
term[7]*2*Hm0*dy/Dv[i]*Ppock*T[-1]/T0;
      IF (bc<>1) THEN
        RHS[j] := RHS[j] +
term[7]*2/Dv[i]*DL*permL[i]/viscL*Rw*T[i-1]*-
2*sigma*(1/R[i-1]-1/R[i+1])/2/Rmax;
```

```
      IF (bc=1) THEN
        RHS[j] := RHS[j] -
2*G*Pv[i]/T[i]*Pamb*(mask[i+1]-mask[i])
      ELSE BEGIN
        IF ((mask[i-1]=0) AND (mask[i]=0) AND
(mask[i+1]=1)) THEN
          RHS[j] := RHS[j] - G*Pv[i]/T[i]*Pamb;
        IF ((mask[i-1]=0) AND (mask[i]=1) AND
(mask[i+1]=1)) THEN
          RHS[j] := RHS[j] + G*Pv[i]/T[i]*Pamb;
      END;
   END

    ELSE
      IF (i<>steps) THEN BEGIN
        MM[j,j-3] := term[12];
        MM[j,j]   := 1+term[13];
        MM[j,j+3] := term[14];
        MM[j,j-2] := term[1]+term[2];
        MM[j,j+1] := term[3];
        MM[j,j+4] := term[4]+term[5];
        MM[j,j-1] := term[6]+term[7];
        MM[j,j+2] := term[8]+term[9];
        MM[j,j+5] := term[10]+term[11];
        RHS[j]    := RHS[j] - G*Pv[i]/T[i]*Pamb*(mask[i-
1]-2*mask[i]+mask[i+1]);
      END

      ELSE BEGIN      {i=steps}
        IF (bc=3) THEN BEGIN
          MM[j,j-3] := term[12]+term[14];
          MM[j,j]   := 1 + term[13];
        END
        ELSE BEGIN
           MM[j,j-3] := term[12] + term[14]*(c/2*M[i]-
d*maxliq)/denom5;
          MM[j,j]   := 1 + term[13] +
term[14]*(c/2*M[i-1]+2*d*maxliq)/denom5;
        END;
        MM[j,j-2] := term[1]+term[2]+term[4]+term[5];
        MM[j,j+1] := term[3] -
(term[4]+term[5])*2*Hs5*dy/k[i];

        IF (bc=3) THEN BEGIN
          MM[j,j-1] := term[6]+term[7] + T[i+1]/T[i-
1]*term[11] + term[10];
          MM[j,j+2] := term[8]+term[9] -
term[11]*2*Hm5*dy/Dv[i]*T[i+1]/T[i];
        END
        ELSE BEGIN
          MM[j,j-1] := term[6]+term[7] + T[i+1]/T[i-
1]*term[11] - term[10];
          MM[j,j+2] := term[8]+term[9] -
2*Hm5*dy/Dv[i]*T[i+1]/T[i]*term[11] + 2*term[10];
```

```
        END;
        RHS[j] := RHS[j] -
(term[4]+term[5])*2*Hs5*dy/k[i]*T5 -
2*Hm5*dy/Dv[i]*Ppock/T5*T[i+1]*term[11];
        IF (bc<>3) THEN
          RHS[j] := RHS[j] +
term[11]*2/Dv[i]*DL*permL[i]/viscL*Rw*T[i+1]*-
2*sigma*(1/R[i+1]-1/R[i-1])/2/Rmax;
        IF (bc=3) THEN
          RHS[j] := RHS[j] - 2*G*Pv[i]/T[i]*Pamb*(mask[i-
1]-mask[i])
        ELSE BEGIN
          IF ((mask[i+1]=0) AND (mask[i]=0) AND (mask[i-
1]=1)) THEN
            RHS[j] := RHS[j] - G*Pv[i]/T[i]*Pamb;
          IF ((mask[i+1]=0) AND (mask[i]=1) AND (mask[i-
1]=1)) THEN
            RHS[j] := RHS[j] + G*Pv[i]/T[i]*Pamb;
        END;
      END;
END;   {SUBPROC}


BEGIN

  MATRIXZERO(MM);
  FOR i := -1 TO (steps+1) DO
    FINDR(M[i]/maxliq,c,d,R[i]);     {calculates R[-1] -
R[6]}

  i := 5;

  FOR i := 0 TO steps DO BEGIN
    FINDR(M[i]/maxliq,c,d,R[i]);     {calculates R[-1] -
R[6]}
    phi := GETPHI(M[i]*steps,T[i]);
    j := 3*i;
    E :=
DL*permL[i]/viscL*2*sigma/Rmax*c/maxliq/SQR(R[i])*dt/dy;
    F := Dv[i]/Rw*dt/dy;
    G := permV[i]/Rw/viscV*dt/dy;
    tt := T[i+1]-T[i-1];
    pp := Pv[i+1]-Pv[i-1];
    ppb := MAX(Pv[i+1],Pamb) - MAX(Pv[i-1],Pamb);
    denom0 := 2*c*M[1] - c*M[0] + d*maxliq;
    denom5 := 2*c*M[steps-1] - c*M[steps] + d*maxliq;

    FOR n := (i-1) TO (i+1) DO
      IF (Pv[n]>Pamb) THEN
        mask[n] := 1
      ELSE
        mask[n] := 0;

    IF (i=0) THEN
```

```
      IF (bc=1) THEN BEGIN
        mask[i-1] := mask[i+1];
        ppb := 0;
      END
      ELSE
        IF (Pamb >= (2*MAX(Pv[i],Pamb) -
MAX(Pv[i+1],Pamb))) THEN BEGIN
          mask[i-1] := 0;
          ppb := MAX(Pv[i+1],Pamb) - Pamb;
        END
        ELSE BEGIN
          mask[i-1] := 1;
          ppb := 2*(MAX(Pv[i+1],Pamb)-MAX(Pv[i],Pamb));
        END;

    IF (i=steps) THEN
      IF (bc=3) THEN BEGIN
        mask[i+1] := mask[i-1];
        ppb := 0;
      END
      ELSE
        IF (Pamb >= (2*MAX(Pv[i],Pamb) - MAX(Pv[i-
1],Pamb))) THEN BEGIN
          mask[i+1] := 0;
          ppb := Pamb - MAX(Pv[i-1],Pamb);
        END
        ELSE BEGIN
          mask[i+1] := 1;
          ppb := 2*(MAX(Pv[i],Pamb)-MAX(Pv[i-1],Pamb));
        END;

    RHS[j] := M[i];

    SUBPROC;

    j := 3*i+1;
    FOR n := 1 TO 11 DO
      term[n] := term[n]*(Hv[i]+Hfg[i])/dy;
    FOR n := 12 TO 14 DO
      term[n] := term[n]*Hl[i]/dy;
    EPC := (1-porosity)*Dfibre*Cpf +
porosity*S[i]*DL*Cpl;
    H := k[i]*dt/SQR(dy);
    Mfactor := porosity*Sinit/Mmax *
(DL*Cpl*T[i]+Cpv*Pv[i]/Rw);
    Pfactor := porosity*Cpv/Rw*(1-S[i]);

    RHS[j] := EPC*T[i] + Mfactor*M[i] + Pfactor*Pv[i];

    IF (i=0) THEN BEGIN
      IF (bc=1) THEN BEGIN
        MM[j,j-1] := Mfactor + term[13];
        MM[j,j+2] := term[14]+term[12];
      END
```

```
      ELSE BEGIN
        MM[j,j-1] := Mfactor+term[13] +
term[12]*(c/2*M[1]+2*d*maxliq)/denom0;
        MM[j,j+2] := term[14] + term[12]*(c/2*M[0]-
d*maxliq)/denom0;
      END;
      MM[j,j]   := EPC + 2*H + term[3] - (-
H+term[1]+term[2])*2*Hs0*dy/k[i];
      MM[j,j+3] := -2*H +
term[4]+term[5]+term[1]+term[2];

      IF (bc=1) THEN BEGIN
        MM[j,j+1] := Pfactor + term[8]+term[9] -
term[7]*2*Hm0*dy/Dv[i]*T[i-1]/T[i];
        MM[j,j+4] := term[10]+term[11] + T[-
1]/T[1]*term[7] + term[6];
      END
      ELSE BEGIN
        MM[j,j+1] := Pfactor + term[8]+term[9] -
2*Hm0*dy/Dv[i]*T[i-1]/T[i]*term[7] + 2*term[6];
        MM[j,j+4] := term[10]+term[11] + T[-
1]/T[1]*term[7] - term[6];
      END;
      RHS[j] := RHS[j] - 2*Hs0*dy/k[i]*T0*(-
H+term[1]+term[2]) - term[7]*2*Hm0*dy/Dv[i]*Ppock*T[-
1]/T0;
      IF (bc<>1) THEN
        RHS[j] := RHS[j] +
term[7]*2/Dv[i]*DL*permL[i]/viscL*Rw*T[i-1]*-
2*sigma*(1/R[i-1]-1/R[i+1])/2/Rmax;
      IF (bc=1) THEN
        RHS[j] := RHS[j] -
2*G*Pv[i]/T[i]*Pamb*(mask[i+1]-mask[i])*(Hv[i]+Hfg[i])/dy
      ELSE BEGIN
        flashoff := DL*PermL[i]/ViscL*dt/SQR(dy)*-
2*sigma/Rmax*(1/R[-1]-1/R[1])/2;
        RHS[j] := RHS[j] + flashoff*(Hv[i]-Hl[i]);
        IF ((mask[i-1]=0) AND (mask[i]=0) AND
(mask[i+1]=1)) THEN
          RHS[j] := RHS[j] -
G*Pv[i]/T[i]*Pamb*(Hv[i]+Hfg[i])/dy;
        IF ((mask[i-1]=0) AND (mask[i]=1) AND
(mask[i+1]=1)) THEN
          RHS[j] := RHS[j] +
G*Pv[i]/T[i]*Pamb*(Hv[i]+Hfg[i])/dy;
      END;
    END

    ELSE
      IF (i<>steps) THEN BEGIN
        MM[j,j-4] := term[12];
        MM[j,j-1] := Mfactor + term[13];
        MM[j,j+2] := term[14];
        MM[j,j-3] := -H+term[1]+term[2];
```

```
            RHS[j] := RHS[j] -
G*Pv[i]/T[i]*Pamb*(Hv[i]+Hfg[i])/dy;
          IF ((mask[i+1]=0) AND (mask[i]=1) AND (mask[i-
1]=1)) THEN
            RHS[j] := RHS[j] +
G*Pv[i]/T[i]*Pamb*(Hv[i]+Hfg[i])/dy;
        END;
      END;

    j := 3*i+2;

    P1 := Psat(T[i]);
    P2 := Psat(T[i]+0.01);
    a := (P2-P1)/0.01;
    b := P1 - (P2-P1)/0.01*T[i];

    MM[j,j-1] := -phi*a;
    MM[j,j]   := 1;
    RHS[j]    := phi*b;

  END;        {i}


  DCMPBKSB(3*(steps+1),MM,RHS,BLU);

  FOR i := 0 TO steps DO BEGIN
    j := 3*i+1;
    M[i] := BLU[j];
    T[i] := BLU[j+1];
    Pv[i]  := BLU[j+2];
  END;

  i := 0;
  T[-1] := T[1] + 2*Hs0*dy/k[0]*(T0 - T[0]);
  Pv[-1]  := Pv[1]*T[-1]/T[1] -
2*Hm0*dy/Dv[0]*(Pv[0]/T[0]-Ppock/T0)*T[-1];
  IF (bc=1) THEN
    M[-1] := M[1]
  ELSE BEGIN
    M[-1] := (c*M[1]*M[0] + 2*M[0]*d*maxliq -
M[1]*d*maxliq)/(2*c*M[1] - c*M[0] + d*maxliq);
    Pv[-1] := Pv[-1] - 2*DL*permL[i]/viscL/Dv[i]*Rw*T[i-
1]*-2*sigma*(1/R[i-1]-1/R[i+1])/2/Rmax;
  END;

  i := steps;
  T[i+1] := T[i-1] - 2*Hs5*dy/k[i]*(T[i]-T5);
  Pv[i+1]  := (Pv[i-1]/T[i-1] -
2*Hm5*dy/Dv[i]*(Pv[i]/T[i]-Ppock/T5))*T[i+1];
  IF (bc=3) THEN
    M[i+1] := M[i-1]
  ELSE BEGIN
    M[i+1] := (c*M[i-1]*M[i] + 2*M[i]*d*maxliq - M[i-
1]*d*maxliq)/(2*c*M[i-1] - c*M[i] + d*maxliq);
```

```
    Pv[i+1] := Pv[i+1] -
2*DL*permL[i]/viscL/Dv[i]*Rw*T[i+1]*-2*sigma*(1/R[i+1]-
1/R[i-1])/2/Rmax;
  END;

END;


PROCEDURE UPDATE;

VAR
  i : integer;
  c,d,liqperm,vapdiff,factor : double;

BEGIN
  FOR i := 0 TO steps DO
    S[i] := M[i]/Mmax*Sinit;

  IF ((bc=1)AND(bcpointer<>1)) THEN BEGIN
    samples := samples+1;
    sampl_air := sampl_air + 1;
    ActualQ[sectnum] := ((samples-1)*ActualQ[sectnum] +
Hs0*(T0-T[0]))/samples;
    Qhood[sectnum] := ((sampl_air-1)*Qhood[sectnum] +
Hs5*(T5-T[steps]))/sampl_air;
  END;

  IF NOT(ODD(bc)) THEN BEGIN
    sampl_air := sampl_air + 1;
    Qhood[sectnum] := ((sampl_air-1)*Qhood[sectnum] +
Hs0*(T0-T[0]) + Hs5*(T5-T[steps]))/sampl_air;
  END;

  IF ((bc=3) AND (bcpointer>24)) THEN BEGIN
    samples := samples+1;
    sampl_air := sampl_air + 1;
    ActualQ[sectnum] := ((samples-1)*ActualQ[sectnum] +
Hs5*(T5-T[steps]))/samples;
    Qhood[sectnum] := ((sampl_air-1)*Qhood[sectnum] +
Hs0*(T0-T[0]))/sampl_air;
  END;

  IF ((bc=3) AND (bcpointer<=24)) THEN BEGIN
    sampl_air := sampl_air + 1;
    Qhood[sectnum] := ((sampl_air-1)*Qhood[sectnum] +
Hs0*(T0-T[0]) + Hs5*(T5-T[steps]))/sampl_air;
  END;

  FOR i := -1 TO (steps+1) DO
    FINDR(M[i]/maxliq,c,d,R[i]);    {calculates R[-1] -
R[6]}

  factor := dt*speed*trim;
```

```
  liqperm := -Dl*permL[0]/viscL*2*sigma/Rmax/dy*(1/R[1]-
1/R[-1])/2;
  IF (ABS(liqperm)>1E-15) THEN
    Mevap[bcpointer,0] := Mevap[bcpointer,0] +
liqperm*factor;
  vapdiff := Dv[0]/Rw/dy*(Pv[1]/T[1]-Pv[-1]/T[-1])/2;
  IF (ABS(vapdiff)>1E-15) THEN
    Mevap[bcpointer,1] := Mevap[bcpointer,1] +
vapdiff*factor;

  liqperm :=
Dl*permL[steps]/viscL*2*sigma/Rmax/dy*(1/R[steps+1]-
1/R[steps-1])/2;
  IF (ABS(liqperm)>1E-15) THEN
    Mevap[bcpointer,2] := Mevap[bcpointer,2] +
liqperm*factor;
  vapdiff := -Dv[steps]/Rw/dy*(Pv[steps+1]/T[steps+1]-
Pv[steps-1]/T[steps-1])/2;
  IF (ABS(vapdiff)>1E-15) THEN
    Mevap[bcpointer,3] := Mevap[bcpointer,3] +
vapdiff*factor;

  Wavprev := Wav;
  Wav := 0;
  FOR i := 0 TO steps DO
    Wav := Wav + M[i]/(steps+1)*(steps/drybasiswt);
  Wfinal := Wav;

END;


PROCEDURE BCMOISTURE;
VAR
  i,j : integer;
  hhh : text;

BEGIN
{  ASSIGN(hhh,'dat\mevap.dat');
  REWRITE(hhh);
  moisture := 0;
  FOR i := 1 TO numcyl*2 DO BEGIN

WriteLn(hhh,i:5,Mevap[i,0]:12:6,Mevap[i,1]:12:6,Mevap[i,2
]:15:6,Mevap[i,3]:12:6);
    moisture :=
moisture+Mevap[i,0]+Mevap[i,1]+Mevap[i,2]+Mevap[i,3];
  END;
  CLOSE(hhh);}

  pocket[1] := Mevap[1,0] + Mevap[1,1] + Mevap[2,0] +
Mevap[2,1];

  FOR i := 2 TO numcyl DO
    FOR j := 2*i-3 TO 2*i DO
```

```
      IF ODD(i) THEN
        pocket[i] := pocket[i]+Mevap[j,0]+Mevap[j,1]
      ELSE
        pocket[i] := pocket[i]+Mevap[j,2]+Mevap[j,3];


{  ASSIGN(hhh,'dat\pocket.dat');
  REWRITE(hhh);
  FOR i := 1 TO numcyl DO
    WriteLn(hhh,i:5,pocket[i]:12:6);
  CLOSE(hhh);}

END;


PROCEDURE AIRCALC;

CONST
  Cpa = 1005;
  T1 = 78;
  T2 = 98;
  T3 = 108;
  Tleak = 25;
  leakratio = 0.65;
  Thr = 30;

VAR
  phi,Mair,steam,correction : array[1..5] of double;
  group : array[0..5] of integer;
  i,j,divide : integer;

M1,M2,M3,M,Tx1,Tx2,Tx3,pocketsum,cylheat,Qair,Hfg,allstea
m : double;
contactarc,paper,SSC,pockavg1,pockavg2,pockavg3,Qh1,Qh2,Q
h3 : double;
  ggg : text;

BEGIN

  IF PM3 THEN BEGIN
    group[0] := 0;
    group[1] := 6;
    group[2] := 12;
    group[3] := 23;
    group[4] := 38;
    group[5] := 48;
    cylheat := 60*(trim*41*(pi*1.52-2.968))*15;
  END
  ELSE BEGIN
    group[0] := 0;
    group[1] := 6;
    group[2] := 12;
    group[3] := 24;
    group[4] := 36;
```

```
    group[5] := 44;
    cylheat := 60*(trim*38*(pi*1.52-2.998))*15;
  END;
  FOR i := 1 TO 5 DO BEGIN
    pocketsum := 0;
    FOR j := (group[i-1]+1) TO group[i] DO BEGIN
      pocketsum := pocketsum + pocket[j];
    END;
    Mair[i] := pocketsum/(w[i]-0.01);
    phi[i] := 101.3E3*w[i]/(0.622+w[i])/Psat(Tpock[i]);
    Qhood[i] := Qhood[i] * trim * (section[i] -
section[i-1]);  {W/m2 - W}
  END;

  IF PM3 THEN BEGIN
    M1 := Mair[1]+Mair[2];
    M2 := Mair[3]+Mair[4]*5/15;
    M3 := Mair[4]*10/15+Mair[5];
    M := M1+M2+M3;

    pockavg1 := (6*Tpock[1]+8*Tpock[2])/14 - 273;
    pockavg2 := (9*Tpock[3]+5*Tpock[4])/14 - 273;
    pockavg3 := (10*Tpock[4]+10*Tpock[5])/20 - 273;

    Qh1 := (6*Qhood[1]+8*Qhood[2])/14;
    Qh2 := (9*Qhood[3]+5*Qhood[4])/14;
    Qh3 := (10*Qhood[4]+10*Qhood[5])/20;

    Tx1 := pockavg1*(14/48*leakratio*M+M1) -
7/41*cylheat/Cpa - M1*T1;
    Tx1 := (Tx1 - 14/48*leakratio*M*Tleak + Qh1/Cpa) /
M1;
    Tx2 := pockavg2*(14/48*leakratio*M+M2) -
14/41*cylheat/Cpa - M2*T2;
    Tx2 := (Tx2 - 14/48*leakratio*M*Tleak + Qh2/Cpa) /
M2;
    Tx3 := pockavg3*(20/48*leakratio*M+M3) -
20/41*cylheat/Cpa - M3*T3;
    Tx3 := (Tx3 - 20/48*leakratio*M*Tleak + Qh3/Cpa) /
M3;
  END
  ELSE BEGIN
    M1 := Mair[1]+Mair[2];
    M2 := Mair[3]+Mair[4]*6/12;
    M3 := Mair[4]*6/12+Mair[5];
    M := M1+M2+M3;

    pockavg1 := (6*Tpock[1]+6*Tpock[2])/12  - 273;
    pockavg2 := (12*Tpock[3]+6*Tpock[4])/18 - 273;
    pockavg3 := (6*Tpock[4]+8*Tpock[5])/14 - 273;

    Tx1 := pockavg1*(12/44*leakratio*M+M1) -
6/38*cylheat/Cpa - M1*T1;
    Tx1 := (Tx1 - 12/44*leakratio*M*Tleak) / M1;
```

```
    Tx2 := pockavg2*(18/44*leakratio*M+M2) -
18/38*cylheat/Cpa - M2*T2;
    Tx2 := (Tx2 - 18/44*leakratio*M*Tleak) / M2;
    Tx3 := pockavg3*(14/44*leakratio*M+M3) -
14/38*cylheat/Cpa - M3*T3;
    Tx3 := (Tx3 - 14/44*leakratio*M*Tleak) / M3;
  END;

  Qair := CPa*(M1*(T1+Tx1-Thr)+M2*(T2+Tx2-
Thr)+M3*(T3+Tx3-Thr));

  allsteam := 0;

  IF PM3 THEN BEGIN
    contactarc := 2.968;
    correction[1] := 0.096;
    correction[2] := 0;
    correction[3] := 0.048;
    correction[4] := 1.083;
    correction[5] := 1.035;
  END
  ELSE BEGIN
    contactarc := 2.998;
    correction[1] := 0.546;
    correction[2] := 0.546;
    correction[3] := 0.819;
    correction[4] := 0.546;
    correction[5] := 0.273;
  END;

  FOR i := 1 TO 5 DO BEGIN
    IF (i<=2) THEN divide := 2
              ELSE divide := 1;
    steam[i] := ActualQ[i]*trim*(contactarc*(group[i]-
group[i-1])/divide - correction[i]); {W}
    Hfg := (2532.29-2.75249*Tsteam[i])*1000;
    steam[i] := steam[i]/Hfg;
    IF (steam[i]<0) THEN steam[i] := 0;
    allsteam := allsteam+steam[i];
  END;
  paper := (1+Wfinal)*drybasiswt*trim*speed;
  allsteam := allsteam + (Qair+cylheat)/2121E3;
  SSC := allsteam/paper;

  ASSIGN(ggg,'summary.dat');
  REWRITE(ggg);
  WriteLn(ggg,'Wfactor ',Wfactor:8:2,'  Tpockoffs
',Tpockoffs:8:2,'  Tsteamoffs ',Tsteamoffs:8:2);
  WriteLn(ggg,'Speed ',60*speed:10:3,'      Final
moisture ',Wfinal:15:9);
  WriteLn(ggg,'Mair
',Mair[1]:10:3,Mair[2]:10:3,Mair[3]:10:3,Mair[4]:10:3,Mai
r[5]:10:3);
```

```
  WriteLn(ggg,'R.H.
',phi[1]:10:3,phi[2]:10:3,phi[3]:10:3,phi[4]:10:3,phi[5]:
10:3);
  WriteLn(ggg,'Steam
',Steam[1]:10:3,Steam[2]:10:3,Steam[3]:10:3,Steam[4]:10:3
,Steam[5]:10:3);
  WriteLn(ggg,'M1   ',M1:10:3,'    M2   ',M2:10:3,'   M3
',M3:10:3,'   M   ',M:10:3);
  WriteLn(ggg,'T1    ',T1+Tx1:10:3,'     T2
',T2+Tx2:10:3,'     T3   ',T3+Tx3:10:3);
  WriteLn(ggg,'Qh1   ',Qh1:10:3,'    Qh2  ',Qh2:10:3,'
Qh3  ',Qh3:10:3);
  WriteLn(ggg,'Qair  ',Qair:10:1);
  WriteLn(ggg,'Allsteam ',Allsteam:7:3);
  WriteLn(ggg,'Paper ',paper:10:3);
  WriteLn(ggg,'SSC   ',SSC:10:3);
  CLOSE(ggg);

END;


PROCEDURE SCRNOUTPUT;

VAR
  i : integer;
  Tav,diff : double;

BEGIN
  Tav := 0;
  FOR i := 0 TO steps DO
    Tav := Tav + T[i]/(steps+1);

  IF (ODD(bc)) THEN
    hotsurfdry := hotsurfdry+(Wavprev-Wav)
  ELSE
    opendrawdry := opendrawdry+(Wavprev-Wav);
  Wfinal := Wav;

  diff := (Wavprev-Wav)*drybasiswt/dt;
  IF ((ROUND(x/dlength) MOD ROUND(1E-2/dt)) = 0) THEN
    WriteLn(fff,x/speed:8:4,'  ',Wav:10:6,'
',diff:12:9,'   ',Tav:10:3);

  CLRSCR;
  Writeln('X = ',x:8:5,'                    bc = ',bc:2);
  IF (x>0) THEN BEGIN
    Writeln;

    Write('M   ');
    FOR i := 0 to steps DO
      Write(M[i]*(steps/drybasiswt):9:7,'    ');
    Writeln;

    Write('T   ');
```

```
    FOR i := 0 TO steps DO
      Write(T[i]:9:4,'    ');
    Writeln;

    Write('Pv  ');
    FOR i := 0 TO steps DO
      Write(Pv[i]:9:2,'    ');
    Writeln;

    WriteLn;
    WriteLn('Average moisture      :  ',Wav:11:9);
    WriteLn('Average Temperature   :  ',Tav:11:5);
  END;

END;

{-------------------------------------------------------}

BEGIN
  PM3 := true;
  Tpockoffs := 0;
  Tsteamoffs := 0;
  Wfactor := 1;

  IF PM3 THEN BEGIN
    speed := 1050/60;
    PM3BC;
    ASSIGN(fff,'pm3.dat');
  END
  ELSE BEGIN
    speed := 880/60;
    PM2BC;
    ASSIGN(fff,'pm2.dat');
  END;

  REWRITE(fff);

  INITVAR;
  PROPERTIES;

  WHILE (x<length-dlength) DO BEGIN
    BCONDS;
    PROPERTIES;
    MASSENERGY;
    UPDATE;
    SCRNOUTPUT;
  END;       {while}

  CLOSE(fff);
  BCMOISTURE;
  AIRCALC;

END.
```

Supporting Routines - SUNCRUN.PAS

```
PROCEDURE LUDCMP(VAR a : glnpbynp; n : integer;
                 VAR indx : glindx);

CONST
  tiny = 1E-20;

VAR
  k,j,imax,i : integer;
  sum,dum,big : double;
  vv : LUglnarray;

BEGIN
  FOR i := 1 TO n DO BEGIN
    big := 0;
    FOR j := 1 TO n DO
      IF (ABS(a[i,j])>big) THEN big := ABS(a[i,j]);
    IF (big=0) THEN BEGIN
      Writeln('Pause in LUDCMP - singular matrix');
      Readln;
    END;
    vv[i] := 1/big;
  END;

  FOR j := 1 TO n DO BEGIN
    FOR i := 1 TO (j-1) DO BEGIN
      sum := a[i,j];
      FOR k := 1 TO (i-1) DO
        sum := sum - a[i,k]*a[k,j];
      a[i,j] := sum;
    END;
    big := 0;
    FOR i := j TO n DO BEGIN
      sum := a[i,j];
      FOR k := 1 TO (j-1) DO
        sum := sum - a[i,k]*a[k,j];
      a[i,j] := sum;
      dum := vv[i]*ABS(sum);
      IF (dum>big) THEN BEGIN
        big := dum;
        imax := i;
      END;
    END;
    IF (j<>imax) THEN BEGIN
      FOR k := 1 TO n DO BEGIN
        dum := a[imax,k];
        a[imax,k] := a[j,k];
        a[j,k] := dum;
      END;
      vv[imax] := vv[j];
    END;
    indx[j] := imax;
```

```
    IF (a[j,j]=0) THEN a[j,j] := tiny;
    IF (j<>n) THEN BEGIN
      dum := 1/a[j,j];
      FOR i := (j+1) TO n DO
        a[i,j] := a[i,j]*dum;
    END;
  END;
END;


PROCEDURE LUBKSB(a : glnpbynp; n : integer; indx :
glindx;
                 VAR b : LUglnarray);

VAR
  j,ip,ii,i : integer;
  sum : double;

BEGIN
  ii := 0;
  FOR i := 1 TO n DO BEGIN
    ip := indx[i];
    sum := b[ip];
    b[ip] := b[i];
    IF (ii<>0) THEN BEGIN
      FOR j := ii TO (i-1) DO
        sum := sum - a[i,j]*b[j];
    END
    ELSE
      IF (sum<>0) THEN ii := i;
    b[i] := sum;
  END;
  FOR i := n DOWNTO 1 DO BEGIN
    sum := b[i];
    IF (i<n) THEN BEGIN
      FOR j := (i+1) TO n DO
        sum := sum - a[i,j]*b[j];
    END;
    b[i] := sum/a[i,i];
  END;
END;


PROCEDURE DCMPBKSB(n : integer; M : matrix; RHS : vector;
                   VAR BLU : LUglnarray);

VAR
  i,j : integer;
  indx : glindx;
  LUM : glnpbynp;

BEGIN
  FOR i := 1 TO n DO BEGIN
    FOR j := 1 TO n DO
```

```
      LUM[i,j] := M[i-1,j-1];
    BLU[i] := RHS[i-1];
  END;
  LUDCMP(LUM,n,indx);
  LUBKSB(LUM,n,indx,BLU);
END;


PROCEDURE MATRIXZERO(VAR M : Matrix);

VAR
  i,j : integer;

BEGIN
  FOR i := 0 TO (3*steps+2) DO
    FOR j := 0 TO (3*steps+2) DO
      M[i,j] := 0;
END;


FUNCTION FACTORIAL(xx : double) : double;

CONST
  stp = 2.50662827465;
  fpf = 5.5;

VAR
  x,tmp,ser,loggam : double;
  j : integer;
  cof : array[1..6] of double;

BEGIN
  xx := xx + 1;
  cof[1] := 76.18009173;
  cof[2] := -86.50532033;
  cof[3] := 24.01409822;
  cof[4] := -1.231739516;
  cof[5] := 0.120858003E-2;
  cof[6] := -0.536382E-5;
  x := xx-1;
  tmp := x + fpf;
  tmp := (x+0.5)*LN(tmp)-tmp;
  ser := 1;
  FOR j := 1 TO 6 DO BEGIN
    x := x+1;
    ser := ser + cof[j]/x;
    loggam := tmp+LN(stp*ser);
    FACTORIAL := EXP(loggam);
  END;
END;


FUNCTION POWER(base,index : double) : double;
```

```
BEGIN
  IF (base=0) THEN POWER := 0
              ELSE POWER := exp(index*(LN(base)));
END;


FUNCTION GETPHI(Z,T : double) : double;

VAR
  b1,b2,W : double;

BEGIN
  W := Z/drybasiswt;
  b1 :=  exp(-17.255*W + 0.121*SQRT(W) - 3.640);
  b2 := -exp(-14.313*W - 2.167*SQRT(W) + 2.772);
  GETPHI := exp(b1*T + b2);
END;


FUNCTION Psat(T : double) : double;
CONST
  Pc = 22.089E6;
  Tc = 647.286;
  Tp = 338.15;
  a = 0.01;

VAR
  F : array[1..8] of double;
  sum : double;
  j : integer;

FUNCTION POWER(base:double; index:integer) : double;
{for integer indices}
VAR
  ans : double;
  k : integer;
BEGIN
  IF (base=0) THEN POWER := 0
  ELSE BEGIN
    ans := 1;
    FOR k := 1 TO index DO
      ans := ans*base;
  END;
  POWER := ans;
END;

BEGIN

  F[1] := -7.419242;
  F[2] := 0.29721;
  F[3] := -0.1155286;
  F[4] := 8.685635E-3;
  F[5] := 1.094098E-3;
  F[6] := -4.39993E-3;
```

```
  F[7] := 2.520658E-3;
  F[8] := -5.218684E-4;
  sum := 0;
  FOR j := 1 TO 8 DO
    sum := sum + F[j]*POWER(a*(T-Tp),j-1);
  Psat := Pc * EXP((Tc/T - 1)*sum);
END;


FUNCTION Qs(W : double) : double;

BEGIN
  Qs := 4186.8*(17.91*EXP(-18.25*W+2.869)+3.567);
END;


FUNCTION GDISTR(r : double) : double;

BEGIN
  GDISTR := Gcoeff*POWER(r,aa)*POWER((1-r),bb);
END;


FUNCTION FUNC(casenum : integcase; x : double) : double;

  FUNCTION VOL(r : double) : double;

  BEGIN
    VOL := SQR(r) * GDISTR(r);
  END;

BEGIN
  CASE casenum OF
    volume :      FUNC := VOL(x);
  END;
END;


FUNCTION MAX(num1,num2 : double) : double;

BEGIN
  IF (num1 > num2) then MAX := num1
                   else MAX := num2
END;


FUNCTION MIN(num1,num2 : double) : double;

BEGIN
  IF (num1 < num2) then MIN := num1
                   else MIN := num2
END;
```

```
PROCEDURE POLINT(xa,ya : glnarray; n : integer; x :
double; VAR y,dy : double);

VAR
  ns,m,i : integer;
  w,hp,ho,dift,dif,den : double;
  c,d : glnarray;

BEGIN
  ns := 1;
  dif := ABS(x-xa[1]);
  FOR i := 1 to n DO BEGIN
    dift := ABS(x-xa[i]);
    IF (dift<dif) THEN BEGIN
      ns := i;
      dif := dift;
    END;
    c[i] := ya[i];
    d[i] := ya[i];
  END;
  y := ya[ns];
  ns := ns-1;
  FOR m := 1 to n-1 DO BEGIN
    FOR i := 1 to n-m DO BEGIN
      ho := xa[i]-x;
      hp := xa[i+m]-x;
      w := c[i+1]-d[i];
      den := ho-hp;
      IF (den=0.0) THEN BEGIN
        Writeln('Pause in routine POLINT');
        Readln;
      END;
      den := w/den;
      d[i] := hp*den;
      c[i] := ho*den;
    END;
    IF (2*ns<(n-m)) THEN BEGIN
      dy := c[ns+1]
    END
    ELSE BEGIN
      dy := d[ns];
      ns := ns-1;
    END;
    y := y+dy;
  END;
END;


PROCEDURE TRAPZD(casenum : integcase; a,b : double; VAR s
: double; n : integer);

VAR
  j : integer;
  x,tnm,sum,del : double;
```

```
BEGIN
  IF (n=1) THEN BEGIN
    s := 0.5*(b-a)*(FUNC(casenum,a)+FUNC(casenum,b));
    glit := 1;
  END
  ELSE BEGIN
    tnm := glit;
    del := (b-a)/tnm;
    x := a + 0.5*del;
    sum := 0.0;
    FOR j := 1 to glit DO BEGIN
      sum := sum + FUNC(casenum,x);
      x := x + del;
    END;
    s := 0.5 *(s+(b-a)*sum/tnm);
    glit := 2 * glit;
  END;
END;


PROCEDURE QROMB(casenum : integecase; a,b : double; VAR ss
: double);

LABEL 99;

CONST
  jmax = 15;
  jmaxp = 16;
  k = 5;

VAR
  i,j : integer;
  eps,dss : double;
  h,s : array[1..jmaxp] of double;
  c,d : glnarray;

BEGIN
  IF (a=b) THEN BEGIN
    ss := 0;
    GOTO 99;
  END;

  eps := 1.0E-4;
  ss := 0;
  h[1] := 1.0;
  FOR j := 1 to jmax DO BEGIN
    TRAPZD(casenum,a,b,s[j],j);
    IF (j>=k) THEN BEGIN
      FOR i := 1 to k DO BEGIN
        c[i] := h[j-k+i];
        d[i] := s[j-k+i];
      END;
      POLINT(c,d,k,0.0,ss,dss);
```

```
      IF(ABS(dss) <= eps*ABS(ss)) THEN GOTO 99;
    END;
    s[j+1] := s[j];
    h[j+1] := 0.25*h[j];
  END;
  Writeln('Pause in QROMB - too many steps');
{  Readln;}

99:
END;

FUNCTION SOLVE(x1,x2,RHS,xlow : double)   : double;

{ Uses the Van Wijngaarden Dekker Brent Method }

LABEL 99;

CONST
  itmax = 100;
  eps = 3.0E-6;
  tol = 1.0E-6;

VAR
  a,b,c,d,e,min1,min2,mini,fa,fb,fc,p,q,r,s,tol1,xm :
double;
  iter : integer;
  again : boolean;

BEGIN
  a := x1;
  b := x2;
  REPEAT
    again := false;
    QROMB(volume,xlow,a,fa);
    QROMB(volume,xlow,b,fb);
    fa := fa - RHS;
    fb := fb - RHS;

    IF (fb*fa>0) THEN BEGIN
      Writeln('Pause in SOLVE');
      IF (fa>0) THEN BEGIN
        Writeln('x = ',' Lower limit too high');
        b := a;
        a := a * 0.99;
        again := true;
      END
      ELSE BEGIN
        Writeln('x = ',' Upper limit too low');
        a := b;
        b := MIN(b*1.01,1);
        again := true;
      END;
    END;
```

```
UNTIL (NOT again);

fc := fb;
FOR iter := 1 TO itmax DO BEGIN
  IF (fb*fc>0) THEN BEGIN
    c := a;
    fc := fa;
    d := b-a;
    e := d;
  END;
  IF (ABS(fc)<ABS(fb)) THEN BEGIN
    a := b;
    b := c;
    c := a;
    fa := fb;
    fb := fc;
    fc := fa;
  END;
  tol1 := 2*eps*ABS(b) + 0.5*tol;
  xm := 0.5*(c-b);
  IF ((ABS(xm)<=tol1) OR (fb=0)) THEN BEGIN
    SOLVE := b;
    GOTO 99;
  END;

  IF((ABS(e)>=tol1) AND (ABS(fa)>ABS(fb))) THEN BEGIN
    s := fb/fa;
    IF (a=c) THEN BEGIN
      p := 2*xm*s;
      q := 1-s;
    END
    ELSE BEGIN
      q := fa/fc;
      r := fb/fc;
      p := s*(2*xm*q*(q-r) - (b-a)*(r-1));
      q := (q-1)*(r-1)*(s-1);
    END;
    IF (p>0) THEN q := -q;
    p := ABS(p);
    min1 := 3*xm*q - ABS(tol1*q);
    min2 := ABS(e*q);
    IF (min1<min2) THEN
      mini := min1
    ELSE
      mini := min2;
    IF (2*p<mini) THEN BEGIN
      e := d;
      d := p/q;
    END
    ELSE BEGIN
      d := xm;
      e := d;
    END;
  END
```

```
    ELSE BEGIN
      d:= xm;
      e := d;
    END;

    a := b;
    fa := fb;
    IF (ABS(d)>tol1) THEN BEGIN
      b := b+d;
    END
    ELSE BEGIN
      IF (xm>0) THEN BEGIN
        b := b+ABS(tol1);
      END
      ELSE BEGIN
        b := b-ABS(tol1);
      END
    END;
    QROMB(volume,xlow,b,fb);
    fb := fb - RHS;
  END;
  Writeln('Pause in SOLVE');
  Writeln('Maximum number of iterations exceeded');
  Readln;
  SOLVE := b;

99:
END;
```